



HAL
open science

Incorporation of metals in zeolite frameworks for catalytic applications

Florent Dubray

► **To cite this version:**

Florent Dubray. Incorporation of metals in zeolite frameworks for catalytic applications. Organic chemistry. Normandie Université, 2020. English. NNT : 2020NORMC210 . tel-03510144

HAL Id: tel-03510144

<https://theses.hal.science/tel-03510144>

Submitted on 4 Jan 2022

HAL is a multi-disciplinary open access archive for the deposit and dissemination of scientific research documents, whether they are published or not. The documents may come from teaching and research institutions in France or abroad, or from public or private research centers.

L'archive ouverte pluridisciplinaire **HAL**, est destinée au dépôt et à la diffusion de documents scientifiques de niveau recherche, publiés ou non, émanant des établissements d'enseignement et de recherche français ou étrangers, des laboratoires publics ou privés.



Normandie Université

THÈSE

Pour obtenir le diplôme de doctorat

Spécialité CHIMIE

Préparée au sein de l'Université de Caen Normandie

Incorporation de métaux dans des zéolithes, pour des applications en catalyse
Incorporation of metals in zeolite frameworks for catalytic applications

Présentée et soutenue par
Florent DUBRAY

Thèse soutenue publiquement le 10/11/2020
devant le jury composé de

M. BENOIT LOUIS	Directeur de recherche au CNRS, Université de Strasbourg	Rapporteur du jury
M. LUDOVIC PINARD	Maître de conférences HDR, Université de Poitiers	Rapporteur du jury
Mme CINDY AQUINO	Ingénieur de recherche, Total Petrochemicals Research Feluy	Membre du jury
Mme DELPHINE MINOUX	Ingénieur, Total Petrochemicals Research Feluy	Membre du jury
Mme SVETLANA MINTOVA	Directeur de recherche au CNRS, Université Caen Normandie	Directeur de thèse
M. JEAN-PIERRE GILSON	Professeur des universités, ENSICAEN	Co-directeur de thèse

Thèse dirigée par SVETLANA MINTOVA et JEAN-PIERRE GILSON, Laboratoire catalyse et spectrochimie (Caen)



UNIVERSITÉ
CAEN
NORMANDIE



Normande de Chimie



Laboratoire
Catalyse & Spectrochimie

Abstract

The development of resilient and stable metal containing zeolite based catalysts able to withstand harsh catalytic conditions is a milestone required for the industrialization of many catalytic processes related to the transition of energy and chemical industries to low-emissions and renewable chemical feedstocks. The stability of metal containing zeolite materials under harsh conditions is mainly ruled by the way the metal is introduced in the zeolite support. Depending on the metal species obtained, the resilience against metal leaching, metal sintering, or structure amorphization and collapse can be changed. In the course of this PhD thesis, two synthesis approaches for molybdenum (Mo) containing nanosized MFI zeolite synthesis were developed, leading to the design of novel highly stable and hydrophobic zeolites. These two processes are more flexible than the standard one-pot direct synthesis approach and allowed the synthesis of not only pure siliceous zeolites but also aluminium containing MFI (Mo-ZSM-5) for the first time. An in-depth characterization of the resulting materials was conducted so as to assess the way the metal was incorporated in the MFI framework. The silanol species of the prepared materials were also evaluated in detail due to their central importance in the Mo incorporation process. Finally, the remarkable stability of the as-prepared Mo containing MFI zeolite sample was evaluated; the catalytic performance of the materials in methane dehydroaromatization reaction (MDA) was evaluated. The hydrophobic Mo containing ZSM-5 having a Si/Al ratio of 110 was free of silanol nests defects and was perfectly stable under MDA operation over 3 successive reaction-regeneration cycles. It displayed high conversion and high selectivity towards the production of both hydrogen and aromatics compared to the state-of-the-art Mo impregnated catalysts. In addition, the stability of the novel Mo-ZSM-5 against thermal treatment up to 1000 °C was demonstrated, as well as against steaming performed at 550 °C. The spent catalyst did show evidence of some dealumination occurring, but no silanol species were generated, and all the molybdenum stayed in the MFI structure unaltered. Thus, this material is promising for the development of efficient MDA catalysts since it solves the issue of molybdenum stability, since no leaching/agglomeration/sintering/fouling occurred.

French Abstract

Le développement de catalyseurs zéolithiques contenant des métaux résilients et stables, et qui soient en mesure de supporter des conditions catalytiques difficiles représente un jalon requis pour l'industrialisation de nombreux procédés catalytiques liés à la transition énergétique, et à l'usage de ressources chimiques renouvelables, ou n'émettant que peu de gaz à effet de serre. La stabilité des zéolithes contenant des métaux lorsqu'elles sont exposées à des conditions catalytiques difficiles est principalement régulée par la façon dont le métal a été introduit dans le support zéolithique. En fonction des espèces métalliques présentes, la résilience du matériau contre la démétallation, le frittage, ou l'amorphisation de la structure cristalline peut être changée. Au cours de cette thèse de doctorat, deux nouvelles approches permettant l'introduction de molybdène (Mo) en position intra-réseau de nanocristaux de zéolithe de type MFI ont été développées, menant au design de zéolithes hydrophobes et stables. Ces deux procédés sont davantage « flexibles » comparé à la procédure standard de synthèse directe, et permettent la synthèse de zéolithes MFI contenant également de l'aluminium (Mo-ZSM-5) pour la première fois. Une caractérisation en profondeur des matériaux résultants a été conduite de façon à évaluer le mécanisme d'incorporation du métal dans la structure zéolithique MFI. Les espèces silanols des matériaux préparés ont été évaluées en détails du fait de leur importance centrale dans le procédé d'incorporation du molybdène dans la structure zéolithique. Enfin, la stabilité remarquable des matériaux préparés contenant du Mo en position réseau de la structure MFI a été évaluée, ainsi que la stabilité de ses performances catalytiques pour la réaction d'aromatation du méthane (MDA). La zéolithe hydrophobe contenant du Mo intra-réseau dans la structure ZSM-5, avec un ratio Si/Al égal à 110, ne contenait pas de nids de silanols, et était parfaitement stable en utilisation catalytique pour la réaction de MDA, sur 3 cycles successifs de réaction-régénération. Le matériau a fait preuve d'une haute conversion et d'une haute sélectivité vers la production d'hydrogène et d'aromatiques une fois comparée à un échantillon standard comportant du molybdène extra-réseau introduit par imprégnation. De plus, la stabilité du nouveau catalyseur Mo-ZSM-5 contre les traitements à haute température (jusque 1000 °C), ainsi qu'en conditions hydrothermales (jusque 550 °C) a été démontrée. Le catalyseur utilisé a montré des signes démontrant la présence de désalumination, mais aucune espèce silanol n'a pour autant été générée, et la totalité du molybdène est restée inchangée dans la structure cristalline MFI. En conséquence, ce matériau est prometteur pour le développement de catalyseurs efficaces pour l'aromatation du méthane (MDA) étant donné qu'il résout les problématiques liées à la stabilité des espèces molybdène, car aucune démétallation/agglomération/frittage ou dégradation des sites métalliques n'a été démontrée.

Acknowledgements

The research work produced in the frame of the present thesis has been performed in the “Laboratoire Catalyse et Spectrochimie” (LCS), in Caen University, under supervision from Svetlana Mintova and Jean-Pierre Gilson. I would like to express here my deepest gratitude for their help, their advises, all the interesting conversations we had, their ideas, their experience, as well as their support all along the course of this PhD thesis. The involvement and the kindness they demonstrated throughout this journey were keys to the success of this PhD thesis all the way to its end.

This PhD thesis being under a CIFRE contract, I would also like to express all my gratitude to my supervisors from Total side: Delphine Minoux and Cindy Aquino. Their precious advises, as well as their kindness were all really precious to me, and I really enjoyed collaborating and working in their company. I also want to stress out the significant help provided by Nikolai Nesterenko, Stijn Van Daele, and Julien Grand. Collaborating with all of them was both enriching and a real pleasure.

I also want to thank deeply all people who helped me with their knowledge, their ideas, or their time, as well as their support and friendship. This includes especially all peoples related to the NanoClean Energy Total’s industrial chair such as Edwin Clatworthy, Stanislav Konnov, Ghinwa Fayad, Mariame Akouche, Vera Bikbaeva, and Izabel Medeiros-Costa. I also want to thank Valérie Ruaux, Aurélie Vicente and Cassandre Kouvatias especially for all the help, knowledge, and advises they shared with me.

My gratitude also goes to Ludovic Pinard and Benoit Louis for accepting to be reporter for this PhD thesis.

In a more general view, I would like to acknowledge all people I collaborated with in the LCS laboratory throughout the course of this PhD thesis, as well as all the other persons I did not have the chance to work with, but still had the opportunity to meet and enjoy the company.

Of course, all this work would not have been possible without the financial support from Total Research and Technology (Feluy, TRTF) and from the ANRT through the CIFRE convention. I also want to thank the University of Caen for being the host university to frame the present PhD thesis.

Last but clearly not the least, I want to express my deepest gratitude to all my friends, colleagues and family for their constant support and friendship throughout the course of this PhD thesis. Those concerned will all recognize themselves.

Table of content

ABSTRACT	1
FRENCH ABSTRACT	2
ACKNOWLEDGEMENTS	3
TABLE OF CONTENT	4
ABBREVIATIONS	7
GOALS OF THE PHD THESIS	8
GENERAL INTRODUCTION	8
FRENCH GOALS OF THE PHD THESIS	13
FRENCH GENERAL INTRODUCTION	13
CHAPTER I: METAL CONTAINING ZEOLITES AS STABLE CATALYSTS UNDER HARSH CONDITIONS: STATE OF THE ART	19
ABSTRACT.....	19
I.1. PROPERTIES OF METAL-CONTAINING ZEOLITES OPERATING AT HIGH TEMPERATURE FOR LIGHT ALKANE CONVERSION BY DEHYDROGENATION.....	20
I.2. FRAMEWORK METAL CONTAINING ZEOLITES.....	31
<i>I.2.1 Metal introduction by direct synthesis approach</i>	33
<i>I.2.3. Metal introduction by post synthesis approach</i>	42
<i>I.2.4. Guidelines for the characterization of metal containing zeolites</i>	46
<i>I.2.5. Properties of framework metal containing zeolites</i>	48
<i>I.2.6. Incorporation of group VI metals in zeolite structures</i>	52
I.3. CONCLUSIONS.....	53
I.4. REFERENCES.....	54
CHAPTER II: EXPERIMENTAL SECTION	68
II.1. MATERIALS.....	68
II.2. SYNTHESIS.....	68
<i>II.2.1. Direct synthesis - Synthesis of Mo-MFI (D) sample:</i>	69
<i>II.2.2. Staged synthesis - Synthesis of Mo-MFI (S5) and Mo-MFI (S48) samples:</i>	69
<i>II.2.3. Hydrothermal post-synthesis - Synthesis of Mo-MFI (P) sample:</i>	70
<i>II.2.4. Hydrothermal post-synthesis - Synthesis of Mo-ZSM-5 (P) sample:</i>	70
<i>II.2.5. Reference samples</i>	71
II.3. MAIN CHARACTERIZATION METHODS.....	72
II.3. EXAMPLES.....	77
II.4. CONCLUSION.....	84
II.5. TABLE OF THE MAIN SAMPLES FROM THE PHD THESIS.....	85
II.6. REFERENCES.....	89

**CHAPTER III: DIRECT EVIDENCE FOR SINGLE MOLYBDENUM ATOMS
INCORPORATED IN THE FRAMEWORK OF MFI ZEOLITE NANOCRYSTALS... 90**

ABSTRACT.....	90
II.1. INTRODUCTION.....	90
II.2. EXPERIMENTAL	91
<i>II.2.1. Synthesis</i>	91
<i>II.2.2. Characterizations</i>	92
II.3. RESULT AND DISCUSSIONS.....	94
II.4. CONCLUSIONS	98
II.5. REFERENCES.....	98
II.6. SUPPORTING INFORMATION	101

**CHAPTER IV: THE CHALLENGE OF SILANOL SPECIES CHARACTERIZATION
IN ZEOLITES 106**

ABSTRACT.....	106
IV.1. INTRODUCTION	106
IV.2. EXPERIMENTAL.....	109
<i>IV.2.1. Synthesis</i>	109
IV.2.1.a. Synthesis of Si-MFI	109
IV.2.1.b. Synthesis of Al-MFI	109
IV.2.1.c. Synthesis of Mo-MFI.....	109
<i>IV.2.2. Characterization</i>	110
IV.3. RESULTS AND DISCUSSION	111
IV.4. CONCLUSIONS.....	118
IV.5. REFERENCES	119

**CHAPTER V: STABILITY AND CATALYTIC PERFORMANCES OF MO-ZSM-5 IN
METHANE DEHYDROAROMATIZATION REACTION 123**

ABSTRACT.....	123
V.1. INTRODUCTION	123
V.2. EXPERIMENTAL SECTION	125
<i>V.2.1. Synthesis</i>	125
V.2.1.a. Synthesis of Mo-free ZSM-5 nanosized zeolite	125
V.2.1.b. Synthesis of single-site [Mo]-ZSM-5 catalyst.....	125
V.2.1.c. Synthesis of reference R-ZSM-5 catalyst	126
V.2.1.d. Hydrothermal treatment of Mo-free ZSM-5 zeolite without sodium molybdate	126
<i>V.2.2. Characterization</i>	126
<i>V.2.3. Catalytic test: non-oxidative high temperature CH₄ conversion to H₂ and higher hydrocarbons.</i>	128
<i>V.2.4. Stability of [Mo]-ZSM-5 and R-ZSM-5 samples</i>	128
V.3. RESULTS AND DISCUSSION	129
<i>V.3.1. Synthesis and comprehensive characterization of Mo-containing zeolites</i>	129

<i>V.3.2. Catalytic test of Mo-containing ZSM-5 zeolite samples: non-oxidative high temperature CH₄ conversion to H₂ and higher hydrocarbons.....</i>	<i>135</i>
<i>V.3.3. Stability of Mo-containing zeolite samples.</i>	<i>138</i>
V.4. CONCLUSION.....	141
V.5. REFERENCES	142
V.6. SUPPORTING INFORMATION	145
CONCLUSIONS AND PERSPECTIVES	153
FRENCH CONCLUSIONS AND PERSPECTIVES	157

Abbreviations

Mo= Molybdenum

Al= Aluminium

Si= Silicon

MDA= methane dehydroaromatization

ZSM-5=Zeolite Socony Mobil-5

XRD= X-Ray diffraction

NMR= Nuclear Magnetic Resonance

MAS= Magic Angle Spinning

IR= Infra Red

TMPO= trimethylphosphine oxide

CD₃CN= deuterated acetonitrile

TEOS= Tetraethylorthosilicate

TPAOH= Tetrapropylammonium hydroxide

SEM= Scanning electron microscopy

TEM= Transmission electron microscopy

Goals of the PhD thesis

The goal of this PhD thesis is to develop a new class of metal containing zeolite-based catalysts for high temperature alkane conversion, and especially, for the non-oxidative conversion of methane into hydrogen and aromatics via methane dehydroaromatization catalytic reaction (MDA). The target catalyst needs to be active, but also to be able to withstand the harsh catalytic conditions that are needed for this process. Molybdenum (Mo) was chosen for its extensive use in MDA state of the art catalysts, as well as the MFI structure. The goals of the PhD thesis were consequently three-fold:

The first goal of the PhD thesis was to be able to synthesize nanosized and silanol point defect-free Mo containing MFI zeolite, with Mo being introduced in the MFI structure as framework species. Detail characterization of the material was required so as to prove the successful occurrence of Mo isomorphous substitution in the MFI framework.

Then, the second goal was to optimize the synthesis procedure, in order to facilitate future scale-up, and make possible the co-introduction of aluminium (Al) in the Mo containing MFI framework. It was then necessary to identify the required synthetic steps from the optional ones, and to understand what was really needed in order to achieve Mo isomorphous substitution.

Once a Mo containing ZSM-5 zeolite was first synthesized, the final (third) goal of the PhD thesis was to evaluate its performances and stability against the catalytic methane dehydroaromatization catalytic reaction. The sample activity and stability was compared to state of the art catalysts.

General Introduction

The development of catalysts able to operate under harsh conditions is of prime interest for the transition of the energy and chemical industries to low-emission and renewable chemical feedstocks. Zeolites are a key player among catalysts, and their stabilization under rough environments is conditioning their development for new processes that are relevant for the energy transition. The main catalytic reactions envisioned are related to the conversion of natural gas and biomass into valuable petrochemical compounds and fuels. These conversions can be efficiently catalysed by using a metal highly dispersed on a zeolite support, but their irreversible deactivation under catalytic conditions remains a challenge. The deactivation mechanisms of such metal containing zeolites are mainly due to metal sintering, amorphization, leaching, fouling, and coking; occurring because of the particularly harsh conditions at which the catalytic reactions needs to be performed (high temperature).

Among the strategies adopted for the stabilization of metal containing zeolites under harsh conditions, the following main strategies were selected: (1) stabilization

of metal atoms so as to prevent their leaching and/or sintering, by introducing them directly into the framework of the zeolite support, (2) hydrophobicity of the support so as to prevent its collapse, by removing most of the silanol defect species from the crystalline structure, (3) use of nanosized zeolite crystals to reduce diffusion limitations and over-reaction. The synthetic strategies allowing the introduction of metal atoms into the framework of zeolites by a process called isomorphous substitution were investigated. So far, only two main synthesis approaches are used for metal introduction in zeolite frameworks : (i) direct synthesis approach, and (ii) post synthesis approach. Both methods possess advantages and disadvantages, but none of these methods are ideal.

In this PhD thesis, the incorporation of molybdenum (Mo) in nanosized MFI zeolite by direct synthesis approach was studied. It was however necessary to be able to efficiently assess whether the Mo was successfully introduced in the MFI framework. As a result, a full in depth characterization of Mo containing MFI zeolite was performed. Valuable comparison with a reference non framework Mo containing MFI zeolite was also provided. The used direct synthesis procedure had a remarkable advantage of favouring the crystallization of silanol defect-free nanosized zeolite crystals. Also, through direct synthesis the metal could be introduced in the zeolitic framework, without co-formation of unwanted non-framework metallic species. However, the synthesis was not ideal due to the lack of flexibility. For instance, the simultaneous introduction of Mo and aluminium (Al) in the MFI framework, so as to synthesize Mo-ZSM-5 zeolite, was not possible due to their high affinity towards the formation of unwanted non-framework aluminium molybdate species. Further development of the synthesis procedure for the Mo isomorphous substitution in MFI framework would be consequently of high interest.

As a result, two novel strategies for the Mo introduction as framework T-atoms in nanosized MFI crystals were developed, both strategies being more or less at the boundaries between what is called direct synthesis and conventional post synthesis approaches in the open literature. The first approach was called “staged synthesis”, and consists in the introduction of a delay before the Mo metal source was added in the precursor suspensions, after a pre-crystallization step. The second approach (called post hydrothermal synthesis) was an extension of the first one, in which the Mo incorporation was performed in fully crystallized and purified samples. These two methods significantly reduced the influence of the Mo atoms on the zeolite crystallization process. Specifically, the two step process used in the post hydrothermal synthesis strategy allowed for the successful co-introduction of both Mo and Al atoms into the MFI framework (Mo-ZSM-5) by preventing the co-existence of Al and Mo in the liquid phase.

The development of the post hydrothermal synthesis method highlighted the central importance of knowing/controlling the nature and amount of silanol species in the zeolite crystals, since Mo atoms are reacting with them during the isomorphous substitution process. Their efficient characterization was consequently a key point in

understanding whether Mo was or not introduced in the MFI framework. A set of characterization techniques were developed to characterize the nature and amount of silanol species in the nanosized zeolites.

The performance of the highly stable Mo-containing nanosized zeolites in a test reaction operated under harsh conditions (850 °C) was evaluated in depth over several reaction-regeneration cycles. It was demonstrated that Mo incorporation in the Al containing ZSM-5 framework created new catalytic active sites that were able to catalyze the methane dehydroaromatization (MDA) reaction with high conversion and selectivity compared to a conventional catalyst. In addition, the stability of the newly developed Mo-MFI catalyst, as well as the stability of its catalytic performances was remarkable. The framework Mo species were completely stable and did not change under the harsh conditions used. This proved the potential of the synthesis procedure developed in the course of this PhD thesis, for the preparation of novel catalysts that are able to withstand harsh catalytic conditions without suffering from fast irreversible deactivation.

This PhD thesis is structured in five chapters as follows:

The first chapter is introducing the state of the art on the subject. Part of this work is published as a review in *Angew. Chem. Int. Ed.* (DOI: 10.1002/anie.202005498). The first part is focused on the most wanted properties for a catalyst to be stable under harsh reaction conditions, mainly for alkane conversion. The second part is focused on the synthesis procedures allowing to prepare stable metal containing zeolites and the main properties of the catalysts associated with the presence of different T-atoms in zeolite framework. It was demonstrated that framework metal containing zeolites are a very promising class of catalysts for stable operation under harsh catalytic conditions, due to the high metal dispersion, low metal loading, and strong interaction with the framework, preventing irreversible deactivation by sintering, agglomeration, or leaching. Two main methods of synthesis can be followed to achieve the preparation of such materials, but neither are ideal. In addition, the characterization of framework metal containing zeolites remains challenging but nonetheless, the properties brought to the zeolite framework by the presence of metal inserted as T-atoms are promising, and might be key for the development of catalysts operating in a stable manner under harsh catalytic conditions.

In the second chapter, the synthesis approaches toward incorporation of Mo in MFI zeolite are presented. The main methods for characterization of zeolites are summarized. Two novel synthetic methods were developed alongside the state of the art direct synthesis approach. The first one is called staged synthesis, and the second one is called post hydrothermal synthesis. Both methods are declination of

the initial direct synthesis in which the metal precursor addition into the synthetic mixture was delayed. In the case of staged synthesis, the precursor gel suspension free of Mo and alkali metals is pre-treated under hydrothermal conditions, before the Mo and alkali sources can be introduced, and the hydrothermal treatment resumed. In the case of the post hydrothermal synthesis treatment, the Mo-free and alkali metal free precursor gel suspension is hydrothermally treated until full crystallization is reached. Then, the solid crystals are harvested, washed, and calcined. Only then, the solid crystals are treated with a solution of Mo and alkali metals under hydrothermal conditions. Both methods allow for the isomorphous substitution of Mo into the MFI framework, but the new methods are associated with higher quality samples (lower particle size, higher local homogeneity), and above all else, the new synthetic procedures are more adaptable/flexible.

In the third chapter, the complete characterization of framework Mo containing MFI zeolite is conducted. This chapter corresponds to a work published in *J. Am. Chem. Soc.* (*J. Am. Chem. Soc.* 2019, 141, 22, 8689). The Mo-MFI sample was prepared by a state of the art direct synthesis approach, and showed atomic homogeneous dispersion of the Mo species based on TEM study. In addition, the Mo introduction in the MFI framework was occurring alongside a symmetry transition of the MFI structure towards its low temperature phase, the monoclinic symmetry. This was shown as being directly related to the incorporation of Mo atoms as T-sites of the zeolite structure as further evidenced by unit cell volume expansion. The absence of molybdenum oxide particles was demonstrated, and the Lewis acidity of the as prepared Mo-MFI was evaluated using the adsorption of two probe molecules (deuterated acetonitrile and trimethylphosphine oxide) monitored by IR and ^{31}P NMR respectively. The Mo sites were shown as being closed Lewis acid sites.

In a fourth chapter (currently being submitted to *Adv. Mat. Interf.*), the characterization of silanols in zeolite framework is further studied and discussed, and comparison between the different techniques available is provided. In addition, the significance of the silanol species characterization will be of critical importance in the future, for the development and scale-up of the isomorphous substitution synthesis process. A comparison between silicalite-1, Mo containing silicalite-1, and ZSM-5 was performed. The silanols quantification and identification was carried out using ^1H NMR, and consolidated with a set of other techniques comprising IR, ^{29}Si NMR, and Raman spectroscopy. It was shown that Mo addition on silicalite-1 sample did cure all silanol nests species, and approximately half of the external silanol species.

In a last fifth chapter (published in *Angew. Chem. Int. Ed.*, DOI: 10.1002/anie.202006524), the stability of the as-prepared Mo containing ZSM-5 zeolite was evaluated by using MDA reaction as a test catalytic reaction. The remarkable stability of the as prepared Mo containing ZSM-5 was discussed according to the structural stability of the material, as well as the stability of its catalytic performances over time on stream and over successive reaction-regeneration cycles. The Mo-ZSM-5 sample displayed higher cumulative conversion

and selectivity in the conversion of methane into aromatics and hydrogen compared to state of the art impregnated samples. Most importantly, full recovery of the catalytic properties of the catalyst was evidenced after each successive catalytic-regeneration cycles. The stability of the material was demonstrated under thermal treatment up to 1000 °C and under steaming conditions at 550 °C, without occurrence of Mo leaching, or sintering. The Mo species remained unchanged, even though some dealumination occurred, but no silanol species were generated. The properties of the Mo-ZSM-5 zeolite prepared according to the synthetic strategy developed in the course of this PhD thesis are very promising, and are opening new horizons towards the smart design of resilient and stable zeolite based metal containing catalysts for applications requiring harsh operation conditions.

French goals of the PhD thesis

L'objectif de cette thèse de doctorat est le développement d'une nouvelle classe de catalyseurs zéolithiques contenant des métaux pour la conversion des alcanes à haute température, et plus particulièrement, pour la conversion non-oxydante du méthane en hydrogène et en aromatiques via la réaction catalytique d'aromatisation du méthane (MDA). Le catalyseur visé doit être actif, mais également en mesure de supporter les conditions catalytiques difficiles requises pour ce procédé catalytique. Le molybdène (Mo) et la structure zéolithique cristalline MFI ont été choisis pour leur usage étendu comme catalyseurs dans la réaction de MDA dans la littérature scientifique. Les objectifs de la thèse de doctorat se découpent par conséquent en trois parties principales :

Le premier objectif de la présente thèse de doctorat correspond au développement de la synthèse de nano-zéolithes MFI contenant du molybdène (Mo) introduit dans la structure cristalline comme espèces métalliques intra-réseau, et qui soient dépourvues de défauts silanols. Une caractérisation approfondie des matériaux a été requise afin de prouver la substitution isomorphe du Mo dans le réseau MFI.

Ensuite, le second objectif consiste en l'optimisation des procédures de synthèse, afin de faciliter un futur *scale-up*, et rendre possible l'introduction simultanée d'aluminium (Al) dans les zéolithes MFI contenant du Mo. Il a par conséquent été requis d'identifier les étapes de synthèses nécessaires parmi les étapes optionnelles, et de comprendre ce qui était réellement nécessaire à la réalisation de la substitution isomorphe du Mo.

Une fois qu'une zéolithe ZSM-5 contenant du Mo a été synthétisée pour la première fois, le troisième objectif de la présente thèse de doctorat a été réalisé ; ce troisième objectif correspond à l'évaluation des performances et de la stabilité du matériau Mo-ZSM-5 lors de la catalyse de la réaction d'aromatisation du méthane. L'activité et la stabilité du matériau ont été comparées à un catalyseur classique de la littérature scientifique.

French general introduction

Le développement de catalyseurs en mesure d'opérer dans des conditions difficiles est d'un grand intérêt pour la transition des industries énergétiques et chimiques vers de faibles émissions de gaz à effet de serre, ou vers l'usage de ressources renouvelables. Les zéolithes représentent une classe de catalyseurs importante, et leur stabilisation contre des environnements difficiles conditionnent leur développement dans le cadre de nouveaux procédés impliqués dans la transition énergétique. Les principales réactions catalytiques envisagées sont liées à la conversion du gaz naturel et de la biomasse en carburants et composés pétrochimiques à haute valeur ajoutée. Ces conversions sont efficacement

catalysées par des métaux hautement dispersés sur un support zéolithique, mais leur désactivation irréversible une fois exposés aux conditions de réactions catalytiques difficiles représente toujours un challenge. Les mécanismes de désactivation de telles zéolithes contenant des métaux sont principalement liés au frittage des métaux, à l'amorphisation de la structure, à la démétallation, à la dégradation des espèces métalliques, ou à la présence de coke ; ces mécanismes apparaissent du fait des conditions particulièrement difficiles auxquelles les réactions catalytiques envisagées doivent être conduites (haute température).

Parmi les stratégies adoptées pour la stabilisation des métaux dans les zéolithes contre les conditions de catalyse difficiles, les principales stratégies suivantes ont été sélectionnées : (1) la stabilisation des atomes métalliques de façon à empêcher leur frittage ou leur perte, via leur introduction en position intra-réseau du support zéolithique, (2) le caractère hydrophobe du support de façon à prévenir l'effondrement de la structure cristalline et son amorphisation, via la réduction de la quantité de défauts silanols, (3) l'utilisation de nanocristaux de zéolithe de façon à réduire les limitations diffusionnelles et les risques de sur-réaction. Les stratégies de synthèse permettant l'introduction d'atomes métalliques dans le réseau des zéolithes, via un procédé appelé substitution isomorphe, ont été étudiées. Il s'avère que jusqu'à présent, uniquement deux méthodologies principales de synthèse sont utilisées pour l'introduction de métaux dans les réseaux zéolithiques : (i) la synthèse directe, et (ii) la post-synthèse. Les deux méthodes possèdent différents avantages/désavantages, mais aucune n'est idéale.

Au cours de cette thèse de doctorat, l'incorporation du molybdène (Mo) dans des nanocristaux de zéolithe MFI par synthèse directe a été étudiée. Cependant, il a été nécessaire de déterminer efficacement si le Mo était introduit dans la structure MFI avec succès ou non. En conséquence, une étude complète et en profondeur des zéolithes MFI contenant du Mo a été réalisée. La comparaison enrichissante avec une zéolithe MFI de référence contenant du Mo en position extra-réseau est également fournie. La synthèse directe utilisée avait comme avantage remarquable sa capacité à favoriser la cristallisation de nanocristaux de zéolithes ne contenant que très peu de défauts silanols. Egalement, en suivant la synthèse directe, la formation de zéolithes MFI contenant des métaux spécifiquement introduits en position intra-réseau a été possible, sans co-formation d'espèces hors-réseau non désirées. Cependant, la synthèse n'était pas idéal, car manquant de flexibilité/adaptabilité. Ainsi, par exemple, l'introduction simultanée de Mo et d'aluminium (Al) dans la structure zéolithique MFI de façon à synthétiser une zéolithe Mo-ZSM-5, n'était pas réalisable du fait de la forte affinité vers la formation de molybdate d'aluminium hors-réseau non souhaités. De nouveaux développements de la procédure de synthèse permettant la substitution isomorphe du Mo dans la structure MFI étaient donc désirables.

En conséquence, deux nouvelles stratégies permettant l'introduction de Mo en temps qu'espèces intra-réseau dans des nanocristaux de zéolithe MFI ont été

développées. Les deux stratégies sont plus ou moins à la frontière entre ce qui est conventionnellement désigné comme synthèse directe, et post synthèse dans la littérature. La première approche développée a été appelée « synthèse par étape », et consiste en l'introduction d'un délai avant l'ajout de la source métallique de Mo dans la suspension initiale, après une étape de pré-cristallisation. La seconde approche développée (appelée post synthèse hydrothermale) est une extension de la première procédure, dans laquelle l'incorporation de Mo est réalisée dans des échantillons entièrement cristallisés et purifiés. Ces deux méthodes de synthèse ont permis de significativement réduire l'influence des atomes de Mo sur le processus de cristallisation de la zéolithe MFI. Spécifiquement, la synthèse en deux étapes proposée par la stratégie de post synthèse hydrothermale a permis la co-incorporation de Mo et d'Al dans la structure MFI (Mo-ZSM-5), en empêchant la coexistence de Mo et Al en phase liquide.

Le développement de la post synthèse hydrothermale a mis en lumière l'importance centrale de connaître/contrôler la nature et la quantité d'espèces silanols dans les cristaux de zéolithe, du fait que les atomes de Mo réagissent avec ces derniers lors du procédé de substitution isomorphe. Leur caractérisation efficace a par conséquent été un point clef dans la compréhension de l'introduction ou non de Mo dans la structure MFI. Un ensemble de techniques de caractérisation a été développée afin d'évaluer la nature et la quantité d'espèces silanols dans les nanocristaux de zéolithe.

Les performances des zéolithes « haute stabilité » contenant du Mo dans la structure MFI ont été évaluées en profondeur dans une réaction test d'aromatization du méthane (MDA), sous conditions difficiles (850 °C), sur une succession de 3 cycles de réaction-réactivation. Il a été démontré que l'incorporation de Mo dans la structure ZSM-5 (rapport Si/Al=110) a permis la création de nouveaux sites actifs capables de catalyser la réaction de MDA avec de hautes conversions et sélectivités, comparées à un catalyseur classique comportant du Mo extra-réseau. De plus, la stabilité du nouveau catalyseur Mo-MFI développé, ainsi que celle de ses performances catalytiques est remarquable. Les espèces Mo intra-réseau sont restées totalement stables et n'ont pas été altérées par les conditions catalytiques difficiles utilisées. Cela prouve le potentiel du processus de synthèse développé dans le cadre de cette thèse de doctorat, pour la préparation de nouveaux catalyseurs qui sont capables de supporter des conditions catalytiques difficiles, sans souffrir d'une désactivation irréversible rapide.

Cette thèse de doctorat est structurée en 5 chapitres, comme suit :

Le premier chapitre introduit l'état de l'art sur le sujet. Une partie de ce travail a été publié dans *Angew. Chem. Int. Ed.* (DOI : 10.1002/anie.202005498). La première partie se concentre sur les principales propriétés désirables pour qu'un catalyseur zéolithique contenant des métaux soit stable lors de son utilisation en conditions catalytiques difficiles, notamment dans le cadre de la conversion des

alkanes. La seconde partie se concentre sur les procédés de synthèse permettant de préparer des zéolithes contenant des métaux stables, ainsi que sur les principales propriétés de ces matériaux liées à la présence d'hétéro-éléments en position tétraédrale des réseaux cristallins zéolithiques. Il a été démontré que les métaux incorporés dans les structures zéolithiques sont une classe de catalyseurs pleine de promesses pour la catalyse en conditions difficiles, du fait de la dispersion des métaux, la faible quantité totale de métaux introduits, et les fortes interactions entre les métaux et le support zéolithique, prévenant les mécanismes de désactivation irréversibles par frittage, agglomération, et démétallation. Deux principales méthodes de synthèses peuvent être suivies de façon à préparer de tels matériaux, mais aucune d'entre-elles n'est idéale. De plus, la caractérisation des métaux dans la structure cristalline des zéolithes reste un défi, mais cependant, les propriétés apportées aux matériaux zéolithiques de par la présence d'ions métalliques en position intra-réseau de leur structure cristalline sont pleines de promesses, et pourraient être la clef pour le développement de catalyseurs zéolithiques en mesure d'être utilisés de façon stable, sous des conditions catalytiques difficiles.

Dans un second chapitre, les approches de synthèse permettant l'incorporation de Mo dans les zéolithes MFI sont présentées. Les principales méthodes de caractérisation des zéolithes sont résumées. Deux nouvelles approches de synthèses ont été développées en parallèle du procédé standard de substitution isomorphe par synthèse directe. La première méthode est appelée « synthèse par étape », et la seconde est appelée « post synthèse hydrothermale ». Les deux méthodes développées sont des déclinaisons de la synthèse directe classique initiale, pour lesquelles l'addition du précurseur métallique dans la suspension est retardée. Dans le cas de la synthèse par étape, la suspension initiale, dépourvue de Mo et d'ions alcalins est prétraitée sous conditions hydrothermales, avant que les sources de Mo et d'ions alcalins ne soient ajoutées, et le traitement hydrothermal, poursuivi. Dans le cas de la post synthèse hydrothermale, la suspension initiale est totalement cristallisée sous conditions hydrothermales. Ensuite, les cristaux obtenus sont lavés et calcinés. Seulement alors, les cristaux solides sont traités avec une solution aqueuse contenant du Mo et un métal alcalin sous conditions hydrothermales. Les deux nouvelles méthodes développées permettent la substitution isomorphe de Mo dans la structure cristalline zéolithique MFI, mais ces nouvelles méthodes sont associées avec des matériaux de meilleure qualité (taille de cristaux réduite, meilleure homogénéité locale), et surtout, ces nouvelles procédures de synthèses sont bien plus adaptables.

Dans un troisième chapitre, la caractérisation complète de zéolithes comportant des atomes de Mo en position intra-réseau du réseau MFI est conduite. Ce travail correspond à un article publié dans le J. Am. Chem. Soc. (J. Am. Chem. Soc. 2019, 141, 22, 8689) L'échantillon Mo-MFI a été préparé via la procédure classique de synthèse directe, et montre une dispersion atomique homogène des espèces Mo, basée sur une étude par TEM. De plus, l'introduction de Mo dans la

structure MFI est accompagnée d'une transition de symétrie de la structure MFI vers sa phase basse température, la symétrie monoclinique. Cela a été montré comme étant directement lié à l'incorporation de Mo dans les positions intra-réseau de la structure MFI, confirmé ensuite via l'accroissement des paramètres de maille et du volume de maille. L'absence d'oxide de molybdène été démontrée, et l'acidité de Lewis du matériau Mo-MFI préparé a été évaluée via l'adsorption de deux molécules sondes (l'acétonitrile deutérée, et l'oxide de triméthylephosphine), contrôlées par IR et ^{31}P MAS NMR respectivement. Les sites Mo ainsi caractérisés sont des sites acides de Lewis fermés.

Dans un quatrième chapitre (actuellement en soumission pour être publié dans *Adv. Mat. Interf.*), la caractérisation des silanols dans la structure des zéolithes est étudiée et discutée, et une comparaison entre les différentes techniques disponibles est apportée. De plus, l'influence de la caractérisation des espèces silanols sera d'une importance centrale dans un futur proche, pour le développement et le scale-up des procédés de synthèses permettant la substitution isomorphe. Une comparaison entre une silicalite-1, la même silicalite-1 après substitution isomorphe avec Mo, et une ZSM-5 est présentée. La quantification et l'identification des silanols a été menée en utilisant la RMN du proton, et consolidée avec un ensemble de techniques de caractérisation additionnelle comportant IR, ^{29}Si NMR, et spectroscopie Raman. Il a été montré que l'addition de Mo sur la silicalite-1 a permis de réparer la totalité des nids de silanols, ainsi qu'environ la moitié des silanols externes.

Dans un dernier cinquième chapitre (publié dans *Angew. Chem. Int. Ed.*, DOI : 10.1002/anie.202006524), la stabilité des zéolithes comprenant du Mo et de l'Al en position intra-réseau de la structure MFI (Mo-ZSM-5) a été étudiée en utilisant la réaction d'aromatization du méthane (MDA) comme réaction catalytique test. La stabilité remarquable de la zéolithe Mo-ZSM-5 est discutée sur la base de la stabilité structurale du matériau, ainsi que celle de ses performances catalytiques sur le temps, et entre chaque cycle de réaction-régénération successifs. Le matériau a montré une conversion cumulée ainsi qu'une sélectivité supérieure vers la formation d'hydrogène et d'aromatiques depuis le méthane, une fois comparée à un catalyseur standard comprenant du Molybdène extra-réseau introduit par imprégnation sur une zéolithe ZSM-5. Cependant, et plus important encore, une récupération totale des propriétés catalytiques du nouveau catalyseur Mo-ZSM-5 est démontrée après chaque cycle de réaction-régénération successif. La stabilité du matériau a été démontrée sous haute température, jusqu'à 1000 °C, et sous condition hydrothermales, jusque 550 °C, sans le moindre signe de démetalation, ou de frittage. Les espèces Mo sont restées inchangées, alors même qu'il a été montré qu'une partie de l'aluminium était sujet à désalumination, mais aucune espèce silanol n'a cependant été générée. Les propriétés de la zéolithe Mo-ZSM-5 préparée via la stratégie de post synthèse hydrothermal développée dans le cadre de cette thèse de doctorat sont vraiment prometteuses, et ouvrent de nouveaux horizons vers le design

intelligent de zéolithes stables et résilientes, comportant des métaux comme catalyseurs pour des applications requérant des conditions d'opérations difficiles.

Chapter I: Metal containing zeolites as stable catalysts under harsh conditions: state of the art

Part of this work is published as a review with the following bibliographic reference:

Clatworthy E.B., Konnov S.V., Dubray F., Nesterenko N., Gilson J-P., Mintova S. Emphasis on the Properties of Metal-Containing Zeolites Operating Outside the Comfort Zone of Current Heterogeneous Catalytic Reactions. *Angew. Chem. Int. Ed.* **2020**, DOI:10.1002/anie.202005498.

Abstract

The development of catalysts that can operate under exceptionally harsh and unconventional conditions is of critical importance for the transition of the energy and chemicals industries to low-emission and renewable chemical feedstocks. Zeolite materials in turn are a very important class of catalysts in the chemical industry, especially in the oil refining and petrochemical fields. Among zeolite catalysts, metal containing zeolite catalysts are of primary importance due to their tunable acidic and redox properties. The use of metal containing zeolite for catalysis under harsh conditions is very tempting, but it is hampered by stability issues. Several examples in the literature highlight the importance of metal dispersion and metal anchoring to the zeolite structure, as counter measures preventing the occurrence of irreversible deactivation by sintering of the metal species. To this degree, a growing interest was devoted towards the introduction and stabilization of metals into the structure of zeolites. The process allowing to synthesize such materials is called isomorphous substitution, and it can be applied using two main variants: (i) the direct synthesis approach, and (ii) the post synthesis approach. While the direct synthesis approach is usually the most selective one for the introduction of metals into the framework of zeolites, it suffers from serious drawbacks that are mainly related to the presence of metallic species inside the gel precursor. On the other hand, the post synthesis approach usually enables the introduction of higher amounts of metal as framework species, but at the cost of co-formation of non framework metallic species. In addition, the post synthesis approach is usually associated with higher hydrophilicity of the synthesized zeolite material, causing a lower hydrothermal stability, and higher operation costs due to the addition of extra synthetic steps. The design of a synthetic method combining the advantages of both approaches while preventing their main drawbacks is consequently highly desirable.

I.1. Properties of metal-containing zeolites operating at high temperature for light alkane conversion by dehydrogenation

The global energy system is undergoing a significant transition in response to a number of major challenges including the reduction of greenhouse gas emissions.¹ Projections of the demand for liquids (fuels and value-added petrochemical products such as benzene, toluene, and xylenes: BTX) over the next half-century predict an increase in the ratio of petrochemicals to fuels as the global population and living standards continue to rise.^{2,3} To satisfy both an increase in petrochemical production and a decrease in global emissions, alternative energy sources and processes will need to be established which will require the development of new catalysts possessing unique and exceptional properties.

Zeolites have proven to be game-changing materials in the petrochemical industry over the last 50 years, and due to their established position have the potential to readily facilitate the development of new and emerging petrochemical processes.^{4,5} One such process is the non-oxidative conversion of CH₄, presenting attractive options for the production of H₂ and chemicals, however, the process typically occurs at high temperature, outside the comfort zone of conventional heterogeneous catalytic reactions.

It is well-known that metal-containing zeolites which operate at high temperature, in the presence of steam, tend to suffer from several types of irreversible damage including: (i) loss of dispersion of the metal phase,⁶ (ii) leaching of the metal phase,⁷ (iii) severe dealumination due to the reaction between volatile metals and framework Al,⁸ and (iv) acid/base catalyzed hydrolysis of Si–O–Al/Si–O–Si bonds.^{9,10} In addition, the formation of coke from CH₄ can result in the poisoning of acid sites and the blocking of pores.^{11,12} Regeneration of the catalyst by calcination can remove coke deposits but often results in the sintering of the metal phase by Ostwald ripening and particle migration.¹³ The dispersion of the metal phase can be restored in some cases via a combination of reductive/oxidative treatments but it brings significant costs and reduces efficiency. Despite the general acceptance of these problems by both the industrial and academic communities, and the significance of these issues for industrial processes, they are seldom addressed in the open literature.

The main current types of dehydrogenation catalysts are not based on zeolites but require either metallic platinum (Oleflex Process) or chromium oxide supported catalysts (Catofin Process), both working in the presence of promoters.^{14–17} The deactivation of platinum-supported catalysts occurs primarily due to the agglomeration and sintering of platinum and the poisoning of active sites by coke. The addition of Sn as a promoter has been found to confer several beneficial geometric and electronic properties to Pt, such as improving the particle dispersion, as well as reducing the acidity of the support, suppressing side reactions, and the transfer of coke from the Pt active sites to the support.¹⁵ Similar to Pt-based

catalysts, chromia-based catalysts deactivate due to the formation of coke and the sintering of the chromia active sites.¹⁸ However, upon regeneration, irreversible deactivation occurs due to the sintering of alumina that reduces the available surface area required to stabilize Cr⁶⁺ species, the incorporation of chromium species into the alumina framework, and the phase transition of γ - to θ - or even α -alumina at high temperatures.¹⁵ Strategies to restrict the phase transformation of γ - to α -alumina have involved the doping of the support with metal oxides.¹⁹ Zeolites-based dehydrogenation catalysts have so far failed due to a lack of regenerability of the metal phase introduced mainly by ion-exchange or impregnation, i.e. in extra-framework positions.

However, the use of zeolites as metal supports is an efficient way to obtain catalysts with highly dispersed metal species.²⁰ The dispersion and stabilization of the metal is facilitated by confinement within the zeolite pore system and its interaction with the zeolite surface, reducing its migration and sintering. Metal-containing zeolites prepared by conventional ion-exchange/impregnation procedures have been investigated for the dehydrogenation of light alkanes, but are susceptible to sintering of the metal species.^{21,22} In addition, impregnation and ion exchange procedures do not always allow for careful control of the location of the metal on the support, resulting in catalysts with poor metal distribution and metal particles located on the external surface of the catalyst.²¹⁻²³

Several recent strategies for improving the resistance to migration and sintering of the metal phase of metal-containing zeolites for propane conversion are highlighted (Table 1), including examples of zeolites containing extra-framework metal species only, extra-framework metal species prepared from framework metal precursors, and zeolites containing both framework and extra-framework metal species.

Liu et al. have developed an innovative approach for the preparation of subnanometric platinum species with high thermal stability in the cages, cups, and channels of zeolites.^{24,25} The novel materials were tested for propane dehydrogenation (PDH) in a fixed-bed reactor at 550–600 °C and in several oxidation-reduction cycles at 650–700 °C, and were compared with Pt-containing zeolite catalysts prepared by wet impregnation.

Liu et al. also achieved the preparation of subnanometric platinum (atomic Pt and Pt clusters) during transformation of a purely siliceous layered MCM-22 precursor to MCM-22 zeolite.²⁴ The Pt subnanometric species were introduced during the swelling of the lamellar MCM-22 precursor using an organic surfactant (hexadecyltrimethylammonium). Calcination of the precursor resulted in the encapsulation of the Pt species in the supercages and exterior cups. The reaction rate of the Pt species of the novel material was approximately 1.7 times higher than that of wet-impregnated material and demonstrated greater stability over multiple cycles. Oxidation-reduction cycles at 650 °C revealed that the Pt atoms and small Pt

clusters were susceptible to aggregation, however, the size distribution of most of the Pt nanoparticles remained below 2 nm. Ultimately the procedure does not fully prevent the aggregation of the metal species but significantly improves their stability in comparison to the wet-impregnated material consisting of metal aggregates between 30 to 50 nm.

Another approach reported by Liu et al. involved the one-pot synthesis of Pt and PtSn clusters stabilized by the presence of K^+ in siliceous MFI zeolite confirmed by HAADF-HRSTEM.²⁵ The initial Pt@MFI and PtSn@MFI materials were prone to fast deactivation and sintering, however, the introduction of a controlled amount of K^+ allowed for the preparation of subnanometric Pt clusters having a size ranging from 0.4 to 0.7 nm. These materials (containing either Pt or PtSn clusters synthesized in the presence of K^+) possessed significantly improved stability, attributed to the stabilizing effect of K^+ . The stability of the subnanometric PtSn clusters was demonstrated up to 700 °C after two oxidation-reduction cycles confirmed by HAADF-HRSTEM.

For zeolites containing both framework and extra-framework metal species, Wang et al. and Xu et al. independently reported on the use of zeolite BEA containing framework Sn to stabilize Pt species for PDH.^{26,27} Both reports begin with a similar synthetic strategy by dealumination of the zeolite BEA followed by different techniques for the incorporation of Sn atoms into the framework and the loading of Pt. Both studies reported the framework Sn sites facilitate the high dispersion of the Pt species. Wang et al.²⁶ reported their optimized catalyst (0.3 wt% Pt, 0.5 wt% Sn) lost only 13% of its initial propene formation rate over 12 h at 600 °C and that it was stable over four reaction cycles at 550 °C with > 99% selectivity to propylene. After reaction at 550 °C (5 h), Pt particles \approx 1.6 nm could be observed indicating that not all of the Pt was stabilized, however, the size of the particles did not significantly increase after further reaction (12 h). TG analysis of the spent catalyst showed a weight loss of 0.6% indicating low coke formation. The healing of silanol defects was confirmed by FTIR spectroscopy, and the incorporation of Sn into the framework was investigated by XRD, diffuse reflectance UV/Vis spectroscopy and XPS. The stable activity and high selectivity to propylene of the catalyst was attributed to the strong interaction between the Pt clusters and framework Sn sites.

Xu et al.²⁷ reported their optimized catalyst (0.5 wt% Pt, 1.0 wt% Sn) demonstrated 50% conversion at the beginning of the reaction, decreasing to 45% over 48 h at 570 °C. The catalyst displayed consistent activity over two reaction cycles with up to 98% selectivity to propylene and low coke formation (2%, TGA). The Pt species were determined to be part of bimetallic Pt/Sn particles (average diameter of 1.26 nm) located on the surface of the zeolite at framework Sn sites. The incorporation of Sn into the framework was studied, and the high dispersion of the Sn and Pt species was attributed to the absence of reflections for SnO_2 and PtO in the XRD patterns. The chemical speciation of Sn from XPS measurements was reported as framework Sn(IV) coordinated to four Si–O–Si linkages, framework Sn(II)

coordinated to two Si–O– Si linkages that interfaces with the Pt particle, and metallic Sn incorporated in the bimetallic Pt/Sn particles.

Attempts to employ zeolites containing first row transition metals for PDH have involved the preparation of cobalt confined in zeolite Beta. Adopting a procedure from Baran et al.,²⁸ Chen et al.²⁹ dealuminated zeolite Beta in nitric acid to form T-atom vacancies, followed by mixing with a solution of cobalt(II) nitrate, and calcination at 600 °C. Calcination of the cobalt-loaded dealuminated zeolite Beta was inferred to extract framework Co^{2+} to form extra-framework CoO_x species. The high dispersion of the CoO_x species was attributed to presence of silanols created at T-atom vacancies. The best performing catalyst, with a 0.5 wt% Co loading, displayed a maximum propane conversion of 53%, plateauing to 40% after 6 h, and a selectivity to propylene > 98%. Regeneration of the catalyst at 600 °C for 2 h in air demonstrated consistent activity over three reaction cycles of 6 h before discernable deactivation during the fourth cycle. The similar activity between the calcined only and reduced samples was attributed to the reduction of CoO_x species to metallic Co during the dehydrogenation reaction.

Similar to their work on Co-BEA, Chen et al. attempted to prepare vanadium containing-BEA zeolites (0.5–10 wt% V) by post-synthetic dealumination and treatment with NH_4VO_3 solution.³⁰ Characterization of the catalysts indicated the formation of extra framework polymeric vanadium species, in particular for high loadings (> 3 wt%). The catalysts were tested for PDH at 600 °C with the higher loaded catalysts (≥ 3 wt% V); the activity dropped initially from approximately 40% conversion to 23% after 6 h, and a maximum propylene selectivity of 95% was observed. The stability of the catalyst was evaluated by regeneration every 2 h after 4 h on stream for a total of 16 h of operation demonstrating consistent behavior.

In addition to cobalt and vanadium, the catalytic properties of framework and extra-framework iron-containing BEA and MFI type zeolites for monomolecular PDH were investigated by Yun and Lobo.³¹ Determination of Fe^{3+} in the MFI framework by XRD and diffuse reflectance UV/Vis revealed that after calcination at 480 °C a large fraction of the framework Fe^{3+} was retained, however, treatment with steaming at 700 °C resulted in the majority of Fe^{3+} migrating to extra-framework positions. With a propane feed of 5 mol% the calcined H-[Fe]ZSM-5 sample displayed a greater rate of dehydrogenation by a factor of 2.7 and 3.8 compared to the H-[Al]ZSM-5 and steamed H-[Fe]ZSM-5 respectively, and a higher relative rate of dehydrogenation to cracking compared to H-[Al]ZSM-5 (22 vs 0.36) at 530 °C. Comparison of the turnover frequencies (TOF) between the calcined Fe-MFI and Fe-BEA samples showed a negligible difference. The results indicate that the conversion of propane occurs mainly on the isolated framework Fe sites, compared to the extra-framework Fe sites, and that the zeolite pore size is not an important factor in the propane reaction. However, with a higher propane feed (16 mol%) at 530 °C the conversion of the H-[Fe]ZSM-5 sample (7.2%) was lower than the H-[Al]ZSM-5 sample (18.7%), but the selectivity was higher (78 vs 20%). In addition, based on the change of the unit

cell volume, approximately 50% of the Fe migrated to extra-framework positions during the reaction. Information concerning the recyclability and catalyst stability over extended time periods was not reported.

Table 1. Examples of metal-containing zeolites operating outside the “comfort zone” of current heterogeneous catalytic reactions: propane dehydrogenation (PDH) and methane dehydroaromatization (MDA).

Entry	Catalyst	Metal State (as synthesized) ^[a]	Synthesis Procedure	Reaction	Reaction Conditions	Performance ^[b]	Identified Deactivation Pathway	Ref.
1	Pt@MCM-22 (0.11 wt% Pt)	EFW	Pt introduction during swelling process of lamellar zeolite precursor	PDH	550 °C, 1 bar, WHSV = 3.2 h ⁻¹	Reaction rate: 0.6 mmol s ⁻¹ g ⁻¹ 5 reaction-regeneration cycles ^[c]	Sintering, coke	24
2	K-PtSn/MFI (0.45 wt% Pt, 0.90 wt% Sn, 0.65 wt% K)	EFW (Pt clusters)	One-pot synthesis in alkaline media	PDH	600 °C, 1 bar, WHSV = 1.8 h ⁻¹	27 s ⁻¹ and 17 s ⁻¹ initial TOF ^[d] Reaction rate: ~80 mmol s ⁻¹ g ⁻¹ 3 reaction-regeneration cycles	Coke	25
3	0.3Pt/0.5Sn-Si-Beta (0.26 wt% Pt, 0.47 wt% Sn)	FW Sn + EFW Pt	Impregnation of dealuminated BEA zeolite	PDH	500–600 °C, 1bar, WHSV = 1 h ⁻¹	4.6 min ⁻¹ initial TOF, propylene formation rate 2.3 mol g ⁻¹ h ⁻¹ (550 °C), 3.1 mol g ⁻¹ h ⁻¹ (600 °C) Deactivation rate: 0.007 h ⁻¹ (550 °C) 4 reaction-regeneration cycles	Coke	26
4	Pt/Sn 2.00-Beta (Si/Al = 440 ; Sn/Pt = 2.00 ; 0.5 wt% Pt)	PtSn alloys (EFW) attached to FW Sn	Post-synthetic incorporation of Sn in BEA framework followed by Pt introduction	PDH	570 °C, WHSV = 2400 h ⁻¹	114 s ⁻¹ TOF, Deactivation rate: 0.0063 h ⁻¹ 2 reaction-regeneration cycles	Coke	27
5	0.5CoSiBeta (0.5 wt% Co)	EFW	Impregnation of dealuminated BEA zeolite	PDH	550–600 °C, 1 bar, WHSV = 0.4 h ⁻¹	32.9 h ⁻¹ TOF (550 °C), Deactivation rate: 21.1% (600 °C) ^[e] 4 reaction-regeneration cycles	Coke	29
6	V-Beta (3 wt% V)	FW + EFW	Impregnation	PDH	600 °C, 1 bar, WHSV = 0.6 h ⁻¹	0.02 s ⁻¹ initial, TOFs and 0.01 s ⁻¹ final TOF Deactivation rate: ~12.5% 4 reaction-regeneration cycles	Coke	30
7	H-[Fe]ZSM-5 (Si/Fe = 26, 48) Fe-BEA (Si/Fe = 15)	FW + minor EFW	Direct isomorphous substitution in alkaline media	PDH	460–530 °C, 1 bar, WHSV = 1.8 h ⁻¹ for experiments with low conversion (TOF and reaction rates)	TOF of dehydrogenation, mol s ⁻¹ (mol H ⁺) ⁻¹ x 10 ⁴ for H-[Fe]beta(15) 5.97 (550 °C)	Coke, demetallation	31
8	Ga-Beta (Si/Ga = 35)	FW + EFW	Direct isomorphous substitution in alkaline media	PDH	600 °C, 1 bar, the amounts of each catalyst were adjusted for a similar conversion level (~7%). 5% C ₃ H ₈ in N ₂ , 20 cm ³ min ⁻¹ .	TOFs ^[f] ~ 120–70 (5 h) mmol h ⁻¹ mol ⁻¹ ~ 45–30 (5 h) mmol h ⁻¹ mol ⁻¹	Coke	32

9	Ga-Beta-200 (Si/Ga = 177.7)	FW	Direct isomorphous substitution in alkaline media	PDH	650 °C, 1 bar, 10 mol% C ₃ H ₈ /90% He, 6.69 cm ³ min ⁻¹ , the amount of the catalyst was not provided.	X ~54–34% (6 h), Y ~32–25% (6 h),	Coke	33
10	Mo/HZSM-5 (Si/Al = 30; 2 wt% Mo)	EFW	Impregnation	MDA	Reaction: 700 °C, 1 bar, WHSV 0.8 h ⁻¹ . Regeneration: 700°C, air	> 50% of initial Y of benzene over 100 reaction-regeneration cycles	Coke, dealumination	8
11	Mo/HZSM-5 (Si/Al = 20; 6 wt% Mo)	EFW	Impregnation	MDA	Reaction: 750 °C, 1 bar, WHSV 3.9 h ⁻¹ , 7h. Regeneration: 450 °C, air (SV 3000 h ⁻¹) with NO (NO/air = 1/50 vol/vol).	Benzene formation rates approximately the same after 8 reaction-regeneration cycles	Coke, dealumination	34
12	Mo/H-ZSM-5 (Si/Al = 15; 5 wt% Mo)	EFW	Impregnation	MDA	Reaction: 700 °C, 1 bar. Regeneration: 450 °C, air	Methane conversion and benzene yield constant over 5 reaction-regeneration cycles	Coke, sintering at high temperature and Mo loading, dealumination	35

^[a] FW = Framework metal sites, EFW = Extra-framework metal sites.

^[b] X, S, Y – Propane conversion, selectivity to propylene, and yield of propylene; TOF – turnover frequency; τ – time required for rates to decrease by a factor of e^{-1} .

^[c] The reaction rates were measured when the conversion of propane is lower than 10% and the values have been normalized to the amount of Pt in the catalysts.

^[d] Initial TOFs of various Pt-zeolite materials for propane dehydrogenation at 600 °C based on the exposed Pt sites determined by CO chemisorption and the exposed surface atoms according to the average particle size derived from electron microscopy and EXAFS results. The TOF values were calculated based on the initial propane conversion at kinetic regime (conversion below < 20%). The reaction conditions were the same as the catalytic tests described in the manuscript, but with a higher space velocity to achieve lower conversion ²⁵.

^[e] Deactivation rate relative to the maximum propane conversion at 6 h on stream.

^[f] TOFs were calculated based on the Brønsted acid site or the total acid site concentrations.

Zeolites containing framework gallium have been studied for several decades due to their ability to dehydroaromatize propane and other light alkanes, and have been used as catalysts in the petrochemical industry since the mid-1980s in the joint UOP and BP Cyclar Process.³⁶ The majority of investigations have been focused on maximizing the selectivity to aromatics while only a small number of investigations have discussed PDH, the first step of aromatization, typically reporting low selectivity and stability.^{32,37}

Choi et al. investigated PDH over gallosilicate MFI obtained by direct synthesis in the presence of (3-Mercaptopropyl)trimethoxysilane (MPS).³² Both framework and non framework Ga sites were formed. The MPS-gallosilicate MFI materials demonstrated a lower rate of deactivation and higher propylene yield, but a lower selectivity to propylene compared to the chromia-alumina catalyst (75% vs 85%). However, at higher levels of conversion the selectivity to propylene was reported to be higher than earlier reports in the literature for gallosilicates under similar conditions. This was attributed to the relatively lower number of Brønsted acid sites which are believed to be active for the oligomerization and cyclization steps of alkane aromatization.

Recently, Nakai et al. investigated high-silica Ga-BEA prepared by dry gel (DGC) conversion method for PDH at 650 °C, and compared it with Ga-BEA prepared by dealumination/wet impregnation and Ga-MFI.³³ The DGC Ga-BEA showed superior performance in terms of propane conversion (54.3% at 15 min) and propylene yield (31.5% at 15 min) compared to the other catalysts, however, the propane conversion and propylene yield decreased to \approx 35% and \approx 25% respectively, after 6 h on stream. It was observed that the Ga-BEA catalyst with a higher Si/Ga ratio demonstrated a higher conversion of propane, higher yield of propylene, and lower formation of coke compared to the equivalent catalyst with a lower Si/Ga ratio. The superior performance of the Ga-BEA with a higher Si/Ga ratio was attributed to the relatively lower number of Brønsted acid sites and higher mesoporosity of the catalyst resulting in a lower amount of coke formation and higher diffusion of the reactant and products. However, information concerning the recyclability and catalyst stability was not presented.

Among alkane catalytic conversions, the non oxidative conversion of methane is of major importance due to its potential. Indeed, the non-oxidative conversion of methane, such as methane dehydroaromatization (MDA), is an attractive reaction for the production of H₂ and chemicals, however, an evaluation of the reaction thermodynamics shows that the production of aromatic is unfavorable below 700 °C and the reaction is highly endothermic. The reaction is therefore significantly hindered by low substrate conversion, poor product selectivity, and catalyst deactivation due to the formation of coke.³⁸ While the formation of coke can be treated with an optimized reaction-regeneration cycle, irreversible deactivation of the catalyst continues to occur over extended time periods.^{8,39} Alternatively, the reaction temperature can be increased

to favor the formation of aromatic products, however this results in severe coke formation and catalyst instability.⁴⁰

Under conventional MDA operating conditions, the typical Mo containing catalyst, obtained by impregnation on HZSM-5, deactivates due to the formation of a carbonaceous layer consisting of polyaromatic hydrocarbons at the external surface. This decreases the accessibility of the Brønsted acid sites in the zeolite micropores, restricts the access of molecules to the acid sites, and facilitates the sintering of molybdenum carbide species due to weak interactions with the zeolite surface.¹¹ In addition, excessive heat treatment and the presence of water during the reaction, especially during the regeneration step, results in the dealumination of the zeolite. Under such conditions the Mo species become mobile and react with framework Al to form aluminium molybdates.^{8,41} The degree of dealumination is strongly influenced by the Mo content and Si/Al ratio.^{8,42,43} These new Mo species cannot form carbides, resulting in irreversible deactivation of the catalyst.^{11,44} Irreversible deactivation such as this prevents continuous recycling of the catalyst which is crucial due to the rapid formation of coke. Several strategies have been proposed to improve the stability of the catalyst during regeneration and to adapt metal-containing zeolites to harsh regeneration conditions (Table 1).^{8,34,35,45,46}

Kosinov et al. investigated the structural and textural stability of HZSM-5 with different loadings of Mo in air at high temperature (550–700 °C).⁸ It was observed that high Mo loading lead to the formation of aluminum molybdate and irreversible damage to the zeolite framework during metal dispersion into the micropores when calcined above 550 °C. In comparison, low Mo loading (1–2%) significantly improved the oxidative stability of the catalyst. Mo species were predominantly located in the zeolite micropores as cationic mono- and di-nuclear Mo-oxo complexes, even at high calcinations temperature. At 2 wt% Mo loading the catalyst retained more than 50% of its initial activity after 100 reaction-regeneration cycles and demonstrated a substantially improved total aromatics yield. Another strategy to improve the stability of the catalyst has been to employ less harsh regeneration procedures. Ma et al. demonstrated the ability to remove carbon deposits by using 2% NO as a promoter in air.³⁴ The removal of coke began at 330 °C and complete removal was achieved at 450 °C, suppressing the migration and sublimation of Mo species and minimizing damage to the structure as confirmed by 8 reaction-regeneration cycles. Han et al. investigated the use of either oxidative or reductive regeneration treatments on Mo/H-ZSM-5 catalysts with different Mo loading (1–7 wt%).³⁵ It was observed for the optimized catalyst (5 wt% Mo) that oxidative regeneration at 450 °C was the most effective treatment attributed to the removal of Mo-associated graphite coke. Higher regeneration temperatures of up to 850 °C caused irreversible deactivation due to the sublimation of MoO₃ and the loss of Brønsted acidity. It was concluded that the selective recovery of Brønsted acid sites

near Mo sites, rather than isolated acid sites, is sufficient to restore the catalytic activity in terms of benzene formation.

In addition to reducing the damage to the zeolite structure, optimizing the reaction and regeneration of the catalyst is of critical importance in order to reduce the migration and sintering of the metal phase. It is widely believed that the dispersion of the metal is the most important factor governing the activity of the MDA catalyst.⁴⁷ However, despite decades of intensive investigation, the synthesis of zeolites with highly dispersed metal is exceptionally challenging. Very few examples of catalysts possessing metals with both high dispersion and stability have been reported in the literature for direct non-oxidative methane conversion. Two examples include lattice-confined single-iron sites embedded within a silica (SiO_2) matrix reported by Guo et al., and nanoceria single-atom platinum catalysts reported by Xie et al.^{48,49} However, these non-zeolite materials operate at extremely high temperatures, above 950 °C.

Thus, despite decades of numerous investigations, the challenge of preparing a suitable catalyst is still unmet. Special attention must be given to the dispersion of the metal phase as single-atom active sites are the most promising for high and stable catalytic performance (Figure 2). In consideration of this goal, new and innovative synthesis procedures will have to be developed, beyond conventional post-synthesis techniques.

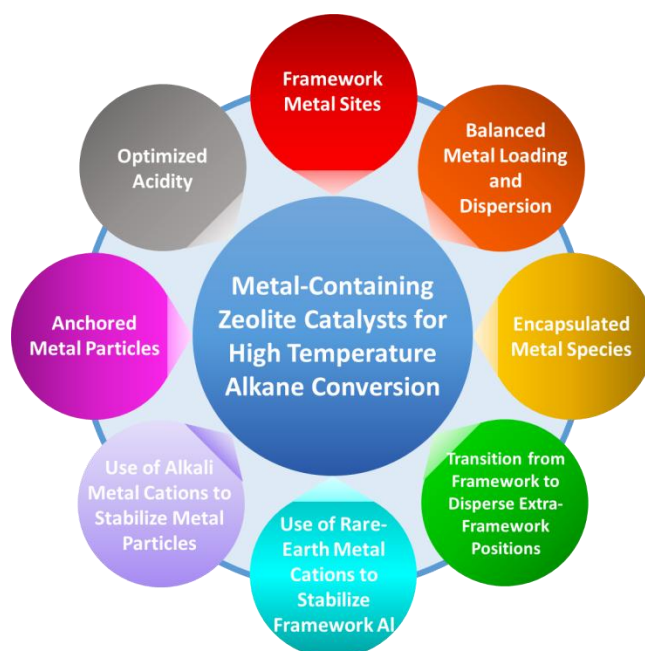


Figure 2. Strategies for improving the performance of metal-containing zeolites catalysts for high temperature alkane conversion.

Zeolites (and zeotypes) that possess metals incorporated at the T-atom positions (tetrahedral Si or Al) of the framework are a promising class of materials for operating under harsh and unconventional reaction conditions. The substitution of T-atoms for metals such as Ti, V, Ga, Mo, Sn or W,⁵⁰ can result in beneficial changes to the catalyst such as: (1) tailored selectivity due to uniformly dispersed metal atoms that can form either closed (non-hydrolyzed) or open (hydrolyzed) Lewis-acidic framework-metal sites;⁵¹ (2) high hydrophobicity due to the reduction in the number of silanol defect sites;⁵² (3) improved mass transfer (in comparison with their impregnated or ion-exchanged counterparts) due to the absence of metal particles that are formed within the micropores during post treatment procedures;⁵³ (4) improved stability of the metal phase due to its high dispersion at low loading in the zeolite framework (reduced Ostwald ripening and metal mobility); and (5) reduced coking rate due to the high distance between/low density of active sites. However, the stability of the metal phase will depend significantly on the preferred coordination environment of the metal as a consequence of its electronic properties and ionic radius, as well as the nature of the site occupied by the metal for any given type of framework.

From the above-mentioned examples, it appears that the incorporation of an isolated metal species into the zeolite framework can indeed be an effective strategy to obtain a catalyst whose active metal species have improved resistance to sintering. However, some metals appear to be relatively less stable when incorporated into the zeolite framework resulting in the formation of extra-framework species and changes in the catalytic behavior of the material are observed.

As the global energy system continues evolving to satisfy both a growing population and a reduction in greenhouse gas emissions, zeolites will continue to play a central role in existing petrochemical and emerging bio-refinery processes. Metal-containing zeolites offer a surplus of opportunities for developing catalysts with desirable and bifunctional properties due to the numerous combinations of framework structures, zeolite morphologies, Si/Al ratios, active site morphologies, and types of metals.

Specifically, strategies that revolve around the substitution of atoms at T-sites show that metals located at these positions can serve as catalytic sites located in the zeolite framework, as anchoring sites for catalytically active metals, and as precursors to highly disperse extra-framework catalytic sites formed during the post-synthetic treatment or catalytic reaction. This reinforces the importance of scrutinizing the activity and stability behavior of the catalyst as different metals clearly demonstrate different degrees of stability within the zeolite framework whereby the observed activity may represent a combination of behaviors from different sites, potentially exhibiting a synergistic interaction.

As we have noted, determining the stability and recyclability of metal-containing zeolite catalysts under industrially relevant conditions is of critical importance yet infrequently reported. General deactivation pathways and stabilization strategies under different reaction conditions have been identified, but further targeted and in-depth analyses are required.

Therefore, framework metal containing zeolites are an ideal candidate for the design of a catalyst that would remain stable even under harsh catalytic and/or regenerative conditions. This is because they meet most of the requirements that are highlighted in this state of the art review such as high metal dispersion, strong anchoring to the structure, low overall metal loading, low silanol content, low Brønsted acidity, and high hydrophobicity.

I.2. Framework metal containing zeolites

Zeolites have a demonstrated track record in many applications such as catalysis, separation and ion exchange due to their unique properties of acidic molecular sieves⁵⁴. Up to now, many efforts have been devoted on tuning zeolite properties in order to improve their performances for existing applications, and to open the doors for new applications. Following this line, the alteration of zeolite acidity or oxidation properties attracted many interests as it allows to tune conversion and selectivity by influencing interactions between zeolite catalyst and reactants⁵⁵. Such modification of zeolite properties is usually performed through the introduction of transition metal atoms which can be performed in several ways; a recent review presenting all known approaches has been published⁵⁶. The way a metal is introduced into a zeolite can alter its chemical nature in the obtained material. Many different metal species can be obtained in a given zeolite⁵⁷ such as metal clusters, metal oxide crystals of different sizes, grafted metal species, or framework metal species, as illustrated in Figure 4. The different metal species are bringing different properties to the zeolite material, and the ratios between any given metal species can be monitored by changing synthesis conditions⁵⁸. The design of efficient synthesis route toward formation of specific metallic sites is consequently of first interest in order to finely tune the zeolite properties.

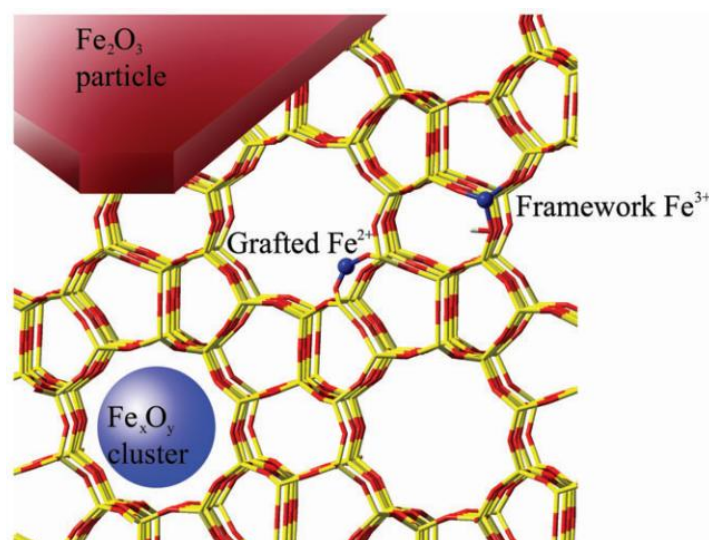


Figure 4. Illustration of different non framework and framework iron species in MFI type framework structure ⁵⁷.

It is possible to distinguish two main kinds of metal species: (i) framework metal species and (ii) non framework metal species. Framework metal species stands for metal being incorporated into a crystallographic tetrahedral position from the zeolite framework through isomorphous substitution, when non framework metal species stands for all other metal species which are not part of the framework itself. Isomorphous substitution consequently stands as the substitution of a silicon atom from a zeolite framework, with another hetero atom ⁵⁹. This hetero element can be metallic or not as in the case of SAPO structures for instance, where Al and P are substituting Si atoms from the framework ⁶⁰. The most often introduced element in zeolite topology is Al; this element is also naturally present as framework species in most of the natural zeolites ⁶¹. However, this section will be focused on the introduction of other metals, namely transition metals, into zeolitic frameworks.

A transition metal introduced into a zeolite framework brings Lewis acidity to the material ^{62,63}, and the corresponding framework Lewis acid sites are of two natures: (i) closed Lewis acid sites, and (ii) open Lewis acid sites ⁶⁴. Open Lewis sites are partially hydrolyzed closed Lewis acid sites such as, for instance, $M(OSi)_4$ (closed site) being hydrolyzed towards $M(OSi)_3OH$ (open site) (Figure 5.). These framework Lewis acid sites possess oxidation potential, and if they interact with adjacent silanol species, they can sometimes generate acid sites having a Brønsted nature (sites that are able to exchange protons) ⁶⁵. Distinction between closed and open Lewis acid sites has already been discussed and characterized using FTIR technique, with the use of several probe molecules adsorption (carbon monoxide: CO, and deuterated acetonitrile: CD₃CN mainly) ⁶⁴⁻⁶⁷.

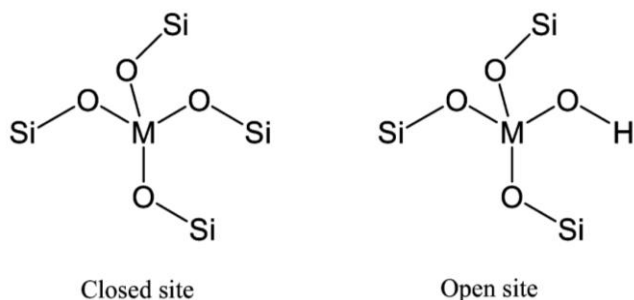


Figure 5. Distinction between closed and open Lewis acid sites ⁶⁴.

There are two main synthesis approaches which are applied so as to perform isomorphous substitution on a zeolite⁶⁸, allowing for the introduction of metal atoms in tetrahedral framework positions of a zeolite structure. These two main approaches are: (i) direct synthesis, and (ii) post-synthesis approach. All synthesis methods applied for the preparation of metal containing zeolite (with metal introduced in the framework) can be related to one of these two approaches. The two approaches are detailed individually in the two sections below.

I.2.1 Metal introduction by direct synthesis approach

The direct hydrothermal synthesis approach consists in the introduction of the transition metal source directly into the synthesis mixture, prior aging and hydrothermal treatment. The idea is to hydrolyze and condense the metal alongside the Si source in order for the metal to be introduced in the structure during the crystallization process. However, this method suffers from several drawbacks linked to the presence of a metal source alongside other reactants in the precursor gel suspension. Indeed, the presence of a hetero-element in a precursor gel suspension can alter the properties of said gel ^{69,70} (solubility of the species, nucleation, condensation, crystallization, pH, alkalinity, counter-ions, kinetics...) in both positive and negative ways. For instance, the rate of hydrolysis of a metal can be different from the one of silica and thus, prevent the linkage between metal and Si units due to the faster condensation of Si during crystallization. The classical way to overcome this issue and still achieve isomorphous substitution is to make a first co-hydrolysis step (prior crystallization) in acidic media. The idea is to reduce the Si hydrolysis rate so that it matches the one of the metal of interest, allowing the formation of Si-O-Me (Me = Metal) linkages, as reported for Co and Cr in BEA, and Sn in MFI zeolite for instance ^{71,72,73}. The oxidation state of the metal source is also of prime interest for allowing isomorphous substitution. This is usually controlled by carefully choosing the metal source, and sometime adjusting the synthesis conditions,

as performed by Chaves et al. for the introduction of V in MWW zeolite structure under inert atmosphere, using a V^{3+} precursor⁷⁴. The discussion regarding the state of vanadium species in the zeolite framework during synthesis, and after post-treatment such as calcination is in full agreement with a theoretical paper discussing oxidation state of group V metal introduced in zeolite frameworks⁷⁵. The introduction of Fe in BEA and MFI zeolite was reported by Naraki et al.⁷⁶, achieving relatively high amount of Fe (up to 7 wt. %); the influence of some parameters (such as OH^-/SiO_2 , SDA/SiO_2 , and SiO_2/Fe_2O_3 ratios, or crystallization temperature) on the synthesis are discussed. The influence of the amount of metal source in the synthesis gel was further studied during the introduction of Zn in ZSM-5 using seeds in another study from Su et al.⁷⁷. In a study from Shah et al.⁷⁸, the Zr/Al ratio influence on the incorporation of Zr in MFI framework topology was studied.

The direct synthesis method is the most used for the incorporation of titanium (Ti) in silicalite-1 (MFI) framework for instance. This material is called TS-1 (for Titanosilicate-1), and was first patented by Taramasso et al. from ENI⁷⁹, standing as the first crystalline microporous oxidation catalyst particularly active and selective in oxidation reactions involving H_2O_2 under mild conditions⁸⁰. The influence of the main synthesis parameters was already reviewed by Perego and Bellussi⁵⁸. Several Si and Ti sources, as well as (organic) structure directing agents (SDA or OSDA) were used. One of the main conclusions was that in order to obtain small particle size ($< 1 \mu m$), it is necessary to use an organic alkaline mineralising agent. In order to obtain the smallest particle size reported in this review, the synthesis system should be prepared from TEOS as Si source and TPAOH as OSDA. However, Xue et al.⁸¹ reported the synthesis of nanosized TS-1 crystals by using ammonia as alkali source, and a mixture of both TPAOH and TPABr as OSDA, in a seed-induced synthesis process. The use of TPABr as a co-templating agent allowed to reduce the amount of TPAOH, thus, making the synthesis less expensive; the use of seeds promoted nucleation and consequently, the particle size was reduced⁸². Still, one of their main findings was that using an appropriate amount of TS-1 colloidal seeds (10-20 wt. %) in the synthesis gel was facilitating the Ti incorporation in MFI framework while decreasing particle size altogether. However, only small evidence is given regarding the effective isomorphous substitution of Si towards Ti atoms, mainly in the form of the observation of an FTIR band at 960 cm^{-1} , attributed to stretching vibration of SiO_4 units strongly influenced by Ti ions in neighbouring coordination sites. It has been demonstrated that using this band as a proof of framework modification (and its quantification) is not a reliable method as it is not directly associated with Ti, but with distortions of Si-O-Si units that can be related to Ti incorporation, but also to defects and/or hydroxyl groups. This can be highlighted by the fact that this band at 960 cm^{-1} can be observed in some purely siliceous Silicalite-1 samples⁸³⁻⁸⁵.

In another work from Fan et al.⁸⁵, $(\text{NH}_4)_2\text{CO}_3$ molecule was used as a modifier, acting as a crystallization mediating agent; the crystallization process of the system was deeply investigated and compared to a classical synthesis system⁸⁶. The purpose of $(\text{NH}_4)_2\text{CO}_3$ molecule was to lower down the pH of the precursor suspension, resulting in a slower crystallization rate, thus making the speed for Ti incorporation into the framework and the crystallization rate match well. The addition of $(\text{NH}_4)_2\text{CO}_3$ molecule also resulted in a considerable modification of the crystallization mechanism, occurring in solid phase instead of the classical liquid-phase transformation, but allowed to start the incorporation of Ti atoms in the structure at earlier stage of the crystallization process (and not only after the crystallization is nearly completed, as it is the case for classical gel systems⁸⁵). Consequently, the Si/Ti ratio in the framework was reduced, as more Ti atoms entered in MFI framework, thanks to the slower crystallization rate. The overall idea in this work was to match the Si condensation rate with the Ti incorporation rate by lowering the pH (lowering the condensation rate of Si). According to this work, it is of primary interest to control the crystallization kinetics in order to successfully incorporate transition metals in zeolite frameworks. It was also shown that Ti tends to be located preferentially at silanol defect sites, making the zeolite more hydrophobic upon Ti incorporation, as shown by the diminution of Q3 species observed in NMR spectroscopy (Figure 6.).

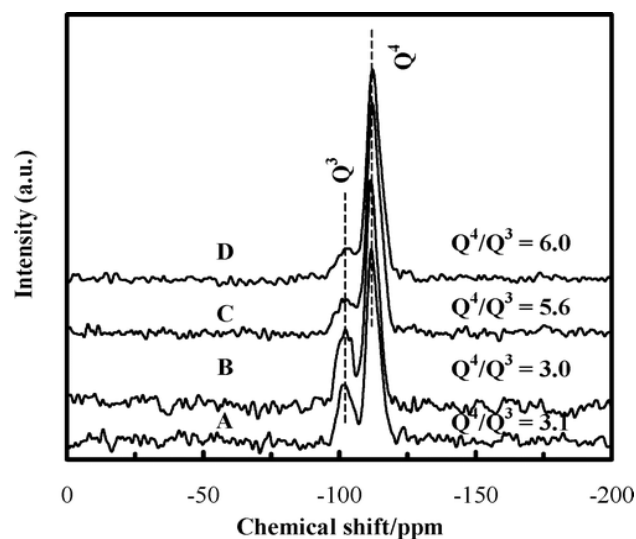


Figure 6. ^{29}Si -NMR spectra of TS-1 samples with different amount of Ti in the MFI framework⁸⁵

The incorporation of Ti species in MFI zeolite framework is not fully understood, but it strongly depends on pH as described above. The incorporation was further studied by Tamura et al.⁸⁷: three synthesis were carried out: one direct synthesis using

tetra n-butoxide titanium as Ti source, another using a Ti peroxo complex prepared by addition of H₂O₂ on tetra n-butoxide titanium, and a last synthesis using the Ti peroxo complex and an already fully crystalline MFI framework as silicon source. From their results, it was found that the reactivity of Ti species formed in liquid phase strongly influence the incorporation process. Non framework Ti are slowly converted into framework Ti species in the already crystalline Si-rich MFI framework, at later stages of crystallization process. Incorporation did not truly start in earlier stages of the hydrothermal treatment. The absence of structure directing agent effect of Ti was highlighted. The successful incorporation of Ti into already fully crystalline purely siliceous MFI framework highlighted the incorporation mechanism, as involving a partial dissolution of Si species from MFI framework, and recrystallization of said species together with Ti species.

In another attempt to reduce synthesis cost of TS-1 zeolite, Borin et al.⁸⁸ were able to obtain crystalline micron-sized TS-1 using a cheap Ti source (hexafluorotitanic acid) and amorphous silica instead of TEOS as Si source. Evidence was given that more Ti is introduced in the framework upon increased crystallization time. In this work, XRD is used to measure unit cell parameters of the crystalline zeolite, and the evolution of these parameters was directly correlated with framework isomorphous substitution of Ti atoms in MFI framework (Figure 7.). Evidence pointed towards a linear increase of cell parameters upon Ti incorporation in framework position, and the absence of any correlation between cell parameters evolution, and non-framework Ti species content. The measurement of these crystallographic parameters using XRD is then described as a very convenient and effective way to provide strong evidence towards isomorphous substitution in zeolite frameworks. This was further supported in a study where the linear correlation between Ti incorporation and unit cell volume expansion observed is described as being a function of the synthesis method used⁸⁹. This is an indirect evidence that Ti incorporation in MFI framework is not random and is in fact dependent on the synthesis method used. Indeed, the maximum unit cell volume expansion observed is not directly linked to Ti incorporation, but to the lattice deformation, and different synthesis could lead to different repartition of Ti in the framework, thus explaining the influence between degree of unit cell volume expansion and synthesis method used. As a result, it is possible to have a similar unit cell volume expansion for very different metal content in the case where synthesis procedure between the two samples is different, making this analysis method very effective for relative quantification between similar samples, but ineffective for absolute quantification of isomorphous substitution. The reason why unit cell parameters are expanded upon Ti introduction in framework position was already described and theoretically calculated⁹⁰, matching very well with experimental measurements. The unit cell parameters expansion is a consequence of the fact that Ti atomic radius is larger than Si atomic radius. The structure must then be distorted in order to be able to accommodate Ti

atoms in framework tetrahedral positions (longer Ti-O bond lengths with regards to Si-O, and smaller Si-O-Ti bond angles with regards to Si-O-Si), resulting in an expansion of the unit cell parameters. The incorporation of metals, even in low amounts, in a zeolite framework might result in a slight modification of the unit cell volume, as long as the radius of the metal is significantly different from the atomic radius of silicon, allowing for relative quantification of isomorphous substitution. The unit cell volume will expand if metal radius is larger than silicon radius, and shrink if it is smaller as it is the case for boron (B) for instance⁹¹. However, this observation is not a standalone proof of metal incorporation in zeolite frameworks, as other parameters can influence it strongly such as adsorbed species, or counter-ions for instance^{92,93}. It is nonetheless not accurate to assess without further discussion that there is framework incorporation if no change of the unit cell volume is observed, as it is the case in the work of Rana et al.⁹⁴. Interestingly, the unit cell volume expansion is not infinite, and at one point, the unit cell volume stops increasing upon metal addition in the zeolite. If the metal loading is increased past this point, non framework metal oxides species start being formed in the corresponding sample, as illustrated in Figure 8. These results further support the direct link between isomorphous substitution and framework expansion. This point is generally described as corresponding to the maximum deformation (induced by the heteroelement presence) that the structure lattice can withstand without collapsing.

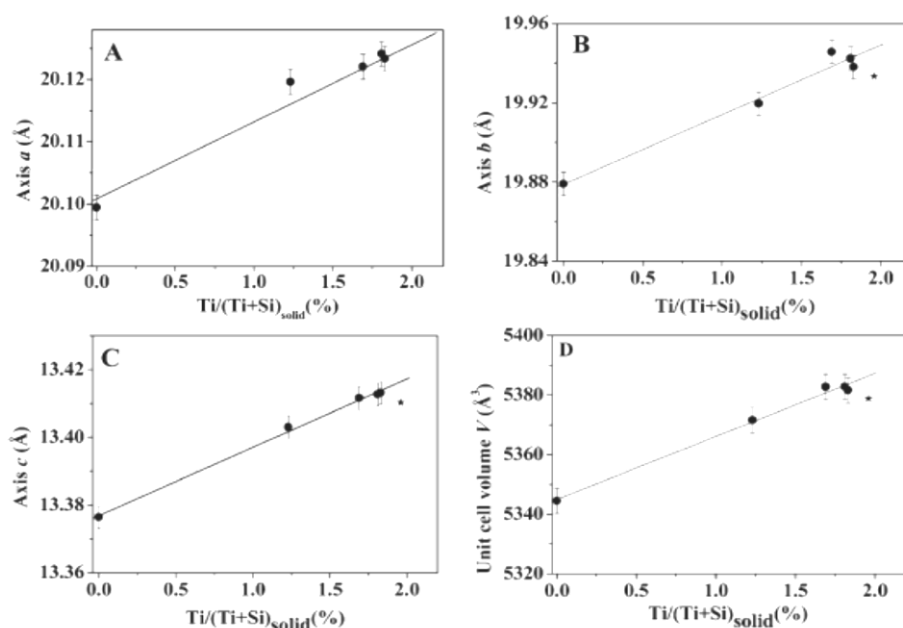


Figure 7. (A,B and C) Unit cell parameters a,b and c, and (D) unit cell volume evolution, as a function of Ti content in MFI framework⁸⁸

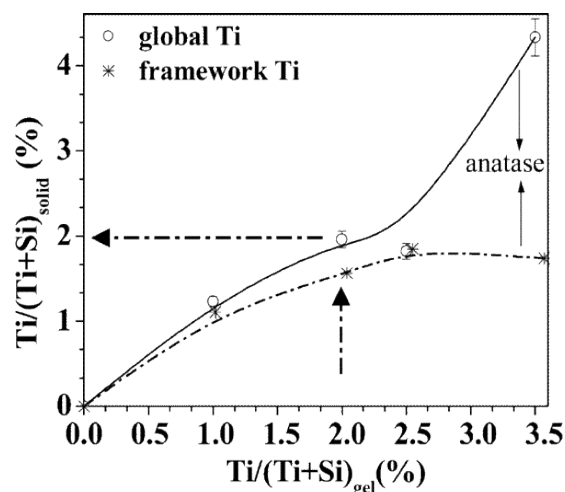


Figure 8. Ti content in the solid (from ICP) and in the framework (determined from volume expansion) as a function of the Ti content in the precursor gel suspension ⁸⁸

The non-random Ti distribution in MFI framework was previously introduced in the above discussion ⁸⁹. This result has been further comforted with a study using Powder Neutron Diffraction (PND) with different Ti isotopes ⁹⁵, where Ti atoms were efficiently located within MFI framework. Titanium is highlighted as being located in 3 of the 12 T-sites of MFI structure: T8, T10 and T3 (in order of decreasing Ti content). Other tetrahedral sites could contain a very low amount or no titanium at all. Silicon vacancies were located in T1 and T5 sites. The conclusion of this study is that the crystallization is likely to be controlled by kinetics rather than thermodynamics, strongly confirming the results obtained by T. Tatsumi et al., describing the synthesis of TS-1 with the use of $(\text{NH}_4)_2\text{CO}_3$ molecule as a modifier, described above ⁸⁵. The non-random repartition of metal in the different framework tetrahedral positions is consequently further confirmed, and differences of Ti content in the T-sites as a function of the synthesis approach used was observed as well, for instance in the case of tin containing Beta zeolite (Sn-BEA) ⁹⁶.

Another consequence of the incorporation of transition metal atoms in MFI framework specifically is the observation of a space group transition from orthorhombic (Pnma) symmetry (for purely siliceous silicalite-1) to monoclinic (P21/n) symmetry at room temperature. More specifically, the observed symmetry transition is linked to a shift of the phase transition temperature value. This phase group transition was already described for Al containing MFI zeolite (ZSM-5) for instance ⁹⁷. The occurrence of this space group transition can be efficiently checked by studying whether diffraction peaks at 23.3 , 23.7 , and 24.4 ° 2θ are split or not, in XRD patterns. However, this is a weaker indication of successful isomorphous substitution than unit cell volume expansion, and is specific to MFI framework. Additionally, in the case where several metal atoms are inserted in a siliceous MFI framework (such as Ti and Al at the same time for instance),

it is impossible to assert whether the space group transition originates from Ti incorporation, Al incorporation, or incorporation of both metals. Moreover, additional parameters can influence space group transition such as adsorbed molecule(s), temperature, and history of sample, and the transition can also be reversible⁹³. Even calcination process can alter this property depending on the availability of some gas such as O₂⁹⁸. Surprisingly, phase group transition from monoclinic to orthorhombic symmetry (instead of orthorhombic to monoclinic) was reported in the case of tantalum (Ta) in MFI framework⁹⁹, with the parallel observation of a linear increase of unit cell volume with regards to Ta content, supporting the successful isomorphous substitution. In this last work, the direct influence between metal content in the synthesis mixture, and in the final crystalline material was emphasized. As a consequence, the use of space group transition to characterize isomorphous substitution should be handled carefully, only through the comparison of similar samples synthesized in a similar manner, and should be considered as weak evidence for metal incorporation.

At this point, it is worth mentioning that if one wants to introduce more than one heteroatom in a zeolite framework, then it is expected to observe competition effect for the incorporation of both atoms¹⁰⁰. For instance, if one wants to introduce both Al and Ti in MFI framework, the two metals will compete together to be incorporated in the MFI structure, and the relative amount of each metal in the zeolite framework will strongly depend on the kinetics of incorporation of each metal^{101–103}. Moreover, the presence of Al in the MFI during crystallization could change properties of the overall MFI framework, and prevent (or favor) the following incorporation of Ti atoms. Ti atoms could also react with framework Al species, so that Ti would be grafted on framework Al sites instead of being embedded in the silica framework. Finally, the presence of a second metallic salt could alter the overall crystallization process, or change the solubility of some species in the precursor gel suspension. Introduction of more than one heteroatom in a zeolite synthesis can consequently result in complex systems.

Another interesting way to study the presence of framework metallic species in a zeolite sample is Raman spectroscopy. An extensive UV/Vis-Raman study of TS-1 materials was already performed by Li et al.^{83,84,104}. Metal containing frameworks are shown to have a charge transfer between framework oxygen, and the framework tetrahedral metal atom, located in the UV range. This transition is at 220 nm for TS-1 materials, 250 nm for iron introduced in ZSM-5, and 280 nm for vanadium containing MCM-41 for instance. It is therefore possible to obtain UV resonance Raman spectra by exciting these transitions with a UV laser. Accordingly, the framework metal atoms can be selectively identified in the Raman spectra based on the resonance Raman effect. Enhanced bands are indeed directly related to framework metal species (Figure 9.). The characterization method is therefore highly sensitive for the detection of metal in low amounts, as framework and/or oxide phase.

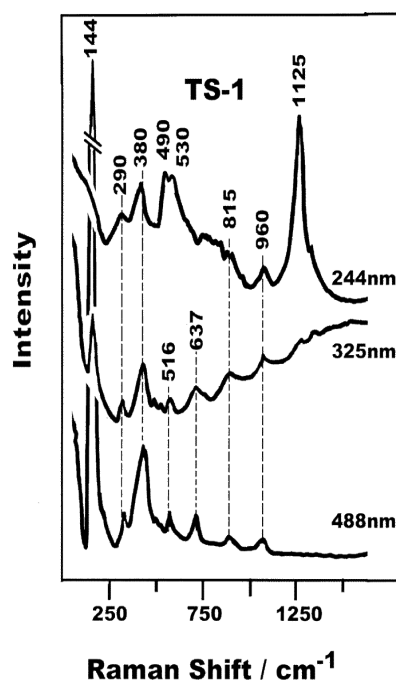


Figure 9. Raman spectra of TS-1 material measured with 244, 325, and 488 nm laser (from top to bottom); showing the increased intensity for framework Ti related bands (490, 530, and 1125 cm^{-1}), and the decreased intensity of bands associated with non-framework Ti anatase (144, 516, 637 cm^{-1}) upon increased laser frequency from visible to UV light.⁸⁴

Apart from TS-1, numerous other metal containing zeolites were prepared in the past decades. Most of the open literature describes TS-1 and Sn-BEA zeolites, but other structures were also reported such as Zr-MFI¹⁰⁵, Al-free hydrophobic Ti-BEA¹⁰⁶, B-MFI, Fe-MFI, Fe-BEA and Fe-MOR¹⁰⁷, or Ga-SBA-15¹⁰⁸ for instance.

One example is zirconium containing BEA zeolite (Zr-BEA). Using the sorption of several probe molecules (mainly carbon monoxide and deuterated acetonitrile) monitored by FTIR, Sushkevich et al.⁶⁴ were able to successfully assess the state of the Zr metal in BEA framework, as closed or open Lewis acid sites. Using several probe molecules with similar functionality and different sizes, one can also assess the accessibility of active sites. Similar study were performed on Sn-BEA sample (tin in BEA zeolite) by Davis and Corma⁶⁵⁻⁶⁷, using deuterated acetonitrile probe molecule to monitor the framework nature of Sn in Sn-BEA sample (Figure 10). The influence of steaming process (hydrothermal treatment) on the opening of closed Lewis acid sites was described, and linked with the catalytic activity of the Sn-BEA. Open Lewis acid sites are described as more active than their closed counter-parts. However, this technique does not allow easy quantification, and the distinction between species can be difficult as bands tends to overlap, and are low intensity.

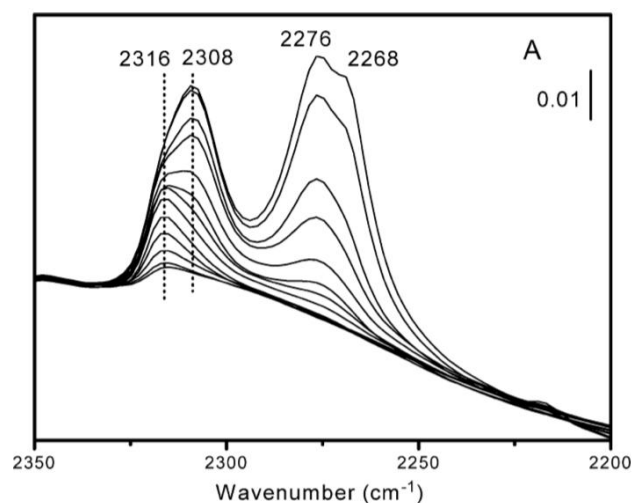


Figure 10. FTIR spectra of CD_3CN adsorbed on Sn-BEA sample ⁶⁷: the band at 2316 cm^{-1} corresponds to open Lewis sites, and the band at 2308 cm^{-1} corresponds to closed Lewis acid sites.

Other metal containing zeolites were synthesized using one-pot direct synthesis approach, such as Sn-BEA zeolite. The tin source was described as strongly influencing the synthesis process, in terms of quantity as well as nature, in a work from Tolborg et al. ¹⁰⁹. Tin content affects crystallization time (4-60 days), crystal size (3-8 μm), and morphology (pyramidal-plate-like) of zeolite crystals. The outer surface of crystals contained more tin, and longer synthesis time resulted in a lower catalytic activity of the material. The incorporation of tin in BEA framework is not very efficient, as the formation of SnO tin oxide particles was highlighted, mainly at the crystal surface. The morphology change was however mainly attributed to the presence of Cl^- anion.

The direct observation and quantification of Tin in Sn-BEA sample synthesized in fluoride media was possible thanks to ^{119}Sn MAS NMR spectroscopy ^{110,111}. Results suggest that Sn atoms were located in T7, T5 and T6 framework position preferentially (T-sites in the 4-membered rings of Beta zeolite), as closed Lewis acid sites located in “defect-free framework positions”, some of them being in proximity with terminal or internal Si-OH groups. NMR spectroscopy is a powerful way to investigate metal framework sites, but unfortunately, it cannot be used for every metal due to their corresponding NMR properties. Correlation has been furthermore drawn between NMR results and DFT calculation ⁹⁶, confirming the attribution of Sn atoms location in T6, T5, and T7 crystallographic positions for fluoride-media synthesized materials. Sn is described as being present as closed Lewis sites than can be partially hydrolysed in presence of water. The location of Sn atoms was highlighted as being a function of synthesis procedure, and catalytic acidity was highly dependent on morphology and hydrophobicity of the material. Surprisingly, both closed and open Sn sites were described as being catalytically active in this work.

The non-random distribution of metal in zeolite framework, with preferential incorporation on double four-membered ring units of germanium (Ge) in ITQ-7 zeolite was also demonstrated based on theoretical calculation; a detailed NMR study was included too¹¹². This non-random distribution of metal in zeolite framework seems valid for most of the zeolites.

Reduction of water content in the fluoride-media synthesis of Sn-BEA samples was conducted and resulting samples were analysed using ¹¹⁹Sn MAS NMR¹¹³. Water content strongly influences crystallization kinetics, and crystallization time could be reduced from 10 to 4 days by decreasing the H₂O/SiO₂ ratio from 7.5 to 5.6. The crystal size was also reduced in the process, as nucleation was promoted thanks to the increased degree of saturation in the initial gel with low water content. Morphology was however unchanged, and no effect on the state of Sn-sites in the final products was observed. This is to be compared with the fact that variation of Sn content in the gel has a tremendous effect on the state of tin in the framework. This implies that Sn/Si ratio has to be controlled in order to monitor the state of Sn atoms in the BEA framework; the Sn/H₂O ratio can be changed without too much influence on the final product in terms of nature of the metal species.

In another work from Wu et al.¹¹⁴, Ti- and Al- containing SBA-15 was prepared in highly acidic conditions (pH<0) with a so-called “pH-adjusting” method described as possibly effective for other metal atoms introduction in SBA-15 framework. The heteroatom source is added at low pH, in a normal direct synthesis approach. Then, after the mesoporous structure is formed, the pH is raised up to neutral, followed by hydrothermal treatment. This method is described as efficient as most of the metal introduced in the initial gel is effectively incorporated in the final material, mostly as framework species. This method is another example of the adjustment of condensation and hydrolysis rates of metal together with silicon and aluminium species, thanks to the management of the pH of the precursor gel suspension.

As shown here-above, the direct synthesis possesses some drawbacks that are mainly related to the presence of metal species in the precursor gel suspension, prior to crystallization. The post synthesis approach (second main way allowing to perform isomorphous substitution) stands as a complementary synthetic method allowing to avoid some of the issues addressed by the direct synthesis approach, as described herein-after.

I.2.3. Metal introduction by post synthesis approach

Isomorphous substitution procedure using direct hydrothermal synthesis approach requires the introduction of metal compounds in the precursor gel suspension

prior crystallization. However, the metal content introduced in the gel and metal content present in the final material are low ¹¹⁴. It has also been demonstrated that metal introduction in the synthesis gel can significantly alter the nucleation and crystallization process, as well as the final formed crystalline materials ^{115,116}. This is particularly true for Sn-BEA samples as illustrated in the work from Tolborg et al. ¹⁰⁹ for instance. Fluoride media is often used in direct hydrothermal synthesis approach in order to dissolve the metal source properly, but using such chemicals has significant drawbacks in terms of toxicity, causticity and pollution ¹¹⁷. Moreover, it can be challenging to introduce high amounts of metals in framework positions as shown for TS-1 materials for instance ^{58,88,89}.

As an alternative, the post synthesis approach consists in the incorporation of the metal in a post-synthetic step. The starting material is consequently already fully crystalline, and the philosophy of the method is to “heal” silanol nest defective sites from this material by using a metal that will consequently be incorporated into the framework structure as a result. Initially, this synthetic approach was used so as to allow the synthesis of metal containing zeolites that were not possible to achieve by direct synthesis pathways, because of kinetics of crystallization issues, or stability of the metal source in the precursor gel suspension for instance. The post synthesis approach can in principle be applied to almost any initial crystalline zeolite material. However, in order for the isomorphous substitution to occur at a maximum rate, the initial material needs to have a maximum amount of silanol nest defect sites for the metal to react with. The metal introduced via post synthesis treatment (usually by chemical vapour deposition – CVD ^{118,119}) is consequently usually anchored to the silanol nests already present in the crystalline material, or purposely introduced after dealumination of the as prepared zeolite for instance ¹²⁰. As a consequence, this post-synthesis approach is usually associated with the preparation of a metal containing zeolite by direct synthesis approach, followed by demetallation of said material, so as to obtain a material full of silanol nest defects that is a perfect candidate for post-synthesis approach. The metal used in the first step is consequently a metal which is relatively easy to introduce in sufficient amounts in zeolite frameworks and usually not that stable in said zeolite structure, so that it is not too hard to remove from framework positions, generating the silanol nests of interest. Therefore, the metal used in the initial step is usually a metal that generates a Brönsted acid sites or an OH group once incorporated in a zeolite tetrahedral environment such as Al, Fe, Ge, B, Ga, ... that can be easily removed using processes such as acid leaching for instance ²⁰. As a classical example for post-synthesis approach, can be cited the introduction of Fe in a dealuminated zeolite BEA ¹²¹. In the work from Gao et al. is also reported the introduction of Ti using TiCl_4 chemical vapour deposition on a boron substituted ZSM-5 (B-ZSM-5) that was previously deboronated using hydrochloric acid ¹²². Germanium can also be used in a similar manner, but its use mainly comes from the stabilization effect of germanium

towards the formation of double 4 membered-ring Ge-containing building units (D4R). The stabilization of 4 ring building blocks allows to achieve the synthesis of large-pore zeolites, that are difficult to access by other means. The Ge can then be removed and other metals can be introduced instead. A good example of that has been reported by Shvets et al., where B-UTL was prepared from the initial germanosilicate Ge-UTL⁷⁰. An original approach for the preparation of Zr containing HY zeolite by post synthesis approach was reported by Sapawe et al.¹²³, as occurring during the preparation of electrogenerated zirconia supported HY using an electrochemical method. Dealumination accompanied by ion exchange with Zr⁴⁺ formed Si-O-Zr bonds during the electrochemical process.

However, the post synthesis approach is generally associated with parallel formation of non-framework metal species on the zeolite material. This has been highlighted and circumvallated in the work from van der Graff et al.¹²⁴, for the Sn-BEA synthesis. Dealumination of zeolite Beta was performed by acid leaching with nitric acid, followed by a subsequent addition of SnCl₄ by CVD. Prior to calcination, a washing step with methanol was performed in order to remove any non-framework stannate species. This approach allowed to insert high amount of Sn (up to 5 wt. %) which is to be compared to direct synthesis approach achieving a maximum of av. 2 wt. %. The sample was free of non-framework stannate species, and the healing of silanol nests upon Sn CVD could be observed by FTIR (Figure 11.). The as prepared zeolite was relatively hydrophilic because of the high silanol content still present in the final material. In another work from Wu et al.¹²⁵, an acid treatment was used after post-introduction of Ti in MWW type structure, to prevent the formation of non-framework anatase (TiO₂).

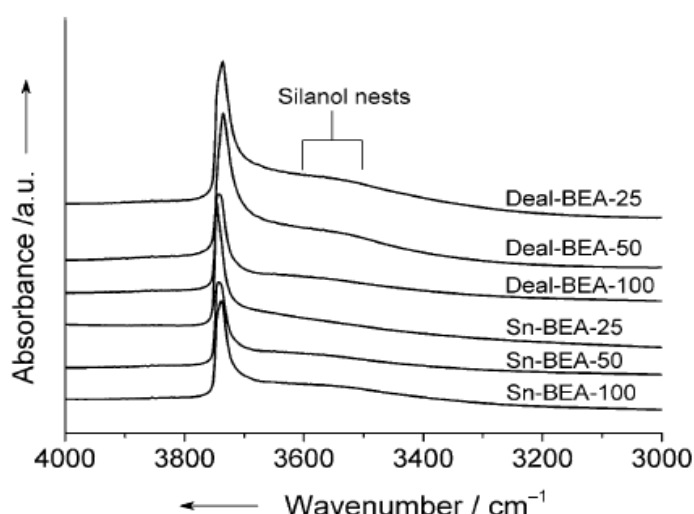


Figure 11. FTIR spectra of Sn-BEA with increased Sn content (from top to bottom), highlighting the silanol nests healing effect upon Sn introduction in framework position of zeolite Beta framework¹²⁴

To this date, numerous metal atoms were introduced in several frameworks using the post synthesis approach. One of them is Ga-ZSM-5, prepared by Bayense et al.¹²⁶, together with Ga-Y. However, the co-formation of non-framework Ga species for both structures, after dealumination and subsequent Ga introduction was observed. The presence of Brønsted acid sites and external silanol groups resulted in the formation of non-framework Ga. The obtained Ga-HZSM-5 samples showed enhanced selectivity to aromatics in the propane conversion. Boron was also introduced in both ZSM-5 and Y structure¹²⁷. The effective framework incorporation was assessed from ¹¹B MAS NMR results. Interestingly, this post synthesis was conducted in fluoride media, in presence of boron source. As a consequence, both dealumination and desilication occurred while boron was introduced in the structure in parallel. This could also explain the partial amorphization of the material, observed after treatment. Only few other examples are provided for isomorphous substitution in zeolite Y. One of them is Ti-Y zeolite¹²⁸, prepared from dealuminated USY (ultra-stable Y) zeolite, followed by Ti incorporation under acidic conditions. The framework nature of Ti atoms was checked using XANES, and cycloalkene epoxidation using hydrogen peroxide as a probe catalytic reaction. Iron was also introduced in ZSM-5 framework using an aerobic aqueous ion exchange with low concentration of iron oxalate (0.01 M)¹²⁹. This method allowed to reduce the non-framework iron clusters content when compared to sample prepared using chemical vapour deposition (CVD). Upon thermal treatment, iron was removed from framework position, achieving highly dispersed non framework iron. Indeed, iron is usually described as not stable in MFI framework at high temperatures. Cr-SiBEA was also successfully prepared by post synthesis approach¹³⁰. Its state was investigated as a function of treatment conditions of the material. As synthesized, calcined, vacuum treated, and rehydrated samples exhibited different content of octahedral, tetrahedral, and pentavalent mononuclear species, according to DR UV-Vis, XAS, and EPR spectroscopy.

The silanol nests used in the post synthesis approach for metal isomorphous substitution can be obtained not only from dealumination, but also from degermanation for instance. This can bring some new application of metal containing zeolite, where the metal is introduced only for its structure directing agent properties, and removed afterwards from the crystallized structure. Indeed, quasi all-silica zeolite could be obtained from Ge-ITQ-22 zeolite in the work from Burel et al.¹³¹. Post introduction of aluminium was then possible. The presence of Ge atom in the initial material, prepared by direct synthesis approach allows to access new structures that are not accessible with traditional Si and Al gel compositions. This is linked to the preferred formation of some secondary building unit accessible in germanium containing hydrothermal synthesis gel (such as 4 member ring units), that are not stable if only made out of Al and Si atoms. Thus, the following de-germanation followed by post synthesis

introduction of aluminium allowed to prepare purely Si/Al zeolite having a structure that is impossible to obtain by direct synthesis approach.

It is also possible to introduce metal in purely siliceous zeolite framework, using their native silanol nest content. This was the case in the work from Mokaya et al.¹³² for instance, where Al was introduced in purely siliceous MCM-41. The as obtained material contained higher Brønsted acid sites content when compared to hydrothermal synthesized Al-containing MCM-41 zeolite as demonstrated from thermally programmed desorption of cyclohexylamine, and the activity of materials in the cracking of cumene catalytic reaction.

In summary, there is no “best” synthesis approach, only two main approaches with variations, and different drawbacks/advantages. However, both synthesis techniques are designed so as to generate the same kind of metal sites, resulting in minor differences from one successful synthesis to the other.

I.2.4. Guidelines for the characterization of metal containing zeolites

After synthesis of metal-containing zeolite frameworks, it is important to correctly evaluate and prove the occurrence or not of isomorphous substitution, meaning, the presence (or not) of framework tetrahedrally coordinated metal atoms linked to the zeolite framework. In current state of the art, there are still many contributions in which the state of the metal atoms is claimed as being framework metal obtained by isomorphous substitution, but no clear evidence supporting this assertion is provided. In result, in several of these contributions, it is sometimes difficult to draw conclusions since the state of the metal in the corresponding structure is still a matter of discussion. As a consequence, we would like here, to stress out the importance of correctly assessing the state of the metals in a given catalyst, so as to draw pertinent conclusions from their catalytic behaviour. To this extent, in this part, we will discuss the main methods allowing to support the occurrence of isomorphous substitution in zeolite frameworks.

One of the first easy-to-perform method that is of high relevance when trying to assess whether an element has been introduced in a zeolite framework is the measurement of the unit cell parameters (and especially the unit cell volume) of the materials. These data are easily extracted from XRD patterns, and when properly compared to relevant references, represent strong indications of possible isomorphous substitution. Indeed, another element than Si has usually a different ionic radius, and thus, needs slightly different bond lengths and bond angles so as to be accommodated in the zeolite framework. A higher ionic radius than Si is going to require longer bonds and smaller bonds angles, and thus, will expand the unit cell parameters of the zeolite

for instance; the inverse being true as well for shorter ionic radius requiring smaller bond length and higher angles (and thus, shrinkage of unit cell parameters/volume)^{71,90,133}.

In parallel, it is usually relevant to assess the state of Si atoms and especially of silanol species. Indeed, they are the active sites of interest when performing isomorphous substitution. Their consumption upon metal introduction is consequently another indication for effective isomorphous substitution¹³⁴.

It is also relatively easy to assess the absence of large oxide species by XRD. In addition, it is usually relevant to assess the absence of oxide species using techniques such as Raman spectroscopy, or UV diffuse reflectance. Electron microscopy can also be used to this extent, so as to demonstrate the metal dispersion (TEM-EDS, HAADF-TEM). TEM-EDS can also be used so as to prove the actual presence of the metal in the sample, similarly to ICP or XRF¹³⁵.

In addition, it is highly relevant to prove tetrahedral coordination of the metallic element, especially when it does not form tetrahedral coordinated oxides on its own. This can usually be shown by NMR/EPR of the metal element (if applicable), XPS, or XANES/EXAFS/XAFS. In addition, these techniques can sometime be used so as to probe the bond lengths, angles, and relative electronegativity of the metal in the structure, bringing relevant information on its neighbour's atoms. This represents relatively strong evidence for actual coordination to a silicon tetrahedral environment, which is expected from isomorphous substitution^{76,136}.

Metal atoms when introduced in the framework of a zeolite can also generate new types of acid sites (purely Lewis sites, or Brønsted sites in some specific cases) that can be probed using different probe molecules monitored with appropriate techniques (Pyridine, CD₃CN, CO/IR, or trimethylphosphine oxide/³¹P MAS NMR for instance). To demonstrate these changes in properties upon metal incorporation is also relevant^{135,137}.

In most of the cases, it is not necessary to show every single possible evidence for effective isomorphous substitution, but it is nonetheless important to assess with sufficient certainty the effectiveness of isomorphous substitution, by combining with intelligence several of these methods. The idea is to oppose simpler explanations (metal present as oxide species, or grafted on Brønsted acid sites for instance), and to demonstrate that the only valuable explanation for what is observed is actual occurrence of isomorphous substitution. This is usually done by showing: (i) unit cell volume expansion, combined with (ii) proof for the presence of the metal in the material, (iii) absence of oxide phase, and (iv) evidence for tetrahedral coordination, silanol consumption, and conservation of Brønsted acid sites if possible.

For instance, in the work from Su et al.⁷⁷, Zn-ZSM-5 was prepared and efficiently characterized using a complementary set of techniques: XRD was performed and shifting of diffraction peaks could be attributed to unit cell volume expansion while absence of large oxide phase was probed, ²⁹Si NMR was measured to evaluate the diminution in silanol content, and EDS showed the presence of highly dispersed homogenous Zn dispersion in ZSM-5 crystals. In the work from Naraki et al.⁷⁶, the tetrahedral nature of iron species in BEA zeolite was evidenced in high details using EPR, XAFS, and UV-DR. Results obtained were in agreement with the actual color of the samples, and the absence/presence of oxide phase was also probed. Fe presence in BEA and MFI topologies could also be evidenced in the work from Yun et al.¹³⁸, by simply using XRD and unit cell parameters measurement from XRD data to probe the absence of oxide phase, and the unit cell volume expansion linked to the metal incorporation. UV spectra were also recorded to support the tetrahedral nature of metal sites. In several contributions, an efficient combination of unit cell volume expansion measured from XRD, new contribution in framework vibrations probed using IR, and absence of oxide phase probed by UV was used to assess the presence of a metal in a zeolite framework^{71,78,139}. In another example, Ga presence in ZSM-5 framework was efficiently assessed using unit cell volume expansion measurement by XRD, IR for the vibration of framework atoms, and an NMR study of Ga, Si and Al nuclei¹⁴⁰. In the work from Grand et al.¹⁴¹, isomorphous substitution was efficiently probed combining XRD for space group transition due to the metal introduction in the framework, Raman and IR for framework vibrations, and ²⁹Si NMR with IR for silanol content.

As shown in the examples here-above, it is not always necessary to show all possible evidence. The idea is mainly to provide enough evidence pointing in the same direction, indicating with enough certainty that metal atoms are in framework positions of a zeolite framework, as the only easy explanation of the observations made.

I.2.5. Properties of framework metal containing zeolites

Most of the metal-containing zeolites (metal being different from Al) described in the open literature (Sn/Ti/Zr/Mo/V-BEA, and Ti/V/Sn-MFI) are catalytically active in reactions involving oxidation of chemicals using H₂O₂ (Summarized in Table 3.) as reviewed by Moliner et al.^{142,143}, Perego et al.⁵⁸, Niederer et al.¹⁴⁴, and Chang et al.¹⁴⁵. These materials are furthermore described as very promising and highly desirable for biomass transformation processes^{51,142}.

Table 3. Activity of metal containing zeolites in different catalytic reactions

Type of materials	Catalytic test	Reference
Sn/Ti-BEA	sugar isomerization	142,143,145
Sn-BEA	epimerization of sugars	142
Sn-BEA	sugar to lactic acid derivatives	142
Zr-BEA	rearrangement of beta-pinene epoxide into myrtanal	142
Sn-BEA	"one-pot" synthesis of furfural-derived products from monosaccharides	142
Zr-BEA	production of gamma-valerolactone (GVL) from furfural	142
Sn/Zr-BEA	synthesis of optically pure gamma-lactones from pyrolysis products	142
Ti/Mo/V-BEA/TS-1/VS-1	olefin epoxidation with H ₂ O ₂	58,142,144,145
Ti/Mo/V-BEA/TS-1/VS-1	selective oxidation of alcohols	144,145
Ti-BEA/TS-1/VS-1	hydroxylation of phenol/aromatics with H ₂ O ₂	142,144,145
Ti-BEA/TS-1/VS-1	ammoximation of ketone (cyclohexanone) with H ₂ O ₂ = main (industrial) application of TS-1)	58,142,144,145
Sn-BEA	Baeyer-Villiger oxidation of ketones to lactones	142
Sn-BEA	Meerwein-Ponndorf-Verley (MPV) reduction of aldehydes and ketones to alcohols	142
TS-1/VS-1/ Sn-BEA/Sn-MFI	oxy-fuctionnalization of alkanes	142,144
TS-1	C-C bond formation (Michael, aldol condensation) with lewis acid catalysis : very few literature	142

Introduction of metal in a zeolite framework can generate both Lewis and Brønsted acidity, depending on the coordination of the metal introduced. For instance, in the case of Al or Fe, the metal atom is trivalent, bringing a negative charge to the zeolite framework once introduced in crystalline tetrahedral position; the negative charge is balanced by a counter ion such as hydrogen (H⁺), and this brings the Brønsted acid properties of zeolites¹⁴⁶. On the other hand, Lewis acid sites are defined as electron density acceptors. A typical example of a Lewis acid site is BF₃ or BCl₃, which possess an empty 2p orbital on trivalent Boron, able to accept electrons from a Lewis base. Lewis acid strength of the boron can be adjusted by changing its ligands from one anion to the other. In a similar way, any tetrahedrally coordinated metals introduced into a silica framework can act as Lewis acids^{62,63}. The metal in zeolite framework can then accept electron pairs from reactants without inducing any charge imbalance. This interaction depends heavily on the identity of both the metal and the reagent, affecting the electronic structure, flexibility, stability and geometry of the resulting adduct⁵¹.

Experimentally, only a loose correlation is observed between catalytic activity and strength of the corresponding Lewis acid sites for various reactions. For instance, Ti containing zeolites such as Ti-MFI and Ti-BEA are active for the epoxidation of linear

alkenes with aqueous H_2O_2 ^{147,148}, but similar Zr and Sn containing MFI and BEA zeolites show no activity for this catalytic reaction¹⁴⁹. On the other hand, Sn containing zeolites were described as active for Baeyer-Villiger, and oxidation of cyclic ketones and aromatic aldehydes with H_2O_2 , whereas Zr-BEA was much less active for these same reactions, and Ti-BEA showed no activity. The main difference between these two types of reactions is the order in which reactants are activated. On one hand, for epoxidation of linear alkenes, the key step was shown as being the activation of positively charged oxygen from H_2O_2 bounded to the metal center¹⁴⁹. On the other hand, for Baeyer-Villiger reaction, the carbonyl group is first activated by the metal center, making the carbon more prone to attack by hydrogen peroxide. However, for Meerwein-Ponndorf-Verley reduction (implying carbonyl activation on the metal center), differences of relative activity were observed between Hf, Zr, Ti, and Sn-BEA zeolite when changing solvent, or reactants¹⁴⁹⁻¹⁵³. These results suggest that intrinsic Lewis acid strength of the metal containing zeolite is not enough to predict the catalytic activity of the material, but other factors are playing a role such as geometric configurations within the pores. Indeed, the nature of the heteroatom introduced cannot explain all the observed differences in reactivity by itself.

As a result, understanding the Lewis acidity of active sites in metal containing zeolites is essential for the design of materials for catalytic applications. Given the fact that evaluated performances will strongly depend on the local geometry, the confinement effect, and the used substrate, the use of probe molecules monitored by spectroscopic methods is of first interest in order to understand and evaluate the activity of a given material. Following this trend, a recent study from Lewis¹⁵⁴ used TMPO (trimethylphosphine oxide) as a probe molecule, followed by ^{31}P MAS NMR to evaluate active sites of Sn-BEA for glucose isomerisation and aldol condensation. They were able to successfully attribute given activity of the materials to given Lewis acid sites observed using ^{31}P NMR with TMPO as a probe molecule. Phosphorus is indeed an abundant (100%) sensitive nucleus towards NMR, with a $\frac{1}{2}$ spin, and high resolution, displayed in a wide window of chemical shifts (more than 650 ppm). Therefore, the use of P-containing probe molecules such as trialkylphosphane (tetramethylphosphane, TMP) and trialkylphosphine oxide (trimethylphosphine oxide, TMPO) were developed for ^{31}P MAS NMR study, and allows to distinguish fine differences between Lewis acid sites such as open against closed sites, and even crystallographic T-positions of the Lewis sites. This characterization method can furthermore be used to study both Lewis and Brønsted acidity. A recent review describes in details the state of the art regarding this characterization method applied to solid and liquid catalysts, and some of the advanced features that could be observed with several advanced NMR experiments¹⁵⁵.

Metals in framework positions can possibly accommodate various molecular connectivity with the framework from fully closed Lewis sites (4 Si-O-M bonds) to

partially-hydrolyzed sites (so-called open sites) from a theoretical point of view. There is consequently different possible degree of open sites, related to the number of metal-framework hydrolyzed bonds, as described in the case of Ti with possible sites ranging from tetrapodal closed sites to open dipodal sites (Figure 12.)¹⁵⁶. The presence of open sites was already shown in the case of Ti, Sn, and Zr containing zeolites by theoretical approach, and experimental approach using EXAFS^{156,157}.

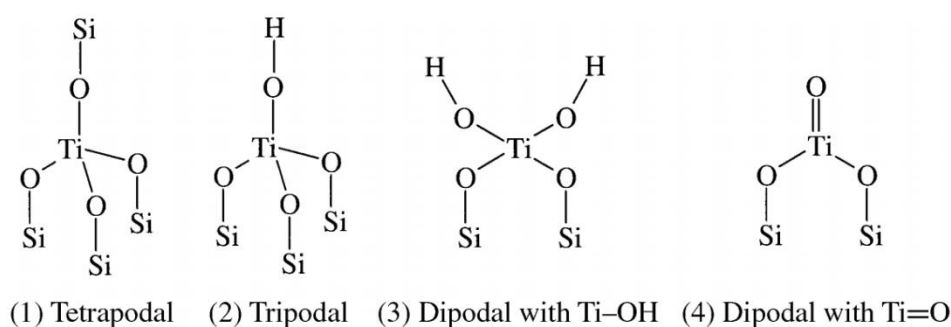


Figure 12. Possible metal-framework connectivity in the case of Ti metal atom in Silicalite-1 (MFI) framework (TS-1)¹⁵⁶

Connectivity of the metal centers with zeolite framework influence its flexibility, which can in return, reduce the required energy for geometric distortion during the formation of a given transition state. This would then explain why open sites are described are active for catalysis with regards to closed sites, mostly considered as inactive. Following this trend, theoretical mechanistic study associated with sodium exchange evidenced that open sites are more active for the epoxidation of alkenes over TS-1 materials¹⁵⁸⁻¹⁶⁰. Moreover, a linear correlation between the number of open sites measured using deuterated acetonitrile (CD_3CN) adsorption monitored by FTIR spectroscopy, and catalytic activity towards Baeyer Villiger oxidation of adamantanone was observed for Sn-BEA materials⁶⁷. Corresponding DFT calculations suggested that metal hydroxyl group was required to bind H_2O_2 . Similarly, initial reaction rates for ethanol condensation catalyzed by Zr-BEA zeolite were correlated with the amount of open Lewis sites observed in the zeolitic material using CO adsorption monitored by IR spectroscopy¹⁶¹.

Interestingly, the presence of open sites comes with the parallel presence of silanol species in direct proximity with the metal center. The modification of such silanol group could then lead to an alteration of the metal center toward its catalytic activity. This was successfully performed by Bermejo-Deval et al.⁶⁶ where epimerization selectivity over isomerisation was optimized thanks to the exchange of adjacent silanol groups with sodium cation in Sn-BEA, thus, altering the metal site properties.

In contrast to these results describing open sites as catalytic active sites, Wolf et al.¹⁶² suggested that both open and closed sites were active towards isomerisation of sugars. They supported this assertion through the analysis by ¹¹⁹Sn DNP MAS NMR of several Sn-BEA samples with different relative amounts of closed and open Lewis acid sites. This assertion was supported by Yang et al.¹⁶³, although they concluded that a nearby silanol nest was beneficial for activation of some substrates. In contrast to these results, Li et al.¹⁶⁴ found that open sites are intrinsically more active than closed sites due to the increased flexibility of the framework metal. We can also point out the fact that only open against closed sites is discussed, the possibility of open sites having more than one hydrolyzed Si-O-M bond is not mentioned. These contradictions are symptomatic of the lack of understanding regarding the real nature and properties of the metal sites generated upon isomorphous substitution of metal in zeolite frameworks.

Aside from catalytic activity, introduction of metals in zeolite framework can also bring other valuable properties to zeolitic materials. This is particularly the case for W-MFI, reported by Grand et al.⁵², where the introduction of tungsten (W) in MFI framework allowed to cure silanol defects, thus, yielding a highly hydrophobic MFI framework. The absence of defects enhanced the thermal stability and promoted the selective adsorption of CO₂ from a gaseous mixture, opening a new array of applications aside from purely catalytic reactions. The material was moreover active towards styrene epoxidation reaction.

I.2.6. Incorporation of group VI metals in zeolite structures

Efforts have been made to incorporate metals such as molybdenum and tungsten into zeolite frameworks due to their high activity in oxidation reactions such as the epoxidation of alkenes¹⁶⁵. However, there are only a few papers on the direct synthesis of molybdenum or tungsten based catalysts¹⁶⁶⁻¹⁶⁹. Raghavan et al.¹⁶⁶ produced molybdenum containing silicalite-2 (ZSM-11) by hydrothermal synthesis from aluminium free alkaline mixture which was active for oxidative dehydrogenation of ethanol to acetaldehyde. The framework position of the metals was evidenced by the expansion of the unit cell volume of the samples measured by XRD. The introduction of Mo in silicalite-1 was also reported from the same group¹⁶⁷, and a non-linear unit cell volume expansion upon Mo loading was observed indicating the co-formation of non-framework metallic species. Interestingly, the samples were more hydrophilic than silicalite-1 and thermally stable; their high activity in the oxidation of thioethers to the corresponding sulfoxides was reported. The incorporation of molybdenum in silicalite-1 framework was also reported by Tavalaro¹⁶⁹. Molybdenum was also introduced in faujasite (zeolite Y)¹⁶⁸, but only very poor evidence for the effective isomorphous substitution was provided.

Niederer and Hölderich¹⁴⁴ described the post synthesis preparation by a gas phase modification of Mo-BEA from the boron analogue, and the catalytic activity of the materials in pentanol oxidation, and epoxidation of allylic alcohol, octane, and cyclohexene was demonstrated. No clear evidence for effective Mo framework incorporation in BEA zeolite was provided. Recently, Grand⁵² described the preparation of tungsten containing MFI zeolite, and assessed the effective framework incorporation using various techniques able to bring indirect evidences, and activity towards styrene epoxidation was reported.

I.3. Conclusions

The development of catalysts that can operate under exceptionally harsh and unconventional conditions (temperatures higher than 500 °C) is of critical importance for the transition of the energy and chemicals industries to low-emission and renewable chemical feedstocks, through the design of new catalytic processes involving the conversion of biomass and natural gas into valuable intermediates.

Metal containing zeolites based catalyst are shown as promising candidates for the catalysis of such reactions, but many issues regarding their stability under such harsh conditions needs to be addressed. High hopes are dedicated into the ability of framework metal containing zeolite to overcome all the issues linked to the catalytic operation under harsh conditions, while providing high stability of the catalytic performances and of the catalyst itself. Indeed, these materials do possess valuable properties such as dispersed metal species, low metal loading, hydrophobicity, strong interaction of the metal to the framework, or resilience against sintering and amorphization.

However, the incorporation of metal in zeolite framework is a complex process. To control the metal introduction during hydrothermal synthesis, care should be taken regarding the synthesis conditions. The isomorphous substitution is mainly driven by kinetic parameters and metal containing zeolites are not initially formed as thermodynamic products.

In an attempt to avoid synthesis limitations, post-synthetic introduction of metal in framework positions was also developed. However, both methods do possess advantages and drawbacks, and therefore, there is no ideal synthesis method. As a result, there is still a lack of a synthesis method that would efficiently combine the advantages of both methods while limiting their drawbacks.

In addition, the characterization of low amount of highly dispersed metals can be quite challenging, but some methods combined together can provide strong evidences

of the presence of such species in a given zeolite sample. The main methods for characterization are XRD, NMR, Raman, and probe molecule adsorption followed by IR (CD_3CN) or ^{31}P MAS NMR (TMPO).

Partly due to the difficult characterization of metal centers in zeolite frameworks, only partial understanding of these sites with regards to their real nature and properties is available in the open literature up to now. Open Lewis sites are generally described as more prone to be active for oxidation reactions with regards to closed sites. The activity of these materials was also illustrated as dependent on local geometry of corresponding adducts, and not directly related with the strength of the Lewis acid sites. Therefore, the nature of the metal inserted does not solely account for the catalytic activity, but local environment, nature of organic substrate, and geometry of adducts are of first importance. Nonetheless, these materials have already been highlighted as very active and selective materials for several catalytic reactions.

I.4. References

1. T. C. E. Progress, International Energy Agency: Paris (2017).
2. Outlook for Energy: A Perspective to 2040. *Exxon Mob. Corp.* (2019).
3. B. Energy, Bp Energy Outlook—2019 Edition. *Br. Pet. London, UK* (2019).
4. W. Vermeiren, J.-P. Gilson, Impact of zeolites on the petroleum and petrochemical industry. *Top. Catal.* **52**, 1131–1161 (2009).
5. A. F. Masters, T. Maschmeyer, Zeolites--From curiosity to cornerstone. *Microporous Mesoporous Mater.* **142**, 423–438 (2011).
6. A. W. Petrov, D. Ferri, F. Krumeich, M. Nachtegaal, J. A. van Bokhoven, O. Kröcher, Stable complete methane oxidation over palladium based zeolite catalysts. *Nat. Commun.* **9**, 1–8 (2018).
7. I. Sádaba, M. L. Granados, A. Riisager, E. Taarning, Deactivation of solid catalysts in liquid media: the case of leaching of active sites in biomass conversion reactions. *Green Chem.* **17**, 4133–4145 (2015).
8. N. Kosinov, F. J. A. G. Coumans, G. Li, E. Uslamin, B. Mezari, A. S. G. Wijkema, E. A. Pidko, E. J. M. Hensen, Stable Mo/HZSM-5 methane dehydroaromatization catalysts optimized for high-temperature calcination-regeneration. *J. Catal.* **346**, 125–133 (2017).
9. T. Ennaert, J. Van Aelst, J. Dijkmans, R. De Clercq, W. Schutyser, M. Dusselier, D. Verboekend, B. F. Sels, Potential and challenges of zeolite chemistry in the catalytic conversion of biomass. *Chem. Soc. Rev.* **45**, 584–611 (2016).

10. A. R. Maag, G. A. Tompsett, J. Tam, C. A. Ang, G. Azimi, A. D. Carl, X. Huang, L. J. Smith, R. L. Grimm, J. Q. Bond, others, ZSM-5 decrystallization and dealumination in hot liquid water. *Phys. Chem. Chem. Phys.* **21**, 17880–17892 (2019).
11. C. H. L. Tempelman, E. J. M. Hensen, On the deactivation of Mo/HZSM-5 in the methane dehydroaromatization reaction. *Appl. Catal. B Environ.* **176**, 731–739 (2015).
12. J. Jae, G. A. Tompsett, A. J. Foster, K. D. Hammond, S. M. Auerbach, R. F. Lobo, G. W. Huber, Investigation into the shape selectivity of zeolite catalysts for biomass conversion. *J. Catal.* **279**, 257–268 (2011).
13. T. W. Hansen, A. T. DeLaRiva, S. R. Challa, A. K. Datye, Sintering of catalytic nanoparticles: particle migration or Ostwald ripening? *Acc. Chem. Res.* **46**, 1720–1730 (2013).
14. E. Rombi, M. G. Cutrufello, V. Solinas, S. De Rossi, G. Ferraris, A. Pistone, Effects of potassium addition on the acidity and reducibility of chromia/alumina dehydrogenation catalysts. *Appl. Catal. A Gen.* **251**, 255–266 (2003).
15. J. J. H. B. Sattler, J. Ruiz-Martinez, E. Santillan-Jimenez, B. M. Weckhuysen, Catalytic dehydrogenation of light alkanes on metals and metal oxides. *Chem. Rev.* **114**, 10613–10653 (2014).
16. R. D. Cortright, J. A. Dumesic, Effects of potassium on silica-supported Pt and Pt/Sn catalysts for isobutane dehydrogenation. *J. Catal.* **157**, 576–583 (1995).
17. R. D. Cortright, J. A. Dumesic, Microcalorimetric, spectroscopic, and kinetic studies of silica supported Pt and Pt/Sn catalysts for isobutane dehydrogenation. *J. Catal.* **148**, 771–778 (1994).
18. R. L. Puurunen, B. M. Weckhuysen, Spectroscopic study on the irreversible deactivation of chromia/alumina dehydrogenation catalysts. *J. Catal.* **210**, 418–430 (2002).
19. L. Wachowski, P. Kirszenstejn, R. Łopatka, B. Czajka, Studies of physicochemical and surface properties of alumina modified with rare-earth oxides I. Preparation, structure and thermal stability. *Mater. Chem. Phys.* **37**, 29–38 (1994).
20. M. Shamzhy, M. Opanasenko, P. Concepción, A. Martínez, New trends in tailoring active sites in zeolite-based catalysts. *Chem. Soc. Rev.* **48**, 1095–1149 (2019).
21. J. M. Hill, R. D. Cortright, J. A. Dumesic, Silica-and L-zeolite-supported Pt, Pt/Sn and Pt/Sn/K catalysts for isobutane dehydrogenation. *Appl. Catal. A Gen.* **168**, 9–21 (1998).
22. R. D. Cortright, J. M. Hill, J. A. Dumesic, Selective dehydrogenation of isobutane

- over supported Pt/Sn catalysts. *Catal. Today*. **55**, 213–223 (2000).
23. M. Shamzhy, M. Opanasenko, P. Concepción, A. Martínez, New trends in tailoring active sites in zeolite-based catalysts. *Chem. Soc. Rev.* **48**, 1095–1149 (2019).
 24. L. Liu, U. Diaz, R. Arenal, G. Agostini, P. Concepción, A. Corma, Generation of subnanometric platinum with high stability during transformation of a 2D zeolite into 3D. *Nat. Mater.* **16**, 132–138 (2017).
 25. L. Liu, M. Lopez-Haro, C. W. Lopes, C. Li, P. Concepcion, L. Simonelli, J. J. Calvino, A. Corma, Regioselective generation and reactivity control of subnanometric platinum clusters in zeolites for high-temperature catalysis. *Nat. Mater.* **18**, 866–873 (2019).
 26. Y. Wang, Z.-P. Hu, W. Tian, L. Gao, Z. Wang, Z.-Y. Yuan, Framework-confined Sn in Si-beta stabilizing ultra-small Pt nanoclusters as direct propane dehydrogenation catalysts with high selectivity and stability. *Catal. Sci. Technol.* **9**, 6993–7002 (2019).
 27. Z. Xu, Y. Yue, X. Bao, Z. Xie, H. Zhu, Propane Dehydrogenation over Pt Clusters Localized at the Sn Single-Site in Zeolite Framework. *ACS Catal.* **10**, 818–828 (2019).
 28. R. Baran, T. Onfroy, S. Casale, S. Dzwigaj, Introduction of Co into the vacant T-atom sites of SiBEA zeolite as Isolated Mononuclear Co Species. *J. Phys. Chem. C*. **118**, 20445–20451 (2014).
 29. C. Chen, S. Zhang, Z. Wang, Z.-Y. Yuan, Ultrasmall Co confined in the silanols of dealuminated beta zeolite: A highly active and selective catalyst for direct dehydrogenation of propane to propylene. *J. Catal.* **383**, 77–87 (2020).
 30. C. Chen, M. Sun, Z. Hu, Y. Liu, S. Zhang, Z.-Y. Yuan, Nature of active phase of VO_x catalysts supported on SiBeta for direct dehydrogenation of propane to propylene. *Chinese J. Catal.* **41**, 276–285 (2020).
 31. J. H. Yun, R. F. Lobo, Catalytic dehydrogenation of propane over iron-silicate zeolites. *J. Catal.* **312**, 263–270 (2014).
 32. S.-W. Choi, W.-G. Kim, J.-S. So, J. S. Moore, Y. Liu, R. S. Dixit, J. G. Pendergast, C. Sievers, D. S. Sholl, S. Nair, others, Propane dehydrogenation catalyzed by gallosilicate MFI zeolites with perturbed acidity. *J. Catal.* **345**, 113–123 (2017).
 33. M. Nakai, K. Miyake, R. Inoue, K. Ono, H. Al Jabri, Y. Hirota, Y. Uchida, S. Tanaka, M. Miyamoto, Y. Oumi, others, Dehydrogenation of propane over high silica* BEA type gallosilicate (Ga-Beta). *Catal. Sci. Technol.* **9**, 6234–6239 (2019).
 34. H. Ma, R. Kojima, R. Ohnishi, M. Ichikawa, Efficient regeneration of Mo/HZSM-5 catalyst by using air with NO in methane dehydro-aromatization reaction. *Appl. Catal. A Gen.* **275**, 183–187 (2004).

35. S. J. Han, S. K. Kim, A. Hwang, S. Kim, D.-Y. Hong, G. Kwak, K.-W. Jun, Y. T. Kim, Non-oxidative dehydroaromatization of methane over Mo/H-ZSM-5 catalysts: A detailed analysis of the reaction-regeneration cycle. *Appl. Catal. B Environ.* **241**, 305–318 (2019).
36. J. R. Mowry, R. F. Anderson, J. A. Johnson, Process makes aromatics from LPG. *Oil gas J.* **83**, 128–131 (1985).
37. P. Meriaudeau, G. Sapaly, C. Naccache, Framework and non-framework gallium in pentasil-like zeolite as studied in the reaction of propane. *J. Mol. Catal.* **81**, 293–300 (1993).
38. P. Schwach, X. Pan, X. Bao, Direct conversion of methane to value-added chemicals over heterogeneous catalysts: challenges and prospects. *Chem. Rev.* **117**, 8497–8520 (2017).
39. M. T. Portilla, F. J. Llopis, C. Martínez, Non-oxidative dehydroaromatization of methane: an effective reaction-regeneration cyclic operation for catalyst life extension. *Catal. Sci. Technol.* **5**, 3806–3821 (2015).
40. C. Sun, G. Fang, X. Guo, Y. Hu, S. Ma, T. Yang, J. Han, H. Ma, D. Tan, X. Bao, Methane dehydroaromatization with periodic CH₄-H₂ switch: A promising process for aromatics and hydrogen. *J. Energy Chem.* **24**, 257–263 (2015).
41. Y.-H. Kim, R. W. Borry III, E. Iglesia, Genesis of methane activation sites in Mo-exchanged H-ZSM-5 catalysts. *Microporous Mesoporous Mater.* **35**, 495–509 (2000).
42. J. Gao, Y. Zheng, J.-M. Jehng, Y. Tang, I. E. Wachs, S. G. Podkolzin, Identification of molybdenum oxide nanostructures on zeolites for natural gas conversion. *Science* (80-.). **348**, 686–690 (2015).
43. R. W. Borry, Y. H. Kim, A. Huffsmith, J. A. Reimer, E. Iglesia, Structure and density of Mo and acid sites in Mo-exchanged H-ZSM5 catalysts for nonoxidative methane conversion. *J. Phys. Chem. B.* **103**, 5787–5796 (1999).
44. B. S. Liu, J. W. H. Leung, L. Li, C. T. Au, A.-C. Cheung, TOF-MS investigation on methane aromatization over 3% Mo/HZSM-5 catalyst under supersonic jet expansion condition. *Chem. Phys. Lett.* **430**, 210–214 (2006).
45. R. W. Borry, E. C. Lu, Y.-H. Kim, E. Iglesia, Non-oxidative catalytic conversion of methane with continuous hydrogen removal. *Stud. Surf. Sci. Catal.* **119**, 403–410 (1998).
46. Z. R. Ismagilov, L. T. Tsikoza, E. V Matus, G. S. Litvak, I. Z. Ismagulova, O. B. Sukhova, Carbonization and regeneration of Mo/ZSM-5 catalysts for methane dehydroaromatization. *Eurasian Chem. J.* **7**, 115–121 (2005).
47. I. Vollmer, A. Mondal, I. Yarulina, E. Abou-Hamad, F. Kapteijn, J. Gascon, Quantifying the impact of dispersion, acidity and porosity of Mo/HZSM-5 on the

- performance in methane dehydroaromatization. *Appl. Catal. A Gen.* **574**, 144–150 (2019).
48. X. Guo, G. Fang, G. Li, H. Ma, H. Fan, L. Yu, C. Ma, X. Wu, D. Deng, M. Wei, others, Direct, nonoxidative conversion of methane to ethylene, aromatics, and hydrogen. *Science (80-.)*. **344**, 616–619 (2014).
 49. P. Xie, T. Pu, A. Nie, S. Hwang, S. C. Purdy, W. Yu, D. Su, J. T. Miller, C. Wang, Nanoceria-supported single-atom platinum catalysts for direct methane conversion. *ACS Catal.* **8**, 4044–4048 (2018).
 50. L. Nemeth, S. R. Bare, in *Advances in Catalysis* (Elsevier, 2014), vol. 57, pp. 1–97.
 51. H. Y. Luo, J. D. Lewis, Y. Román-Leshkov, Lewis acid zeolites for biomass conversion: Perspectives and challenges on reactivity, synthesis, and stability. *Annu. Rev. Chem. Biomol. Eng.* **7**, 663–692 (2016).
 52. J. Grand, S. N. Talapaneni, A. Vicente, C. Fernandez, E. Dib, H. A. Aleksandrov, G. N. Vayssilov, R. Retoux, P. Boullay, J.-P. Gilson, others, One-pot synthesis of silanol-free nanosized MFI zeolite. *Nat. Mater.* **16**, 1010–1015 (2017).
 53. S. Narayanan, A. Sultana, Aniline alkylation with ethanol over zeolites and vanadium modified zeolites prepared by solid state exchange method. *Appl. Catal. A Gen.* **167**, 103–111 (1998).
 54. Y. Li, L. Li, J. Yu, Applications of zeolites in sustainable chemistry. *Chem.* **3**, 928–949 (2017).
 55. P. Nachtigall, M. Davidová, M. Šilhan, D. Nachtigallová, in *Studies in Surface Science and Catalysis* (Elsevier, 2002), vol. 142, pp. 101–108.
 56. N. Kosinov, C. Liu, E. J. M. Hensen, E. A. Pidko, Engineering of transition metal catalysts confined in zeolites. *Chem. Mater.* **30**, 3177–3198 (2018).
 57. A. Zecchina, M. Rivallan, G. Berlier, C. Lamberti, G. Ricchiardi, Structure and nuclearity of active sites in Fe-zeolites: comparison with iron sites in enzymes and homogeneous catalysts. *Phys. Chem. Chem. Phys.* **9**, 3483–3499 (2007).
 58. C. Perego, A. Carati, P. Ingallina, M. A. Mantegazza, G. Bellussi, Production of titanium containing molecular sieves and their application in catalysis. *Appl. Catal. A Gen.* **221**, 63–72 (2001).
 59. C. T. Briden, C. D. Williams, D. Apperley, A study of the chemistry of isomorphous substitution and characterization of Al-ZSM-5 and Sc-ZSM-5 synthesized in fluoride media. *Inorg. Mater.* **43**, 758–769 (2007).
 60. S. Wilson, P. Barger, The characteristics of SAPO-34 which influence the conversion of methanol to light olefins. *Microporous Mesoporous Mater.* **29**, 117–126 (1999).

61. A. Ruíz-Baltazar, R. Pérez, Kinetic adsorption study of silver nanoparticles on natural zeolite: experimental and theoretical models. *Appl. Sci.* **5**, 1869–1881 (2015).
62. J. Zhuang, Z. Yan, X. Liu, X. Liu, X. Han, X. Bao, U. Mueller, NMR study on the acidity of TS-1 zeolite. *Catal. Letters.* **83**, 87–91 (2002).
63. R. S. Drago, S. C. Dias, J. M. McGilvray, A. L. M. L. Mateus, Acidity and Hydrophobicity of TS-1. *J. Phys. Chem. B.* **102**, 1508–1514 (1998).
64. V. L. Sushkevich, A. Vimont, A. Travert, I. I. Ivanova, Spectroscopic evidence for open and closed Lewis acid sites in ZrBEA zeolites. *J. Phys. Chem. C.* **119**, 17633–17639 (2015).
65. R. Otomo, R. Kosugi, Y. Kamiya, T. Tatsumi, T. Yokoi, Modification of Sn-Beta zeolite: characterization of acidic/basic properties and catalytic performance in Baeyer–Villiger oxidation. *Catal. Sci. Technol.* **6**, 2787–2795 (2016).
66. R. Bermejo-Deval, M. Orazov, R. Gounder, S.-J. Hwang, M. E. Davis, Active sites in Sn-Beta for glucose isomerization to fructose and epimerization to mannose. *ACS Catal.* **4**, 2288–2297 (2014).
67. M. Boronat, P. Concepción, A. Corma, M. Renz, S. Valencia, Determination of the catalytically active oxidation Lewis acid sites in Sn-beta zeolites, and their optimisation by the combination of theoretical and experimental studies. *J. Catal.* **234**, 111–118 (2005).
68. T. Pang, X. Yang, C. Yuan, A. A. Elzatahry, A. Alghamdi, X. He, X. Cheng, Y. Deng, Recent advance in synthesis and application of heteroatom zeolites. *Chinese Chem. Lett.* (2020), doi:10.1016/j.ccllet.2020.04.018.
69. W. Zhang, W. Hou, T. Meng, W. Zhuang, J. Xie, Y. Zhou, J. Wang, Direct synthesis of V-containing all-silica beta-zeolite for efficient one-pot, one-step conversion of carbohydrates into 2,5-diformylfuran. *Catal. Sci. Technol.* **7**, 6050–6058 (2017).
70. O. V. Shvets, M. V. Shamzhy, P. S. Yaremov, Z. Musilová, D. Procházková, J. Čejka, Isomorphous introduction of boron in germanosilicate zeolites with UTL topology. *Chem. Mater.* **23**, 2573–2585 (2011).
71. Y. Yao, F. Cao, J. Gu, Y. Wu, Y. Zhou, J. Wang, Direct hydrothermal synthesis and characterization of framework-substituted Co(Mn)-Beta zeolites. *J. Porous Mater.* **20**, 891–896 (2013).
72. J. Wang, J. Xie, Y. Zhou, J. Wang, New facile way to isomorphously substituted Cr-β zeolite and its catalytic performance. *Microporous Mesoporous Mater.* **171**, 87–93 (2013).
73. C. Xia, Y. Liu, M. Lin, X. Peng, B. Zhu, X. Shu, Confirmation of the isomorphous substitution by Sn atoms in the framework positions of MFI-typed zeolite. *Catal.*

- Today*. **316**, 193–198 (2018).
74. T. F. Chaves, A. R. Passos, V. Briois, L. Martins, S. H. Pulcinelli, C. V. Santilli, J. Pérez-Pariente, Vanadosilicate with MWW zeolite structure synthesized from VCl₃ by cooperative assembly of organic templates. *Microporous Mesoporous Mater.* **279**, 252–261 (2019).
 75. F. Tielens, S. Dzwigaj, Group v metal substitution in silicate model zeolites: In search for the active site. *Chem. Phys. Lett.* **501**, 59–63 (2010).
 76. Y. Naraki, K. Ariga, H. Oka, H. Kurashige, T. Sano, An Isomorphously Substituted Fe-BEA Zeolite with High Fe Content: Facile Synthesis and Characterization. *J. Nanosci. Nanotechnol.* **18**, 11–19 (2017).
 77. X. Su, K. Zhang, Y. Snatenkova, Z. Matieva, X. Bai, N. Kolesnichenko, W. Wu, High-efficiency nano [Zn,Al]ZSM-5 bifunctional catalysts for dimethyl ether conversion to isoparaffin-rich gasoline. *Fuel Process. Technol.* **198**, 106242 (2020).
 78. K. K. Shah, J. Saikia, D. Saikia, A. K. Talukdar, Synthesis and characterization of isomorphously zirconium substituted Mobil Five (MFI) zeolite. *Mater. Chem. Phys.* **134**, 43–49 (2012).
 79. M. Taramasso, G. Perego, B. Notari, Preparation of porous crystalline synthetic material comprised of silicon and titanium oxides (1983).
 80. G. Bellussi, R. Millini, P. Pollesel, C. Perego, Zeolite science and technology at Eni. *New J. Chem.* **40**, 4061–4077 (2016).
 81. T. Xue, H. Liu, Y. Wang, H. Wu, P. Wu, M. He, Seed-induced synthesis of small-crystal TS-1 using ammonia as alkali source. *Chinese J. Catal.* **36**, 1928–1935 (2015).
 82. S. Gonthier, R. W. Thompson, in *Studies in surface science and catalysis* (Elsevier, 1994), vol. 85, pp. 43–73.
 83. C. Li, G. Xiong, Q. Xin, J. Liu, P. Ying, Z. Feng, J. Li, W. Yang, Y. Wang, G. Wang, others, UV Resonance Raman Spectroscopic Identification of Titanium Atoms in the Framework of TS-1 Zeolite. *Angew. Chemie Int. Ed.* **38**, 2220–2222 (1999).
 84. C. Li, G. Xiong, J. Liu, P. Ying, Q. Xin, Z. Feng, Identifying framework titanium in TS-1 zeolite by UV resonance Raman spectroscopy. *J. Phys. Chem. B.* **105**, 2993–2997 (2001).
 85. W. Fan, R.-G. Duan, T. Yokoi, P. Wu, Y. Kubota, T. Tatsumi, Synthesis, crystallization mechanism, and catalytic properties of titanium-rich TS-1 free of extraframework titanium species. *J. Am. Chem. Soc.* **130**, 10150–10164 (2008).
 86. M. G. Clerici, G. Bellussi, U. Romano, Synthesis of propylene oxide from

- propylene and hydrogen peroxide catalyzed by titanium silicalite. *J. Catal.* **129**, 159–167 (1991).
87. M. Tamura, W. Chaikittisilp, T. Yokoi, T. Okubo, Incorporation process of Ti species into the framework of MFI type zeolite. *Microporous mesoporous Mater.* **112**, 202–210 (2008).
88. M. F. Borin, T. da Silva, R. F. Felisbino, D. Cardoso, Synthesis of TS-1 molecular sieves using a new Ti source. *J. Phys. Chem. B.* **110**, 15080–15084 (2006).
89. A. Tuel, Y. Ben Taârit, Influence of the nature of silicon and titanium alkoxides on the incorporation of titanium in TS-1. *Appl. Catal. A Gen.* **110**, 137–151 (1994).
90. R. C. Deka, V. A. Nasluzov, E. A. Ivanova Shor, A. M. Shor, G. N. Vayssilov, N. Rösch, Comparison of all sites for Ti substitution in zeolite TS-1 by an accurate embedded-cluster method. *J. Phys. Chem. B.* **109**, 24304–24310 (2005).
91. A. Cichocki, J. Parasiewicz-Kaczmarek, M. Michalik, M. Buś, Synthesis and characterization of boralites with the MFI structure. *Zeolites.* **10**, 577–582 (1990).
92. G. Ricchiardi, J. M. Newsam, Predicted effects of Site-Specific aluminum substitution on the framework geometry and unit cell dimensions of zeolite ZSM-5 materials. *J. Phys. Chem. B.* **101**, 9943–9950 (1997).
93. E. L. Wu, S. L. Lawton, D. H. Olson, A. C. Rohrman, G. T. Kokotailo, ZSM-5-type materials. Factors affecting crystal symmetry. *J. Phys. Chem.* **83**, 2777–2781 (1979).
94. R. K. Rana, B. Viswanathan, Mo incorporation in MCM-41 type zeolite. *Catal. Letters.* **52**, 25–29 (1998).
95. P. F. Henry, M. T. Weller, C. C. Wilson, Structural investigation of TS-1: Determination of the true nonrandom titanium framework substitution and silicon vacancy distribution from powder neutron diffraction studies using isotopes. *J. Phys. Chem. B.* **105**, 7452–7458 (2001).
96. P. Wolf, M. Valla, F. Nunez-Zarur, A. Comas-Vives, A. J. Rossini, C. Firth, H. Kallas, A. Lesage, L. Emsley, C. Coperet, others, Correlating synthetic methods, morphology, atomic-level structure, and catalytic activity of Sn- β catalysts. *Acc Catal.* **6**, 4047–4063 (2016).
97. G. L. Marra, G. Artioli, A. N. Fitch, M. Milanese, C. Lamberti, Orthorhombic to monoclinic phase transition in high-Ti-loaded TS-1: an attempt to locate Ti in the MFI framework by low temperature XRD. *Microporous mesoporous Mater.* **40**, 85–94 (2000).
98. M. K. Dongare, P. Singh, P. P. Moghe, P. Ratnasamy, Synthesis, characterization, and catalytic properties of [Zr]-ZSM-5. *Zeolites.* **11**, 690–693 (1991).

99. Y. S. Ko, W. S. Ahn, Synthesis and characterization of tantalum silicalite molecular sieves with MFI structure. *Microporous mesoporous Mater.* **30**, 283–291 (1999).
100. J. B. Nagy, R. Aiello, G. Giordano, A. Katovic, F. Testa, Z. Konya, I. Kiricsi, in *Characterization II* (Springer, 2006), pp. 365–478.
101. T. Blasco, M. A. Camblor, A. Corma, J. Perez-Pariente, The state of Ti in titanoaluminosilicates isomorphous with zeolite. beta. *J. Am. Chem. Soc.* **115**, 11806–11813 (1993).
102. M. A. Camblor, A. Corma, J. Perez-Pariente, Synthesis of titanoaluminosilicates isomorphous to zeolite Beta, active as oxidation catalysts. *Zeolites.* **13**, 82–87 (1993).
103. G. Bellussi, A. Carati, M. G. Clerici, A. Esposito, in *Studies in Surface Science and Catalysis* (Elsevier, 1991), vol. 63, pp. 421–429.
104. C. Li, Identifying the isolated transition metal ions/oxides in molecular sieves and on oxide supports by UV resonance Raman spectroscopy. *J. Catal.* **216**, 203–212 (2003).
105. B. Rakshe, V. Ramaswamy, S. G. Hegde, R. Vetrivel, A. V Ramaswamy, Crystalline, microporous zirconium silicates with MFI structure. *Catal. Letters.* **45**, 41–50 (1997).
106. T. Blasco, M. A. Camblor, A. Corma, P. Esteve, J. M. Guil, A. Martinez, J. A. Perdigon-Melon, S. Valencia, Direct synthesis and characterization of hydrophobic Aluminum-free Ti- beta zeolite. *J. Phys. Chem. B.* **102**, 75–88 (1998).
107. R. Aiello, J. B. Nagy, G. Giordano, A. Katovic, F. Testa, Isomorphous substitution in zeolites. *Comptes Rendus Chim.* **8**, 321–329 (2005).
108. Z. El Berrichi, B. Louis, J. P. Tessonnier, O. Ersen, L. Cherif, M. J. Ledoux, C. Pham-Huu, One-pot synthesis of Ga-SBA-15: Activity comparison with Ga-post-treated SBA-15 catalysts. *Appl. Catal. A Gen.* **316**, 219–225 (2007).
109. S. Tolborg, A. Katerinopoulou, D. D. Falcone, I. Sádaba, C. M. Osmundsen, R. J. Davis, E. Taarning, P. Fristrup, M. S. Holm, Incorporation of tin affects crystallization, morphology, and crystal composition of Sn-Beta. *J. Mater. Chem. A.* **2**, 20252–20262 (2014).
110. Y. G. Kolyagin, A. V Yakimov, S. Tolborg, P. N. R. Vennestrøm, I. I. Ivanova, Application of ¹¹⁹Sn CPMG MAS NMR for fast characterization of Sn sites in zeolites with natural ¹¹⁹Sn isotope abundance. *J. Phys. Chem. Lett.* **7**, 1249–1253 (2016).
111. Y. G. Kolyagin, A. V Yakimov, S. Tolborg, P. N. R. Vennestrøm, I. I. Ivanova, Direct Observation of Tin in Different T-Sites of Sn-BEA by One-and Two-

- Dimensional ^{119}Sn MAS NMR Spectroscopy. *J. Phys. Chem. Lett.* **9**, 3738–3743 (2018).
112. T. Blasco, A. Corma, M. J. Díaz-Cabañas, F. Rey, J. A. Vidal-Moya, C. M. Zicovich-Wilson, Preferential location of Ge in the double four-membered ring units of ITQ-7 zeolite. *J. Phys. Chem. B.* **106**, 2634–2642 (2002).
 113. A. V Yakimov, Y. G. Kolyagin, S. Tolborg, P. N. R. Vennestrøm, I. I. Ivanova, Accelerated synthesis of Sn-BEA in fluoride media: effect of H₂O content in the gel. *New J. Chem.* **40**, 4367–4374 (2016).
 114. S. Wu, Y. Han, Y.-C. Zou, J.-W. Song, L. Zhao, Y. Di, S.-Z. Liu, F.-S. Xiao, Synthesis of heteroatom substituted SBA-15 by the “pH-adjusting” method. *Chem. Mater.* **16**, 486–492 (2004).
 115. T. R. Gaffney, R. Pierantozzi, M. R. Seger, (ACS Publications, 1989).
 116. N. Lang, P. Delichere, A. Tuel, Post-synthesis introduction of transition metals in surfactant-containing MCM-41 materials. *Microporous mesoporous Mater.* **56**, 203–217 (2002).
 117. M. Ziolk, I. Sobczak, M. Trejda, A. Wojtaszek-Gurdak, in *Structure and Reactivity of Metals in Zeolite Materials* (Springer, 2017), pp. 179–249.
 118. M. Liu, S. Jia, C. Li, A. Zhang, C. Song, X. Guo, Facile preparation of Sn- β zeolites by post-synthesis (isomorphous substitution) method for isomerization of glucose to fructose. *Cuihua Xuebao/Chinese J. Catal.* **35**, 723–732 (2014).
 119. H. Xu, J. G. Jiang, B. Yang, L. Zhang, M. He, P. Wu, Post-synthesis treatment gives highly stable siliceous zeolites through the isomorphous substitution of silicon for germanium in germanosilicates. *Angew. Chemie - Int. Ed.* **53**, 1355–1359 (2014).
 120. S. Krijnen, P. Sánchez, B. T. F. Jakobs, J. H. C. Van Hooff, A controlled post-synthesis route to well-defined and active titanium Beta epoxidation catalysts. *Microporous mesoporous Mater.* **31**, 163–173 (1999).
 121. M. M. Diallo, J. Mijoin, S. Laforge, Y. Pouilloux, Preparation of Fe-BEA zeolites by isomorphous substitution for oxidehydration of glycerol to acrylic acid. *Catal. Commun.* **79**, 58–62 (2016).
 122. J. Gao, M. Liu, X. Wang, X. Guo, Characterization of Ti-ZSM-5 prepared by isomorphous substitution of B-ZSM-5 with TiCl₄ and its performance in the hydroxylation of phenol. *Ind. Eng. Chem. Res.* **49**, 2194–2199 (2010).
 123. N. Sapawe, A. A. Jalil, S. Triwahyono, S. H. Adam, N. F. Jaafar, M. A. H. Satar, Isomorphous substitution of Zr in the framework of aluminosilicate HY by an electrochemical method: Evaluation by methylene blue decolorization. *Appl. Catal. B Environ.* **125**, 311–323 (2012).

124. W. N. P. van der Graaff, G. Li, B. Mezari, E. A. Pidko, E. J. M. Hensen, Synthesis of Sn-Beta with Exclusive and High Framework Sn Content. *ChemCatChem*. **7**, 1152–1160 (2015).
125. P. Wu, T. Tatsumi, T. Komatsu, T. Yashima, A novel titanosilicate with MWW structure. I. Hydrothermal synthesis, elimination of extraframework titanium, and characterizations. *J. Phys. Chem. B*. **105**, 2897–2905 (2001).
126. C. R. Bayense, J. H. C. Van Hooff, J. W. De Haan, L. J. M. de Ven, A. P. M. Kentgens, Introduction of gallium in HZSM5 and HY zeolites by post-synthesis treatment with trimethylgallium. *Catal. Letters*. **17**, 349–361 (1993).
127. S. Han, K. D. Schmitt, S. E. Schramm, P. T. Reischman, D. S. Shihabi, C. D. Chang, Isomorphous substitution of boron into zeolites ZSM-5 and Y with aqueous NH₄BF₄. *J. Phys. Chem.* **98**, 4118–4124 (1994).
128. Y. Oumi, T. Manabe, H. Sasaki, T. Inuzuka, T. Sano, Preparation of Ti incorporated y zeolites by a post-synthesis method under acidic conditions and their catalytic properties. *Appl. Catal. A Gen.* **388**, 256–261 (2010).
129. M.-T. Nechita, G. Berlier, G. Ricchiardi, S. Bordiga, A. Zecchina, New precursor for the post-synthesis preparation of Fe-ZSM-5 zeolites with low iron content. *Catal. Letters*. **103**, 33–41 (2005).
130. S. Dzwigaj, T. Shishido, State of Chromium in CrSiBEA Zeolite Prepared by the Two-Step Postsynthesis Method: XRD, FTIR, UV- Vis, EPR, TPR, and XAS Studies. *J. Phys. Chem. C*. **112**, 5803–5809 (2008).
131. L. Burel, N. Kasian, A. Tuel, Quasi All-Silica Zeolite Obtained by Isomorphous Degermanation of an As-Made Germanium-Containing Precursor. *Angew. Chemie Int. Ed.* **53**, 1360–1363 (2014).
132. R. Mokaya, Post-synthesis grafting of Al onto MCM-41. *Chem. Commun.*, 2185–2186 (1997).
133. M. F. Borin, T. Da Silva, R. F. Felisbino, D. Cardoso, Synthesis of TS-1 molecular sieves using a new Ti source. *J. Phys. Chem. B*. **110**, 15080–15084 (2006).
134. M. M. Diallo, S. Laforge, Y. Pouilloux, J. Mijoin, Highly Efficient Dehydration of Glycerol to Acrolein Over Isomorphously Substituted Fe-MFI Zeolites. *Catal. Letters*. **148**, 2283–2303 (2018).
135. F. Dubray, S. Moldovan, C. Kouvatas, J. Grand, C. Aquino, N. Barrier, J. P. Gilson, N. Nesterenko, D. Minoux, S. Mintova, Direct Evidence for Single Molybdenum Atoms Incorporated in the Framework of MFI Zeolite Nanocrystals. *J. Am. Chem. Soc.* **141**, 8689–8693 (2019).
136. A. K. Patra, A. Dutta, M. Pramanik, M. Nandi, H. Uyama, A. Bhaumik, Synthesis of hierarchical mesoporous Mn-MFI zeolite nanoparticles: A unique architecture of heterogeneous catalyst for the aerobic oxidation of thiols to disulfides.

- ChemCatChem*. **6**, 220–229 (2014).
137. V. L. Sushkevich, A. Vimont, A. Travert, I. I. Ivanova, Spectroscopic Evidence for Open and Closed Lewis Acid Sites in ZrBEA Zeolites. *J. Phys. Chem. C*. **119**, 17633–17639 (2015).
 138. J. H. Yun, R. F. Lobo, Catalytic dehydrogenation of propane over iron-silicate zeolites. *J. Catal.* **312**, 263–270 (2014).
 139. G. L. Wang, W. Wu, W. Zan, X. F. Bai, W. J. Wang, X. Qi, O. V. Kikhtyanin, Preparation of Zn-modified nano-ZSM-5 zeolite and its catalytic performance in aromatization of 1-hexene. *Trans. Nonferrous Met. Soc. China (English Ed.)*. **25**, 1580–1586 (2015).
 140. X. Su, G. Wang, X. Bai, W. Wu, L. Xiao, Y. Fang, J. Zhang, Synthesis of nanosized HZSM-5 zeolites isomorphously substituted by gallium and their catalytic performance in the aromatization. *Chem. Eng. J.* **293**, 365–375 (2016).
 141. J. Grand, S. N. Talapaneni, A. Vicente, C. Fernandez, E. Dlb, H. A. Aleksandrov, G. N. Vayssilov, R. Retoux, P. Boullay, J. P. Gilson, V. Valtchev, S. Mintova, One-pot synthesis of silanol-free nanosized MFI zeolite. *Nat. Mater.* **16**, 1010–1015 (2017).
 142. M. Moliner, State of the art of Lewis acid-containing zeolites: lessons from fine chemistry to new biomass transformation processes. *Dalt. Trans.* **43**, 4197–4208 (2014).
 143. M. Moliner, Y. Román-Leshkov, M. E. Davis, Tin-containing zeolites are highly active catalysts for the isomerization of glucose in water. *Proc. Natl. Acad. Sci.* **107**, 6164–6168 (2010).
 144. J. P. M. Niederer, W. F. Hölderich, Oxidation capabilities of BEA isomorphously substituted with molybdenum, vanadium and titanium: an explorative study. *Appl. Catal. A Gen.* **229**, 51–64 (2002).
 145. C.-C. Chang, Z. Wang, P. Dornath, H. J. Cho, W. Fan, Rapid synthesis of Sn-Beta for the isomerization of cellulosic sugars. *Rsc Adv.* **2**, 10475–10477 (2012).
 146. C. T. W. Chu, C. D. Chang, Isomorphous substitution in zeolite frameworks. 1. Acidity of surface hydroxyls in [B]-, [Fe]-, [Ga]-, and [Al]-ZSM-5. *J. Phys. Chem.* **89**, 1569–1571 (1985).
 147. J. C. der Waal, M. S. Rigutto, H. Van Bekkum, Zeolite titanium beta as a selective catalyst in the epoxidation of bulky alkenes. *Appl. Catal. A Gen.* **167**, 331–342 (1998).
 148. J. C. van der Waal, H. van Bekkum, Zeolite titanium beta: A versatile epoxidation catalyst. Solvent effects. *J. Mol. Catal. A Chem.* **124**, 137–146 (1997).
 149. M. Boronat, A. Corma, M. Renz, P. M. Viruela, Predicting the activity of single

- isolated Lewis acid sites in solid catalysts. *Chem. Eur. J.* **12**, 7067–7077 (2006).
150. Y. Zhu, G. Chuah, S. Jaenicke, Chemo- and regioselective Meerwein–Ponndorf–Verley and Oppenauer reactions catalyzed by Al-free Zr-zeolite beta. *J. Catal.* **227**, 1–10 (2004).
 151. H. Y. Luo, D. F. Consoli, W. R. Gunther, Y. Román-Leshkov, Investigation of the reaction kinetics of isolated Lewis acid sites in Beta zeolites for the Meerwein–Ponndorf–Verley reduction of methyl levulinate to γ -valerolactone. *J. Catal.* **320**, 198–207 (2014).
 152. J. D. Lewis, S. de Vyver, Y. Román-Leshkov, Acid–base pairs in Lewis acidic zeolites promote direct aldol reactions by soft enolization. *Angew. Chemie Int. Ed.* **54**, 9835–9838 (2015).
 153. J. D. Lewis, S. de Vyver, A. J. Crisci, W. R. Gunther, V. K. Michaelis, R. G. Griffin, Y. Román-Leshkov, A Continuous Flow Strategy for the Coupled Transfer Hydrogenation and Etherification of 5-(Hydroxymethyl) furfural using Lewis Acid Zeolites. *ChemSusChem.* **7**, 2255–2265 (2014).
 154. J. D. Lewis, M. Ha, H. Luo, A. Faucher, V. K. Michaelis, Y. Román-Leshkov, Distinguishing Active Site Identity in Sn-Beta Zeolites Using ^{31}P MAS NMR of Adsorbed Trimethylphosphine Oxide. *ACS Catal.* **8**, 3076–3086 (2018).
 155. A. Zheng, S.-B. Liu, F. Deng, ^{31}P NMR chemical shifts of phosphorus probes as reliable and practical acidity scales for solid and liquid catalysts. *Chem. Rev.* **117**, 12475–12531 (2017).
 156. D. Gleeson, G. Sankar, C. R. A. Catlow, J. M. Thomas, G. Spanó, S. Bordiga, A. Zecchina, C. Lamberti, The architecture of catalytically active centers in titanosilicate (TS-1) and related selective-oxidation catalysts. *Phys. Chem. Chem. Phys.* **2**, 4812–4817 (2000).
 157. R. Bermejo-Deval, R. S. Assary, E. Nikolla, M. Moliner, Y. Román-Leshkov, S.-J. Hwang, A. Palsdottir, D. Silverman, R. F. Lobo, L. A. Curtiss, others, Metalloenzyme-like catalyzed isomerizations of sugars by Lewis acid zeolites. *Proc. Natl. Acad. Sci.* **109**, 9727–9732 (2012).
 158. D. H. Wells Jr, W. N. Delgass Jr, K. T. Thomson, Evidence of defect-promoted reactivity for epoxidation of propylene in titanosilicate (TS-1) catalysts: a DFT study. *J. Am. Chem. Soc.* **126**, 2956–2962 (2004).
 159. C. B. Khouw, M. E. Davis, Catalytic activity of titanium silicates synthesized in the presence of alkali-metal and alkaline-earth ions. *J. Catal.* **151**, 77–86 (1995).
 160. S. Bordiga, F. Bonino, A. Damin, C. Lamberti, Reactivity of Ti (iv) species hosted in TS-1 towards H_2O_2 – H_2O solutions investigated by ab initio cluster and periodic approaches combined with experimental XANES and EXAFS data: a review and new highlights. *Phys. Chem. Chem. Phys.* **9**, 4854–4878 (2007).

161. V. L. Sushkevich, D. Palagin, I. I. Ivanova, With open arms: open sites of ZrBEA zeolite facilitate selective synthesis of butadiene from ethanol. *ACS Catal.* **5**, 4833–4836 (2015).
162. P. Wolf, M. Valla, A. J. Rossini, A. Comas-Vives, F. Núñez-Zarur, B. Malaman, A. Lesage, L. Emsley, C. Copéret, I. Hermans, NMR Signatures of the Active Sites in Sn- β Zeolite. *Angew. Chemie Int. Ed.* **53**, 10179–10183 (2014).
163. G. Yang, E. A. Pidko, E. J. M. Hensen, Structure, stability, and Lewis acidity of mono and double Ti, Zr, and Sn framework substitutions in BEA zeolites: a periodic density functional theory study. *J. Phys. Chem. C.* **117**, 3976–3986 (2013).
164. Y.-P. Li, M. Head-Gordon, A. T. Bell, Analysis of the reaction mechanism and catalytic activity of metal-substituted beta zeolite for the isomerization of glucose to fructose. *Acs Catal.* **4**, 1537–1545 (2014).
165. K. A. Jørgensen, Transition-metal-catalyzed epoxidations. *Chem. Rev.* **89**, 431–458 (1989).
166. P. S. Raghavan, S. Kannan, A. A. Belhekar, Synthesis and characterization of molybdenum containing silicalite-2 (MoS-2) molecular sieve (1997).
167. P. S. Raghavan, V. Ramaswamy, T. T. Upadhya, A. Sudalai, A. V Ramaswamy, S. Sivasanker, Selective catalytic oxidation of thioethers to sulfoxides over Mo-silicalite-1 (MoS-1) molecular sieves. *J. Mol. Catal. A Chem.* **122**, 75–80 (1997).
168. P.-S. E. Dai, J. H. Lunsford, Catalytic properties of molybdenum-containing zeolites in epoxidation reactions: I. Catalysts preparation and characterization. *J. Catal.* **64**, 173–183 (1980).
169. A. Tavolaro, Thermal characterization of the metal-silicalites obtained from aqueous nonalkaline fluoride gels. *J. Therm. Anal. Calorim.* **47**, 171–179 (1996).

Chapter II: Experimental Section

II.1. Materials

All samples were prepared using the following chemicals without further purification: tetraethyl orthosilicate (TEOS, 98 %, Aldrich), tetra n-propylammonium hydroxide (TPAOH, 20 wt. % in water solution, Alfa Aesar), sodium molybdate dehydrated ($\text{Na}_2\text{MoO}_4, 2\text{H}_2\text{O}$, 98 %, Alfa Aesar), ammonium chloride (NH_4Cl , 99.5 %, Alfa Aesar), and aluminum nitrate nonahydrated ($\text{Al}(\text{NO}_3)_3, 9\text{H}_2\text{O}$, 97%, prolabo). Double distilled water was used in all synthesis steps and post synthesis treatments.

II.2. Synthesis

All the main synthesis procedures are summarized in Scheme 1.

The direct synthesis procedure corresponds to a classical direct synthesis approach in which Mo source is introduced alongside other reactants in the precursor gel suspension prior crystallization (sample Mo-MFI (D)). In this procedure, the molybdenum salt is introduced alongside TEOS, TPAOH, and water prior aging. The presence of alkali cation is required, which is usually done by using a sodium molybdate salt as the Mo and Na source.

The staged synthesis procedure corresponds to a direct synthesis approach in which the metal addition is delayed (samples Mo-MFI (S5) and (S48)). The Mo-free precursor gel suspension (composed of TEOS, TPAOH and water) is aged and is subjected to hydrothermal treatment for a variable time (pre-crystallization step), before Mo source is added into the gel (introduction of sodium molybdate). Then, the gel resumes its hydrothermal treatment. This novel synthesis method is just on the boundaries between state-of-the-art direct synthesis and conventional post synthesis approaches.

The so-called hydrothermal post synthesis procedure is a prolongation of the staged synthesis in which the two steps are completely separated. This hydrothermal post synthesis procedure was applied on purely siliceous (Mo-MFI (P) sample) and Al containing MFI frameworks (Mo-ZSM-5 (P) sample). In this procedure, Mo-free silicalite-1 and ZSM-5 zeolite is first synthesized, separated from the gel suspension and purified (washed and calcined). Then, the Mo addition is performed in a new post synthesis treatment in which the zeolite is hydrothermally treated in the presence of the Mo metal source (solution of sodium molybdate). The resulting zeolite is then washed so as to

remove any possible unreacted Mo species that would tend to form non framework Mo species during the drying step.

The synthesis of Mo impregnated on MFI zeolite is not discussed in this section since (i) it does not consists in framework modification of the MFI structure and thus is not really part of the PhD thesis work, only serving as a reference sample, and (ii) the impregnation procedure is fully described and compared to framework modification of the MFI structure in Chapter 3.

II.2.1. Direct synthesis - Synthesis of Mo-MFI (D) sample:

In a 125 mL polypropylene bottle, was added the following molar gel composition: 1 SiO₂ : 0.28 TPAOH : 40 H₂O : 0.08 MoO₃. The resulting clear suspension was stirred for 1 h at room temperature, and further hydrolyzed for 18 h on an orbital shaker (aging step). Hydrothermal treatment was performed at 90 °C for 48 h; the as prepared zeolite suspension was then separated using high speed centrifugation (20,000 rpm) and further washed with water until a pH of 7 was reached. The harvested zeolite was dried at 80 °C overnight, and calcined (550 °C, 5h). The H-form of the zeolite was then retrieved by washing two times the zeolite powder with NH₄Cl (0.2 M, 1h), then once with water, before being dried at 80 °C overnight and calcined again (550 °C, 5h). The as obtained sample is named Mo-MFI (D), with “D” coming from “Direct synthesis”.

II.2.2. Staged synthesis - Synthesis of Mo-MFI (S5) and Mo-MFI (S48) samples:

In a 125 mL polypropylene bottle, the following molar gel composition was added: 1 SiO₂ : 0.28 TPAOH : 40 H₂O. The resulting clear suspension was stirred for 1 h at room temperature, and further hydrolyzed for 18 h on an orbital shaker (aging step). Hydrothermal treatment was then performed at 90 °C for 5 h for sample Mo-MFI (S5), and for 48h for sample Mo-MFI (S48). To the as retrieved suspension (amorphous suspension after 5 h, and fully crystalline silicalite-1 after 48h) is added the sodium molybdate diluted in a minimum volume of water (0.08 MoO₃ : 1 SiO₂). The two gel suspensions were then stirred 1 h at room temperature before hydrothermal treatment was allowed to be resumed for an additional 43 h in case of sample Mo-MFI (S5) and 24 h in case of sample Mo-MFI (S48). The as retrieved sample was then purified and washed with water using high speed centrifugation (20,000 rpm) until a pH value of 7 was reached. The harvested crystals were dried at 80 °C overnight, calcined (550 °C, 5h), before H-form was retrieved by washing the calcined crystals twice with NH₄Cl (0.2 M, 1h). The as-obtained samples are washed once with water, dried overnight (80 °C) and calcined again (550 °C, 5h). The as-prepared samples were named Mo-MFI (S5)

and Mo-MFI (S48); “S” for “Staged synthesis”, and respectively “5” and “48” for the delay before metal addition after the start of the initial hydrothermal treatment step, given in hours.

II.2.3. Hydrothermal post-synthesis - Synthesis of Mo-MFI (P) sample:

Purely siliceous Si-MFI was prepared using the following procedure; in a 125 mL polypropylene bottle was added the following gel composition: 1 SiO₂ : 0.40 TPAOH : 40 H₂O. The suspension was stirred 1h at room temperature and placed on an orbital shaker for 18 h, at room temperature (aging step). The suspension was then subjected to hydrothermal treatment at 90 °C for 48 h. The silicalite-1 crystals were then harvested and purified using high speed centrifugation (20,000 rpm) and water washing steps, until the pH value reached 7. The crystals were then dried overnight (80 °C), and calcined (550 °C, 5h).

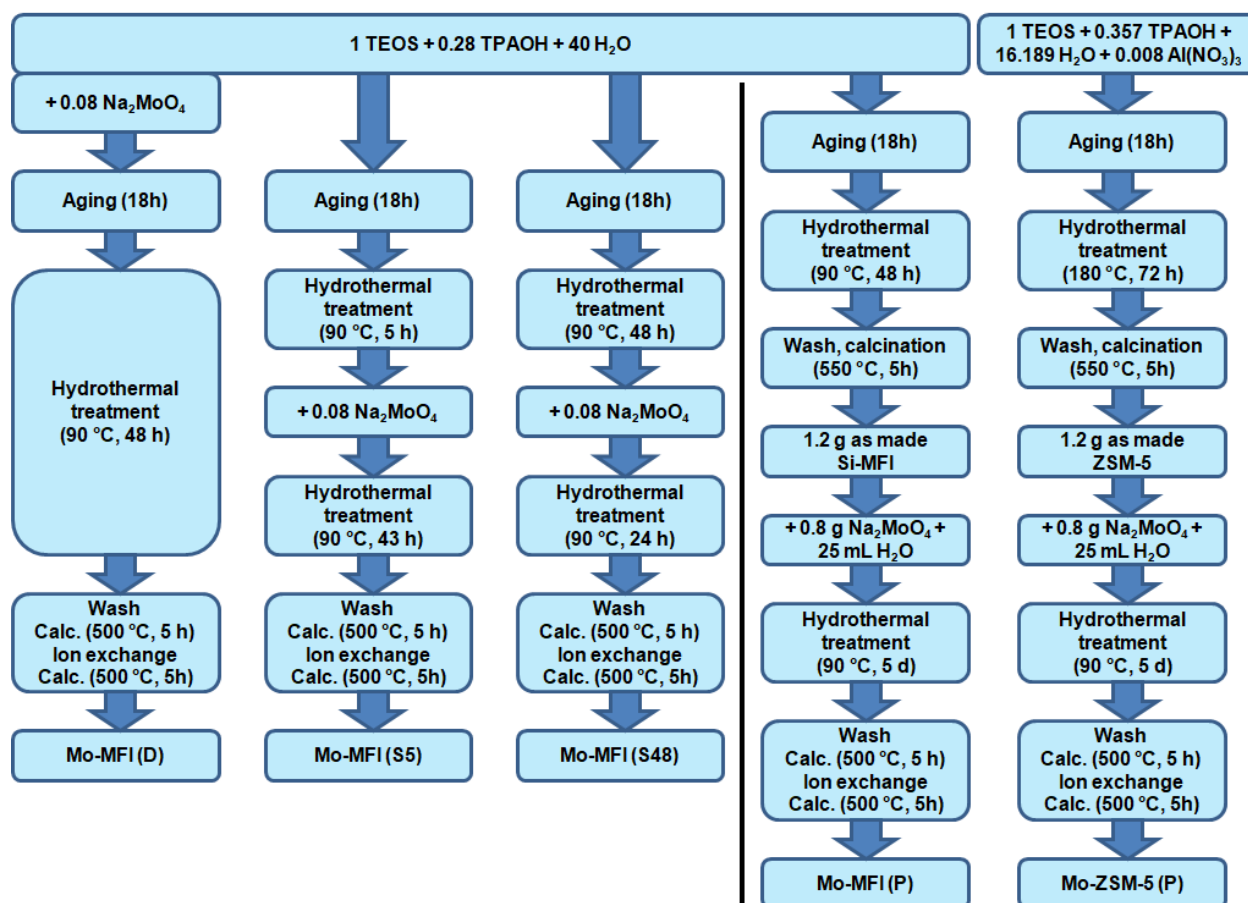
Then, 1.2 g of the as-prepared purely siliceous silicalite-1 was treated with 0.8 g Na₂MoO₄ diluted in 25 mL H₂O. The corresponding suspension was hydrothermally treated 5 days at 90 °C, before being purified with high speed centrifugation and water washing steps, until no molybdenum species is present in the spent water (as determined by colorimetry using H₂O₂: if Mo is present, the color-free liquid phase will turn deep red in presence of H₂O₂). The sample is then dried overnight (80 °C), calcined (550 °C, 5 h), ion exchanged (H-form of the sample is retrieved by treating the crystals twice with 0.2 M NH₄Cl followed by one water washing step), dried overnight (80 °C), and calcined again (550 °C, 5h). The as obtained sample is called Mo-MFI (P), “P” standing for “Post synthesis treatment”.

II.2.4. Hydrothermal post-synthesis - Synthesis of Mo-ZSM-5 (P) sample:

ZSM-5 was prepared from the following molar gel composition: 1 SiO₂ : 0.357 TPAOH : 16.189 H₂O : 0.008 Al(NO₃)₃. The aged suspension (1h under magnetic stirring, 18h on orbital shaker) was transferred in Teflon lined autoclaves and hydrothermally treated at 180 °C for 72 h. The crystals were then harvested and purified using high speed centrifugation (20,000 rpm) and water washing steps, until a pH value of 7 is reached. The sample is then dried overnight (80 °C) and calcined (550 °C, 5h).

Then, 1.2 g of the as-prepared ZSM-5 (Si/Al=110 based on ICP measurement) was treated with 0.8 g Na₂MoO₄ diluted in 25 mL H₂O. The corresponding suspension was hydrothermally treated 5 days at 90 °C, before being purified with high speed centrifugation and water washing steps, until no molybdenum species is present in the

spent water (as determined by colorimetry using H_2O_2 as described above). The sample is then dried overnight ($80\text{ }^\circ\text{C}$), calcined ($550\text{ }^\circ\text{C}$, 5 h), ion exchanged (H-form of the sample is retrieved by treating the crystals twice with $0.2\text{ M NH}_4\text{Cl}$ followed by one water washing step), dried overnight ($80\text{ }^\circ\text{C}$), and calcined again ($550\text{ }^\circ\text{C}$, 5h). The obtained sample is called Mo-ZSM-5 (P), “P” standing for “Post synthesis treatment”.



Scheme 1. Summary of synthesis procedure for Mo-MFI (D), Mo-MFI (S5), Mo-MFI (S48), Mo-MFI (P), and Mo-ZSM-5 (P) samples. “Calc.” corresponds to calcinations, “ion exchange” designates the washing step of the samples with NH_4Cl (0.2 M). All compositions are molar compositions unless indicated otherwise.

II.2.5. Reference samples

A reference Mo-free silicalite-1 (Si-MFI) is prepared by interrupting the synthesis process described above in II.2.3. after the Si-MFI crystals are retrieved (before starting the Mo treatment, 2nd paragraph of II.2.3.).

Similarly, a reference Mo-free ZSM-5 (or Al-MFI) is prepared by interrupting the synthesis process described above in II.2.4. after the ZSM-5 crystals are retrieved (before starting the Mo treatment, 2nd paragraph of II.2.4.).

The corresponding Mo impregnated samples (Mo impregnated on silicalite-1, and Mo impregnated on ZSM-5) can be prepared by performing wet impregnation using ammonium molybdate $(\text{NH}_4)_6\text{Mo}_7\text{O}_{24}$.

These samples were prepared for comparison purposes only.

II.3. Main characterization methods

Powder X-Ray diffraction (XRD) was used as a mean to access valuable information regarding the crystalline phase of samples. The technique is based on the diffraction patterns of X-rays by the atoms of a given sample, usually performed in the conventional Bragg-Brentano geometry ($\theta - 2\theta$). This characterization method is allowing to investigate the crystalline structure of a framework with long range order of repetition through space. It consists in the emission of X-ray photons onto the solid analyzed, which is going to be elastically diffused, generating interferences as a function of the symmetry of the sample. The more the solid is ordered, the more interference will be generated. The photons are emitted toward the solid and are deflected in specific directions depending on the crystal framework structure, and the photon wavelength. By measuring the angles and intensities of the diffracted photons, it is possible to gain insight in the geometry of the framework structure (size of unit cell, symmetries). It is a powerful tool to examine materials in a long-range order, and to extract first important information such as the sample's space group, and with the help of a fitting procedure called LeBail profile refinement, its unit cell parameters. The size of crystallites can also be determined from the PXRD patterns. In a practical point of view, this technique is used first to determine the crystalline structure/phase of a sample. Indeed, each zeolite phase have different crystalline structure, resulting in different and unique PXRD patterns. Additionally, fine details can be extracted too, such as symmetry transitions, presence of additional crystalline phase (like metal oxides, or changes of unit cell parameters and volume.

Nuclear magnetic resonance (NMR) spectroscopy is an extremely complete characterization tool that allows to examine materials in a small-range order. It is from that point of view complementary to XRD. The NMR technique is based on the spectroscopy of the Zeeman effect applied to nuclear spins. The NMR technique is based on the observation of the NMR phenomena, which is produced by atoms with spins value different from 0, placed in an external magnetic field, and excited with a radio frequency electromagnetic wave corresponding to the energies of the different

state available for the spin of the studied nuclei (called Larmor frequency of a given nucleus). Each isotope has a different gyro magnetic moment, so the NMR analysis allows to observe each isotope independently, since their Larmor frequency differ. However, the precise Larmor resonance frequencies are not only a function of the nuclei, but also of its near environment. The interaction with the environment is of electrical (in the case of quadrupolar interaction, with spin value other than 1/2) and/or magnetic nature (coupling and chemical shift). The NMR technique is consequently a powerful tool for the characterization of the local environment of each NMR-active nucleus present in a given sample. Indeed, the technique is highly sensitive to local interactions such as chemical bonding, molecular conformation, inter-atomic distances, magnetic and/or electric interactions between nucleus, geometry, oxidation state, etc... The solid-state NMR corresponds to the NMR technique applied to solid samples. For all experiments, rotation around the magic angle (MAS, 54.74°) was performed so as to average the orientation-dependent interactions (dipolar, quadrupolar, and chemical shift anisotropy), for the acquired spectra to be interpretable. In the framework of this thesis, 4 isotopes are investigated: ^{29}Si , ^{27}Al , ^1H , and ^{31}P . The NMR of ^{95}Mo was aborted due to high quadrupolar interactions, low natural abundance, low sensitivity, and low Larmor frequency. ^{29}Si nuclei however, has a $\frac{1}{2}$ spin and is ideal for NMR study, although its sensitivity and natural abundance are fairly low, requiring time-consuming acquisitions. ^{27}Al nuclei use in NMR is common since it has the advantage of having 100 % abundance, and fairly good sensitivities, but its spin is $\frac{5}{2}$, bringing quadrupolar interactions. Of course, the ^1H NMR is the most common nuclei to be studied, with its ideal high sensitivity, $\frac{1}{2}$ spin, and its high natural abundance, combined with high Larmor frequency. Then, the NMR of ^{31}P nuclei was used to investigate the state of phosphorous probe molecules in zeolite samples. Indeed, ^{31}P nuclei is 100% abundant, has high sensitivity, and has spin $\frac{1}{2}$ so that it is easy to analyze using NMR, but most importantly, it has a very wide chemical shift range, allowing to discriminate even the slightest differences of local environment of each ^{31}P nuclei in a given probe molecule, adsorbed on a sample. Its use as a probe molecule consequently makes full use of its NMR properties. Overall, ^1H MAS NMR was mostly used to characterize hydroxyls groups in zeolites (silanols, or Brønsted sites), while ^{29}Si MAS NMR was used to characterize the coordination of Si atoms and the local homogeneity of the framework. ^{27}Al MAS NMR was used on Al containing samples, so as to determine the coordination of Al atoms (tetrahedral – in the framework, or octahedral – out of the zeolite framework). Additionally, ^{31}P MAS NMR was used for the characterization of the trimethylphosphine oxide probe molecule (TMPO), allowing to probe the acid sites of the zeolite samples, and to distinguish metal Lewis centers, from silanols and Brønsted acid sites. Following, is a table summarizing the main NMR properties of NMR-active nucleus of interest for this PhD thesis.

Table 1. Main NMR properties of the nucleus analyzed in the course of the present PhD thesis.

Isotope	Spin	Natural abundance (%)	Molar receptivity rel. ^1H	Larmor Frequency at 11.7467 T (in MHz)
^1H	1/2	99.9885	1	500.130
^{27}Al	5/2	100.0	2.07e-1	130.318
^{29}Si	1/2	4.685	7.86e-3	99.362
^{31}P	1/2	100.0	6.65e-2	202.457

Infra red spectroscopy (IR) is a spectroscopic technique allowing to investigate the vibration modes of different molecular bonds in a sample, through the absorption of IR light (measured in absorbance as a function of wavelength) by the sample under investigation. The zeolite powders were first pelletized into self-supported wafers (1 t/cm, 2 cm²) prior analysis in IR. This technique is focused on vibration modes of chemical bonds, and as a consequence, it gives valuable information on the nature of bonds present in a given sample. In the case of zeolite frameworks, the main vibrations will be framework vibrations of Si-O-Si units, and Si-O-Al units in case Al is present. These vibrations are high intensity (due to their number), and as a consequence, their absorbance is saturated when measured on self-supported wafers. For this precise case, it was therefore necessary to dilute the sample in KBr (which is transparent in IR), so as to form a self supported wafer comprising around 0.5 mg of zeolite for 100 mg of KBr. However, silanol species (Si-OH groups) and acid sites (Al-OH groups) are easily observed on undiluted self-supported wafers. In addition, IR spectroscopy can be used with probe molecules interacting with the zeolite sample under investigation. Indeed, each adduct of a probe molecule chemisorbed on zeolite surface sites will display altered vibration modes, that will translate into modification of the frequency of IR light absorbance. The frequency for absorbance of a chemical bond vibration mode from a free probe molecule will be different from the same vibration mode of the chemisorbed probe molecule. Thus, characterization of zeolite surface is easily achievable using IR technique combined with the use of different probe molecules such as pyridine, deuterated acetonitrile, CO, NO₂, ... However, the technique has poor quantification since absorption of IR light is highly dependent on absorption coefficients that are often difficult to estimate with precision.

Raman spectroscopy is a characterization technique relying on the inelastic scattering of monochromatic light on mater. Raman spectroscopy is also based on sample's chemical bonds vibration modes (as in IR), and thus, can provide structural information as well. The frequency of the monochromatic light source that is used can be changed so as to enhance given transitions in the material of interest. The technique is powerful in proving the presence of metal oxide species, and in seeing fine details in

the framework vibration modes since no sample dilution is required (as in the case of IR). Its comparison with IR data is therefore of first interest. In the course of the PhD thesis, this technique was mostly used to check the presence (or absence) of molybdenum oxide species, and as a way to observe framework vibration modes related with the presence of Mo as framework species in the zeolite. However, the technique does not allow for quantification, and only qualitative characterization is possible. In addition, its detection limits are highly dependent upon measurement conditions (especially laser wavelength, power, and integration time), and are also sample dependent (influence of sample/matrix polarity on the Raman scattering cross-section of the analyte).

Scanning electron microscopy (SEM) and transmission electron microscopy (TEM) are both imaging techniques relying on the interaction of electrons with matter. Zeolites crystals are dispersed with ethanol on a holey carbon grid prior TEM measurement, or dispersed on a carbon tape and subjected to metal (Pt/Pd) vapor deposition prior SEM measurement. In these techniques, electrons are directed with electromagnetic lenses, and a 2D projection of detected electrons is retrieved. The main difference between SEM and TEM is that SEM detects electrons that are reflected (from the sample) while TEM detects transmitted electrons (going through the sample). The SEM (Scanning Electron Microscopy) is a method of visualisation by reflection of electrons. An electron flow is sent under vacuum on the surface of the sample, generating particles (such as secondary electrons for instance) in response, that we can collect and analyse in order to build a picture out of them. The HRTEM method relies on transmitted electrons going through the sample. Due to the high interaction of electron with matter, only small sized samples can be analyzed in TEM. Both techniques are complementary, and can be adapted with add-on equipments such as energy dispersive spectroscopy (EDS) for elemental analysis. TEM resolution goes down to less than 1 Å while SEM resolution only goes down to 10-20 nm, making TEM particularly efficient for detailed analysis of samples, in an atomic/subnanometric level. Regarding TEM especially, it is possible to combine 2D views taken at different tilt angle of the sample holder, to reconstruct a 3D picture of a sample. Two main picture acquisition methods exist on TEM: the picture mode, and the diffraction mode in which electrons diffracted by the crystal lattice are detected. In this PhD thesis work, TEM was mostly used for detailed analysis of Mo containing samples, and especially the high resolution HAADF (dark field annular imaging) was used in combination with EDS to probe metal species size and dispersion. SEM on the other hand was mostly used for morphology investigation, and crystals size determination.

Thermo gravimetric (TG) analysis is a thermal analysis in which changes in physical and chemical properties of a material are measured as a function of increasing temperature (constant heating rate), or as a function of time (constant temperature or

weight loss). In a TG analysis, the sample is constantly weighed during heating. TG can bring information about second order physical transition (vaporization, sublimation, absorption, desorption, adsorption, chemisorptions, desolvation, decomposition, ...). It is a powerful method for evaluating the amount of coke on a catalyst, or to characterize a metal oxide, which is changing its crystalline form at a given temperature for instance. It is also a way of evaluating the thermal resistance of a material.

The N_2 sorption is a technique allowing to evaluate textural properties of a given zeolite sample, and to determine its porosity. The samples are activated prior to measurement at 500 °C. Then, nitrogen adsorption and desorption isotherms are recorded at 77 K. Based on modelisation of obtain isotherms, information on pore geometry, porosity, pore size distribution, surface area, or adsorption mechanisms (BET, Langmuir) can be easily extracted. The shape of the adsorption-desorption isotherms can be of type I, II, III, IV, V, or VI depending if the sample is: (i) microporous, (ii) non porous or macroporous, (iii) non porous or macroporous with weak interaction with N_2 , (iv) mesoporous with capillary condensation occurring, (v) mesoporous with weak interactions with N_2 , and (vi) a porous solid in which adsorbed layers are formed one after the other respectively.

The inductively coupled plasma analysis combined with mass spectrometry (ICP-MS) technique was used to assess the elemental compositions of zeolite samples. The zeolite samples (50 mg) were first digested using a mixture of aqua regia ($HCl+HNO_3$) and hydrofluoric acid (HF), in closed PTFE vessels at 90 °C. The HF is then neutralized using boric acid (H_3BO_4). The as obtained samples are diluted in a jauged volume of 1000 mL prior analysis. The ICP analysis consists in the atomization/ionisation of the elements contained in the analyte solution using high energy Ar-plasma. The ionized elements are then accelerated in a mass spectrometer, allowing the acquisition of the mass spectrum of the analyte solution. This analytical method is efficient in determining with precision low amount of most of the isotopes in a given sample. However, the precision of the equipment is highly dependent on possible environmental contaminations of the samples, and on the efficiency of the sample digestion process.

The diffusion light scattering technique (DLS) can be used so as to evaluate the particle size distribution of a liquid suspension (water suspension of zeolites nano-particles in the case of this PhD thesis). A laser light is diffused by going through a colloidal suspension. Analysis of this diffusion allows to obtain the average size of the particles in suspension, and the dispersion around this averaged value.

II.3. Examples

All samples prepared following the direct synthesis approach (Mo-MFI (D)), the staged synthesis approach (Mo-MFI (S5) and Mo-MFI (S48)), and the hydrothermal post synthesis approach (Mo-MFI (P) and Mo-ZSM-5 (P)) are investigated using a set of characterization techniques so as to evaluate the efficiency of the isomorphous substitution.

First of all, the crystallinity of all samples was evaluated using XRD (Figure 1). All samples displays well resolved and highly crystalline MFI structure with monoclinic symmetry (as evidenced by the splitted peaks at around 23.30, 23.75, and 24.50 ° 2 θ).¹ No amorphous phase, and no peaks attributed to molybdenum oxide phase were visible, proving the absence of large molybdenum oxide particles. The monoclinic symmetry of the samples indicate the successful molybdenum incorporation, as previously reported in our group.¹ These results were further supported by LeBail profile refinement, where the monoclinic symmetry of all samples was confirmed. In addition, the unit cell volume of all samples was measured, and results are displayed in Table 2. All samples have unit cell volumes exceeding 5350 Å³, while purely siliceous MFI zeolite does have a volume of approximately 5330 Å³ (as measured from a Si-MFI sample prepared according to the exact same procedure as sample Mo-MFI (D), minus the sodium molybdate addition). The ZSM-5 sample used for the synthesis of Mo-ZSM-5 (P) had a unit cell volume of 5359 Å³. The successful isomorphous substitution for all synthesis method is thus confirmed due to the expanded unit cell volumes. Indeed, the volume expansion does originate from the fact that Mo atoms have a higher ionic radius than Si atoms.² As a result, Mo atoms need higher bond length and lower bond angles, and thus, need higher unit cell volume so as to be accommodate in the MFI structure once compared to silicon. In addition, the unit cell volume is even higher when high delay before Mo addition is applied in case of the staged synthesis (Mo-MFI (S48)), and in the case of post synthesis approach (Mo-MFI (P)), which can be attributable to a higher degree of isomorphous substitution for these two approaches, once compared to the direct synthesis approach.^{3,4} The highest unit cell volumes were achieved using the hydrothermal post synthesis methods which yields unit cell volume that are significantly larger by more than 10 Å³ once compared to staged synthesis method. From these results, it is evident that unit cell volume is a function of the synthesis approach used, and that isomorphous substitution is most effective (ie: higher degree of isomorphous substitution) when using post synthesis treatment. In addition, the use of post synthesis approach allowed to prepare Mo containing ZSM-5 material, which is impossible to obtain via direct and staged syntheses since the co-presence of Mo and Al in solution always results in the precipitation of both atoms as aluminium molybdate species, preventing their co-incorporation in the MFI framework. The use of a two steps

approach (post synthesis) solved this issue by preventing Mo from being in direct contact with Al atoms in the liquid phase.

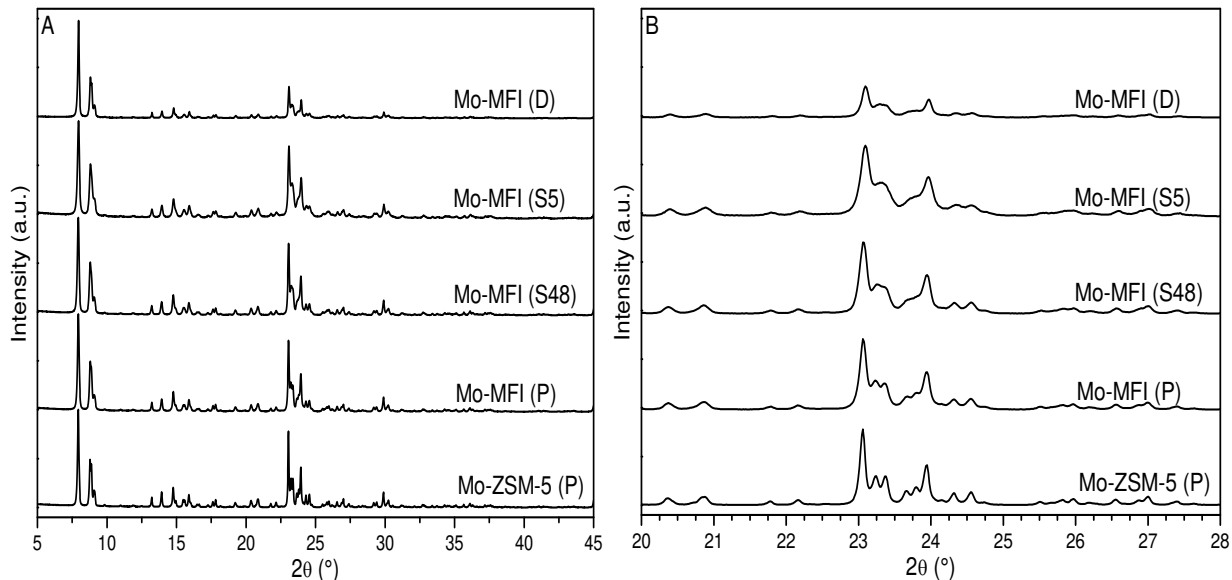


Figure 1. X-Ray diffraction patterns of Mo-MFI (D), Mo-MFI (S5), Mo-MFI (S48), Mo-MFI (P) and Mo-ZSM-5 (P) zeolite samples: (a) from 5 to 45 ° 2 θ , and (b) from 20 to 28 ° 2 θ .

Table 2. Leball profile refinement of Mo-MFI (D), Mo-MFI (S5), Mo-MFI (S48), Mo-MFI (P) and Mo-ZSM-5 (P) zeolite samples. For comparison purposes, is added the Mo-free ZSM-5 and Si-MFI used during the post hydrothermal synthesis of Mo-MFI (P) and Mo-ZSM-5 (P).

Sample	Symmetry	<i>a</i> (Å)	<i>b</i> (Å)	<i>c</i> (Å)	β (°)	Volume (Å ³)	wRp ^a
Mo-MFI (D)	<i>P21/n</i>	19.902	20.121	13.387	90.529	5360.57	5.75
Mo-MFI (S5)	<i>P21/n</i>	19.888	20.118	13.386	90.549	5355.38	3.57
Mo-MFI (S48)	<i>P21/n</i>	19.909	20.136	13.391	90.608	5367.97	4.07
Mo-MFI (P)	<i>P21/n</i>	19.924	20.143	13.399	90.609	5377.11	3.42
Mo-ZSM-5 (P)	<i>P21/n</i>	19.910	20.139	13.392	90.609	5369.27	3.97
Si-MFI	<i>Pnma</i>	19.887	20.058	13.370	90.000	5333.13	5.08
ZSM-5	<i>Pnma</i>	19.904	20.097	13.397	90.000	5359.28	5.87

^a Weight Profile R-factor

The morphology and crystal size of all samples was also evaluated using SEM (Figure 2). The morphology is slightly different between purely siliceous and Al containing zeolite (sample Mo-ZSM-5 (P) due to the fact that the synthesis are very different (temperature, time of synthesis, and gel compositions). All samples displayed spherical particles (average 150 nm in size) that were mostly unaffected by the synthesis method used. However, sample Mo-MFI (D) does possess a much larger particle size once compared to samples prepared using both the staged and the hydrothermal post synthesis treatment. Indeed, the synthesis performed in absence of Mo salt achieves crystals of approximately 150 nm in diameter (similar to what is obtained for staged and post synthesis) while the synthesis of Mo-MFI (D) (direct synthesis) yields crystals of approximately 300 nm in diameter. This is a consequence of the presence of Mo in the precursor gel suspension that is interacting with the nucleation and crystallization process. By performing staged and post synthesis approaches, this interaction was suppressed, allowing to achieve isomorphous substitution in crystals that are two times smaller in diameter. However, no significant difference in morphology could be observed between staged synthesis and post synthesis treatments. The reduced particle size for Mo containing MFI crystals in case of staged and post synthesis approaches is highly desirable for catalytic application where diffusion limitations might be an issue to be addressed.⁵

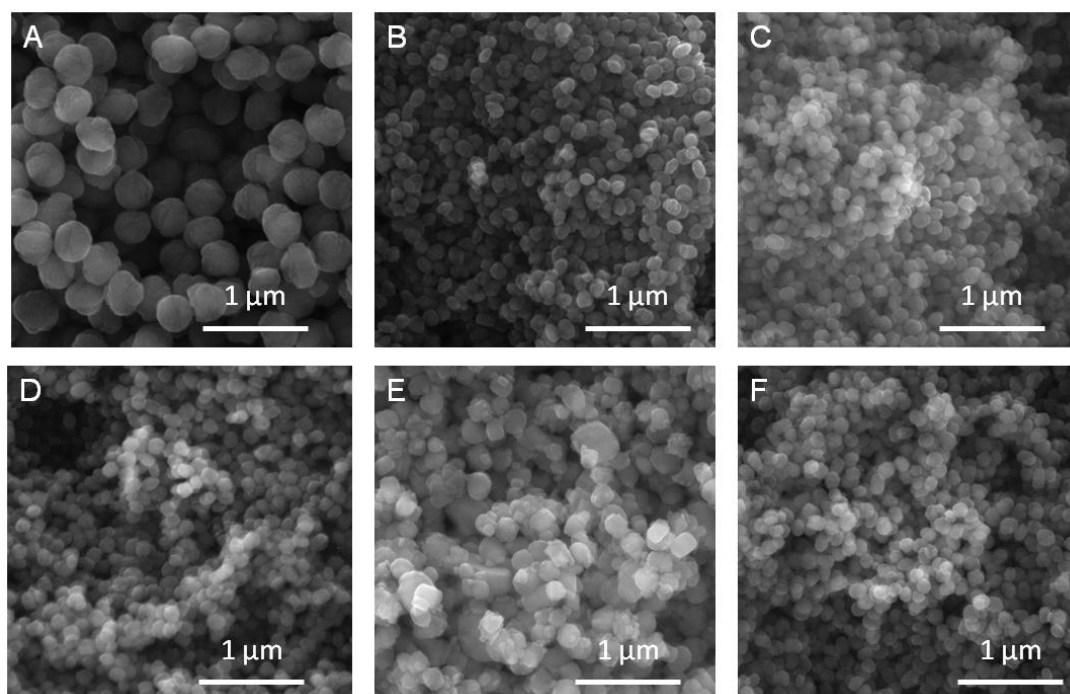


Figure 2. SEM images of (A) Mo-MFI (D), (B) Mo-MFI (S5), (C) Mo-MFI (S48), (D) Mo-MFI (P), and (E) Mo-ZSM-5 (P) samples. The SEM of Mo-free Si-MFI (F) is given for comparison purpose.

The bonding of Mo species was assessed using Raman spectroscopy (Figure 3). No peaks corresponding to Mo oxide species (MoO_3) were observed for any of the samples (247 , 621 , 890 , and 980 cm^{-1})⁶. In addition, no broad band is observed at 980 cm^{-1} for all samples, indicating the low amount of Si-OH species in all framework Mo-containing samples. However, the presence of new bands at 332 , 416 , 803 , and 820 cm^{-1} were attributed to the presence of framework Mo species.^{1,7} Bands at 332 and 416 cm^{-1} were attributed to Si-O-Mo vibrations, while bands at 803 and 820 cm^{-1} do not have clear attributions yet. This highlights the fact that by using the direct, the staged, or the post synthesis treatment described earlier for performing Mo isomorphous substitution in MFI zeolite, only framework Mo species are formed since no undesired non framework Mo oxide phase is formed.

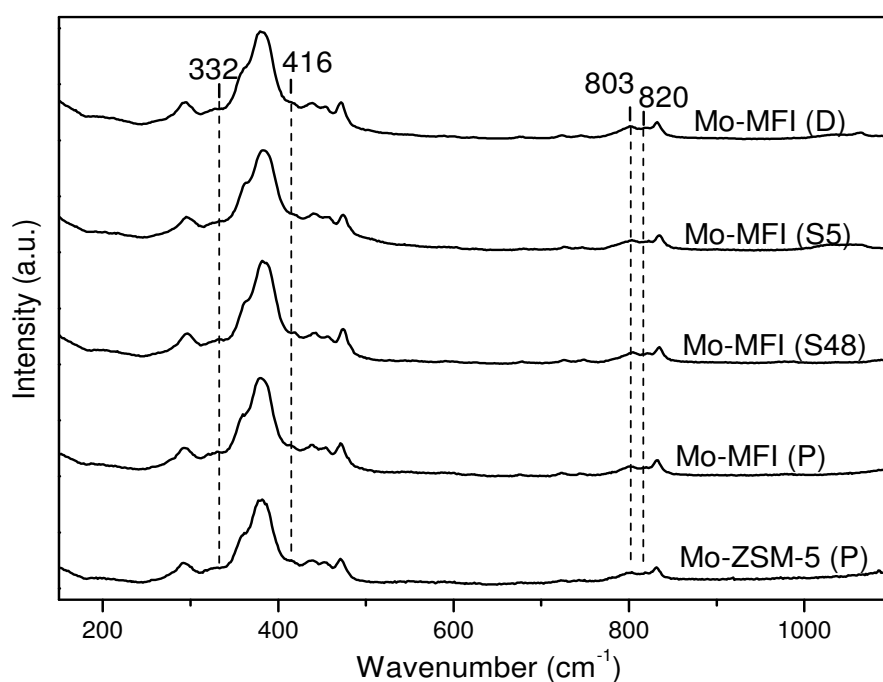


Figure 3. Raman spectra of Mo-MFI (D), Mo-MFI (S5), Mo-MFI (S48), Mo-MFI (P) and Mo-ZSM-5 (P) zeolite samples.

The silicon environments were studied using ^{29}Si MAS NMR (Figure 4). The ^{29}Si MAS NMR spectra was very similar for all samples: no Q^3 species are seen, proving the remarkably low amount of silanol species present in all samples, and in addition, Q^4 species are “resolved”, which is indicative of the very high local homogeneity of the Si environments.^{1,8} This local homogeneity of the framework structure is linked to the extremely low amount of silanol species and structural defects. To a molecular level, the framework is consequently highly homogeneous and hydrophobic due to the absence of silanol species. The local homogeneity of the framework was shown as being the highest for samples prepared using the hydrothermal post synthesis approach (Mo-MFI

(P)), and the lowest for samples prepared according to the direct synthesis approach (Mo-MFI (D)). This was demonstrated by the fact that Mo-MFI (P) possessed the highest Q⁴ species resolution, followed by samples prepared by staged synthesis (Mo-MFI (S5) and Mo-MFI (S48)), the lowest Q⁴ resolution being achieved by Mo-MFI (D) sample. However, this observation does not apply to the Mo-ZSM-5 (P) sample which has slightly lower Q⁴ species resolution, due to the inhomogeneity brought by the presence of framework Al species in the MFI structure.

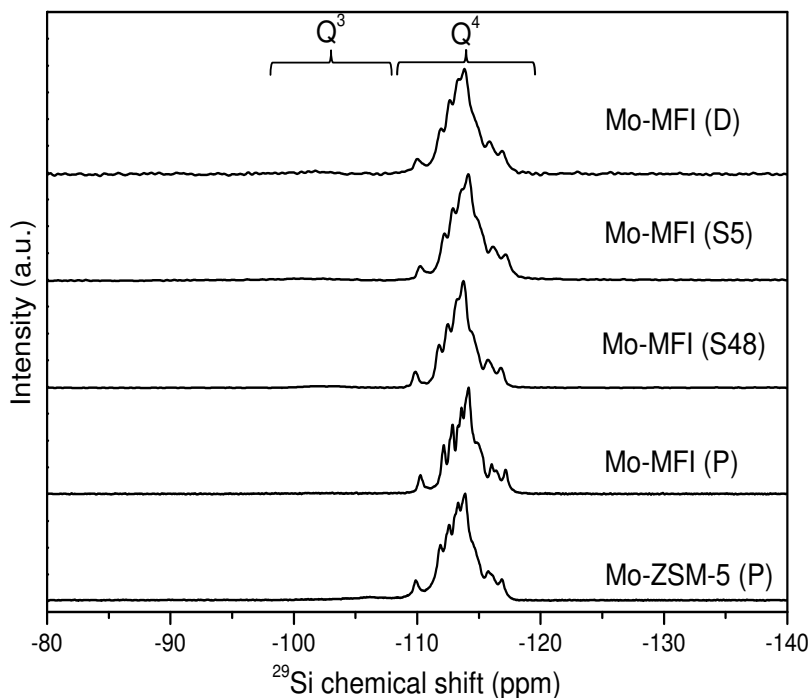


Figure 4. ²⁹Si MAS NMR of Mo-MFI (D), Mo-MFI (S5), Mo-MFI (S48), Mo-MFI (P) and Mo-ZSM-5 (P) zeolite samples.

In addition, the silanol species were investigated using FTIR spectroscopy (Figure 5). All samples possessed one low intensity band at 3745 cm⁻¹, attributable to isolated silanol species while no band corresponding to silanol nests species (3520 cm⁻¹) could be observed.⁹ This is due to the fact that silanol nests species are fully healed upon Mo addition in the zeolite framework, as well as a significant part of isolated silanol species. An additional band at 3610 cm⁻¹ can be seen for sample Mo-ZSM-5 (P) sample, due to the presence of Al-OH species (Brønsted acid sites).

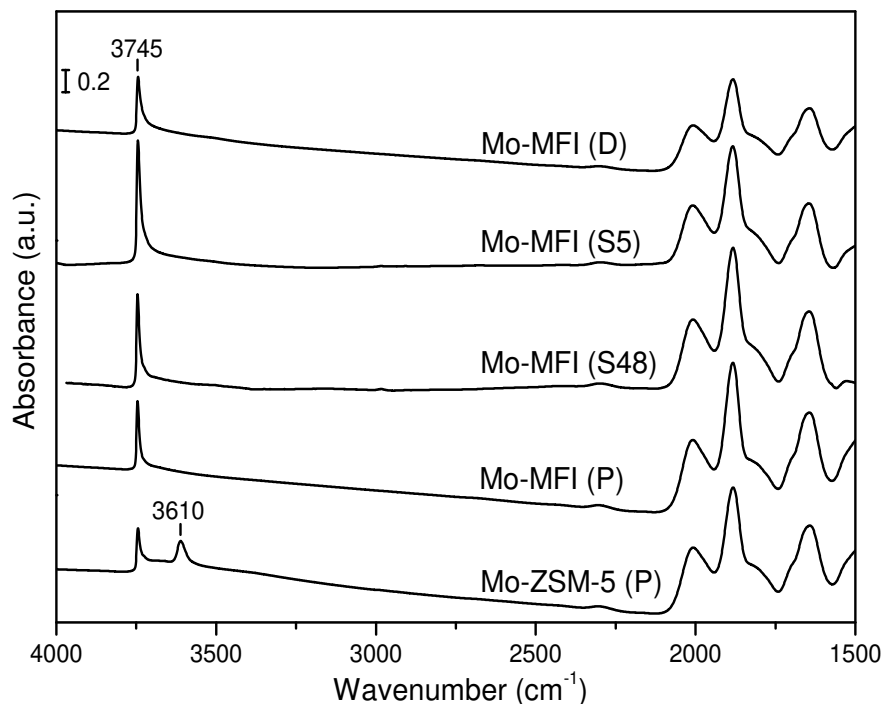


Figure 5. FT-IR spectra of Mo-MFI (D), Mo-MFI (S5), Mo-MFI (S48), Mo-MFI (P) and Mo-ZSM-5 (P) zeolite samples. All samples were activated at 500 °C for 4 h prior measurement.

In addition, the acidity of the samples was evaluated using trimethylphosphine oxide (TMPO) probe molecule adsorption, monitored by ^{31}P MAS NMR (Figure 6, attributions summarized in Table 3).¹⁰ All samples showed a contribution at approximately 45 ppm, attributed to the presence of framework Mo atoms interacting with the TMPO probe molecule while no signal coming from silanol species (50 ppm) is observed. In addition, for sample Mo-ZSM-5 (P), the Brønsted acid sites were fully preserved after Mo addition as shown by the presence of peaks attributed to TMPO adsorbed on Brønsted acid sites at 65 and 74 ppm. The peak at approximately 29 ppm is due to the presence of physisorbed TMPO, and the small peak at 36 ppm is attributed to hydrolyzed TMPO. Since all samples do possess physisorbed TMPO (29 ppm), and since the signals were normalized according to the total amount of TMPO present in the NMR rotor, a comparison of the peak intensity/area at 45 ppm is relevant due to the fact that for these materials, only one TMPO is interacting with each sites (mono-adsorption).¹ As a result, we can conclude that the amount of framework Mo introduced in all samples is quite similar from sample to sample based on LeBail profile refinement results, as discussed above. However, based on LeBail profile refinement, Mo-ZSM-5 (P) contains slightly less framework Mo, because of the co-presence of framework Al (the Mo-free ZSM-5 is

already at approximately 5359 \AA^3 while Mo-free Si-MFI is at 5333 \AA^3 , thus, the unit cell volume difference attributable to Mo is lower in the case of the Al-containing zeolite). Approximative quantification could be performed by ^{31}P MAS NMR since it was proven that only one TMPO molecule interacts with each Mo sites (See chapter 3), and gave an approximative amount of Mo in the MFI framework of 1 wt. %. However, this result could not be confirmed using ICP-MS, hypothetically because the digestion procedure that is used ($\text{HF}+\text{HNO}_3+\text{HCl}$) might be inappropriate for the breaking of the Mo-O-Si bond, given its strongness (discussed in Chapter 5).

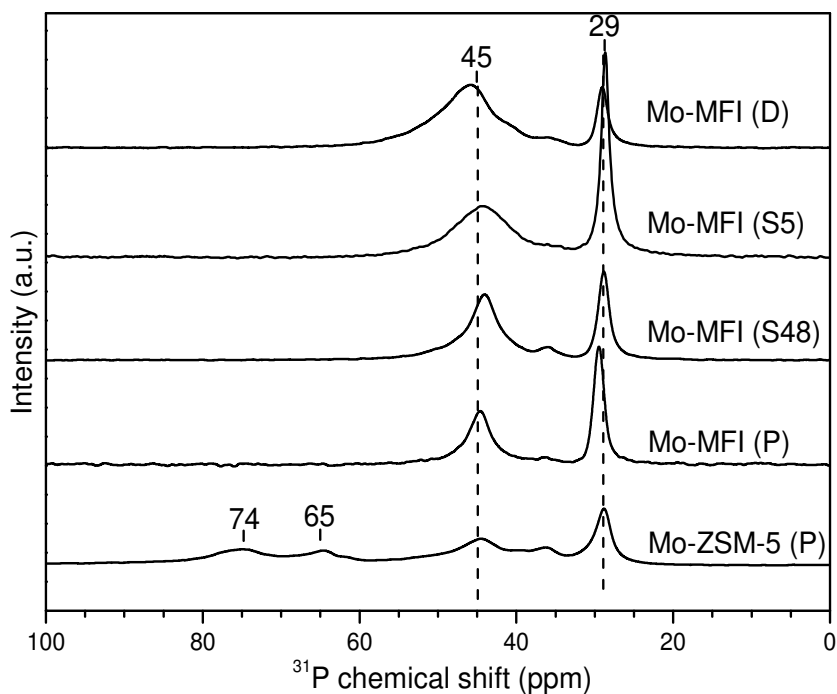


Figure 3. ^{31}P MAS NMR spectra of TMPO adsorbed on Mo-MFI (D), Mo-MFI (S5), Mo-MFI (S48), Mo-MFI (P) and Mo-ZSM-5 (P) zeolite samples. Intensities normalized according to the total mass of TMPO present in the corresponding NMR rotor.

Table 3. Attribution of ^{31}P MAS NMR chemical shifts observed for TMPO adsorbed in zeolite samples.

Chemical shift [ppm]	Attribution
29	Physisorbed TMPO
36	Hydrolyzed TMPO
43	Crystalline TMPO
45	TMPO interacting with framework Mo
50	TMPO interacting with silanols
64 and 75	TMPO interacting with bridging hydroxyl groups

II.4. Conclusion

In this work, different synthesis methods were attempted to perform isomorphous substitution of Mo in MFI frameworks. The first synthesis method is a state-of-the-art direct synthesis approach, that was compared to two novel synthesis methods allowing to perform isomorphous substitution: (i) the staged synthesis, and (ii) the hydrothermal post synthesis method.

The staged synthesis method consists in the introduction of the metal to the precursor gel suspension after a pre-crystallization step. The introduction of this delay allowed a drastic reduction of the particle size compared to samples synthesized according to the direct synthesis route. This reduction of particle size was occurring since the Mo source was no longer able to influence the nucleation step, and had limited effect on crystallization, thanks to the delay imposed before Mo addition into the synthesis gel. In addition, it was observed that the higher the delay for Mo addition, the higher the unit cell volume, attributable to higher Mo loading. Similarly, a higher local homogeneity of the framework based on ^{29}Si MAS NMR study was observed for the sample where a higher delay for Mo addition was applied.

The hydrothermal post synthesis approach was designed as a prolongation of the staged synthesis in which the pre-crystallization step is completely separated from the Mo addition. In this method, the initial MFI framework is synthesized and purified, and then treated with the Mo source. The hydrothermal post synthesis approach yielded zeolite materials with an even higher unit cell volume, indicative of a higher Mo loading,

and higher local homogeneity of the framework when compared to both staged and direct synthesis approaches. In addition, with the crystallization being fully separated from the Mo addition step, the latter was no longer conditioned by issues regarding the solubility of Mo species in the synthesis gel. As a consequence, the post synthesis approach represents the key to introduce both Al and Mo in the MFI framework, since the solubility of Mo in presence of Al species in solution is no longer a concern.

In conclusion, all synthesis approaches allow isomorphous substitution, and the resulting materials are very similar. However, the quality of samples in terms of Mo loading and local homogeneity was slightly improved by using staged synthesis and post synthesis treatment (according to higher unit cell volume of the sample, attributable to slightly higher Mo loading, and higher resolution of Q⁴ species in ²⁹Si MAS NMR). The main improvement however is with regards to the synthesis itself: the staged synthesis allowed to significantly reduce the negative influence of Mo species in the synthesis gel, allowing a higher degree of optimization of the synthesis process. This last observation was even more pronounced in the case of the hydrothermal post synthesis treatment, which is extremely adaptable/flexible. In the latter, many variables can be potentially changed with minimum impact on the obtained material such as Mo concentration, solide/liquid ratio, pH, etc. The two novel synthesis methods are consequently more adaptable/flexible, versatile and efficient than the initial direct synthesis approach, without addition of any drawbacks. This type of versatility guarantees a greater spectrum of applications for Mo-zeolites and opportunities for the optimization of the synthesis process for possible future scale-up. It is for instance possible, by using the post synthesis treatment, to recycle the metal solution used, or to export with much more ease the process to other structures and other metals.

II.5. Table of the main samples from the PhD thesis

In the following table (Table 3.) the synthesis conditions of the main Mo-containing MFI zeolites prepared during the PhD thesis are summarized. They will be associated with the names and date from the corresponding powerpoint presentations given to TOTAL during the PhD thesis in which they appear.

Sample name	Occurrence in manuscript	Presentation date	Mo incorporation	nature of Mo sites	Description
Mo-MFI-C	Chapter 3: Mo-MFI-D	10/04/2018	direct synthesis	framework	18h aging, 48h hydrothermal treatment (90 °C), from sodium molybdate
Mo-MFI-C 24h	#	10/04/2018	direct synthesis	framework	18h aging, 24h hydrothermal treatment (90 °C), from sodium molybdate
Si-MFI-C	Chapter 4: Si-MFI	10/04/2018	#	#	18h aging, 48h hydrothermal treatment (90 °C)
Mo-MFI-I-1	#	10/04/2018	impregnation	non framework	impregnation of ammonium heptamolybdate on Si-MFI-C
Mo-MFI-I-2	#	10/04/2018	impregnation	non framework	impregnation of sodium molybdate on Si-MFI-C
Mo-MFI-C	Chapter 3: Mo-MFI-D	25/10/2018	direct synthesis	framework	18h aging, 48h hydrothermal treatment (90 °C), also called Mo-MFI-C (48h) and Mo-MFI-C (0h) in the presentation, from sodium molybdate
Si-MFI-C	Chapter 4: Si-MFI	25/10/2018	#	#	Silicalite-1 synthesis
Mo-MFI-I	Chapter 3: Mo-MFI-I	25/10/2018	impregnation	non framework	impregnation using ammonium heptamolybdate
I-Mo-MFI-1-6	#	25/10/2018	direct synthesis	framework and non framework	repeatability tests for Mo-MFI-C synthesis
II-Mo-MFI (8h)	#	25/10/2018	direct synthesis	non framework	18h aging, hydrothermal treatment (90°C, 8h), from sodium molybdate
II-Mo-MFI (24h)	#	25/10/2018	direct synthesis	framework	18h aging, hydrothermal treatment (90°C, 24h), from sodium molybdate
II-Mo-MFI (528h)	#	25/10/2018	direct synthesis	framework	18h aging, hydrothermal treatment (90°C, 528h), from sodium molybdate

III-Mo-MFI (5h)	Chapter 2: Mo-MFI (S5)	25/10/2018	staged synthesis	framework	18h aging, hydrothermal treatment (90°C, 48h), delay before Mo addition = 5h, from sodium molybdate
III-Mo-MFI (25h)	#	25/10/2018	staged synthesis	framework	18h aging, hydrothermal treatment (90°C, 48h), delay before Mo addition = 25h, from sodium molybdate
III-Mo-MFI (48h)	Chapter 2: Mo-MFI (S48)	25/10/2018	staged synthesis	framework	18h aging, hydrothermal treatment (90°C, 72h), delay before Mo addition = 48h, from sodium molybdate
Mo-MFI-0	Chapter 3: Mo-MFI-I	21/06/2019	direct synthesis	framework	18h aging, 48h hydrothermal treatment (90 °C), from sodium molybdate
Mo-MFI-1	#	21/06/2019	staged synthesis	framework	18h aging, hydrothermal treatment (90°C, 72h), delay before Mo addition = 48h, from sodium molybdate
Mo-MFI-2	Chapter 2: Mo-MFI (P)	21/06/2019	post synthesis	framework	Mo incorporation from sodium molybdate (0,8g/25mL H2O for 1,2 g zeolite), on silicalite-1
AlMo-MFI	Chapter 5: [Mo]-ZSM-5	21/06/2019	post synthesis	framework	Mo incorporation from sodium molybdate (0,8g/25mL H2O for 1,2 g zeolite), on ZSM-5 (Si/Al=110)
MoZSM-5-I	Chapter 5: R-ZSM-5	20/11/2019 and 24/01/2020	impregnation	non framework	impregnation of 1 wt. % Mo on ZSM-5 (Si/Al=112)
MoSiMFI-D	Chapter 3: Mo-MFI-D	20/11/2019 and 24/01/2020	direct synthesis	framework	18h aging, 48h hydrothermal treatment (90 °C), from sodium molybdate
MoSiMFI-S	#	20/11/2019 and 24/01/2020	staged synthesis	framework	18h aging, hydrothermal treatment (90°C, 48h), delay before Mo addition = 5h, from sodium molybdate
MoSiMFI-P (1)	#	20/11/2019 and 24/01/2020	post synthesis	framework	from silicalite-1 and a recycled sodium molybdate solution from a previous synthesis
MoSiMFI-P (2)	#	20/11/2019 and	post synthesis	framework	from silicalite-1 and a solution prepared

		24/01/2020			from Mo oxide, NaNO ₃ , and H ₂ O ₂
MoSiMFI-P (3)	#	20/11/2019 and 24/01/2020	post synthesis	framework	from silicalite-1 and a solution prepared from Mo oxide, NaOH, and H ₂ O ₂
MoZSM-5-P (1)	Chapter 5: [Mo]-ZSM-5	20/11/2019 and 24/01/2020	post synthesis	framework	ZSM-5 and sodium molybdate solution concentrated
MoZSM-5-P (2)	#	20/11/2019 and 24/01/2020	post synthesis	framework	ZSM-5 and sodium molybdate solution diluted
MoZSM-5-P (3)	#	20/11/2019 and 24/01/2020	post synthesis	framework	ZSM-5 and sodium molybdate solution higher concentration of Mo, but same dilution of the suspension
Silicalite-1 with different metal cations	#	29/03/2019	staged synthesis	framework (and non framework for some cases)	incorporation after 5h delay on silicalite-1 synthesis gel, using Li ₂ MoO ₄ , (Li, Na, K, Cs)VO ₃ , Na ₂ SnO ₃ , AgNO ₃ +NaNO ₃ , CuN ₂ O ₆ +NaCl, Na ₂ WO ₄ , Cs ₂ WO ₄)
Mo-MFI	Chapter 4: Mo-MFI	11/06/2020	post synthesis	framework	Silicalite-1 modification with sodium molybdate solution
Al-MFI	Chapter 4: Al-MFI	11/06/2020	#	#	ZSM-5 synthesis
Si-MFI	Chapter 4: Si-MFI	11/06/2020	#	#	Silicalite-1 synthesis

Table 3. Main samples from powerpoint presentation performed with Total with associated dates and short description.

II.6. References

1. Dubray, F. *et al.* Direct Evidence for Single Molybdenum Atoms Incorporated in the Framework of MFI Zeolite Nanocrystals. *J. Am. Chem. Soc.* **141**, 8689–8693 (2019).
2. Deka, R. C. *et al.* Comparison of all sites for Ti substitution in zeolite TS-1 by an accurate embedded-cluster method. *J. Phys. Chem. B* **109**, 24304–24310 (2005).
3. Borin, M. F., Silva, T. Da, Felisbino, R. F. & Cardoso, D. Synthesis of TS-1 molecular sieves using a new Ti source. *J. Phys. Chem. B* **110**, 15080–15084 (2006).
4. Tuel, A. & Taârit, Y. Ben. Influence of the nature of silicon and titanium alkoxides on the incorporation of titanium in TS-1. *Appl. Catal. A Gen.* **110**, 137–151 (1994).
5. Yan, Y., Guo, X., Zhang, Y. & Tang, Y. Future of nano-/hierarchical zeolites in catalysis: Gaseous phase or liquid phase system. *Catal. Sci. Technol.* **5**, 772–785 (2015).
6. Dieterle, M. & Mestl, G. Raman spectroscopy of molybdenum oxides: Part II. Resonance Raman spectroscopic characterization of the molybdenum oxides Mo₄O₁₁ and MoO₂. *Phys. Chem. Chem. Phys.* **4**, 822–826 (2002).
7. Xia, C. *et al.* Confirmation of the isomorphous substitution by Sn atoms in the framework positions of MFI-typed zeolite. *Catal. Today* **316**, 193–198 (2018).
8. Chezeau, J. M., Delmotte, L., Guth, J. L. & Gabelica, Z. Influence of synthesis conditions and postsynthesis treatments on the nature and quantity of structural defects in highly siliceous MFI zeolites: A high-resolution solid-state ²⁹Si n.m.r. study. *Zeolites* **11**, 598–606 (1991).
9. Hadjiivanov, K. *Identification and Characterization of Surface Hydroxyl Groups by Infrared Spectroscopy. Advances in Catalysis* vol. 57 (Elsevier Inc., 2014).
10. Zheng, A., Liu, S.-B. & Deng, F. ³¹P NMR chemical shifts of phosphorus probes as reliable and practical acidity scales for solid and liquid catalysts. *Chem. Rev.* **117**, 12475–12531 (2017).

Chapter III: Direct Evidence for Single Molybdenum Atoms Incorporated in the Framework of MFI Zeolite Nanocrystals.

This work is published as a research article with the following bibliographic reference:

Dubray F., Moldovan S., Kouvatas C., Grand J., Aquino C., Barrier N., Gilson J-P., Nesterenko N., Minoux D., Mintova S. Direct evidence for Single Molybdenum Atoms Incorporated in the Framework of MFI Zeolite Nanocrystals. *J. Am. Chem. Soc.* **2019**, 141, 22, 8689-8693.

Abstract

Direct evidence of the successful incorporation of atomically dispersed molybdenum (Mo) atoms into the framework of nanosized highly crystalline MFI zeolite is demonstrated for the first time. Homogeneous distribution with a size of 0.05 nm is observed by STEM-HAADF. ^{31}P MAS NMR and FTIR spectroscopy, using trimethylphosphine oxide (TMPO) and deuterated acetonitrile as probe molecules, reveal a homogeneous distribution of Mo in the framework of MFI nanozeolites, and the presence of Lewis acidity. ^{31}P MAS NMR of TMPO shows probe molecules interacting with isolated Mo atoms in the framework, and physisorbed probe molecules in the zeolite channels. Moreover, 2D ^{31}P - ^{31}P MAS radio frequency-driven recoupling (RFDR) NMR indicates the presence of one type of Mo species in different crystallographic positions in the MFI framework. The substitution of framework Si by Mo significantly reduces the silanol defect content, making the resulting zeolite highly hydrophobic. In addition, the insertion of Mo into the MFI structure induces a symmetry lowering, from orthorhombic ($Pnma$), typical of high silica MFI, to monoclinic ($P21/n$), as well as an expansion of unit cell volume. The novel material opens many opportunities of catalysts design for application in mature and emerging fields.

II.1. Introduction

The introduction of metal ions into zeolites is known to modify their acid and/or redox properties, and can be achieved by different routes as recently reviewed.¹ One such route is framework isomorphous substitution where framework silicon ions are replaced by transition metal ions. The classic zeolite literature states that elements such as Ga, Ce, Be, B, Fe, Cr, P, and Mg can isomorphously substitute Si and Al in zeolite framework.^{2,3} In the 80s the introduction of Ti in the MFI zeolites was reported by ENI researchers.⁴ Two years ago the introduction of W into the framework of MFI zeolite was reported by our group.⁵ In general, this substitution greatly influences the physicochemical properties of the materials and opens many opportunities for new application in catalysis and adsorption.⁶⁻¹⁰ Ti-containing materials (TS-1) are very

active and selective in partial catalytic oxidation of fine chemicals, in particular in the presence of H_2O_2 . The best known examples of such transformations are propylene epoxidation (Hydrox. Process, HPPO), hydroxylation of phenol, and cyclohexanone ammoximation.⁹

Properties of the metal-containing zeolites, such as Lewis acidity and higher resilience to water, are very valuable for future application in biomass upgrading.⁴ Our group described the preparation of a nanosized MFI zeolite containing atomically dispersed tungsten.⁵ The resulting W-containing MFI zeolite possessed exceptional stability, high hydrophobicity, and no silanol defects. These properties give them a great potential in catalysis as silanols (often referred to as framework and external defects) display unwanted hydrophilic properties related to water adsorption on silanol sites.^{11,12}

However, the proven incorporation of the molybdenum atoms in the MFI was not described in literature so far. Attempts were reported by Raghavan et al.¹³ who prepared a molybdenum containing silicalite-2 (MEL structure) by hydrothermal synthesis in aluminum-free alkaline mixtures that was active for the oxidative dehydrogenation of ethanol to acetaldehyde. Then, the synthetic effort to introduce Mo in silicalite-1 (MFI structure) was also reported by the same group.¹⁴ Interestingly, the samples were more hydrophilic than silicalite-1 (more defects) and thermally stable; they displayed a high activity in the catalytic oxidation of thioethers to the corresponding sulfoxides. A non-linear unit cell volume expansion with the introduction of molybdenum was observed, indicating a significant co-formation of non-framework metallic species. The partial incorporation of molybdenum in the silicalite-1 framework synthesized in fluoride media was reported by Tavalaro.¹⁵ The framework insertion of a portion of the molybdenum was claimed to occur based on the thermal decomposition behavior of TPA^+ cations blocked in the zeolite micropores without any further evidences.

Here we present for the first time direct evidence for the hydrothermal synthesis of a nanosized MFI zeolite containing atomically dispersed Mo in the zeolite framework, hereinafter referred to as Mo-MFI-D. A reference sample, prepared by molybdenum wet-impregnation of silicalite-1, hereinafter referred to as Mo-MFI-P, was used for comparative purposes. Both samples are in H-form, obtained by ion exchange with ammonium chloride. The residual concentration of alkali metals was below 500 ppm in the samples after ion-exchange.

II.2. Experimental

II.2.1. Synthesis

Mo-MFI-P and Mo-MFI-D zeolite samples were synthesized using the following chemicals without any further purification: tetraethyl orthosilicate (TEOS,

98%, Aldrich), tetra n-propylammonium hydroxide (TPAOH, 20 wt. % in water solution, Alfa Aesar), and sodium molybdate dihydrate ($\text{Na}_2\text{MoO}_4 \cdot 2\text{H}_2\text{O}$, Alfa Aesar, 98%). Doubly deionized water was used in the synthesis and post-synthetic treatments. Syntheses were carried out in 125 mL polypropylene (PP) bottles at autogenous pressure, without agitation. Two different gels were prepared with the following molar composition:



Synthesis gels were prepared with magnetic stirring at room temperature. The resulting clear suspensions were stirred for 1h at room temperature, further hydrolysed for 18 h on an orbital shaker and the hydrothermal synthesis took place at 90 °C for 48 h. The harvested crystalline products were water washed and centrifugated (20,000 rpm) until a pH of 7 was reached, and subsequently dried at 80 °C in an oven. The samples were then calcinated in a muffle furnace at 550 °C for 5 h prior any post treatment.

The obtained zeolite gel (1) was then loaded with molybdenum by wet impregnation with Na_2MoO_4 (700 mg zeolite/mL of molybdate solution at 1.5 mg/mL), dried at room temperature and calcined (550 °C, 5 h). Its H-form was obtained by ion-exchanging the zeolite twice in a NH_4Cl solution (0.2 M) for 1 h, washing once with water, dried at 80 °C and calcined (550 °C, 5 h); this reference sample was labelled Mo-MFI-I (*i.e.* MFI with Mo atoms introduced in a impregnation post-synthetic step).

The H-form of the zeolite obtained from gel (2) was prepared by ion-exchanging with a NH_4Cl solution (0.2 M) for 1 h twice. The sample was then washed with water, dried at 80 °C and calcined (550 °C, 5 h); this sample was labelled Mo-MFI-D (MFI where Mo was introduced during the hydrothermal synthesis).

II.2.2. Characterizations

Powder X-ray diffraction (XRD) patterns of the zeolites were collected with a PANalytical X'Pert Pro diffractometer equipped with a Johansson monochromator using the Cu $\text{K}\alpha_1$ radiation ($\lambda = 1.540598 \text{ \AA}$). The unit cell parameters, volume, and space group of Mo-MFI-P and Mo-MFI-D were obtained from a Le Bail profile refinements using the JANA2006 software.²⁹

The crystallinity and defects of nanosized zeolites were determined by ^{29}Si and $\{^1\text{H}\}^{29}\text{Si}$ cross-polarization (CP) solid-state MAS NMR on a Bruker Avance III-HD 500 (11.7 T) spectrometer operating at 99.3 MHz, using a zirconia rotor of 4 mm outer diameter spun at 12 kHz. For ^{29}Si MAS NMR, a single pulse excitation (30 ° flip

angle) was used with a recycle delay of 30 s. For $\{^1\text{H}\}^{29}\text{Si}$ CP-MAS NMR, a contact time of 5 ms and a recycle delay of 2 s were used, respectively. Chemical shifts were referenced to tetramethyl silane (TMS).

The acidity of the Mo-MFI-I and Mo-MFI-D zeolites was characterized by IR spectroscopy using a Nicolet Magna 550-FT-IR spectrometer (4 cm^{-1} optical resolution). The self-supported wafers (1 cm^2 , av. 20 mg, hydraulic press at 1 T/cm^2) of zeolites were activated at $480\text{ }^\circ\text{C}$ for 3h under vacuum (av. 2.5×10^{-6} Torr) prior to measurements. Successive small doses (2 to 30×10^{-3} mmol/g loading range) of acetonitrile (CD_3CN) were then adsorbed at room temperature.

The acidity of the Mo-MFI-I and Mo-MFI-D zeolites was also characterized by monitoring the adsorption of trimethylphosphine oxide (TMPO) by ^{31}P -NMR under ^1H decoupling. All preparation steps were conducted under an Ar atmosphere to prevent any reaction of TMPO with air, and water adsorption on the zeolite. Sodium free samples, *vide-supra*, were dehydrated at $400\text{ }^\circ\text{C}$ under vacuum (av. 4.0×10^{-5} Torr) while a solution of TMPO dissolved in dichloromethane (CH_2Cl_2) was prepared. This solution was then added to the dehydrated zeolite sample, and the resulting suspension treated in an ultrasonic bath for 15 min. The suspension was then dried by evaporating dichloromethane under vacuum for 2 h. The TMPO loaded zeolites were then packed in zirconium rotors for ^{31}P MAS NMR characterization. All NMR experiments were performed on a 11.7 T Bruker Avance 500 spectrometer operating at a frequency of 500.0 MHz and 202.4 MHz for ^1H and ^{31}P respectively, and. All MAS NMR spectra were recorded on a 4mm MAS probe-head at a spinning rate of 14 kHz. ^{31}P $\pi/2$ and π -pulses lengths were 7 and 14 μs respectively for all measurements. 1D and 2D ^{31}P MAS NMR experiments were conducted under spinal-64 $^{30}\text{ }^1\text{H}$ decoupling using a field strength of 71.2 kHz, with a recycle delay were carefully set according to preliminary relaxation time measurements. The single-pulse ^{31}P MAS NMR spectra were acquired with 256 scans. Two-dimensional homonuclear ^{31}P - ^{31}P radio-frequency driven recoupling (RFDR) ^{31}P experiments were also performed, using 80 scans and 4K complex points in the t_2 dimension. The t_1 dwell was rotor-synchronized, and 192 time increments were set for 0.2 ms mixing time. ^{31}P and ^1H chemical shifts and RF pulses were calibrated on phosphoric acid (85%) and TMS respectively.

Raman spectra were collected on a Jobin Yvon Labram 300 confocal Raman spectrometer coupled to a microscope (objective: 50 \times) and a CCD detector. A 532 nm wavelength laser was used, and spectra were accumulated 3 times for 60 s each. The power on the sample did not exceed 20 mW upon measurement.

The crystal size and morphology were measured by transmission electron microscopy (TEM); experiments were carried out on an Analytical double (objective and probe) corrected JEOL ARM200CF equipped with a 100 mm Centurio EDS detector and a Quantum GIF for the EELS. A probe of 0.1 nm was used to scan the specimen in STEM mode and Bright Field and high Angular Annular Dark Field

detectors were simultaneously employed for imaging. The camera length was fixed at 8 cm. Two different accelerating voltages of 200 kV and 80 kV were employed in the STEM mode for imaging and chemical analysis, respectively. Owing to the enhanced Z contrast developed at 200 kV, this configuration was used for imaging and a high speed scanning protocol (10 $\mu\text{sec}/\text{px}$) was employed in order to minimize the specimen degradation under the beam. To avoid material degradation the STEM-EDS analytical essays were carried out at 80 kV with a high scanning speed of 3 $\mu\text{s}/\text{px}$ and for a mean duration of 60 minutes. A cross-correlation algorithm implemented in the Jeol Analysis Station software was applied every 30 seconds in an effort to compensate for the special drift occurring during the test. The microstructure of samples was checked prior and after each EDS scan.

II.3. Result and discussions

The distribution of molybdenum in the Mo-MFI-I and Mo-MFI-D samples was investigated by STEM-EDS (Figure 1). Both Mo-containing samples show a homogeneous distribution of molybdenum with a mean content of 0.8 to 1.2 wt. %. STEM-HAADF results reveal structural information of the materials by providing Z-contrast images. The white dot-like features identified by the high-resolution STEM-HAADF micrographs disclose the homogeneous distribution of Mo in Mo-MFI-D. The size of the white dots is 0.05 nm, which is approximately 10 times smaller than the crystalline fringes. This indicates that atomically dispersed Mo atoms are part of the MFI framework (Figure 2a). Similar dots that are of a larger size (1.5 nm) are observed in Mo-MFI-I (Figure 2b). For comparison, the STEM-HAADF micrograph of the pure siliceous calcined MFI zeolite used for the preparation of sample Mo-MFI-I is presented in Figure S1. Said larger-sized dots observed in sample Mo-MFI-I correspond to small molybdenum oxide clusters homogeneously distributed in the MFI sample as indicated by Raman spectroscopy (Figure S2). The bands at 247, 621, 890, and 980 cm^{-1} in the Raman spectrum of Mo-MFI-I are assigned to molybdenum oxide.¹⁶ These bands are not observable in Mo-MFI-D, indicating the absence of any oxide phases in this sample. A small peak at 980 cm^{-1} in Mo-MFI-D is not attributed to an oxide phase (narrow signal), but to a small amount of silanols (wide band). Furthermore, in Mo-MFI-D, two new bands (803 and 820 cm^{-1}) possibly originate from single Mo atoms in the MFI framework positions. Two shoulders (332 and 416 cm^{-1}) are attributed to the perturbation of Si-O-Si vibrations linked to the presence of neighboring Mo-O-Si species, or possibly Mo-O-Si vibrations.¹⁷ This last attribution is further supported by the presence of a broadening of the 1105 cm^{-1} band in the FTIR spectra in the region below 1200 cm^{-1} , corresponding to Si-O-Mo framework vibration (Figure S3). These two samples differ substantially; Mo-MFI-D contains Mo atoms in the MFI framework and no oxide phase, with a negligible amount of isolated silanols (3745 cm^{-1}), Mo-MFI-I contains molybdenum oxide and silanols as shown by FTIR (Figure S4).

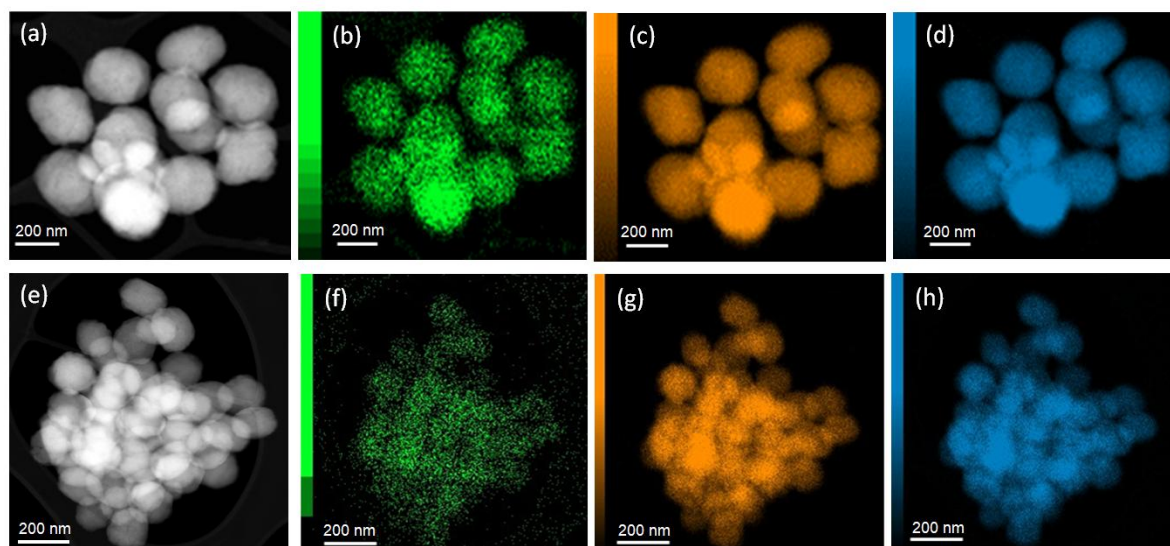


Figure 1. STEM-EDS elemental maps of (a,b,c,d) Mo-MFI-D and (e,f,g,h) Mo-MFI-I: Si (orange), O (blue), and Mo (green)

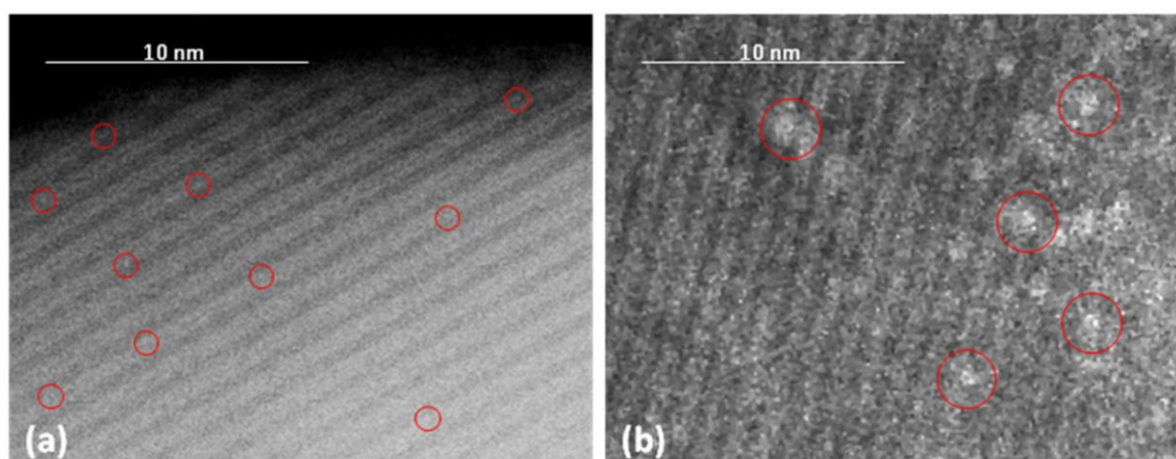


Figure 2. STEM-HAADF micrographs revealing the distribution of Mo species in (a) Mo-MFI-D and (b) Mo-MFI-I

Both Mo-MFI-I and Mo-MFI-D are highly crystalline. Upon direct introduction of molybdenum in the MFI framework (Mo-MFI-D), the diffraction peaks at 23.30 , 23.75 , and 24.50 ° 2θ split (Figure S5). This is a direct consequence of the symmetry lowering from orthorhombic ($Pnma$) to monoclinic ($P21/n11$), confirmed by Le Bail profile refinements of the respective diffraction patterns (see Table S1 and Figure S5). The unit cell volume of Mo-MFI-D expands also from 5337.4 to 5360.6 Å³ compared to Mo-MFI-I. Such a polymorphic transition is always observable in MFI zeolite, and its transition temperature depends on the incorporation of elements such as aluminum and titanium into the MFI framework.¹⁸⁻²⁰ It is still unclear however why Mo-MFI-D sample exhibits monoclinic symmetry, when incorporation of Mo is expected to lower the transition temperature of the monoclinic-orthorhombic phase transition instead.²¹ This result is probably a consequence of the hydrophobic and

silanol defect-free properties of the material. An increase in the unit cell volume proportional to the amount of metals introduced into the zeolite framework has been previously reported.^{22,23} The unit cell volume expansion and symmetry change of the MFI type zeolite are due to distortion of the framework to accommodate Mo atoms with an ionic radius larger than Si.²⁴ The space group transition and volume expansion observed for Mo-MFI-D provide additional evidence for the incorporation of molybdenum atoms into the framework of the MFI type zeolite. In contrast, Mo-MFI-P does not show any evidence for the presence of framework Mo. This is based on its orthorhombic symmetry and its unit cell volume that are both similar to purely siliceous MFI type zeolite (orthorhombic symmetry, measured volume = 5333.1 Å³).

The nature of the silicon environment in the MFI type zeolite framework was investigated by ²⁹Si magic-angle spinning (MAS) NMR and [¹H] cross-polarization (CP) ²⁹Si MAS NMR spectroscopy (Figure S6). The absence of Q³ species in Mo-MFI-D is highlighted by a one-pulse experiment (absence of a -104 ppm peak). Few silanols are observed by ²⁹Si CP MAS NMR for Mo-MFI-D, while for Mo-MFI-I a higher concentration of Q³ species is detected. Moreover, well resolved Q⁴ species in Mo-MFI-D are attributed to the local homogeneity of the sample. Mo-MFI-D can be described as a silanol-free material with a high degree of local homogeneity.

The nature of the Mo and the acidity of the zeolites is studied using trimethylphosphine oxide (TMPO) adsorption monitored by ³¹P MAS NMR spectroscopy (Figure 3). The spectra of Mo-MFI-D exhibits contributions from TMPO interacting with framework Mo atoms (45 ppm) as well as physisorbed TMPO (29 ppm).²⁵ The absence of a peak at 50 ppm indicates that no or few silanols are present on Mo-MFI-D.²⁵ This is further supported by 2D ³¹P-³¹P MAS RFDR NMR (Figure 3). The symmetry and shape of the 45 ppm peak related to framework molybdenum Lewis acid sites indicates the presence of a single chemical species, with some small variations in its environment. This is potentially indicative of Mo atoms in different crystalline positions of the framework. In contrast, the spectra of Mo-MFI-I exhibits contributions from silanols (50 ppm), crystalline TMPO (42 ppm), and physisorbed TMPO (29 ppm). The 50 ppm peak in Mo-MFI-I is attributed to the presence of different species such as Q², Q³, silanol nests, and isolated silanols. The absence of correlation in the 2D experiment indicates that the amount of TMPO is too low to observe interactions between probe molecules and high enough to observe physisorbed species. Moreover, the peak at 29 ppm attributed to physisorbed TMPO is narrower on Mo-MFI-D than on Mo-MFI-I. This indicates that the local geometry for the physisorbed TMPO is different in the two samples, possibly due to a lower anisotropy of the local environment in Mo-MFI-D compared to Mo-MFI-I. The higher anisotropy of the TMPO would then be attributed to the presence of different species in the zeolite pores, such as Mo oxides and silanols in Mo-MFI-I. In Mo-MFI-D, the narrow peak at 29 ppm may be attributed to the local homogeneity in the micropores, i.e., a single type of Lewis acid site as discussed above. Additionally, the peak corresponding to physisorbed TMPO on Mo-MFI-D is shifted by -0.5 ppm compared

to Mo-MFI-I. A slightly lower chemical shift in Mo-MFI-D is linked to the absence of silanol groups and thus to a higher hydrophobicity compared to Mo-MFI-I. It was reported that the higher the chemical shift of TMPO, the stronger the acidity of the zeolite.²⁵ The presence of a significant number of silanol groups in Mo-MFI-I, compared to Mo-MFI-D, makes the material more acidic, as observed by a shifting of the peak attributed to physisorbed TMPO to higher ppm values compared to Mo-MFI-D.

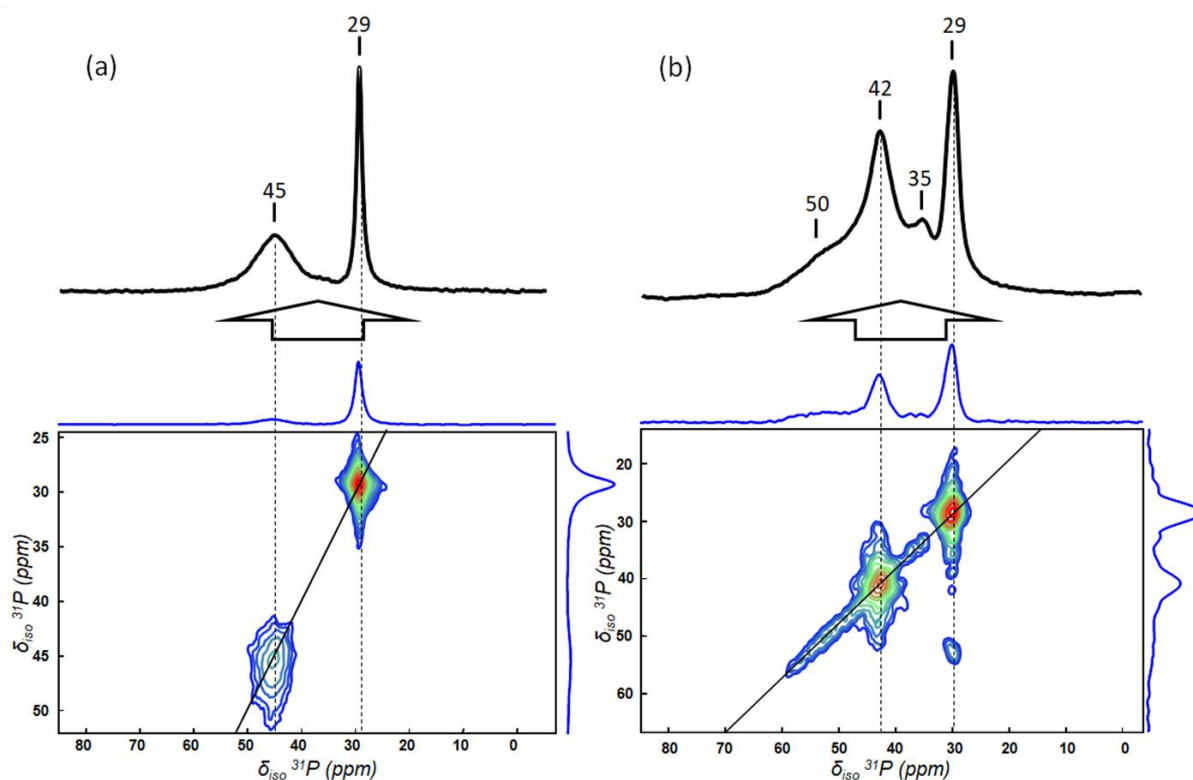


Figure 3. ^{31}P - ^{31}P MAS RFDR NMR spectra (top: 1D ^{31}P MAS NMR spectra) of (a) Mo-MFI-D and (b) Mo-MFI-I under ^1H spinal-64 decoupling (magnetic field of 500 MHz, MAS at 12 kHz and 14 kHz for 1D and RFDR spectra, respectively)

The acidity of these two molybdenum containing zeolites is also investigated by the adsorption of deuterated acetonitrile (CD_3CN) monitored by FTIR spectroscopy (Figure 4). The spectra of Mo-MFI-D exhibits one band at 2308 cm^{-1} corresponding to CD_3CN adsorbed on the Lewis acid sites brought by the atomically dispersed framework molybdenum and low intensity bands at 2283 and 2274 cm^{-1} indicative of trace amounts of alkali metal and silanols. The 2308 cm^{-1} band is attributed to closed Lewis acid sites, i.e. non-hydrolysed framework Mo, that may also correspond to Mo^{VI} in the MFI framework ($\text{O}=\text{Mo}(\text{-OSi})_4$), based on previous reports on Me-containing zeolites.²⁶⁻²⁸ In contrast, the spectra of Mo-MFI-I exhibits two bands at 2317 and 2303 cm^{-1} indicating the presence of molybdenum oxide species. In addition, low intensity band at 2283 cm^{-1} is due to trace amounts of alkali metals, and peak at 2274 cm^{-1} corresponds to silanol groups.

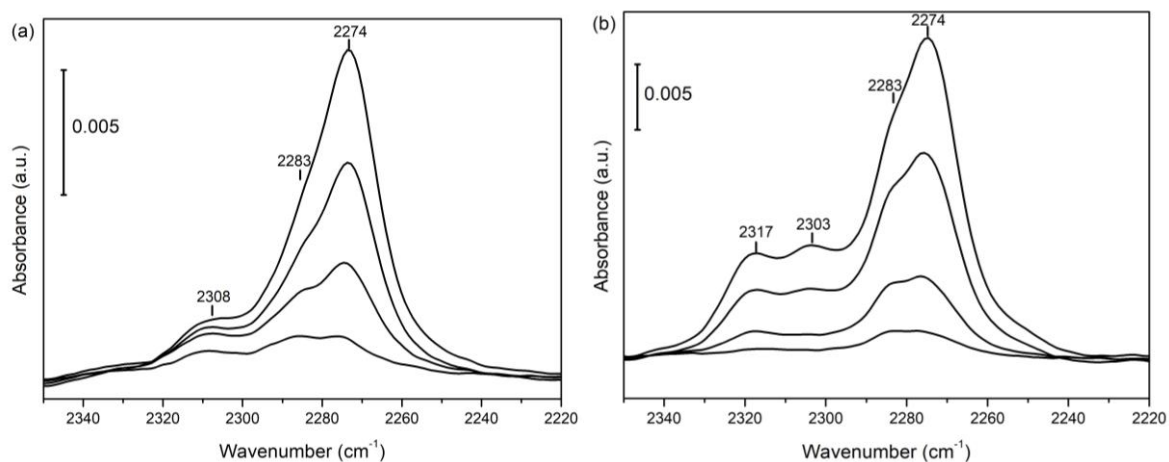


Figure 4. FTIR spectra of CD₃CN adsorbed on (a) Mo-MFI-D (3.7, 11.3, 26.2, 41.4 x10⁻³ mmol/g), and (b) Mo-MFI-I (2.6, 7.8, 18.1, 28.0 x10⁻³ mmol/g) at room temperature.

II.4. Conclusions

In summary, a nanosized MFI type zeolite with atomically dispersed molybdenum in framework is prepared. Mo-MFI zeolite displays high local homogeneity of the atomically dispersed Mo atoms, low silanol content, and high hydrophobicity. These properties originate from the incorporation of Mo atoms into the MFI framework as closed Lewis acid sites (O=Mo(-OSi)₄). The insertion of Mo in the MFI structure induces a space group transition and increase of the unit cell volume. The uniform nature of the Mo incorporated into the MFI framework is confirmed by IR spectroscopy (deuterated acetonitrile probe) and ³¹P MAS NMR spectroscopy (trimethylphosphine oxide probe). The homogeneous distribution of the atomically distributed Mo in the MFI framework is proven by STEM-HAADF. The materials open many opportunities of catalysts and adsorbents design for applications in mature and emerging fields.

II.5. References

1. Kosinov, N.; Liu, C.; Hensen, E.J.M.; Pidko, E.A. Engineering of Transition Metal Catalysts Confined in Zeolites. *Chem. Mater.* **30** (10), 3177-3198 (2018).
2. Barrer, R.M. Hydrothermal Chemistry of Zeolites. *Academic Press*, London, 1982.
3. Jacobs, P.A.; Leuven K.U. Acid Zeolites: an Attempt to Develop Unifying Concepts. *Catal. Rev. Sci. Eng.* **24** (3), 415-440 (1982).

4. Moliner, M. State of the Art of Lewis Acid-Containing Zeolites: Lessons from Fine Chemistry to New Biomass Transformation Processes. *Dalton Trans.* **43**, 4197-4208 (2014).
5. Grand, J.; Talapaneni, S.N.; Vicente, A.; Fernandez, C.; Dib, E.; Aleksandrov, H.A.; Vayssilov, G.N.; Retoux, R.; Boullay, P.; Gilson, J-P; Valtchev, V.; Mintova, S. One-Pot Synthesis of Silanol-Free Nanosized MFI Zeolite. *Nat. Mater.* **16**, 1010-1017 (2017).
6. Price, G.L.; Kanazirev, V. Ga₂O₃/HZSM-5 Propane Aromatization Catalysts: Formation of Active Centers via Solid-State Reaction. *J. Catal.* **126** (1), 267-278 (1990).
7. Kharitonov, A.S.; Aleksandrova, T.N.; Vostrikova, L.A.; Sobolev, V.I.; Ione, K.G.; Panov, G.I. Selective Oxidation of Benzene to Phenol over FeAlPO Catalysts Using Nitrous Oxide as Oxidant *USSR Pat.* 1805127 June 22, 1988.
8. Panov, G.I.; Shevelena, G.A.; Kharitonov, A.S.; Romannikov, V.N.; Vostrikova, L.A. Oxidation of Benzene to Phenol by Nitrous Oxide over Fe-ZSM-5 Zeolites. *App. Catal. A* **82** (1), 31-36 (1992).
9. Bellussi, G.; Millini, R.; Pollesel, P.; Perego, C. Zeolite Science and Technology at Eni. *New. J. Chem.* **40**, 4061-4077 (2016).
10. Taramasso, M.; Perego, G.; Notari, B. Preparation of Porous Crystalline Synthetic Material Comprised of Silicon and Titanium Oxides *US pat.* 4410501 June 29, 1982.
11. Mintova, S.; Jaber, M.; Valtchev, V. Nanosized Microporous Crystals: Emerging Applications. *Chem.Soc.Rev.* **44**, 7207-7233 (2015).
12. Chezeau, J.M.; Delmotte, L.; Guth, J.L. Influence of Synthesis Conditions and Postsynthesis Treatments on the Nature and Quantity of Structural Defects in Highly Siliceous MFI Zeolites: A High-Resolution Solid-State ²⁹Si n.m.r. Study. *Zeolites* **11** (6), 598-606 (1991).
13. Raghavan, P.S.; Kannan, S.; Belhekar, A.A. Synthesis and Characterization of Molybdenum Containing Silicalite-2 (MoS-2) Molecular Sieve. *Indian J. Chem. Sec. A* **36** (10), 905-907 (1997).
14. Raghavan, P.S.; Ramaswamy, V.; Upadhya, T.T.; Sudalai, A.; Ramaswamy, A.V.; Sivasanker, S. Selective Catalytic Oxidation of Thioethers to Sulfoxides over Mo-Silicalite-1 (MoS-1) Molecular Sieves. *J. Mol. Catal. A.* **122** (1), 75-80 (1997).
15. Tavolaro, A. Thermal Characterization of the Metal-Silicalites Obtained from Aqueous Nonalkaline Fluoride Gels. *J. Therm. Anal.* **47** (1), 171-179 (1996).

16. Dieterle, M.; Mestl, G. Raman Spectroscopy of Molybdenum Oxides – Part II. Resonance Raman Spectroscopic Characterization of the Molybdenum Oxides Mo₄O₁₁ and MoO₂. *Phys. Chem. Chem. Phys.* **4**, 822-826 (2002).
17. Xia, C.; Liu, Y.; Lin, M.; Peng, X.; Zhu, B.; Shu, X. Confirmation of the Isomorphous Substitution by Sn Atoms in the Framework Positions of MFI-Typed Zeolite. *Catal. Today* **316**, 193-198 (2018).
18. Wu, E.L.; Lawton, S.L.; Olson, D.H.; Rohrman, A.C.; Kokotailo, Jr.; Kokotailo, G.T. ZSM-5-Type Materials. Factors Affecting Crystal Symmetry. *J. Phys. Chem.* **83** (21), 2777-2781 (1979).
19. Van Kningsveld, H.; Jansen, J.C.; Van Bekkum, H. The Monoclinic Framework Structure of Zeolite H-ZSM-5. Comparison with the Orthorhombic Framework of As-Synthesized ZSM-5. *Zeolites* **10** (4), 235-242 (1990).
20. Marra, G.L.; Artioli, G.; Fitch, A.N.; Milanesio, M.; Lamberti, C. Orthorhombic to Monoclinic Phase Transition in High-Ti-Loaded TS-1: an Attempt to Locate Ti in the MFI Framework by Low Temperature XRD. *Micropor. Mesopor. Mat.* **40** (1-3), 85-94 (2000).
21. Ardit, M.; Martucci, A.; Cruciani, G. Monoclinic-Orthorhombic Phase Transition in ZSM-5 Zeolite: Spontaneous Strain Variation and Thermodynamic Properties. *J. Phys. Chem. C* **119**, 7351-7359 (2015).
22. Borin, M.F.; da Silva, T.; Felisbino, R.F.; Cardoso, D. Synthesis of TS-1 Molecular Sieves Using a New Ti Source. *J. Phys. Chem. B* **110** (31), 15080-15084 (2006).
23. Tuel, A.; Taârit, Y.B. Influence of the Nature of Silicon and Titanium Alkoxides on the Incorporation of Titanium in TS-1 *App. Chem. A* **110** (1), 137-151 (1994).
24. Ch. Deka, R.; Nasluzov, V.A.; Shor, E.A.I.; Shor, A.M.; Vayssilov, G.N.; Rösch, N. Comparison of All Sites for Ti Substitution in Zeolite TS-1 by an Accurate Embedded-Cluster Method. *J. Phys. Chem. B* **109** (51), 24304-24310 (2005).
25. Zheng, A.; Liu, S.B.; Deng, F. ³¹P NMR Chemical Shifts of Phosphorous Probes as Reliable and Practical Acidity Scales for Solid and Liquid Catalysts. *Chem. Rev.* **117** (19), 12475-12531 (2017).
26. Bermejo-Deval, R.; Orazov, M.; Gounder, R.; Hwang, S-J.; Davis, M.E. Active Sites in Sn-Beta for Glucose Isomerization to Fructose and Epimerization to Mannose. *ACS Catal.* **4** (7), 2288-2297 (2017).
27. Boronat, M.; Concepcion, P.; Corma, A.; Renz, M.; Valencia, S. Determination of the Catalytically Active Oxidation Lewis Sites in Sn-Beta Zeolites, and Their

- Optimisation by the Combination of Theoretical and Experimental Studies. *J. Catal.* **234** (1), 111-118 (2005).
28. Otomo, R.; Kosugi, R.; Kamiya, Y.; Tatsumi, T.; Yokoi, T. Modification of Sn-Beta Zeolite: Characterization of Acidic/Basic Properties and Catalytic Performances in Baeyer-Villiger Oxidation. *Catal. Sci. Technol.* **6**, 2787-2795 (2016).
 29. Petříček, V.; Dušek, M.; Palatinus, L. Crystallographic Computing System JANA2006: General Features. *Z. Kristallogr.* **229** (5), 345-352 (2014).
 30. Fung, B.M.; Khitrin, A.K.; Ermolaev, K. An Improved Broadband Decoupling Sequence for Liquid Crystals and Solids. *J. Magn. Reson.* **142** (1), 97-101 (2000).
 31. Bennett, A.E.; Griffin, R.G.; Ok, J.H.; Vega, S. Chemical Shift Correlation Spectroscopy in Rotating Solids: Radio Frequency-Driven Dipolar Recoupling and Longitudinal Exchange. *J. Chem. Phys.* **96** (11), 8624-8627 (1992).

II.6. Supporting Information

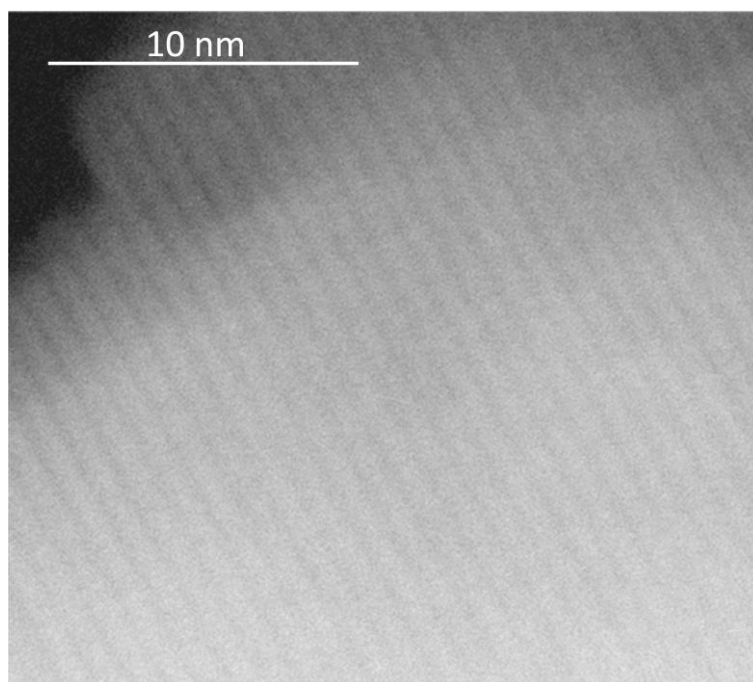


Figure S1. STEM-HAADF micrograph of purely siliceous calcined MFI zeolite, prior Mo introduction by ion exchange conducted in order to get sample Mo-MFI-I

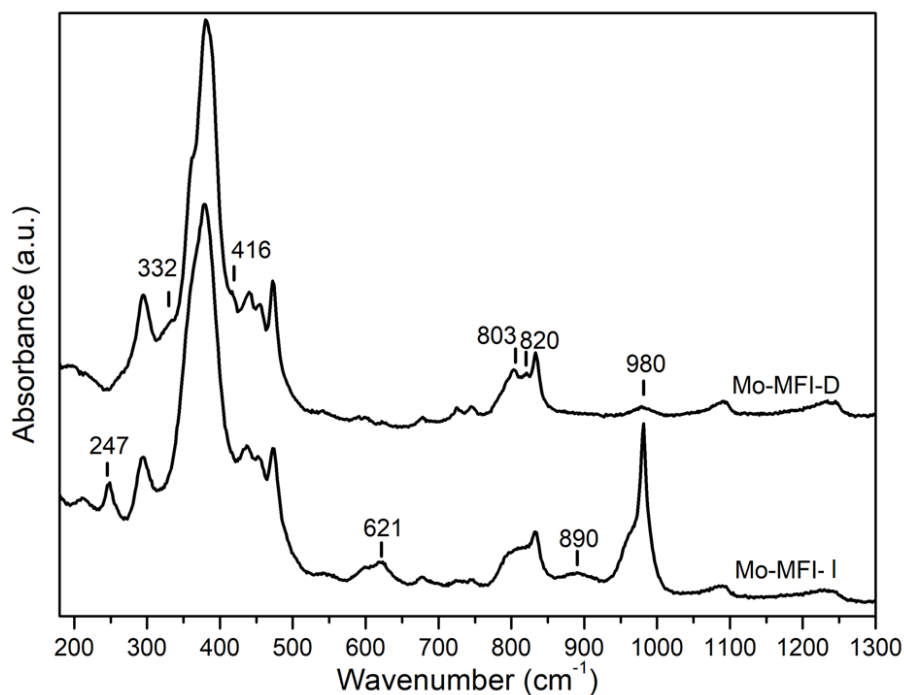


Figure S2. Raman spectra of samples Mo-MFI-I and Mo-MFI-D

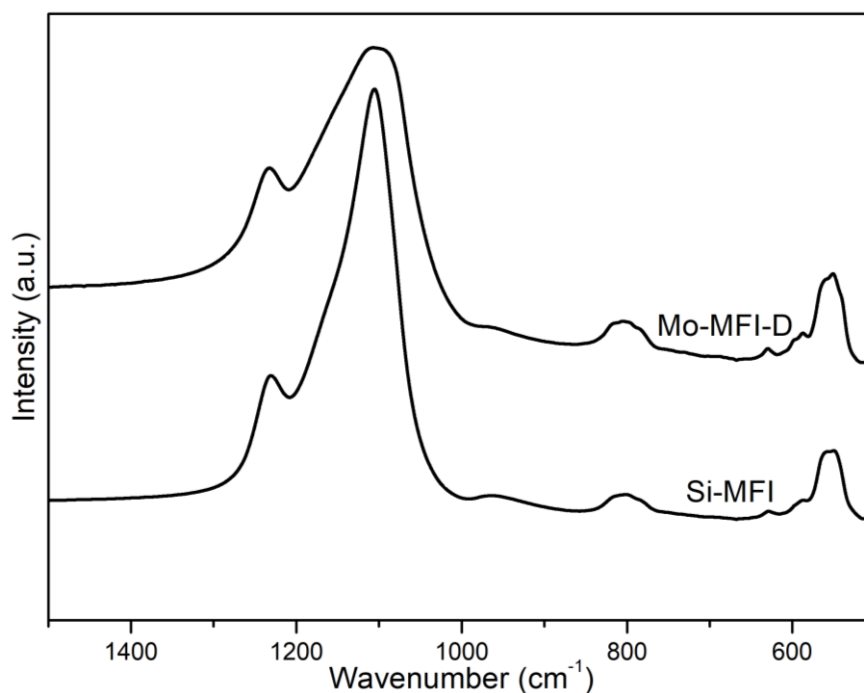


Figure S3. FTIR spectra of sample Mo-MFI-D and Si-MFI (standing for purely siliceous calcined MFI zeolite, prior Mo introduction by ion exchange conducted in order to get sample Mo-MFI-P), measured from self-supported wafers made of 1 wt.% of zeolite sample diluted in 99 wt.% of KBr.

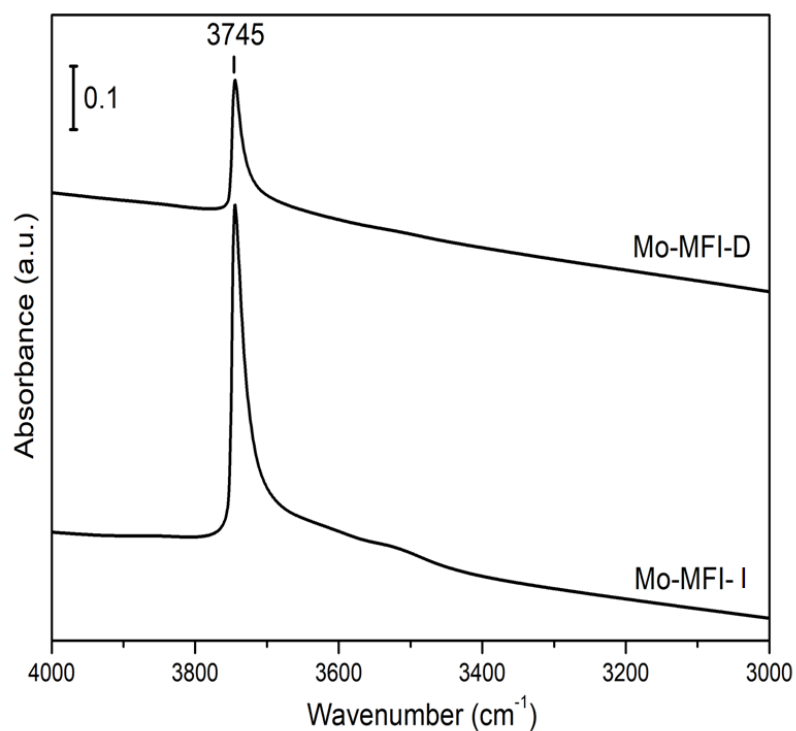


Figure S4. FTIR spectra of activated Mo-MFI-D and Mo-MFI-P samples (480°C, 3h) in the silanol region.

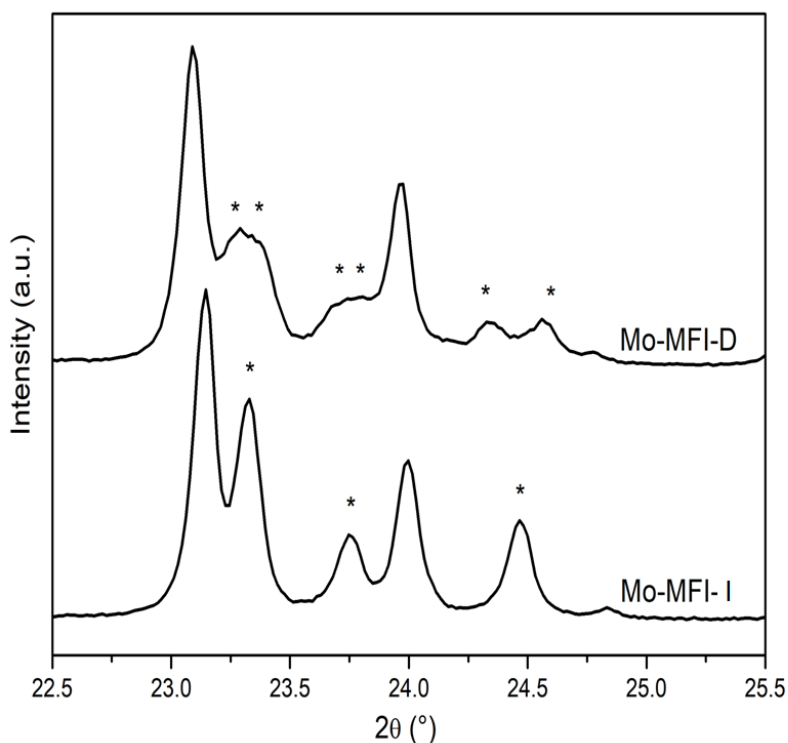


Figure S5. XRD patterns of Mo-MFI-D and Mo-MFI-P samples in the range of 22-26 ° 2θ.

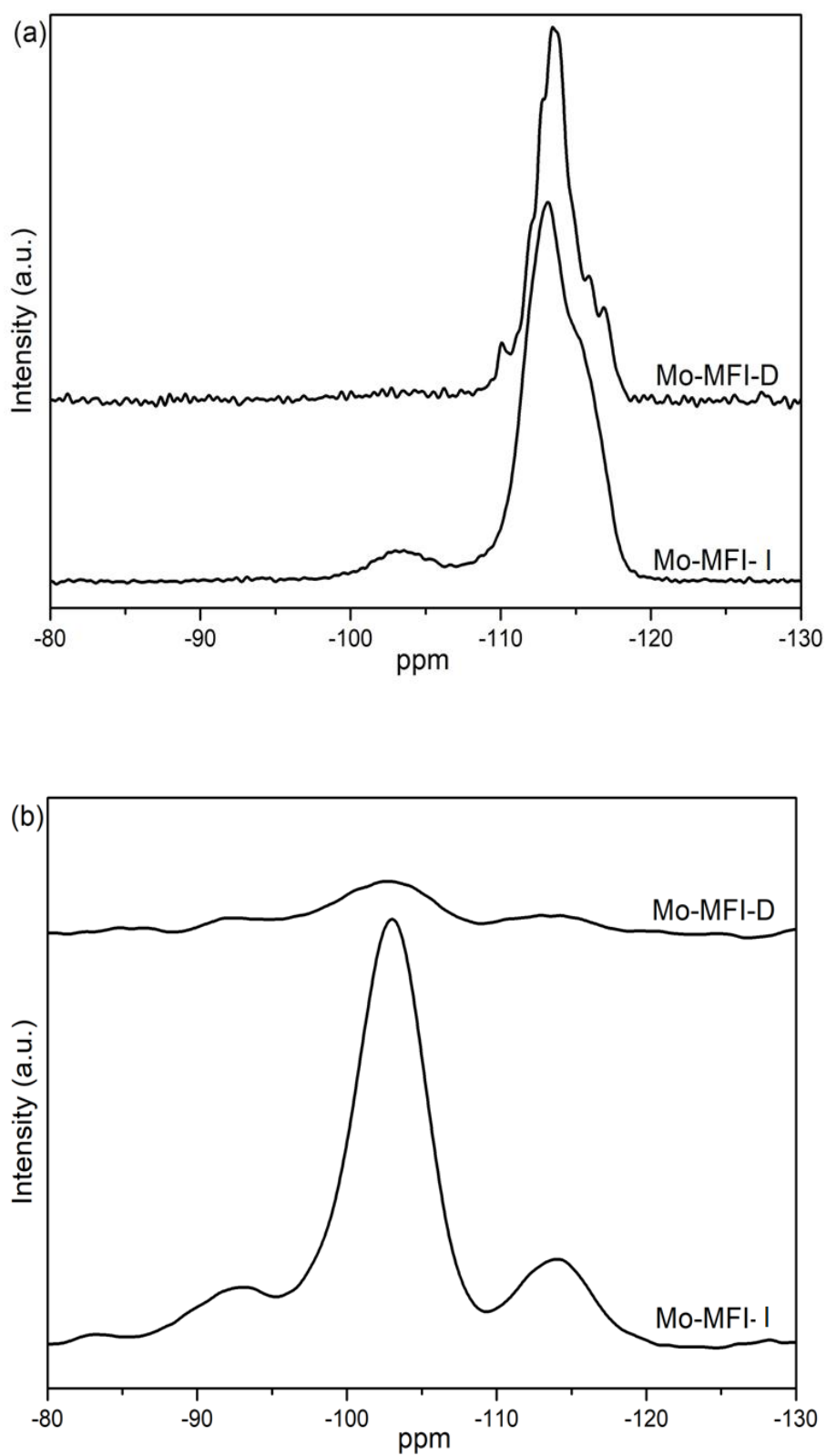


Figure S6. (a) ^{29}Si MAS NMR and (b) CP $\{^1\text{H}\}$ ^{29}Si MAS NMR spectra of samples Mo-MFI-P and Mo-MFI-D

Table S1. Le Bail refinement results of samples Mo-MFI-D and Mo-MFI-P

	Space group	a(Å)	b(Å)	c(Å)	α (°)	Volume (Å ³)	GOF ^a	Rp ^b	wRp ^c
Mo-MFI-D	<i>P2₁/n11</i> (monoclinic)	20.121(1)	19.902(1)	13.386(8)	90.528(7)	5360.5(7)	1.53	4.32	5.75
Mo-MFI-I	<i>Pnma</i> (orthorhombic)	20.061(2)	19.898(4)	13.370(8)	90.000(0)	5337.4(2)	1.56	4.39	5.75

^a Goodness Of Fit

^b Expected R-factor

^c Weight Profile R-factor

Chapter IV: The challenge of silanol species characterization in zeolites

This work is currently being submitted to *Advanced Materials Interfaces*.

Abstract

The chemistry of silica-based materials, including zeolites, is strongly influenced by the nature and amount of their silanols. In zeolites, they are either surface isolated silanol species, or silanol nests corresponding to internal hydrolyzed Si-O-Si bonds; their hydrophilic nature will in turn impact the overall properties of the corresponding material. It is therefore important to assess the nature and to quantify silanol species. This work pools spectroscopic techniques to that effect. The zeolites with a very relevant MFI type structure were prepared as (i) pure siliceous silicalite-1, (ii) aluminium-containing ZSM-5 (Si/Al=110), and (iii) molybdenum-containing silicalite-1 providing a rich spectrum of chemical compositions. The occurrence of silanol nest sites in silicalite-1 is confirmed as well as their removal by isomorphous substitution with molybdenum. The latter also removes part of external silanol species, compared to the purely siliceous silicalite-1. The ZSM-5 highlights the effect of silanol species in the presence of strong Brønsted acid. A protocol for evaluation of silanol species in zeolites using spectroscopic approaches (IR, Raman and NMR) is proposed.

IV.1. Introduction

The extensive use of zeolite-based materials in liquid and gas separation as well as in catalysis is well known, and was a driver to their in depth characterization, so as to optimize their efficiency and better control their synthesis¹. Zeolites are primarily composed of silicon (Si) and aluminium (Al) atoms tetrahedrally coordinated with oxygen (O) bridges forming a three-dimensional framework². A “point defect” in the zeolite framework is an irregularity in the periodic crystalline structure, linked to the presence of silanol (Si-OH) species. They consist of either: (i) terminal silanols located at the edges or on the surface of the crystals, or (ii) internal silanols located within the periodic structure due to the absence of a framework tetrahedrally coordinated Si atom, thus generating a vacancy^{3,4,5}. Usually, these silanol species are described as external (isolated) or germinal silanols, and internal silanol, or silanol nests, respectively. These silanol species are considered as weakly acidic⁶.

In the case of aluminium containing zeolites, other hydroxyl groups are present in the zeolite structure: the so-called Brønsted acid sites. Brønsted acid sites emerge in zeolites due to the presence of hetero-elements such as Al, Ti, Fe, etc. in the framework^{6,7}. These hetero-elements in the zeolite framework are tetrahedrally

coordinated, and thus bring a negative charge to the framework due to their valence, located on one of the bridging oxygen atoms linking the hetero-element to the zeolite framework; the negative charge is therefore compensated by a neighbour cation. A Brønsted acid site is generated when the corresponding cation is a hydrogen atom. Brønsted acid sites are not far away from being silanols or aluminium hydroxides, and thus often referred to as “bridging hydroxyl groups”. Their structure can be summarized as follows: $(\text{SiO})_3\text{-Si-O(H)-Al-(OSi)}_3$. These hydroxylated sites are however very different in nature and properties from usual silanols, and are therefore not considered as silanol species.

The nature and amount of silanols are directly linked to the synthesis procedures or post-synthesis modifications applied towards the preparation of zeolites. By variation of the synthesis conditions, zeolites with variable properties such as crystal size, crystal morphology, aggregation degree, chemical composition and elemental homogeneity can be designed.

A non-exhaustive list of silanol features in zeolites is for instance:

- They are weak points in zeolite structures that will lead to their collapse under harsh conditions^{8,9}. These weak points are for instance the base for the generation of hollow zeolite materials, thanks to the fact that the center of zeolite crystals usually contains more silanol nests, and are consequently more prone to dissolution under controlled conditions⁸.
- Silanols can be seen as reactive species that are able to stabilize metals into zeolite tetrahedral positions through a process called isomorphous substitution.^{10,11}
- Silanol species affect the surface properties of zeolites, such as their hydrophobicity¹²⁻¹⁵, in turn modifying their sorption properties depending on the polarity and nature of the guest molecules^{13,16}.
- Silanol sites can act (synergistically or on their own) as active site in catalysis, influencing the selectivity^{17,18}, or the formation of coke, and coke retention in other cases¹⁹⁻²².

The characterization of silanol species is therefore of major interest, since their presence, amount, location, and nature plays a significant role in the design of fit-for-purpose zeolitic materials.

FT-IR spectroscopy is one of the most widely used techniques to characterize silanols in zeolites. The IR spectral region of 3000 - 4000 cm^{-1} (stretching vibrations) is commonly used to distinguish bridging hydroxyl groups (Brønsted acid sites, linked to the presence of Al-OH, around 3608 cm^{-1}) from isolated silanols (3745 cm^{-1}), or silanol nests (3500 - 3600 cm^{-1}).^{11,23-27} While the stretching vibrations provide valuable information on the nature of the silanols (internal, external, ...), they cannot be quantified since both band positions and extinction coefficients are affected by the

environment of the different hydroxyl groups and H-bonding (depending whether the silanols are germinal, vicinal, isolated, ...).^{9,28,29}

To quantify the total amount of silanols in zeolites, the combination ($\nu+\delta$) OH bands in the 4800 - 4200 cm^{-1} range is valuable. The silanol and water contents of various porous silicas were quantified and reported by Gallas *et al.*²⁸, by combining a simultaneous *in-situ* recording of IR spectroscopy with thermogravimetric analysis (TG-IR); the extinction coefficient of the ($\nu+\delta$) OH combination band was determined. In addition, deuterium isotopic exchange was carried out on the silanols using deuterated water. Back-exchange with alcohols of different sizes was subsequently performed, allowing the quantification of silanols and the drawing of a silanol accessibility map: silanols were consumed based on their accessibility by each alcohols as a function of its size, since the ($\nu+\delta$) OD combination band is shifted with regards to the corresponding ($\nu+\delta$) OH combination band. In a similar study, Ide *et al.*³⁰ treated the silanols with silanes of different sizes to derive their accessibility.

Alternatively, silanol quantification was also attempted using pyridine as a probe molecule³¹. However, the variation of extinction coefficient and significant overlap between the coordinated and physisorbed pyridine bands makes this approach of little use³². The relative acidity of silanols was assessed using CO as a probe molecule monitored by FTIR; some silanols displayed strong acidity related to the nature of the material under consideration (crystalline vs. amorphous, hydrophobic vs. hydrophilic).³³

In addition to IR spectroscopy, a commonly used technique for silanols evaluation is solid-state ^1H NMR as ^1H possesses a spin $\frac{1}{2}$ and quantification is more straightforward than with IR. ^1H NMR can therefore quantify and distinguish silanols based on their chemical shifts (non-acidic isolated silanols: ~ 1.4 ppm, silanol nests: ~ 2.2 ppm, Brønsted acid sites: ~ 4.3 ppm) although the chemical shift range is rather narrow and overlapping.³⁴ By comparing the relative quantity of different silanols in as synthesized zeolites, after template removal by calcination, and ion exchange, the formation mechanism of internal silanols as a function of the template location could be elucidated.³⁵⁻³⁷ Deuterium exchange of ZSM-5 zeolite studied by both ^1H and ^2H NMR spectroscopy was used to reveal silanol species based on their geometry.³⁸ While ^{29}Si NMR could estimate the total amount of silanols by quantifying the Q² (-91 ppm) and Q³ (-103 ppm) species as presented by Zhang *et al.*³⁴

In this chapter, spectroscopic techniques are used to determine the nature and to quantify silanols in three zeolite samples, all MFI framework types, namely: (i) silicalite-1 (Si-MFI), (ii) ZSM-5 (Al-MFI), and (iii) molybdenum containing silicalite-1 (Mo-MFI). Their silanols are thoroughly characterised by FTIR, Raman, ^{29}Si MAS NMR, $\{^1\text{H}\}$ ^{29}Si CP-MAS NMR, ^1H MAS NMR, and ^{31}P MAS NMR of adsorbed trimethylphosphine oxide (TMPO)^{39,40}.

IV.2. Experimental

IV.2.1. Synthesis

Si-MFI, Al-MFI and Mo-MFI zeolites were prepared using the following chemicals without further purification: tetraethyl orthosilicate (TEOS, 98%, Aldrich), tetra n-propylammonium hydroxide (TPAOH, 20 wt. % in water solution, Alfa Aesar), aluminium nitrate ($\text{Al}(\text{NO}_3)_3 \cdot 9\text{H}_2\text{O}$, 97%, Prolabo), and sodium molybdate dihydrate ($\text{Na}_2\text{MoO}_4 \cdot 2\text{H}_2\text{O}$, Alfa Aesar, 98%). Double distilled water was systematically used in all synthesis steps requiring the use of water. Syntheses were carried out in closed 125 mL polypropylene (PP) bottles under autogenous pressure and quiescent conditions (Si-MFI and Mo-MFI), or in Teflon-lined autoclaves under autogenous pressure and quiescent conditions (Al-MFI). All harvested sample have approximately the same particle size (around 150 nm).

IV.2.1.a. Synthesis of Si-MFI

The chemical composition of the precursor mixture was: 1 SiO_2 : 0.28 TPAOH : 40 H_2O . The resulting clear suspension was stirred 1h at room temperature, before hydrolysis for 18 h on an orbital shaker. Then, hydrothermal synthesis was carried out at 90 °C for 48 h. The crystalline product was recovered and purified by high speed centrifugation (20,000 rpm) until a pH of 7 was reached; the product was then dried at 80 °C and calcined in a muffle furnace (550 °C, 5 h); this sample was abbreviated as Si-MFI.

IV.2.1.b. Synthesis of Al-MFI

The chemical composition of the precursor mixture was: 1 SiO_2 : 0.357 TPAOH : 0.004 Al_2O_3 : 16.189 H_2O . The resulting clear suspension was stirred 1h at room temperature, before hydrolysis for 18h on an orbital shaker. The precursor mixture was then transferred into Teflon-lined autoclaves, and hydrothermal synthesis was carried out at 180 °C for 72 h. The crystalline product was recovered and purified following the procedure described above. The sample with a Si/Al ratio of 110 according to ICP was abbreviated as Al-MFI.

IV.2.1.c. Synthesis of Mo-MFI

To an aqueous and homogeneous solution of sodium molybdate (0.107 M, 8 mL) was added 300 mg of sample Si-MFI *vide-supra*; the resulting suspension was stirred for 1 h and further heated at 90 °C for 96 h in quiescent conditions (post hydrothermal synthesis method). The crystalline product was recovered following the procedure described above so as to prevent any unreacted Mo species from staying in the microporous volume of the zeolite sample. The H-form of the Mo-MFI zeolite was prepared by ion exchange treatment: the calcined powder is dispersed in an ammonium chloride solution (NH_4Cl , 0.2 M, solid/liquid weight ratio = 0.1), and stirred for 1 h, prior being subjected to calcination (550 °C; 5h). The sample was abbreviated as Mo-MFI.

IV.2.2. Characterization

The silanols in the zeolite were characterized by FTIR spectroscopy using a Nicolet Magna 550-FT-IR spectrometer (4 cm^{-1} optical resolution). Self-supported zeolite wafers (1 cm^2 , av. 20 mg, hydraulic press at 1 t/cm^2) were first activated at $480\text{ }^\circ\text{C}$ for 3h under vacuum (av. 2.5×10^{-6} Torr) prior to the measurements. Additionally, the zeolites were mixed with KBr and directly measured; the wafer mass was 100 mg with approximately 0.5 wt. % of zeolite in this case.

Raman spectra were collected on a Jobin Yvon Labram 300 confocal Raman spectrometer coupled with a microscope (objective: 50x) and a CCD detector. A 532 nm laser was used, and the spectra were accumulated three times for 60 s each.

^{29}Si , ^1H , and ^{31}P NMR spectra were all collected on a Bruker Avance III-HD (11.7 T) spectrometer operating at 99.3, 500, and 202.4 MHz, respectively; a 4 mm outer diameter zirconia rotor spun at 12 KHz in the case of ^{29}Si and ^1H NMR, and a 3.2 mm outer diameter zirconia rotor spun at 22 KHz in the case of ^{31}P NMR were used. Single pulse excitations were used, with a flip angle of 30° for ^{29}Si , and 90° for ^1H and ^{31}P spectra, corresponding to radio frequency fields of 114, 94, and 41 KHz for ^{29}Si , ^1H , and ^{31}P respectively. $\{^1\text{H}\}$ ^{29}Si CP-MAS NMR cross-polarization experiments were performed with a contact time of 5 ms, and a recycle delay of 2 s. Chemical shifts were referenced to tetramethyl silane (TMS) for ^1H and ^{29}Si , and to phosphoric acid (H_3PO_4 , 1M) for ^{31}P .

Prior to the ^1H MAS NMR experiments, the samples (loaded in unsealed rotors) were dehydrated at $200\text{ }^\circ\text{C}$ for 12 h, and promptly sealed inside the oven so as to prevent rehydration. Prior to the ^{31}P MAS NMR experiments, trimethylphosphine oxide (TMPO) was impregnated on the zeolitic sample according to the following procedure. All steps were conducted under an inert Argon (Ar) atmosphere to prevent any reaction of the TMPO with moisture in the air and zeolitic water. The zeolite samples were first dehydrated at $400\text{ }^\circ\text{C}$ under vacuum (4.0×10^{-5} Torr) while a solution of TMPO dissolved in dichloromethane (CH_2Cl_2) was prepared in parallel. The solution was then mixed with the dehydrated zeolite powder followed by sonication for 15 min. The obtained suspensions were then evaporated for 2 h at room temperature and under vacuum. The harvested TMPO loaded samples were then transferred into 3.2 mm outer diameter zirconia rotors, still under Ar atmosphere, so as to record ^{31}P MAS NMR spectra. The (excess) precise TMPO loading was chosen so as to not have too much non-chemisorbed species (crystalline and/or physisorbed TMPO) that might “hide” the NMR signals of interest.

IV.3. Results and discussion

The FTIR spectra of Si-MFI, Al-MFI, and Mo-MFI samples are depicted in Figure 1. The Si-MFI spectrum displays one intense narrow band at 3746 cm^{-1} , attributed to the presence of isolated silanols, and a band located at 3520 cm^{-1} , attributed to the presence of silanol nests. Another band at 4550 cm^{-1} related with all silanols (combination ($\nu+\delta$) OH bands) is observed as well, but its low intensity prevents a reliable quantification. In sample Al-MFI, a new band appears at 3615 cm^{-1} , and is the usual signature of bridged hydroxyls, the so-called Brønsted acid sites. The bands at 3746 and 3520 cm^{-1} are still observed, indicating that both isolated silanols and silanol nests species are also present in the Al-MFI sample. However, sample Mo-MFI does not show bands at 3520 cm^{-1} (silanol nests) and at 3615 cm^{-1} (bridged hydroxyls) as this zeolite sample is Al-free. Furthermore, the band at 3746 cm^{-1} (isolated silanols) is still present albeit with a much lower intensity, while the band at 4550 cm^{-1} is absent due to the very low amount of silanols in Mo-MFI zeolite sample. Figure 2 shows a schematic representation of the different types of silanols.

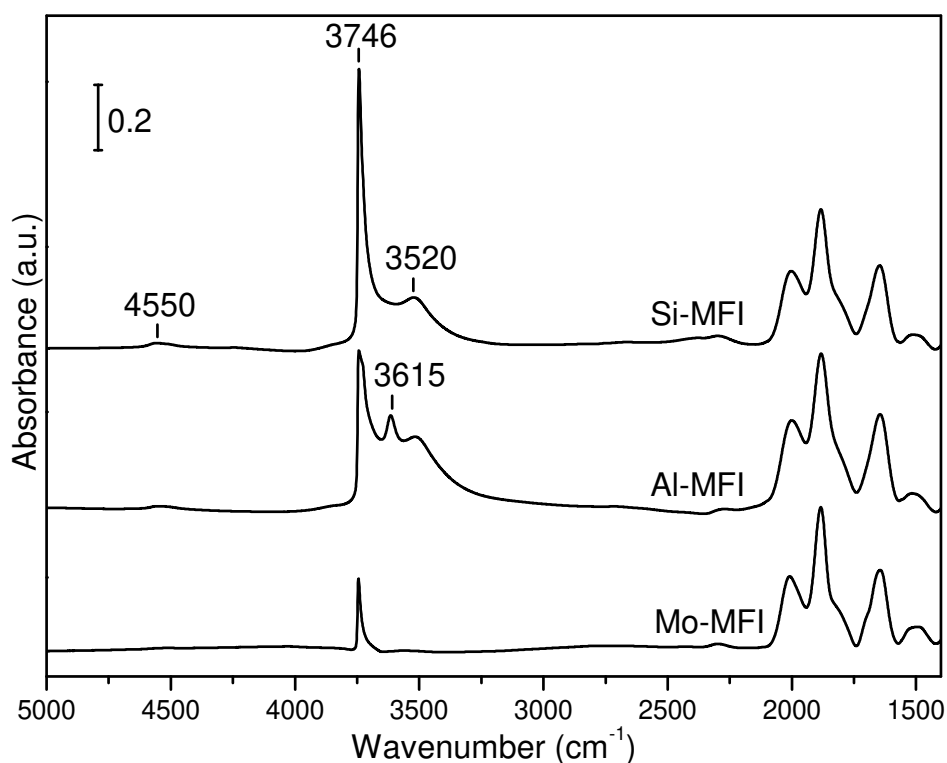


Figure 1. FTIR spectra of (dehydrated) zeolite samples: Si-MFI, Al-MFI, and Mo-MFI.

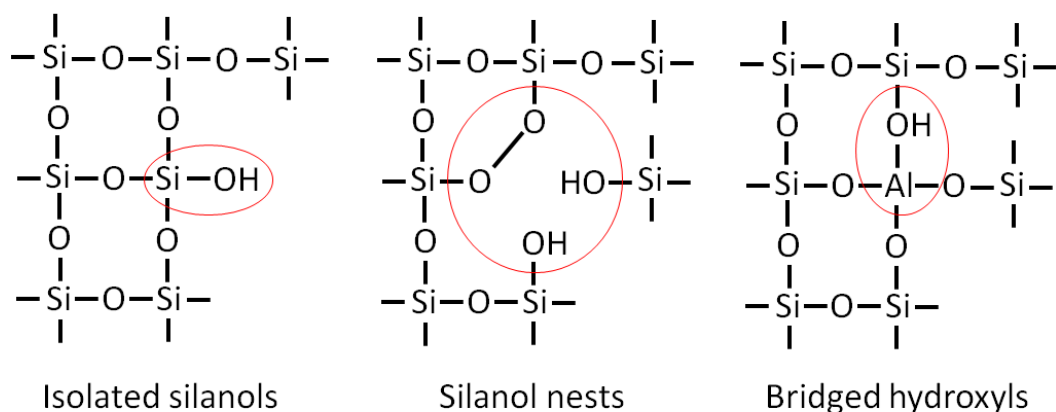


Figure 2. Visual representation of isolated silanols, silanol nests, and bridged hydroxyls (Brønsted acid sites).

Silanols could also be observed based on IR spectroscopy of framework vibration region as shown in Figure 3. The band attributed to silanols at 980 cm^{-1} is clearly observed in the IR spectrum of Si-MFI sample, and slightly red-shifted towards 965 cm^{-1} for the Al-MFI sample due to the presence of framework Al species.^{41,42,43} While, Mo-MFI sample does not display any band in this region, due to the very low amount of silanols present in this sample.

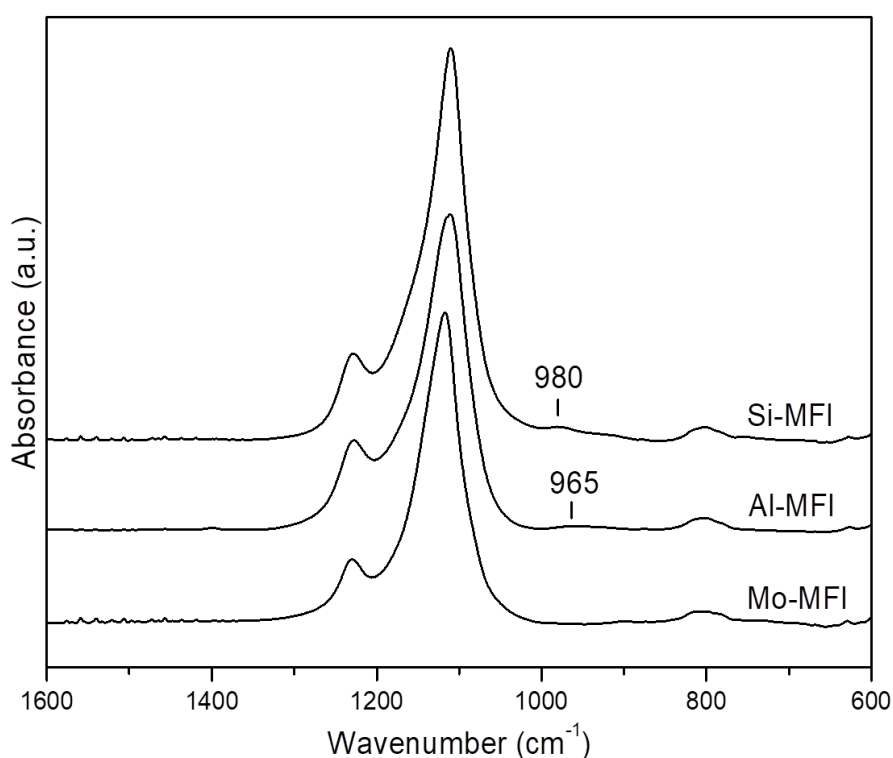


Figure 3. FTIR spectra of samples Si-MFI, Al-MFI, and Mo-MFI (zeolites : KBr= 0.5 wt.%, spectra recorded under ambient conditions).

Silanols were also observed by Raman spectroscopy (Figure 4) where the 980 cm^{-1} band is attributed to silanol species^{41,42}. This band is intense on both samples Si-MFI and Al-MFI, but slightly red-shifted in Al-MFI due to the presence of bridged hydroxyls⁴³. However, on the Mo-MFI sample, almost no signal is observable at 980 cm^{-1} in agreement with the low concentration of silanols as observed by IR as well as the absence of MoO_3 species, while new bands (332, 416, 803, and 820 cm^{-1}) indicate the presence of framework Mo^{40,44}. The bands at 332 and 416 cm^{-1} are attributed to Si-O-Mo framework vibrations while attribution of the bands at 803 and 820 cm^{-1} remains unclear.

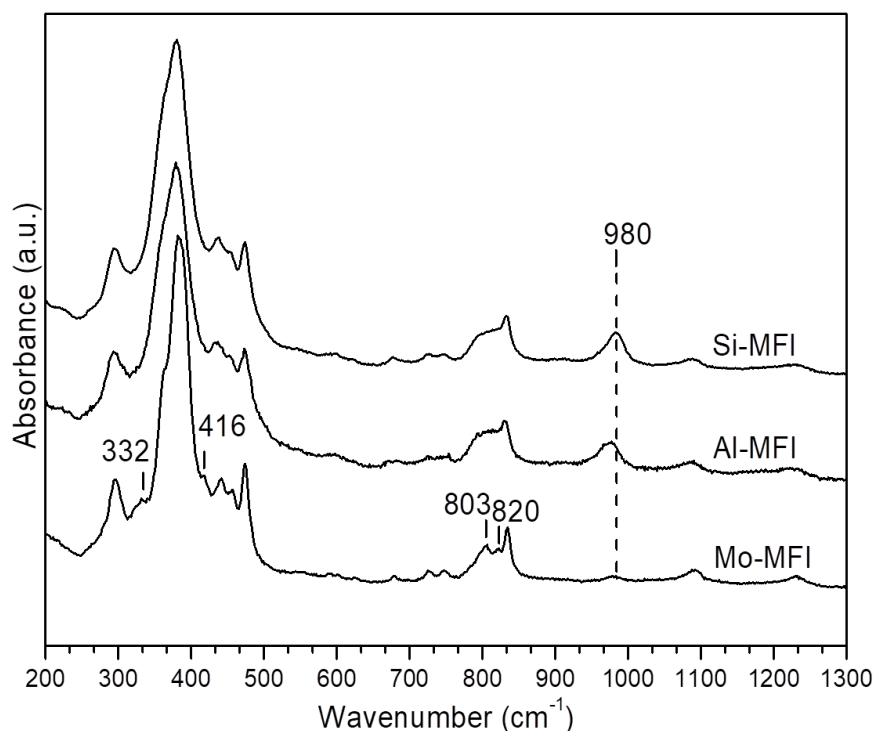


Figure 4. Raman spectra of zeolite samples Si-MFI, Al-MFI, and Mo-MFI.

The local environment of Si atoms in the zeolites was further investigated by ^{29}Si MAS NMR (Figure 5). Both Si-MFI and Al-MFI samples contain Q^3 ($(\text{SiO})_3\text{-OH}$) and unresolved Q^4 (SiO_4) species, indicating the presence of silanol species. However, for sample Mo-MFI, no Q^3 species are observed, and well-resolved Q^4 species are present pointing out the extremely low amount of silanol species, and the exceptionally high local homogeneity of the sample due to the absence of silanol nests⁴⁰. Indeed, the relative homogeneity between T-sites of the crystalline structure is linked to the presence of silanol species: by removing silanols, the local structure homogeneity is improved. This clearly demonstrates that Mo introduced in the MFI framework by isomorphous substitution reacts with silanol species, and especially with silanol nests, leading to a crystalline structure free of any silanol nests, and containing in addition a greatly reduced amount of isolated silanols.

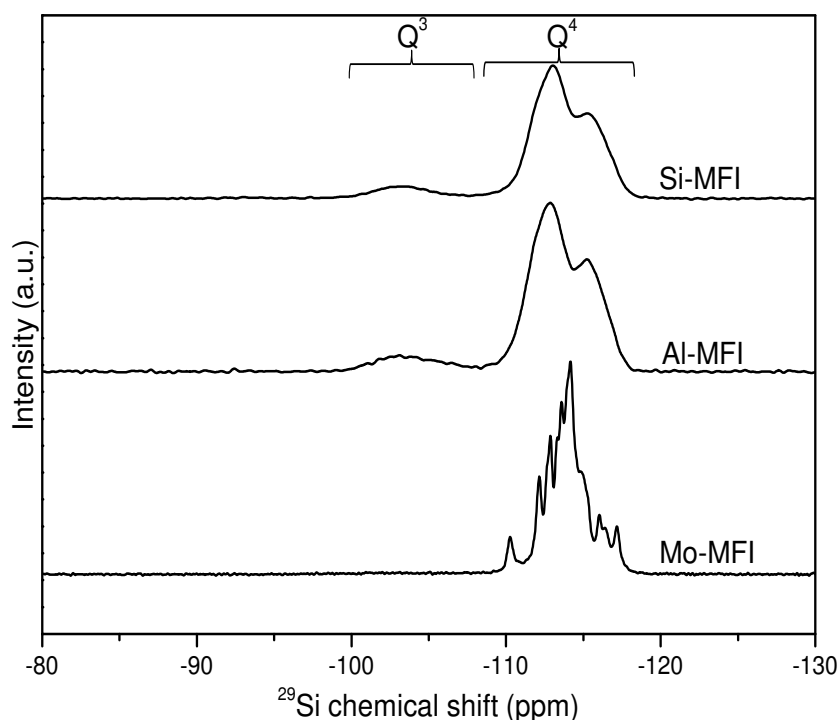


Figure 5. ^{29}Si MAS NMR spectra of Si-MFI, Al-MFI, and Mo-MFI samples.

The samples were also characterized by Cross-Polarization $\{^1\text{H}\}$ ^{29}Si CP MAS NMR spectroscopy (Figure 6). The presence of Q^2 ($(\text{SiO})_2(\text{OH})_2$), Q^3 and Q^4 species is observed in both Si-MFI and Al-MFI samples while no signal is present in the spectrum of sample Mo-MFI. This indicates that almost no hydrogen atoms are spatially in close proximity to any Si in sample Mo-MFI, in line with its very low silanol content, in contrast to samples Si-MFI and Al-MFI. In sample Al-MFI, however, almost no Q^2 species are observed even though silanol species are still present. This indicates a low amount of Q^2 , due to the preferential location of Al in silanol nests. Unfortunately, such a spectroscopic study does not provide any quantitative information and further NMR studies are necessary, as ^1H MAS NMR, *vide infra*.

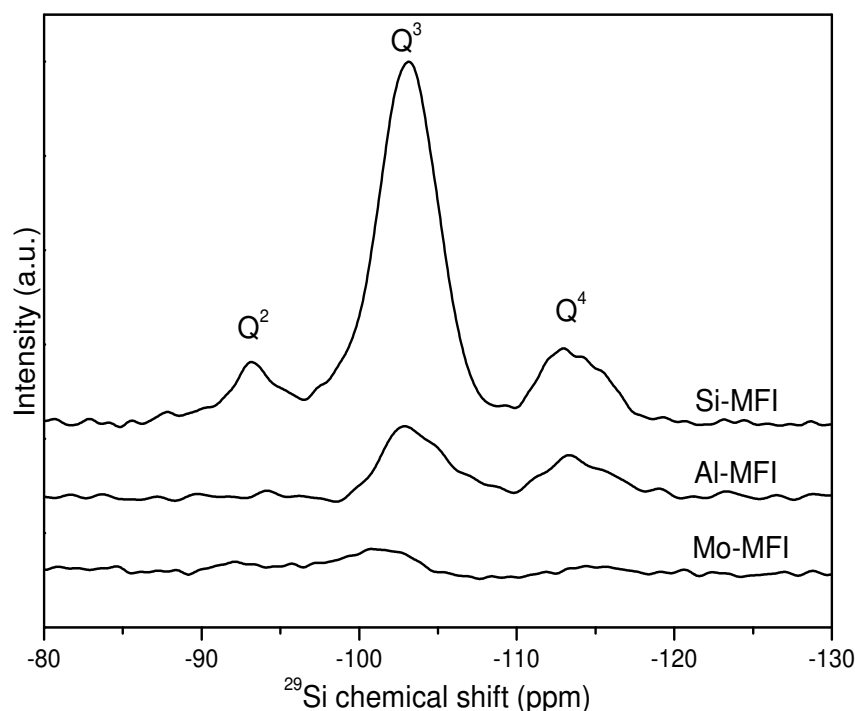


Figure 6. $\{^1\text{H}\}$ ^{29}Si CP MAS NMR spectra of samples Si-MFI, Al-MFI, and Mo-MFI.

^1H MAS NMR is a well-established technique to quantify hydroxyl groups. A complete dehydration of the samples is required to prevent an unwanted contribution of water (Figure 7). In the ^1H MAS NMR spectrum of Si-MFI sample, the two peaks at 2.2 and 3.9 ppm observed are attributed to isolated silanol species and silanol nests, respectively. In Al-MFI sample, one additional peak located at 5.5 ppm appears, attributed to bridged hydroxyls. While, in the ^1H MAS NMR spectrum of sample Mo-MFI, a single low-intensity signal at 2.2 ppm is present, which is in full agreement with the IR *vide supra*. To quantify the silanol species, all samples were measured under identical conditions, and the total area of the signal from 0 to 8 ppm was integrated (a rotor containing a known amount of water was used as a reference for calibration of the relation “signal vs. quantity in moles”). Since samples are dehydrated, all ^1H nucleus observed are due to silanols. As a result, the content of silanol species as isolated, nests, and bridged hydroxyls can be precisely evaluated. Based on ^1H MAS NMR spectroscopic study, samples Si-MFI, Al-MFI, and Mo-MFI contained 4.0 mmol/g, 3.7 mmol/g, and 1.1 mmol/g of total silanol species (bridging hydroxyl groups + silanol nests + isolated silanols), respectively. More precisely, all the silanol nests (3.9 ppm, 1.9 mmol/g) observed in sample Si-MFI were cured under introduction of Mo (Mo-MFI sample). While only half of the isolated silanol species (2.2 ppm) were suppressed, i.e., 2.1 mmol/g for Si-MFI, and 1.1 mmol/g for Mo-MFI were measured, respectively. Sample Al-MFI shows signals at 2.2, 3.9, and 5.5 ppm accountable for approximately 0.9, 2, and 0.9 mmol/g of isolated silanols, silanol nests and bridging hydroxyl groups, accordingly. A summary of the quantification performed on ^1H MAS NMR data is given in Table 1.

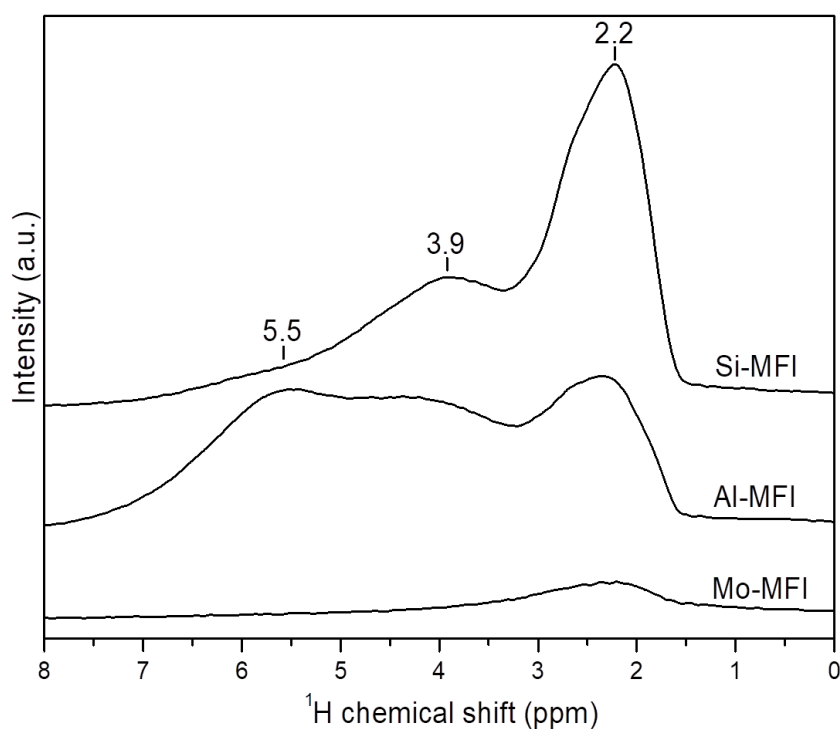


Figure 7. ^1H MAS NMR spectra of dehydrated samples Si-MFI, Al-MFI, and Mo-MFI.

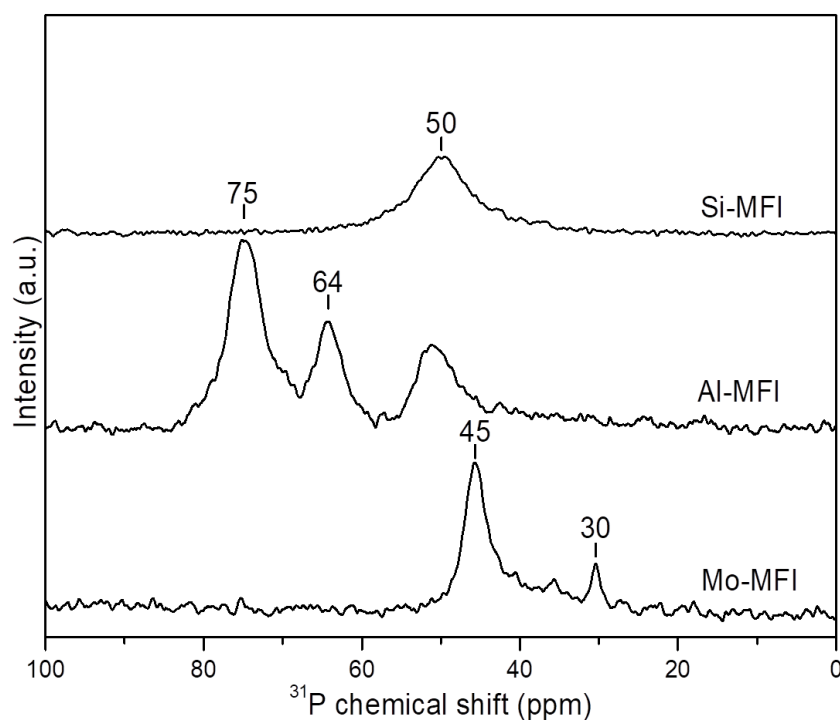
Table 1. Quantification of silanol species in Si-MFI, Al-MFI, and Mo-MFI samples based on ^1H MAS NMR.

Sample	Si-MFI	Al-MFI	Mo-MFI
Isolated silanols (mmol/g)	2.1	0.9	1.1
Silanol nests (mmol/g)	1.9	2.0	0.0
Bridging OH groups (mmol/g)	0.0	0.9	0.0
Total silanols (mmol/g)	4.0	3.7	1.1

Additionally, the hydroxyl groups of the three samples were investigated by impregnation of the dehydrated samples with trimethyl phosphine oxide (TMPO) and monitored by ^{31}P MAS NMR (Figure 8). Peaks at 43 ppm and 30 ppm (appearing as a function of the TMPO loading of the sample) correspond to crystalline and physisorbed TMPO, respectively and do not provide relevant information on the zeolite surface and will not be considered further (Table 2). On Si-MFI, the peak at 50 ppm is attributed to the presence of TMPO interacting with silanols. On Al-MFI, two additional peaks appear at 64 and 75 ppm, corresponding to TMPO adsorbed on bridged hydroxyls. Mo-MFI displays only one peak at 45 ppm, attributed to TMPO interacting with framework molybdenum Lewis acidity⁴⁰. This result clearly highlights the removal of most of the Si-OH species (complete removal of silanol nests, and partial removal of isolated silanol species) upon introduction of Mo by isomorphous substitution in the MFI framework.

Table 2. Attribution of ^{31}P MAS NMR chemical shifts observed for TMPO adsorbed in zeolite samples.^{39,40}

Chemical shift (ppm)	Attribution
30	Physisorbed TMPO
43	Crystalline TMPO
45	TMPO interacting with framework Mo
50	TMPO interacting with silanols
64 and 75	TMPO interacting with bridging hydroxyl groups

**Figure 8.** ^{31}P MAS NMR of TMPO adsorbed on Si-MFI, Al-MFI, and Mo-MFI samples.

The summary of the characterization techniques with the information revealed for evaluation of silanols in zeolites is provided in Table 3.

Table 3. Comparison of our different techniques to characterize (nature and quantity) zeolitic hydroxyls.

Technique	Quantification	Comments
FTIR	Yes, but low precision	Identification of silanols using the 4000-3000 cm^{-1} bands; no precise quantification ^{9,28,29} . Total silanol content is determined using the 5000-4000 cm^{-1} bands; low sensitivity due to weak intensity of IR bands. No quantification and poor identification in the framework vibration region (500-1500 cm^{-1}), observed by dilution in KBr.
^1H MAS NMR	Yes	Identification of the nature of silanol species based on their chemical shifts. Quantification of silanols on dehydrated samples.
^{29}Si MAS NMR	Relative	Identification of silanols but very poor quantification (only relative comparison between samples). Silanols mostly visible as Q^3 , and undistinguishable from aluminium-induced Q^3 .
$\{^1\text{H}\} ^{29}\text{Si}$ CP-MAS NMR	Relative	Identification of silanols depending on their coordination to the framework (Q^2 , Q^3 species) is possible. No absolute quantification is possible.
TMPO/ ^{31}P MAS NMR	Yes, but low precision	Identification of silanol as a function of their relative acidity is possible (as long as they are accessible for TMPO), but with poor precision and resolution. Approximative quantification of TMPO accessible sites possible when the peak attributed to silanol is relatively isolated, and all sites are covered (presence of physisorbed TMPO).
Raman	No	Poor identification of silanols, quantification is impossible unless a probe molecule is used; the results have a low precision.

IV.4. Conclusions

Hydroxyl groups, silanols in particular, in three nanosized MFI type zeolites (Si-MFI, Al-MFI, and Mo-MFI) with identical particle size, have been characterized by IR, Raman, and NMR spectroscopies. The nature and amount of the various silanols were determined unambiguously by cross-checking the results of different techniques. The complete removal of silanol nests from the pure silica sample (Si-MFI) upon post-synthesis introduction of molybdenum (Mo-MFI) leads to a full isomorphous substitution of Mo in framework positions. Based on this study, a summary evaluation of the used characterization techniques towards identification and quantification of silanol species is provided (Table 3). Accordingly, the most efficient way to identify and quantify silanols simultaneously was the use of ^1H MAS NMR of dehydrated zeolites. However, the use of other techniques and especially of

IR was complementary, in particular for the identification of silanols. The characterization of silanols in zeolite samples is challenging and therefore several spectroscopic techniques are required.

IV.5. References

1. C. J. Rhodes, Properties and applications of zeolites. *Sci. Prog.* **93**, 223–284 (2010).
2. J. Weitkamp, Zeolites and catalysis. *Solid State Ionics.* **131**, 175–188 (2000).
3. B. Bonelli, L. Forni, A. Aloise, J. B. Nagy, G. Fornasari, E. Garrone, A. Gedeon, G. Giordano, F. Trifirò, Beckmann rearrangement reaction: About the role of defect groups in high silica zeolite catalysts. *Microporous Mesoporous Mater.* **101**, 153–160 (2007).
4. T. Karbowski, M. A. Saada, S. Rigolet, A. Ballandras, G. Weber, I. Bezverkhy, M. Soulard, J. Patarin, J. P. Bellat, New insights in the formation of silanol defects in silicalite-1 by water intrusion under high pressure. *Phys. Chem. Chem. Phys.* **12**, 11454–11466 (2010).
5. S. Bordiga, I. Roggero, P. Ugliengo, A. Zecchina, V. Bolis, G. Artioli, R. Buzzoni, G. Marra, F. Rivetti, G. Spano, C. Lamberti, Characterisation of defective silicalites. *J. Chem. Soc. Dalton Trans.*, 3921–3929 (2000).
6. M. Boronat, A. Corma, Factors Controlling the Acidity of Zeolites. *Catal. Letters.* **145**, 162–172 (2015).
7. G. L. Woolery, G. H. Kuehl, On the nature of framework Brønsted and Lewis acid sites in ZSM-5. *Zeolites.* **19**, 288–296 (1997).
8. Y. Wang, A. Tuel, Nanoporous zeolite single crystals: ZSM-5 nanoboxes with uniform intracrystalline hollow structures. *Microporous Mesoporous Mater.* **113**, 286–295 (2008).
9. L. Zhang, K. Chen, B. Chen, J. L. White, D. E. Resasco, Factors that Determine Zeolite Stability in Hot Liquid Water. *J. Am. Chem. Soc.* **137**, 11810–11819 (2015).
10. S. Dzwigaj, P. Massiani, A. Davidson, M. Che, Role of silanol groups in the incorporation of V in β zeolite. *J. Mol. Catal. A Chem.* **155**, 169–182 (2000).
11. P. Wolf, C. Hammond, S. Conrad, I. Hermans, Post-synthetic preparation of Sn-, Ti- and Zr-beta: A facile route to water tolerant, highly active Lewis acidic zeolites. *Dalt. Trans.* **43**, 4514–4519 (2014).
12. E. E. Mallon, M. Y. Jeon, M. Navarro, A. Bhan, M. Tsapatsis, Probing the relationship between silicalite-1 defects and polyol adsorption properties. *Langmuir.* **29**, 6546–6555 (2013).
13. J. Grand, S. N. Talapaneni, A. Vicente, C. Fernandez, E. Dib, H. A. Aleksandrov, G. N. Vayssilov, R. Retoux, P. Boullay, J. P. Gilson, V. Valtchev,

- S. Mintova, One-pot synthesis of silanol-free nanosized MFI zeolite. *Nat. Mater.* **16**, 1010–1015 (2017).
14. H. Zhou, J. Mouzon, A. Farzaneh, O. N. Antzutkin, M. Grahn, J. Hedlund, Colloidal Defect-Free Silicalite-1 Single Crystals: Preparation, Structure Characterization, Adsorption, and Separation Properties for Alcohol/Water Mixtures. *Langmuir.* **31**, 8488–8494 (2015).
 15. C. H. Wang, P. Bai, J. I. Siepmann, A. E. Clark, Deconstructing hydrogen-bond networks in confined nanoporous materials: Implications for alcohol-water separation. *J. Phys. Chem. C.* **118**, 19723–19732 (2014).
 16. J. W. Harris, M. J. Cordon, J. R. Di Iorio, J. C. Vega-Vila, F. H. Ribeiro, R. Gounder, Titration and quantification of open and closed Lewis acid sites in Sn-Beta zeolites that catalyze glucose isomerization. *J. Catal.* **335**, 141–154 (2016).
 17. X. Meng, Q. Yu, Y. Gao, Q. Zhang, C. Li, Q. Cui, Enhanced propene/ethene selectivity for methanol conversion over pure silica zeolite: Role of hydrogen-bonded silanol groups. *Catal. Commun.* **61**, 67–71 (2015).
 18. N. Rai, S. Caratzoulas, D. G. Vlachos, Role of silanol group in Sn-beta zeolite for glucose isomerization and epimerization reactions. *ACS Catal.* **3**, 2294–2298 (2013).
 19. K. Lee, S. Lee, Y. Jun, M. Choi, Cooperative effects of zeolite mesoporosity and defect sites on the amount and location of coke formation and its consequence in deactivation. *J. Catal.* **347**, 222–230 (2017).
 20. L. Lakiss, F. Ngoye, C. Canaff, S. Laforge, Y. Pouilloux, Z. Qin, M. Tarighi, K. Thomas, V. Valtchev, A. Vicente, L. Pinard, J. P. Gilson, C. Fernandez, On the remarkable resistance to coke formation of nanometer-sized and hierarchical MFI zeolites during ethanol to hydrocarbons transformation. *J. Catal.* **328**, 165–172 (2015).
 21. F. Thibault-Starzyk, A. Vimont, J.-P. Gilson, 2D-COS IR study of coking in xylene isomerisation on H-MFI zeolite. *Catal. today.* **70**, 227–241 (2001).
 22. C. Fernandez, I. Stan, J.-P. Gilson, K. Thomas, A. Vicente, A. Bonilla, J. Pérez-Ramírez, Hierarchical ZSM-5 zeolites in shape-selective xylene isomerization: role of mesoporosity and acid site speciation. *Chem. Eur. J.* **16**, 6224–6233 (2010).
 23. J. N. Kondo, E. Yoda, H. Ishikawa, F. Wakabayashi, K. Domen, Acid property of silanol groups on zeolites assessed by reaction probe IR study. *J. Catal.* **191**, 275–281 (2000).
 24. S. Dzwigaj, P. Massiani, A. Davidson, M. Che, Role of silanol groups in the incorporation of V in β zeolite. *J. Mol. Catal. A Chem.* **155**, 169–182 (2000).
 25. G. L. Woolery, L. B. Alemany, R. M. Dessau, A. W. Chester, Spectroscopic evidence for the presence of internal silanols in highly siliceous ZSM-5. *Zeolites.* **6**, 14–16 (1986).

26. P. Hoffmann, J. A. Lobo, Identification of diverse silanols on protonated ZSM-5 zeolites by means of FTIR spectroscopy. *Microporous Mesoporous Mater.* **106**, 122–128 (2007).
27. J. Chen, Q. Li, R. Xu, F. Xiao, Distinguishing the silanol groups in the mesoporous molecular sieve MCM-41. *Angew. Chemie (International Ed. English)*. **34**, 2694–2696 (1996).
28. J. P. Gallas, J. M. Goupil, A. Vimont, J. C. Lavalley, B. Gil, J. P. Gilson, O. Miserque, Quantification of water and silanol species on various silicas by coupling IR spectroscopy and in-situ thermogravimetry. *Langmuir*. **25**, 5825–5834 (2009).
29. J. M. Chezeau, L. Delmotte, J. L. Guth, Z. Gabelica, Influence of synthesis conditions and postsynthesis treatments on the nature and quantity of structural defects in highly siliceous MFI zeolites: A high-resolution solid-state ²⁹Si n.m.r. study. *Zeolites*. **11**, 598–606 (1991).
30. M. Ide, M. El-Roz, E. De Canck, A. Vicente, T. Planckaert, T. Bogaerts, I. Van Driessche, F. Lynen, V. Van Speybroeck, F. Thybault-Starzyk, P. Van Der Voort, Quantification of silanol sites for the most common mesoporous ordered silicas and organosilicas: Total versus accessible silanols. *Phys. Chem. Chem. Phys.* **15**, 642–650 (2013).
31. S. Ashtekarl, J. J. Hastingsz, P. J. Barriel, L. F. Gladden, Quantification of the Number of Silanol Groups in. **33**, 569–584 (2000).
32. V. Zholobenko, C. Freitas, M. Jendrlin, P. Bazin, A. Travert, F. Thibault-Starzyk, Probing the acid sites of zeolites with pyridine: Quantitative AGIR measurements of the molar absorption coefficients. *J. Catal.* **385**, 52–60 (2020).
33. A. A. Gabrienko, I. G. Danilova, S. S. Arzumanov, A. V. Toktarev, D. Freude, A. G. Stepanov, Strong acidity of silanol groups of zeolite beta: Evidence from the studies by IR spectroscopy of adsorbed CO and ¹H MAS NMR. *Microporous Mesoporous Mater.* **131**, 210–216 (2010).
34. W. Zhang, X. Bao, X. Guo, X. Wang, A high-resolution solid-state NMR study on nano-structured HZSM-5 zeolite. *Catal. Letters*. **60**, 89–94 (1999).
35. E. Dib, J. Grand, S. Mintova, C. Fernandez, Structure-Directing Agent Governs the Location of Silanol Defects in Zeolites. *Chem. Mater.* **27**, 7577–7579 (2015).
36. M. Hunger, D. Freude, H. Pfeifer, W. Schwieger, MAS NMR studies of silanol groups in zeolites ZSM-5 synthesized with an ionic template. *Chem. Phys. Lett.* **167**, 21–26 (1990).
37. M. Hunger, J. Kärger, H. Pfeifer, J. Caro, B. Zibrowius, M. Bülow, R. Mostowicz, Investigation of internal silanol groups as structural defects in ZSM-5-type zeolites. *J. Chem. Soc. Faraday Trans. 1 Phys. Chem. Condens. Phases*. **83**, 3459–3468 (1987).
38. J. M. Kobe, T. J. Gluszak, J. A. Dumesic, T. W. Root, Deuterium NMR

- characterization of bronsted acid sites and silanol species in zeolites. *J. Phys. Chem.* **99**, 5485–5491 (1995).
39. A. Zheng, S.-B. Liu, F. Deng, ³¹P NMR chemical shifts of phosphorus probes as reliable and practical acidity scales for solid and liquid catalysts. *Chem. Rev.* **117**, 12475–12531 (2017).
 40. F. Dubray, S. Moldovan, C. Kouvatas, J. Grand, C. Aquino, N. Barrier, J. P. Gilson, N. Nesterenko, D. Minoux, S. Mintova, Direct Evidence for Single Molybdenum Atoms Incorporated in the Framework of MFI Zeolite Nanocrystals. *J. Am. Chem. Soc.* **141**, 8689–8693 (2019).
 41. B. A. Morrow, A. J. McFarlan, Surface vibrational modes of silanol groups on silica. *J. Phys. Chem.* **96**, 1395–1400 (1992).
 42. J. L. Koenig, P. T. K. Shih, Raman and Infrared Spectroscopic Studies of the Reactions of Silica and Glass Surfaces. *Mater. Sci. Eng.* **20**, 127–135 (1975).
 43. M. A. Cambor, A. Corma, J. Pérez-Pariante, Infrared spectroscopic investigation of titanium in zeolites. A new assignment of the 960 cm⁻¹ band. *J. Chem. Soc. Chem. Commun.*, 557–559 (1993).
 44. M. Dieterle, G. Mestl, Raman spectroscopy of molybdenum oxides: Part II. Resonance Raman spectroscopic characterization of the molybdenum oxides Mo₄O₁₁ and MoO₂. *Phys. Chem. Chem. Phys.* **4**, 822–826 (2002).

Chapter V: Stability and catalytic performances of Mo-ZSM-5 in methane dehydroaromatization reaction

This work is published as a research article with the following bibliographic reference:

Konnov S.V., Dubray F., Clatworthy E.B., Kouvas C., Gilson J-P., Dath J-P., Minoux D., Aquino C., Valtchev V., Moldovan S., Koneti S., Nesterenko N., Mintova M. Novel Strategy for the Synthesis of Ultra-Stable Single-Site Mo-ZSM-5 Zeolite Nanocrystals. *Angew. Chem. Int. Ed.* **2020**, DOI: 10.1002/anie.202006524.

Abstract

The current energy transition presents many technological challenges, such as the development of highly stable catalysts. Herein, we report a novel “top-down” synthesis approach for preparation of a single-site Mo-containing nanosized ZSM-5 zeolite possessing atomically dispersed framework-molybdenum homogeneously distributed through the zeolite crystals. The introduction of Mo heals most of the native point defects in the zeolite structure resulting in an extremely stable material. The important features of this single-site Mo-containing ZSM-5 zeolite are provided by an in-depth spectroscopic and microscopic analysis. The material demonstrates superior thermal (up to 1000 °C), hydrothermal (steaming), and catalytic (converting methane to hydrogen and higher hydrocarbons) stability, maintaining the atomically dispersed Mo, structural integrity of the zeolite, and preventing the formation of silanols.

V.1. Introduction

As the world undergoes a decades-long transformation of the energy industry to low or zero carbon-based resources and fuels, natural gas (mainly CH₄) and biomass will play increasingly important roles in transitioning away from traditional fossil fuel feedstocks such as coal, light and heavy oils.^{1–3} The shift in focus to other energy sources will require the modification of existing and the development of emerging industrial processes. Zeolites, already a key player in catalysis and separations in oil refining and petrochemistry¹ are poised to play an important role in such technologies if the stability of metal sites in zeolite-based catalysts can be insured.⁴ Moreover, dedicated crude-to-chemicals technologies will start to boost the production of chemicals from oil at refineries from ≈ 10–15% at present to ≈ 30–80% in the coming decades and many traditional facilities are already considering changing their product slate from transportation fuels to chemical feedstocks.⁵ Such scenarios would benefit from the development of novel and stable metal-containing zeolite catalysts.

For example, the dehydrogenation of propane to propylene employs alumina-supported catalysts,⁶ however, state of the art synthetic procedures have demonstrated several new strategies to improve the activity and stability of zeolite-supported catalysts such as the encapsulation of metal atoms and clusters during the zeolite synthesis,⁷ stabilisation of the metal phase in the zeolite channels by alkali metals,⁴ and the use of framework-metal sites to stabilise extra-framework active sites.^{8,9} Similar to the dehydrogenation of propane, there are no commercial zeolite-based catalysts for the non-oxidative conversion of methane to hydrogen and industrially important chemicals (olefins, aromatics). This process is a direct route to decarbonize methane to petrochemicals while co-producing a clean energy vector - hydrogen. A big competitive advantage relative to the other routes to produce hydrogen from methane (*e.g.* steam reforming process) is in no direct CO₂ emission and, as a consequence, no requirement for CO₂ capture. The route is also more carbon efficient and requires lower capital investments relative to syngas routes, which are the only industrial processes currently available to transform methane to petrochemicals. This reaction faces two critical issues: (1) low conversion due to unfavorable thermodynamics and (2) catalyst deactivation due to coke deposition at high temperatures (> 700 °C) causing irreversible damage to the zeolite structure. Recent studies on metal-containing zeolites for the non-oxidative conversion of methane, such as Mo-impregnated ZSM-5, have focussed on the optimization of the metal loading, reaction process, and catalyst regeneration.^{10–12}

For this process to be industrially viable, the catalysts envisioned will have to possess, among other features, a low density of similar active sites (single sites), short diffusion path lengths of guest molecules (nanosized crystalline domains) to minimize secondary reactions (*e.g.* coking), shape selectivity (selective production of high-value aromatics such as *p*-xylene) and superior hydrothermal stability. It is clear that such catalysts will have to operate outside the current “comfort zone” of conventional industrial catalytic processes. At present, metal-containing zeolites operating at high temperature in the presence of steam suffer from irreversible damages including: (1) the loss of dispersion of the metal phase, (2) structural collapse, (3) strong dealumination due to the reaction between volatile metals and framework Al, and (4) hydrolysis of Al–O–Si bonds. Such challenges are seldom addressed in the current literature. Thermal and hydrothermal stability of zeolites and the currently available methodologies for their stabilization remain important issues for the industrial scale application of novel materials or even known zeolite catalysts. In addition to the recent examples for propane dehydrogenation mentioned earlier, reported methods for the stabilization of zeolites include the addition of phosphorous in MFI,^{13–16} ion-exchange with rare-earth metals in FAU,¹⁷ dealumination/silication by (NH₄)₂SiF₆ treatments and/or partial dealumination combined with extraction of Al extra-framework species (USY).¹⁸ Most of these stabilization strategies of zeolites are based on defect healing, or the creation of substantially “defect free” structures. Very recently, Iyoki *et al.* demonstrated the stabilization of high-silica zeolites (SiO₂/Al₂O₃ > 240, BEA, MFI and MOR type) using a liquid-mediated treatment

consisting of hydroxide anions, fluoride anions and organic structure directing cations, without requiring the addition of silylating agents. The treated zeolites were able to withstand high temperature steaming conditions of 900–1150 °C.¹⁹

In this work we report for the first time the “top-down” synthesis of novel single-site Mo-containing ZSM-5 nanozeolite with superior stability (up to 1000 °C) by treatment of calcined nanosized zeolite with sodium molybdate under autogenous pressure. Mo is atomically dispersed in the framework of an aluminium containing MFI zeolite ([Mo]-ZSM-5) and homogeneously distributed through the crystals. Mo effectively heals silanol defects and the resulting catalyst demonstrates stable activity over consecutive catalytic reactions. The exceptional stability and performance of the single-site Mo-containing nanozeolite for H₂ and higher hydrocarbons production from CH₄ under methane dehydroaromatization (MDA) conditions was demonstrated. The single-site Mo-containing ZSM-5 nanozeolite is stable under oxidative, reductive, and steaming conditions.

V.2. Experimental section

V.2.1. Synthesis

V.2.1.a. Synthesis of Mo-free ZSM-5 nanosized zeolite

The Mo-free ZSM-5 zeolite was synthesized using the following chemicals without any further purification: tetraethyl orthosilicate (TEOS, 98%, Aldrich), tetra-n-propylammonium hydroxide (TPAOH, 20 wt.% in aqueous solution, Alfa Aesar), and aluminum nitrate (Al(NO₃)₃•9H₂O, 97%, Prolabo). Double-distilled water was used for both synthesis and post-synthesis treatments. The ZSM-5 precursor suspension with the following chemical composition: 1 SiO₂: 0.357 TPAOH: 0.004 Al₂O₃: 16.189 H₂O, was prepared under stirring and then aged for 18 h on an orbital shaker. The aged precursor suspension was then transferred into a 20 mL Teflon-lined autoclave, and subjected to hydrothermal treatment at 180 °C for 72 h under autogenous pressure and quiescent conditions. Separation and purifications of the harvested solids were performed by high speed centrifugation (20,000 rpm) and double-distilled water until the pH of the supernatant was 8. The sample was dried at 80 °C and calcined at 550 °C for 5 h. The as-synthesized ZSM-5 zeolite had a Si/Al ratio of 110 and a particle size of about 150 nm.

V.2.1.b. Synthesis of single-site [Mo]-ZSM-5 catalyst

The single-site Mo-zeolite catalyst ([Mo]-ZSM-5) was prepared as follows: in a 125 mL polypropylene bottle, 3.0 g of the Mo-free calcined ZSM-5 nanosized zeolite, *vide supra*, was mixed with a solution containing 1.5 g of sodium molybdate (Na₂MoO₄, 4H₂O, 98%, Alfa Aesar) solubilized in 50 mL of water under stirring. The

as-prepared mixture was then heated at 90 °C for 5 days under autogenous pressure. The [Mo]-ZSM-5 crystals were purified by high speed centrifugation (20,000 rpm) until complete removal of unreacted Mo species from the supernatant. The crystals were then dried at 80 °C and calcined at 550 °C for 6 h in air flow.

The [Mo]-ZSM-5 was then ion-exchanged with a NH₄Cl solution (0.2 M) to remove the sodium associated with the Mo source, followed by calcination (550 °C, 5 h), to provide its H-form. The [Mo]-ZSM-5 sample contained 0.5 wt.% Mo as determined by TEM-EDS. The Si/Al ratio of the pristine ZSM-5 used in this process was 110, and remained unchanged after the treatment.

V.2.1.c. Synthesis of reference R-ZSM-5 catalyst

Molybdenum was introduced in the pure ZSM-5 nanosized zeolite (Mo-free ZSM-5) by wet-impregnation as follows: ZSM-5 was impregnated with a solution of ammonium heptamolybdate ((NH₄)₆Mo₇O₂₄, 4H₂O, 99%, Alfa Aesar). The obtained mixture was then dried at 120 °C for 3 hours and calcined at 550 °C for 6 h in air flow. This impregnated reference sample, R-ZSM-5, contained 1 wt.% Mo as determined by ICP.

V.2.1.d. Hydrothermal treatment of Mo-free ZSM-5 zeolite without sodium molybdate

The procedure to obtain the pristine treated Mo-free zeolite (the ZSM-5 zeolite prior Mo introduction either by impregnation or by isomorphous substitution) was as follows: water was added to the pristine ZSM-5 crystals (6.65 g H₂O for 300 mg ZSM-5), the obtained suspension was treated at 90 °C for 5 days, before being washed with water, dried at 90 °C overnight, and calcined at 550 °C for 5 h. This procedure is the same for the preparation of the single site [Mo]-ZSM-5 sample, but without the presence of sodium molybdate in the suspension.

V.2.2. Characterization

Powder X-Ray diffraction (XRD) patterns of the materials were collected on a PANalytical X'Pert Pro diffractometer equipped with a Johansson monochromator set up for Cu K α 1 radiation ($\lambda = 1.540598 \text{ \AA}$). Unit cell parameters, volume, and space group were determined from Le Bail profile refinements of XRD patterns using the JANA2006 software. Crystallinity and silanol defects were determined by ²⁹Si and ²⁷Al solid-state MAS NMR. ²⁹Si and ²⁷Al NMR spectra were acquired on a Bruker Avance III-HD 500 (11.7 T) spectrometer operating at 99.3 MHz and 130.3 MHz for ²⁹Si and ²⁷Al respectively, using a zirconia rotor of 4 mm outer diameter, spun at 12

KHz. Single pulse excitations were used, with a flip angle of 30° and 90° for ^{29}Si and ^{27}Al respectively, corresponding to radio frequency fields of 114 KHz and 188 KHz respectively. Additionally, ^1H MAS NMR spectra were recorded using a 3 mm outer diameter rotor spun at 12 KHz, with the spectrometer operating at 500 MHz, with a flip angle of 90°, corresponding to a radio frequency field of 94 KHz (all samples were dehydrated at 200 °C overnight prior measurements).

FTIR spectra of self-supported zeolite pellets (1 cm², 20 mg) were recorded using a Nicolet Magna 550-FT-IR spectrometer (4 cm⁻¹ optical resolution); prior to the measurements the samples were activated at 480 °C for 3 h under vacuum ($\approx 2.5 \times 10^{-6}$ Torr).

The crystal size and morphology were measured by transmission electron microscopy (TEM); experiments were carried out on an Analytical double (objective and probe) corrected JEOL ARM200CF equipped with a 100 mm Centurio EDS detector and a Quantum GIF for the EELS. A probe of 0.09 nm was used to scan the specimen in STEM mode and Bright Field, and high Angular Annular Dark Field detectors were simultaneously employed for imaging. The camera length was fixed at 8 cm. Two different accelerating voltages of 200 kV and 80 kV were employed in the STEM mode for imaging and chemical analysis respectively. Owing to the enhanced Z contrast developed at 200 kV, this configuration was used for imaging, and a high speed scanning protocol (12 $\mu\text{sec}/\text{px}$) was employed in order to minimize the specimen degradation under the beam. To avoid material degradation, the STEM-EDS analytical essays were carried out at 80 kV with a high scanning speed of 2 $\mu\text{s}/\text{px}$ and for a mean duration of 60 minutes. A cross-correlation algorithm implemented in the JEOL Analysis Station software was applied every 60 seconds to compensate for the spatial drift occurring during the test. The microstructure of samples was checked before and after each EDS scan in order to exclude the microstructural changes induced by the beam and during the scan.

The acidity of the catalysts was characterized by monitoring the adsorption of a probe molecule, trimethylphosphine oxide (TMPO), by ^{31}P MAS NMR. All preliminary preparation steps were conducted in a glove bag under an Ar atmosphere to prevent any reaction of the TMPO with moisture in the air and zeolitic water. The catalysts were first dehydrated at 400 °C under vacuum (4.0×10^{-5} Torr). In parallel, a solution of TMPO dissolved in dichloromethane (CH_2Cl_2) was prepared and added to the dehydrated catalyst. To ensure homogeneous dispersion of the probe molecule (TMPO) in the zeolite porosity, the samples were ultrasonicated in a bath for 15 min. The suspensions were then evaporated for 2 h at room temperature under vacuum. The TMPO loaded catalysts were then transferred and packed into a sealed zirconia rotor of 3.2 mm outer diameter and spun at 22 kHz during the ^{31}P MAS NMR measurements. All ^{31}P MAS NMR spectra were also recorded on a Bruker Avance III-HD 500 (11.7 T) spectrometer operating at 202.4 MHz. A single pulse excitation was used, with a flip angle of 90°, corresponding to a radio frequency field of 41 KHz. The ^{29}Si , ^1H , ^{27}Al , and ^{31}P NMR spectra were referenced to the spectrum of

tetramethylsilane (TMS, for both ^{29}Si and ^1H), aluminium nitrate ($\text{Al}(\text{NO}_3)_3$) and phosphoric acid (H_3PO_4) respectively.

V.2.3. Catalytic test: non-oxidative high temperature CH_4 conversion to H_2 and higher hydrocarbons.

The zeolite samples were pelletized, crushed, sieved and the 200–400 μm fraction retained for catalytic testing. The catalytic tests were carried out in a quartz downflow tubular reactor (367 mm long and 6.0 mm of internal diameter) loaded with 0.3 g of catalyst (sandwiched between quartz wool layers).

The testing conditions were 850 $^\circ\text{C}$, 1 bar, WHSV = 1.2 h^{-1} . Before reaction, all catalysts were activated by heating from room to reaction temperature (ramp rate of 10 $^\circ\text{C}/\text{min}$) under a flow of CH_4/N_2 (80/20 vol. %). The products were analyzed online with an Interscience Compact GC chromatograph fitted with three channels. The GC three-channel configuration included two TCDs and one FID on dedicated columns (Molsieve 5A, Rt-QBond, Rtx-1) to analyse light gases (H_2 , N_2 , CO , CO_2), light hydrocarbons (CH_4 , C_2H_4 , C_2H_6) and aromatic hydrocarbons (benzene, toluene, xylenes, ethylbenzene, naphthalene). Nitrogen was used as an internal standard. The main products of the reaction were hydrogen, aromatic hydrocarbons (benzene, toluene, naphthalene) and aliphatic hydrocarbons (mostly ethylene, ethane). Ethylbenzene, xylenes, acetylene and $\text{C}_3\text{-C}_4$ hydrocarbons were formed in negligible amounts.

Successive reaction-regeneration cycles of the catalysts were performed. After each catalytic test, the reactor was cooled down to room temperature under a dry nitrogen flow (10 mL/min). This was followed by the catalyst regeneration under a dry air flow (15 mL/min) with an increase (2 $^\circ\text{C}/\text{min}$) of the temperature to 750 $^\circ\text{C}$ which was maintained for 3 h. The first reaction-regeneration cycle was used to equilibrate the performance of the catalysts.

Steaming treatment of the samples (0.3 g) was carried out in a tubular quartz reactor. The temperature was increased (5 $^\circ\text{C}/\text{min}$) to 550 $^\circ\text{C}$ under a dry nitrogen flow of 20 mL/min, and steaming took place at 550 $^\circ\text{C}$ for 6 h; the flow of water used during the treatment was 6.2 g/h.

V.2.4. Stability of [Mo]-ZSM-5 and R-ZSM-5 samples

The stability of both [Mo]-ZSM-5 and R-ZSM-5 samples (prepared according to the procedure described above) was investigated as follows:

The fresh samples [Mo]-ZSM-5 and R-ZSM-5 were used as catalysts for the non-oxidative conversion of CH_4 (according to the conditions described in the

catalytic section) in 3 successive reaction-regeneration cycles. The as-retrieved samples subjected to these 3 reaction-regeneration cycles are respectively called [Mo]-ZSM-5 (3 cycles) and R-ZSM-5 (3 cycles).

The spent catalysts [Mo]-ZSM-5 (3 cycles) and R-ZSM-5 (3 cycles) are then subjected to a steaming treatment, also described in the catalytic section. These spent catalysts after steaming are called [Mo]-ZSM-5 (S) and R-ZSM-5 (S).

The stability of the samples was studied by comparing their catalytic stability, as well as by studying their structural stability based on spectroscopic characterizations before and after catalytic and steaming treatments.

V.3. Results and discussion

V.3.1. Synthesis and comprehensive characterization of Mo-containing zeolites

The single-site [Mo]-ZSM-5 zeolite sample was synthesized following the novel procedure outlined in the experimental section and presented in Scheme S1. The synthesis approach is based on the treatment of calcined Mo-free ZSM-5 nanosized zeolite with sodium molybdate at 90 °C for 5 days under autogenous pressure, followed by purification and calcination (550 °C for 6 h). The prepared [Mo]-ZSM-5 contains 0.5 wt.% of Mo according to EDS-TEM and ICP analyses. The reference sample, R-ZSM-5, was prepared by incipient wetness impregnation of the parent Mo-free ZSM-5 nanozeolite with 1 wt.% of Mo according to standard procedures reported in the MDA literature.²⁰ In contrast to the direct synthesis approach reported earlier in chapter 3,²¹ the current method allows stabilization of single metal species in already synthesized aluminium containing MFI type (ZSM-5) zeolites (Scheme S1). This new procedure can in principle be applied to any calcined pure silica and aluminosilicate zeolites including commercially available materials.

The structural properties of the novel single-site [Mo]-ZSM-5 zeolite sample were characterized by in-depth diffraction and spectroscopic analyses. The XRD patterns of the single-site [Mo]-ZSM-5 and reference R-ZSM-5 zeolite samples are depicted in Figure 1A. The [Mo]-ZSM-5 sample is monoclinic (P21/n) while the R-ZSM-5 is orthorhombic (Pnma). Pristine untreated calcined Mo-free ZSM-5 was orthorhombic and the XRD pattern is provided in Figure S1 for comparison. In addition, orthorhombic symmetry was maintained for the pristine ZSM-5 that was subjected to the same treatment as that used for the preparation of the [Mo]-ZSM-5 sample, however, without the presence of sodium molybdate (Figure S1). The characteristic splitting of the diffraction peaks at 23.3, 23.8, and 24.5° 2 θ in the XRD pattern of the single-site [Mo]-ZSM-5 zeolite sample is clearly seen (Figure 1B); stars marked the splitting of the single peaks typical for orthorhombic R-ZSM-5. The monoclinic symmetry is an indication for the isomorphous substitution of a metal with an ionic radius larger than Si in the MFI framework, however, the specific T-site

locations occupied by Mo in the ZSM-5 framework could not be determined.²¹ The Le Bail profile refinements of the XRD patterns are summarized in Table S1. The larger unit-cell volume of the single-site [Mo]-ZSM-5 zeolite sample further indicates the substitution of Si^{IV} (ionic radius: 0.26 Å) for Mo^{VI} (ionic radius: 0.59 Å) in the MFI framework.²¹ The morphology, size and elemental composition of both samples [Mo]-ZSM-5 and R-ZSM-5 are studied by STEM- HAADF (Figure 2). The statistical analysis of the particle size (measured for about 200 particles) is presented as inserts in the Figure 2A and 2B. They reveal the average particles size is about 150 (+/- 20) nm for both Mo-ZSM-5 and R-ZSM-5 samples. The most striking differences between the samples are found in the morphology of the particles. The crystals of [Mo]-ZSM-5 exhibit smooth surfaces and sharp edges, whereas in the case of R-ZSM-5 crystals, the outer surface is less regular and the inner crystals morphology is marked by the presence of mesopores (darker circular areas). The sharpness of the edges in the case of specimen [Mo]-ZSM-5 can be interpreted as a signature of its monocrystalline nature, whilst the irregular outer edges of the R-ZSM-5 crystals are associated with their polycrystallinity. The polycrystalline nature of the R-ZSM-5 crystals is also associated with the presence of an abundant number of defects (notably the mesopores), which is further confirmed by NMR (¹H and ²⁹Si MAS NMR), and IR spectroscopy (see below). The atomically dispersed Mo in [Mo]-ZSM-5 (seen as light points in the micrographs) are highlighted with circles in the STEM-HAADF micrographs, and confirm the presence of homogeneously distributed Mo atoms within the zeolite crystals (Figure 2A). The size of Mo light points in STEM-HAADF micrographs is similar in the two samples, however, they differ substantially in their stability under high temperature treatment (up to 1000 °C) and steaming. The chemical composition of the single-site [Mo]-ZSM-5 crystals is determined by ICP and confirmed by EDS-TEM. The elemental distributions in the [Mo]-ZSM-5 and R-ZSM-5 samples are shown in Figure S2. The shape and morphology of the pristine ZSM-5 was examined by STEM-EDS (Figure S3). The agglomerated crystals have irregular shapes, and a mean size of 170 nm. The crystals in the reference sample (R-ZSM-5) have a similar shape and size (Figure S2); the distribution of both Si and Al in the pristine and reference sample is homogeneous suggesting that no changes under impregnation occurred.

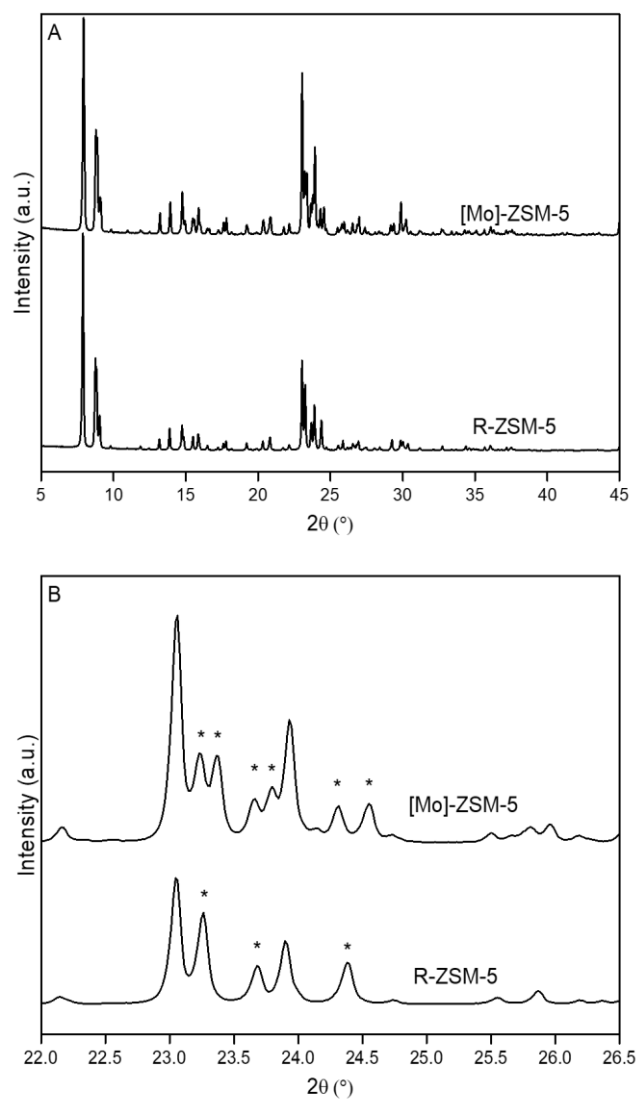


Figure 1. XRD patterns of [Mo]-ZSM-5 and R-ZSM-5 zeolite samples in the range of (A) $5\text{--}45^{\circ}2\theta$ and (B) $22\text{--}26.5^{\circ}2\theta$

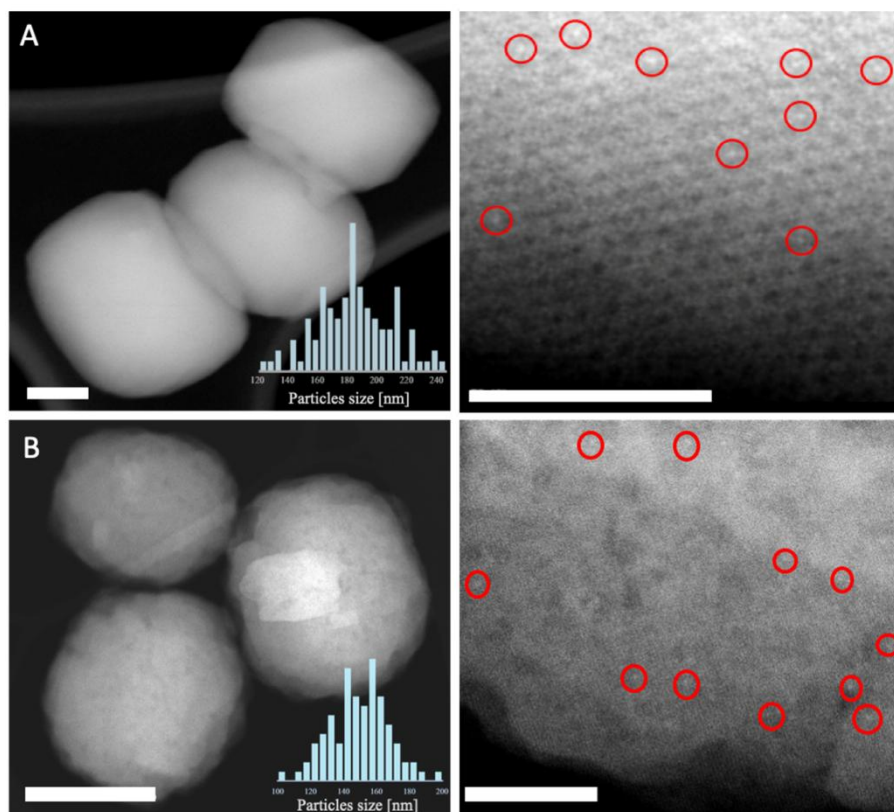


Figure 2. STEM-HAADF micrographs of (a) [Mo]-ZSM-5: left scale bar = 100 nm, right scale bar = 10 nm, and (B) R-ZSM-5: left scale bar = 100 nm, right scale bar = 10 nm. Inset: particle size distribution.

Further structural information of the single-site [Mo]-ZSM-5 sample is provided by ^{29}Si MAS NMR spectroscopy (Figure 3A). The spectrum of the calcined [Mo]-ZSM-5 sample reveals well-resolved Q^4 ($(\text{SiO})_4\text{Si}$) and no Q^3 ($(\text{SiO})_3\text{Si-OH}$) species, indicating an almost total absence of silanols. In comparison, the reference R-ZSM-5 sample displays unresolved Q^4 and Q^3 species, indicating the presence of silanol defects. These results are consistent with the HRTEM observations revealing the formation of [Mo]-ZSM-5 crystals with smooth surface, while the R-ZSM-5 particles contain additional mesopores and surface defects. The presence of Al in the framework of both samples is confirmed by ^{27}Al MAS NMR spectroscopy (Figure 3B). The spectra for both the [Mo]-ZSM-5 and R-ZSM-5 samples contain a sharp peak at 60 ppm corresponding to Al in tetrahedral coordination, and no octahedral species are detected at 0 ppm.

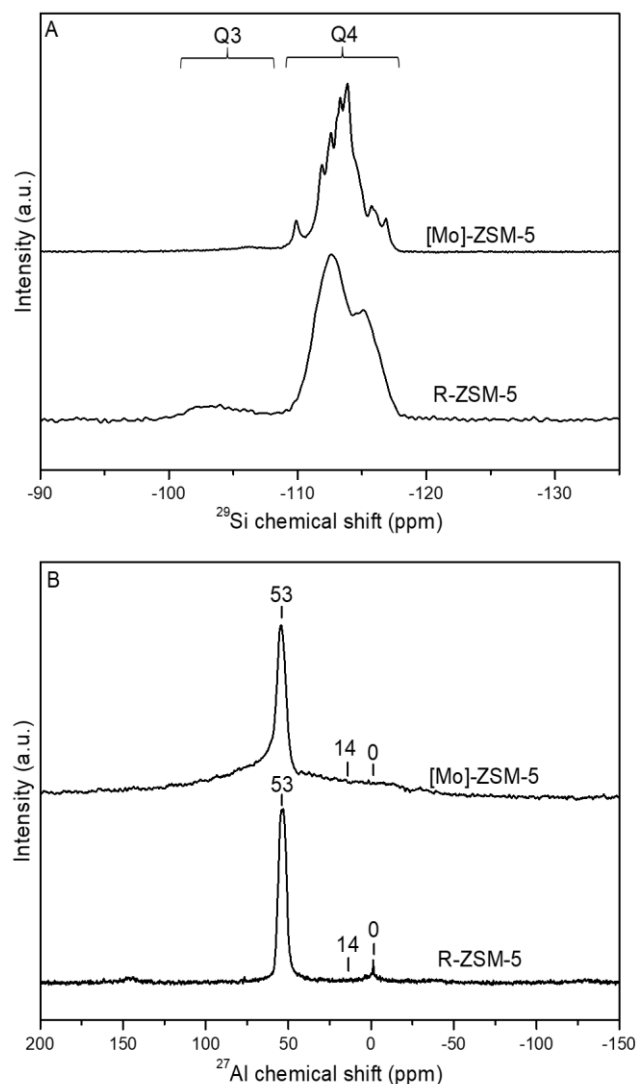


Figure 3. (A) ^{29}Si MAS NMR and (B) ^{27}Al MAS NMR spectra of samples [Mo]-ZSM-5 and R-ZSM-5.

The results from the ^{29}Si and ^{27}Al NMR analyses are consistent with the IR observations performed in the silanol region for the two samples (Figure 4A). Sample [Mo]-ZSM-5 contains a negligible amount of isolated silanols represented by the peak at 3745 cm^{-1} , and no silanol nests. In comparison, sample R-ZSM-5 contains a significant amount of isolated silanols and silanol nests represented by the highly intense peaks at 3745 cm^{-1} and 3510 cm^{-1} , respectively. The peak corresponding to bridging silanol species at 3610 cm^{-1} in both samples remains unchanged, confirming the preservation of Brönsted acid sites (Figure 4A). Additionally, the low amount of silanol defects in the [Mo]-ZSM-5 is confirmed by ^1H MAS NMR spectroscopy (Figure 4B); the samples were dehydrated at $200\text{ }^\circ\text{C}$ overnight prior to the measurements to remove the zeolitic water. One peak at 2.3 ppm corresponding to isolated silanol species is present in the spectrum of [Mo]-ZSM-5, while no peaks in the range 4–5.5 ppm are observed which is attributed to the absence of silanol nests. For the R-ZSM-5 reference sample, broad peaks at 2.3, and 4.0–5.5 ppm related to isolated silanols,

and silanol nests and/or bridging hydroxyl groups respectively are observed (Figure 4B).²²

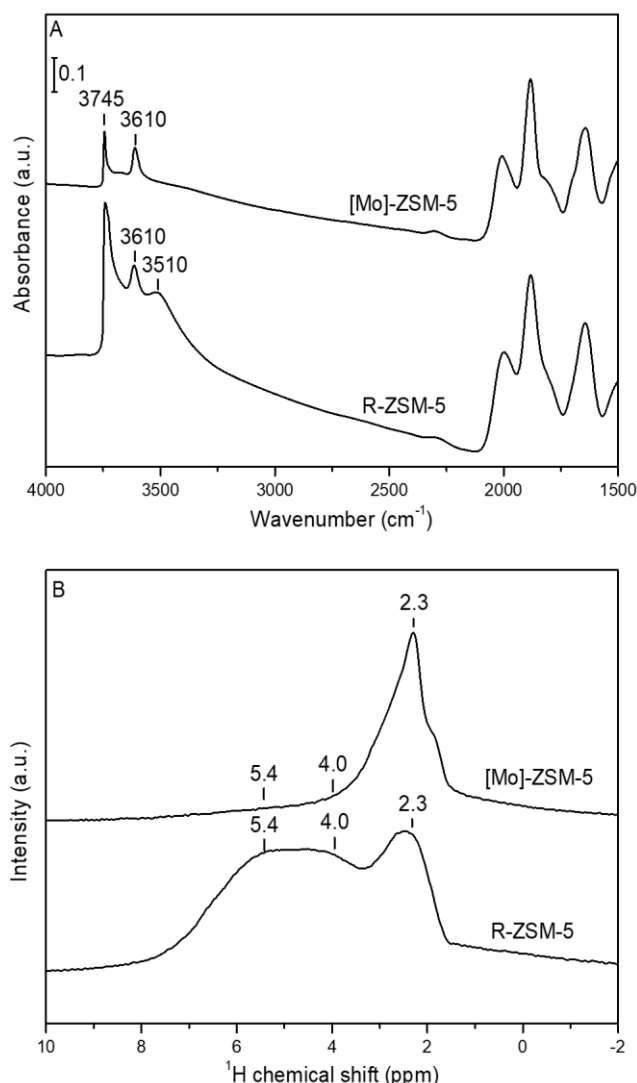


Figure 4. (A) FTIR spectra and (B) ¹H MAS NMR spectra of dehydrated [Mo]-ZSM-5 and R-ZSM-5 samples.

The location and state of the Mo are further studied by ³¹P MAS NMR spectroscopy. The spectra of adsorbed trimethylphosphine oxide (TMPO) on the single-site [Mo]-ZSM-5 and reference R-ZSM-5 samples are presented in Figure 5. The presence of Mo in the framework positions of the [Mo]-ZSM-5 zeolite is confirmed by the resonance at 45 ppm which is consistent with previous work,²¹ while a small amount of silanols are also observed (50 ppm).^{23–25} Two Brønsted acid sites (64 and 74 ppm) as well as crystalline (43 ppm) and physisorbed (29 ppm) TMPO are present, indicating that TMPO accesses all acidic and metallic sites.^{25,26} The peak at 38 ppm was attributed to hydrated TMPO. In contrast, for the Mo impregnated R-ZSM-5 sample, Brønsted acid sites (64 and 74 ppm) and silanols (50 ppm) are present, however, no framework Mo is detected as the resonance at 45 ppm is not observed (Figure 5).

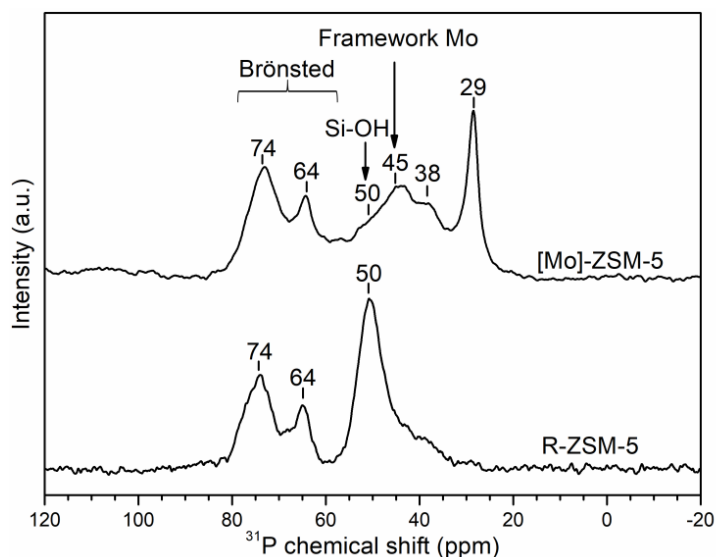


Figure 5. ^{31}P MAS NMR spectra of TMPO adsorbed on samples [Mo]-ZSM-5 and R-ZSM-5.

V.3.2. Catalytic test of Mo-containing ZSM-5 zeolite samples: non-oxidative high temperature CH_4 conversion to H_2 and higher hydrocarbons

The catalytic performances of the Mo single-site [Mo]-ZSM-5 and reference R-ZSM-5 samples were assessed for the high temperature non-oxidative conversion of CH_4 (850 °C, atmospheric pressure, 0.3 g of catalyst, WHSV 1.2 h^{-1}) over 12 h (Figure 6). The reference sample, R-ZSM-5, rapidly deactivates until the conversion of CH_4 plateaus after 7 h. In contrast, the single-site [Mo]-ZSM-5 zeolite sample with only 0.5 % Mo shows exceptional stability after three consecutive reaction-regeneration cycles. It is worth noting that for [Mo]-ZSM-5, we deal with Mo-sites which remain within the zeolite framework allowing for the presence of either non-carburized or partially carburized Mo-sites. The location and retention of Mo in the zeolite framework results in the high stability of the catalyst, allowing it to operate under severe conditions over multiple reaction-regeneration cycles. However, further in-depth study is required to determine the exact structure and evolution of the active sites. Mo remains in the framework structure of the [Mo]-ZSM-5 zeolite and does not undergo any discernible changes over the three reaction-regeneration cycles, *vide infra*. The total methane conversion to hydrogen and the detailed product yields of the two catalysts are compared in Figure 6B. The [Mo]-ZSM-5 sample affords a significantly higher yield of hydrogen and ethylene in comparison to the R-ZSM-5 reference sample. It is also worth noting that the [Mo]-ZSM-5 sample produces a relatively high proportion of ethylene in the C_2 fraction (> 90%). The production of $\text{C}_3\text{-C}_4$ hydrocarbons is negligible for both samples.

To assess the stability of the Mo in the single-site [Mo]-ZSM-5 zeolite sample, the catalysts were subjected to multiple cycles of reaction (MDA, i.e. reducing

conditions) and regeneration (calcination, i.e. oxidative conditions). Under typical MDA operating conditions, the classical Mo containing zeolite (R-ZSM-5) deactivates due to the sintering and migration of molybdenum carbide species as a consequence of weak interactions with the zeolite.²⁷ During the exothermic catalyst regeneration, the molybdenum carbide is oxidized, and steam is generated from the oxidation of coke. Under such conditions the Mo species become mobile and react with framework Al to form aluminium molybdates. These new Mo species cannot form carbides, resulting in irreversible deactivation of the catalyst.^{23,28} In contrast, the single-site [Mo]-ZSM-5 nanozeolite shows exceptional stability for the conversion of CH₄ after three reactions at 850 °C and regeneration cycles at 750 °C (Figure 6A). Moreover, the [Mo]-ZSM-5 catalyst produces relatively stable amounts of hydrogen and aliphatics throughout the cycles in comparison with the R-ZSM-5 sample (Figure S4). Such a stable catalytic performance of the [Mo]-ZSM-5 over three reaction-regeneration cycles clearly demonstrates that the catalytically active sites attributed to the single-site Mo in the MFI structure are maintained, in strong contrast with the reference R-ZSM-5 sample. That the catalyst demonstrates stable activity at a high reaction temperature (850 °C) allows for the targeted production of ethylene which requires more severe conditions. The [Mo]-ZSM-5 catalyst can operate over a greater temperature range (compared to R-ZSM-5 state-of-the-art catalyst) without significant changes in its catalytic performance, which is one of the critical points for process design. The significant improvement in the stability of the metal phase is highly beneficial, in particular for catalysts working under harsh conditions (e.g. high temperatures and continuous oxidation/reduction cycles).

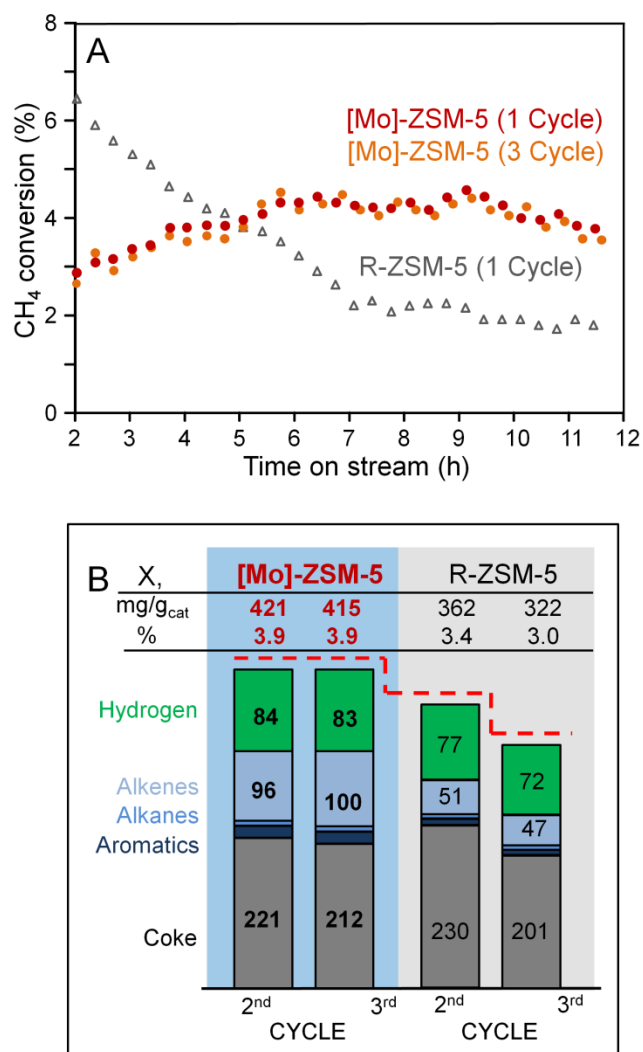


Figure 6. (A) CH₄ conversion after the first and third consecutive cycles of reaction-regeneration as a function of time on stream for the [Mo]-ZSM-5 and reference R-ZSM-5 catalysts and (B) total CH₄ conversion (X: milligrams per gram of catalyst or %), products yield (milligrams per gram of catalyst) corresponding to 2–12 h time gap of calculation over the [Mo]-ZSM-5 and R-ZSM-5. Reaction conditions: T = 850 °C, atmospheric pressure, WHSV = 1.2 h⁻¹, time on stream window = 2–12 h.

As shown above, the single-site metal species incorporated into the zeolite framework results in stable catalytic performance. Further investigation of the thermal and hydrothermal stability of the single-site Mo-containing [Mo]-ZSM-5 zeolite and the reference sample is provided below. Emphasis is placed on the characterization of the samples in an attempt to describe the structural evolution of the catalysts under harsh reaction and regeneration conditions.

V.3.3. Stability of Mo-containing zeolite samples.

The stability of the single-site [Mo]-ZSM-5 and the reference [R]-ZSM-5 zeolite samples was evaluated after the catalytic reaction and subsequent recycling treatments. The samples subjected to 3 catalytic (reaction-regeneration) cycles are denoted with “(3 cycles)”, while the samples that are subjected to 3 catalytic cycles followed by steaming are denoted with “(S)”. The XRD patterns of the calcined ([Mo]-ZSM-5) and used ([Mo]-ZSM-5 (3 cycles)) samples after 3 catalytic cycles (methane conversion and regeneration at 750 °C) clearly show that all the Bragg peaks are identical, confirming the preservation of the crystalline structure (Figure S5). A marginal decrease of the unit cell volume for [Mo]-ZSM-5 (3 cycles) is observed, suggesting that the sample underwent a degree of dealumination (Table S1). In contrast, the unit cell volume of R-ZSM-5 sample decreased substantially from 5359.283 to 5344.653 Å³, which is indicative of significant structural change occurring in the sample R-ZSM-5 (3 cycles). Remarkably, the ²⁹Si MAS NMR spectrum of the single-site [Mo]-ZSM-5 (3 cycles) sample is almost identical to that of the calcined [Mo]-ZSM-5 sample (Figure S6). The ²⁹Si MAS NMR spectra of [Mo]-ZSM-5 (3 cycles) still displays highly resolved Q⁴ species and no Q³ species, in stark contrast to R-ZSM-5 (3 cycles) where both Q³ and Q⁴ species are observed. This further demonstrates the exceptional stability of the framework Mo in the [Mo]-ZSM-5 zeolite under reductive (catalytic reaction) and oxidative (regeneration) conditions. The intensity and high resolution of the Q⁴ peaks in the spectrum of the [Mo]-ZSM-5 (3 cycles) sample is related to the degree of dealumination, the conservation of Mo in the structure, and the absence of silanols. The occurrence of dealumination in both the [Mo]-ZSM-5 (3 cycles) and R-ZSM-5 (3 cycles) samples was revealed in the ²⁷Al MAS NMR spectra by the presence of octahedral aluminum species at 0 ppm (Figure S7). Based on ²⁷Al MAS NMR spectroscopy, dealumination occurred to a slightly greater degree for the [Mo]-ZSM-5 (3 cycles) sample in comparison to the R-ZSM-5 (3 cycles) sample. This suggests that the Brønsted sites due to framework Al in the Mo impregnated ZSM-5 (R-ZSM-5 sample) are more resilient to dealumination than in pure ZSM-5. This discrepancy could be attributed to the presence of a protective molybdenum oxide shell around the framework Al species in the R-ZSM-5 sample consistent with recent work reporting a preferential location of Mo near framework Al species in ZSM-5.²⁹

Additionally, the stability of the samples after 3 catalytic cycles was studied after a subsequent steaming treatment performed at 550 °C. The XRD patterns and ²⁹Si MAS NMR spectra of the [Mo]-ZSM-5 (S) and R-ZSM-5 (S) samples (Figure 7) establishes the outstanding hydrothermal stability of the framework Mo species in [Mo]-ZSM-5 zeolite. All the Bragg peaks are identical for the calcined [Mo]-ZSM-5 and the steamed [Mo]-ZSM-5 (S) samples, while the diffraction pattern of the R-ZSM-5 (S) sample reveals the appearance of several Bragg peaks (Figure 7A). In addition, the ²⁹Si MAS NMR spectra of the [Mo]-ZSM-5 (S) sample (Figure 7B) displays highly resolved Q⁴ species and no Q³ species, demonstrating that no silanol species were

generated after the combined reaction-regeneration cycles and steaming treatments despite the simultaneous occurrence of dealumination. These observations further support the conclusion that the Mo atoms are retained in the MFI framework. This is the first example of a zeolite structure that contains heteroelements, such as Mo, able to withstand such harsh treatment (3 high temperature reaction/regeneration cycles in MDA, followed by steaming at 550 °C). In contrast, the R-ZSM-5 (S) sample displays both unresolved Q^4 and Q^3 species attributed to the presence of silanol species. The formation of aluminium molybdates and the occurrence of dealumination of the R-ZSM-5 (S) sample were further supported by ^{27}Al MAS NMR analysis (Figure 8A) due to the clear appearance of a peak at 14 ppm, which was not observed for the [Mo]-ZSM-5 (S) sample. Indeed, in the case of the [Mo]-ZSM-5 (S) sample, a portion of the tetrahedral Al (53 ppm) is converted to distorted framework Al and/or penta-coordinated Al species (27 ppm), and octahedral Al. Critically, no aluminum molybdate is formed, in stark contrast with the R-ZSM-5 (S) sample. Indeed, it has been reported that MoO_3 reacts with framework Al above 550 °C to form aluminum molybdate and possibly surface AlMo_6 Anderson entities.¹⁰ Consequently, the absence of aluminum molybdate in [Mo]-ZSM-5 (S) further indicates that all Mo atoms remain atomically dispersed in the framework of [Mo]-ZSM-5 after steam treatment. ^{31}P MAS NMR spectra (using TMPO) of the steamed samples are depicted in Figure 8B. The number of Brønsted acid sites in the [Mo]-ZSM-5 (S) sample decreased substantially after steaming due to dealumination and the subsequent formation of extra-framework aluminium, evidenced from both ^{31}P MAS NMR (Figure 8B) and ^{27}Al MAS NMR (Figure 8A) spectroscopy, *vide supra*. Importantly, no silanols are observed after the reaction-regeneration cycles and subsequent steaming of the [Mo]-ZSM-5 sample according to the ^{31}P MAS NMR spectra (Figure 8B), even though dealumination occurs. This demonstrates that atomically dispersed Mo introduced into the MFI zeolite framework stabilizes the crystalline structure and prevents the formation of silanols. This is further supported by the fact that, despite the occurrence of dealumination, the resonance at 45 ppm remains unchanged, suggesting that Mo is retained in the framework.

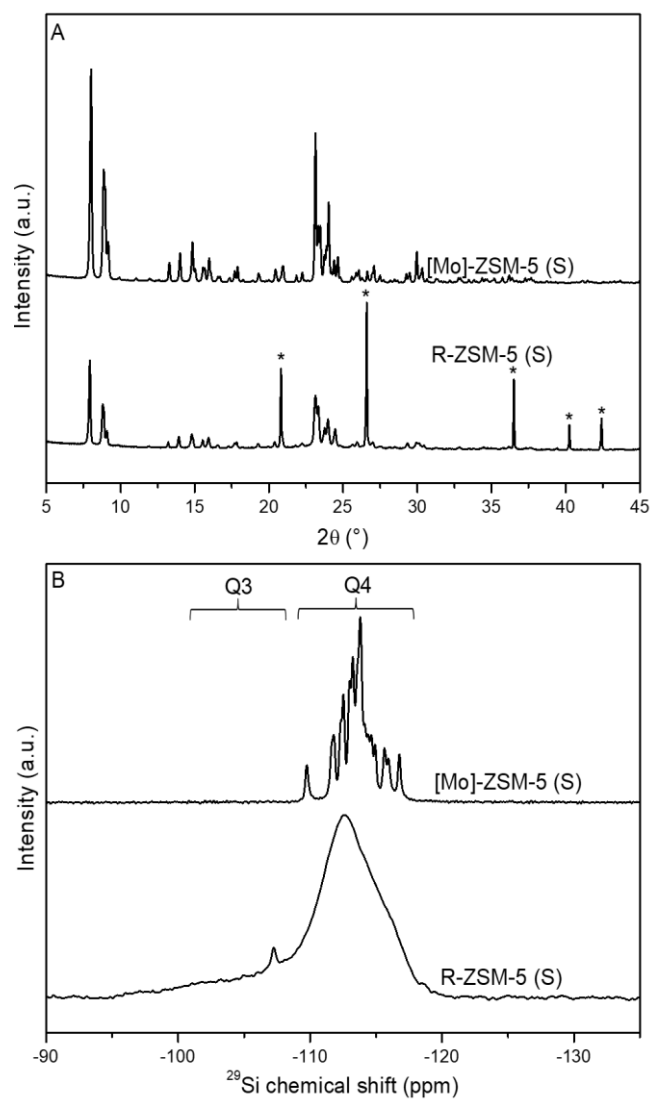


Figure 7. (A) XRD patterns, and (B) ^{29}Si MAS NMR spectra of samples [Mo]-ZSM-5 (S) and R-ZSM-5 (S). Diffraction peaks marked by “*” at 20.8° , 26.6° , 36.5° , 40.2° , and 42.4° 2θ on sample R-ZSM-5 (S) are attributed to the formation of catalytically inactive aluminium molybdate species.

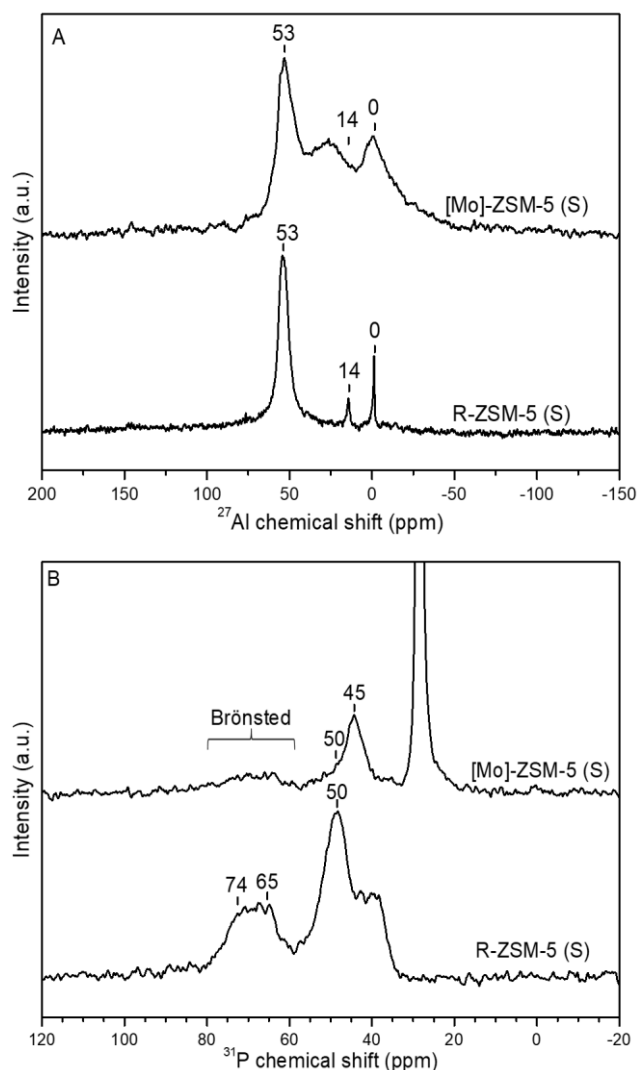


Figure 8. (A) ^{27}Al MAS NMR spectra of dehydrated [Mo]-ZSM-5 (S) and R-ZSM-5 (S) samples, and (B) ^{31}P MAS NMR spectra of TMPO adsorbed on dehydrated [Mo]-ZSM-5 (S) and R-ZSM-5 (S) samples.

V.4. Conclusion

Here we report the synthesis of a novel single-site [Mo]-ZSM-5 zeolite using a Mo-free ZSM-5 nanosized zeolite subjected to treatment with sodium molybdate under autogenous pressure. The single-site [Mo]-ZSM-5 zeolite contains highly disperse Mo (0.5 wt.%) according to EDS-TEM and ICP analyses; the [Mo]-ZSM-5 zeolite was compared with a reference sample prepared with 1 wt.% Mo by the classical impregnation method (R-ZSM-5). The properties of the single-site Mo containing ZSM-5 zeolite were characterized at the atomistic and molecular level using diffraction, microscopy and spectroscopy methods.

The novel single-site Mo-containing nanozeolite possesses atomically dispersed framework-molybdenum atoms homogeneously distributed through the

zeolite crystals. The introduction of atomically dispersed Mo in the zeolite framework heals silanol defects resulting in an extremely stable material, resistant to severe structural degradation. The novel single-site Mo-containing ZSM-5 nanozeolite exhibits superior performance for CH₄ conversion to H₂ and higher hydrocarbons operating under successive reductive and oxidative atmospheres at high temperature (850 and 750 °C), as well as demonstrating exceptional structural stability under hydrothermal steaming conditions.

In summary, zeolites have so far been used successfully and extensively in oil refining and petrochemistry and will continue to play an important role by meeting the challenges in these fields. However, the operating conditions (e.g. temperatures in the 750–850 °C range) of some emerging industrial processes will push zeolites outside this “comfort zone” and successful zeolitic catalysts will require exceptional thermal and hydrothermal resilience.

The single-site Mo-containing ZSM-5 represents a strong example of a zeolite material able to operate “outside” of the comfort zone. This novel synthesis approach can be applied for the introduction of other metals (e.g. V, W, Cu, Zn) in other calcined zeolites including pure silica and aluminosilicates.

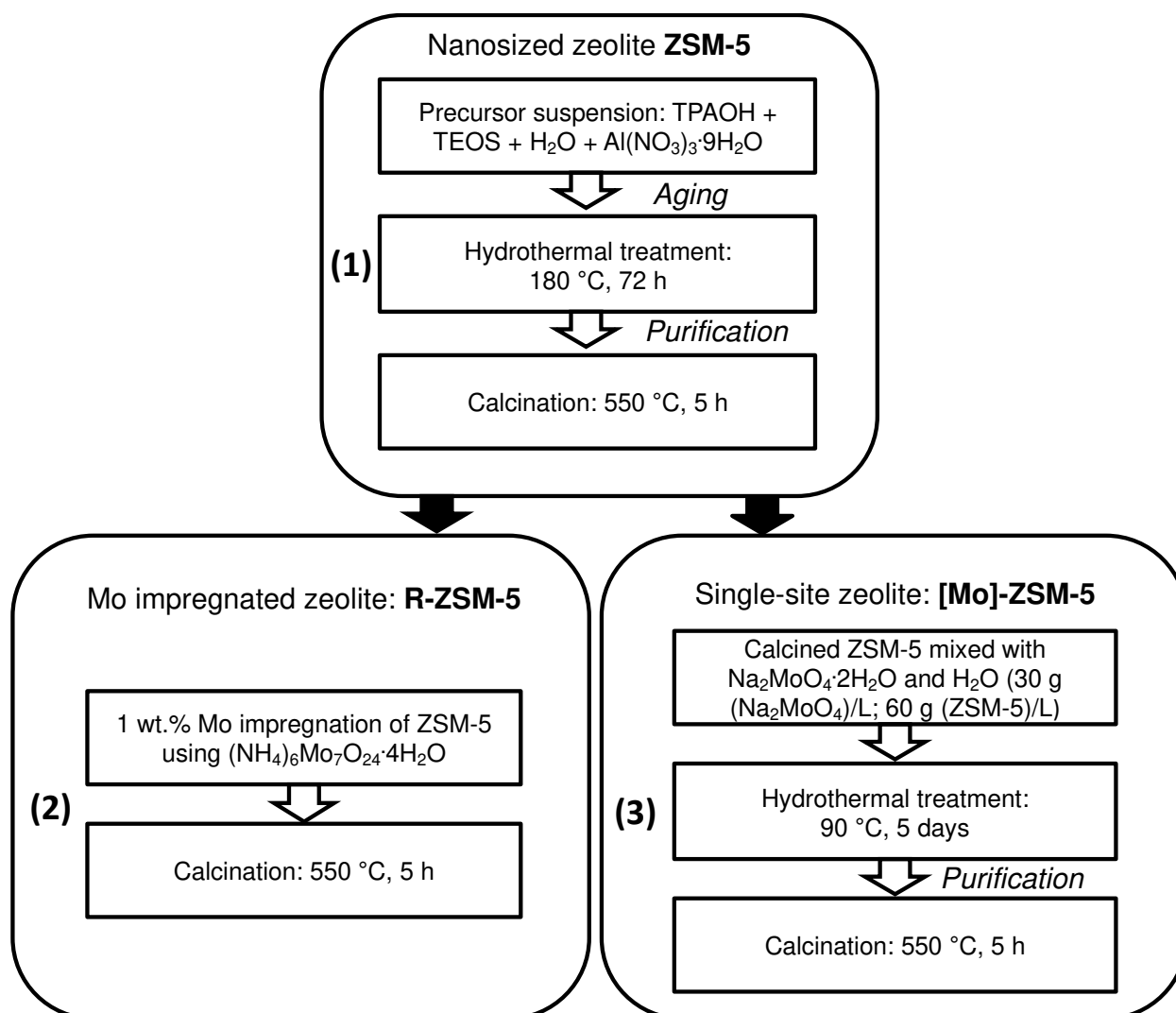
V.5. References

1. M. Jefferson, V. Smil, *Energy and Civilization: A History*, MIT Press, Cambridge, Massachusetts and London, England (2017). (2017).
2. V. Smil, *Energy transitions: global and national perspectives* (ABC-CLIO, 2016).
3. W. Vermeiren, J.-P. Gilson, Impact of zeolites on the petroleum and petrochemical industry. *Top. Catal.* **52**, 1131–1161 (2009).
4. L. Liu, M. Lopez-Haro, C. W. Lopes, C. Li, P. Concepcion, L. Simonelli, J. J. Calvino, A. Corma, Regioselective generation and reactivity control of subnanometric platinum clusters in zeolites for high-temperature catalysis. *Nat. Mater.* **18**, 866–873 (2019).
5. M. Chadwick, G. McManus, S. Zinger, G. Haire, *Crude-to-Chemicals: Opportunity or Threat?* (Wood Mackenzie, 2019).
6. J. J. H. B. Sattler, J. Ruiz-Martinez, E. Santillan-Jimenez, B. M. Weckhuysen, Catalytic dehydrogenation of light alkanes on metals and metal oxides. *Chem. Rev.* **114**, 10613–10653 (2014).
7. L. Liu, U. Diaz, R. Arenal, G. Agostini, P. Concepción, A. Corma, Generation of subnanometric platinum with high stability during transformation of a 2D zeolite into 3D. *Nat. Mater.* **16**, 132–138 (2017).
8. Y. Wang, Z.-P. Hu, W. Tian, L. Gao, Z. Wang, Z.-Y. Yuan, Framework-confined Sn in Si-beta stabilizing ultra-small Pt nanoclusters as direct propane

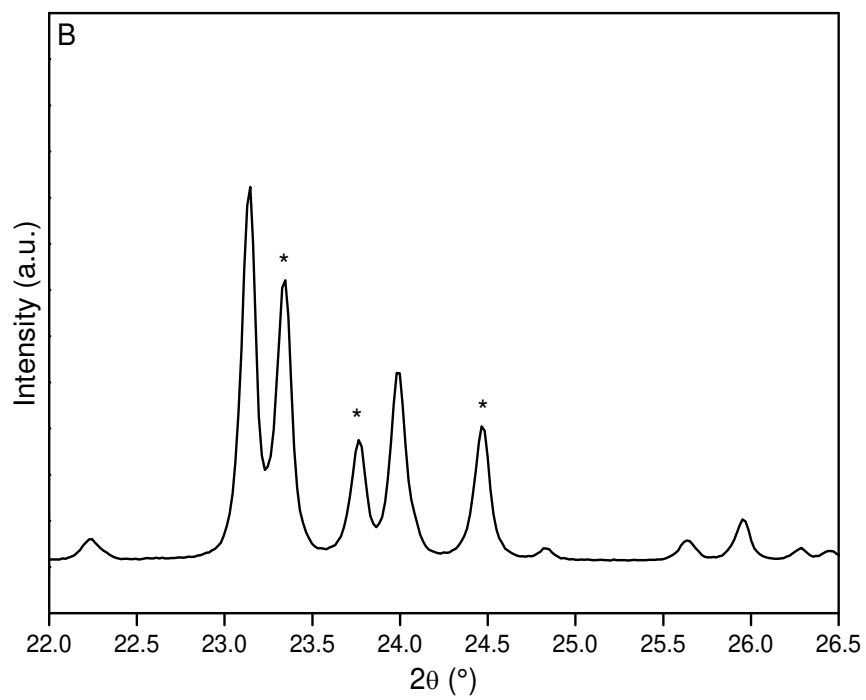
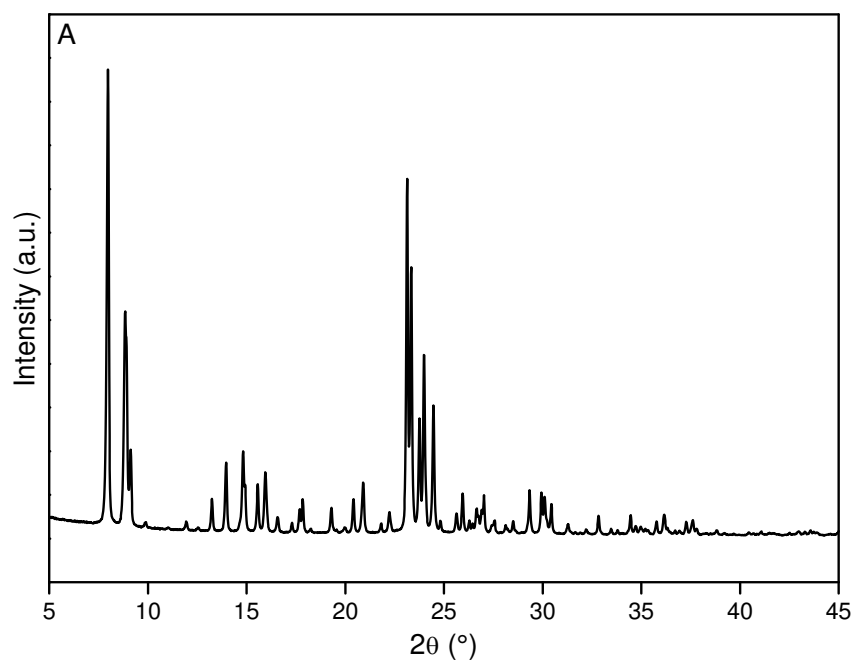
- dehydrogenation catalysts with high selectivity and stability. *Catal. Sci. Technol.* **9**, 6993–7002 (2019).
9. Z. Xu, Y. Yue, X. Bao, Z. Xie, H. Zhu, Propane Dehydrogenation over Pt Clusters Localized at the Sn Single-Site in Zeolite Framework. *ACS Catal.* **10**, 818–828 (2019).
 10. N. Kosinov, F. J. A. G. Coumans, G. Li, E. Uslamin, B. Mezari, A. S. G. Wijkema, E. A. Pidko, E. J. M. Hensen, Stable Mo/HZSM-5 methane dehydroaromatization catalysts optimized for high-temperature calcination-regeneration. *J. Catal.* **346**, 125–133 (2017).
 11. H. Ma, R. Kojima, R. Ohnishi, M. Ichikawa, Efficient regeneration of Mo/HZSM-5 catalyst by using air with NO in methane dehydro-aromatization reaction. *Appl. Catal. A Gen.* **275**, 183–187 (2004).
 12. S. J. Han, S. K. Kim, A. Hwang, S. Kim, D.-Y. Hong, G. Kwak, K.-W. Jun, Y. T. Kim, Non-oxidative dehydroaromatization of methane over Mo/H-ZSM-5 catalysts: A detailed analysis of the reaction-regeneration cycle. *Appl. Catal. B Environ.* **241**, 305–318 (2019).
 13. T. Blasco, A. Corma, J. Martínez-Triguero, Hydrothermal stabilization of ZSM-5 catalytic-cracking additives by phosphorus addition. *J. Catal.* **237**, 267–277 (2006).
 14. W. W. Kaeding, S. A. Butter, Production of chemicals from methanol: I. Low molecular weight olefins. *J. Catal.* **61**, 155–164 (1980).
 15. A. Jentys, G. Rumpelmayr, J. A. Lercher, Hydroxyl groups in phosphorus-modified HZSM-5. *Appl. Catal.* **53**, 299–312 (1989).
 16. H. E. van der Bij, B. M. Weckhuysen, Phosphorus promotion and poisoning in zeolite-based materials: synthesis, characterisation and catalysis. *Chem. Soc. Rev.* **44**, 7406–7428 (2015).
 17. J. Biswas, I. E. Maxwell, Recent process-and catalyst-related developments in fluid catalytic cracking. *Appl. Catal.* **63**, 197–258 (1990).
 18. A. Corma, V. Fornes, F. Rey, Extraction of extra-framework aluminium in ultrastable Y zeolites by (NH₄)₂SiF₆ treatments: I. physicochemical characterization. *Appl. Catal.* **59**, 267–274 (1990).
 19. K. Iyoki, K. Kikumasa, T. Onishi, Y. Yonezawa, A. Chokkalingam, Y. Yanaba, T. Matsumoto, R. Osuga, S. P. Elangovan, J. N. Kondo, others, Extremely Stable Zeolites Developed via Designed Liquid-Mediated Treatment. *J. Am. Chem. Soc.* **142**, 3931–3938 (2020).
 20. D. Wang, J. H. Lunsford, M. P. Rosynek, Characterization of a Mo/ZSM-5 catalyst for the conversion of methane to benzene. *J. Catal.* **169**, 347–358 (1997).
 21. F. Dubray, S. Moldovan, C. Kouvatas, J. Grand, C. Aquino, N. Barrier, J. P. Gilson, N. Nesterenko, D. Minoux, S. Mintova, Direct Evidence for Single Molybdenum Atoms Incorporated in the Framework of MFI Zeolite

- Nanocrystals. *J. Am. Chem. Soc.* **141**, 8689–8693 (2019).
22. W. Zhang, X. Bao, X. Guo, X. Wang, A high-resolution solid-state NMR study on nano-structured HZSM-5 zeolite. *Catal. Letters.* **60**, 89–94 (1999).
 23. B. S. Liu, J. W. H. Leung, L. Li, C. T. Au, A.-C. Cheung, TOF-MS investigation on methane aromatization over 3% Mo/HZSM-5 catalyst under supersonic jet expansion condition. *Chem. Phys. Lett.* **430**, 210–214 (2006).
 24. J. D. Lewis, M. Ha, H. Luo, A. Faucher, V. K. Michaelis, Y. Román-Leshkov, Distinguishing Active Site Identity in Sn-Beta Zeolites Using ^{31}P MAS NMR of Adsorbed Trimethylphosphine Oxide. *ACS Catal.* **8**, 3076–3086 (2018).
 25. A. Zheng, S.-B. Liu, F. Deng, ^{31}P NMR chemical shifts of phosphorus probes as reliable and practical acidity scales for solid and liquid catalysts. *Chem. Rev.* **117**, 12475–12531 (2017).
 26. C. Bornes, M. Sardo, Z. Lin, J. Amelse, A. Fernandes, M. F. Ribeiro, C. Geraldes, J. Rocha, L. Mafra, ^1H - ^{31}P HETCOR NMR elucidates the nature of acid sites in zeolite HZSM-5 probed with trimethylphosphine oxide. *Chem. Commun.* **55**, 12635–12638 (2019).
 27. P. Schwach, X. Pan, X. Bao, Direct conversion of methane to value-added chemicals over heterogeneous catalysts: challenges and prospects. *Chem. Rev.* **117**, 8497–8520 (2017).
 28. C. H. L. Tempelman, E. J. M. Hensen, On the deactivation of Mo/HZSM-5 in the methane dehydroaromatization reaction. *Appl. Catal. B Environ.* **176**, 731–739 (2015).
 29. L. Liu, N. Wang, C. Zhu, X. Liu, Y. Zhu, P. Guo, L. Alfifil, X. Dong, D. Zhang, Y. Han, *Angew. Chemie-Int. Ed.* 2019, 58, 2--9. *Angew. Chem.* **132**, 829–835 (2020).

V.6. Supporting information



Scheme S1. Synthesis procedure for the preparation of (1) pure nanosized ZSM-5 zeolite, (2) Mo single-site ZSM-5 zeolite ([Mo]-ZSM-5) and (3) Mo-impregnated ZSM-5 zeolite (reference R-ZSM-5).



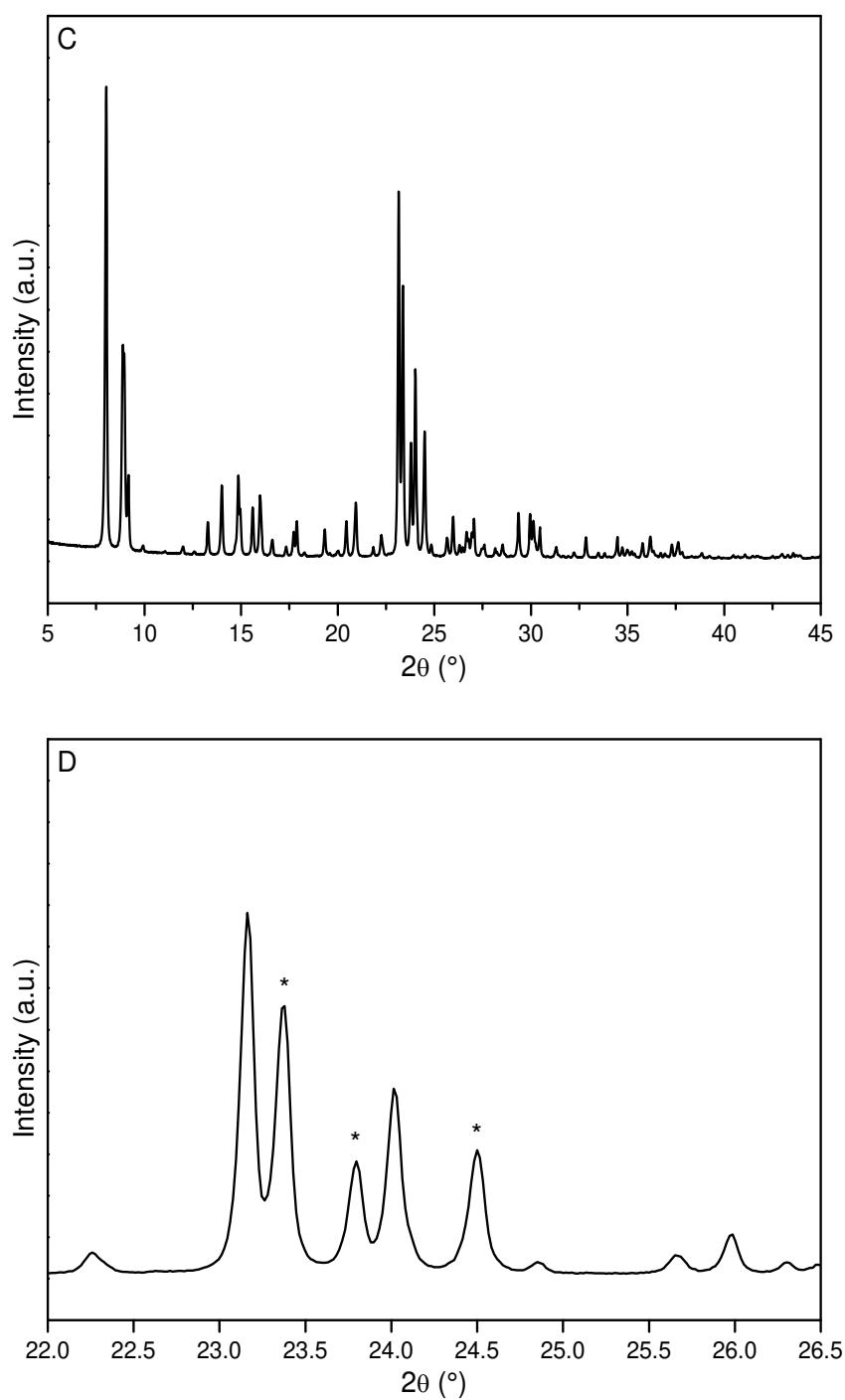


Figure S1. The XRD patterns of pristine untreated calcined Mo-free ZSM-5 in the range (A) 5–45 $^{\circ}$ 2θ and (B) 22–26.5 $^{\circ}$ 2θ , and pristine calcined Mo-free ZSM-5 treated in pure water (5 days, 90 $^{\circ}$ C), in the range (C) 5–45 $^{\circ}$ 2θ and (D) 22–26.5 $^{\circ}$ 2θ .

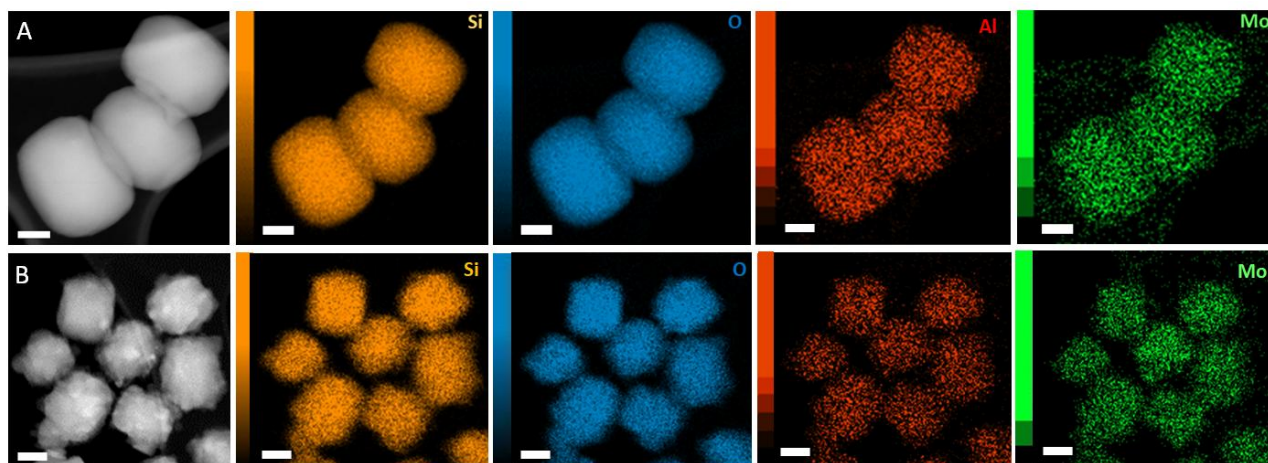


Figure S2. STEM-EDS elemental maps: from left to the right are Si, O, Al, and Mo, for (A) [Mo]-ZSM-5 and (B) R-ZSM-5 zeolite samples. All scale bars are 100 nm.

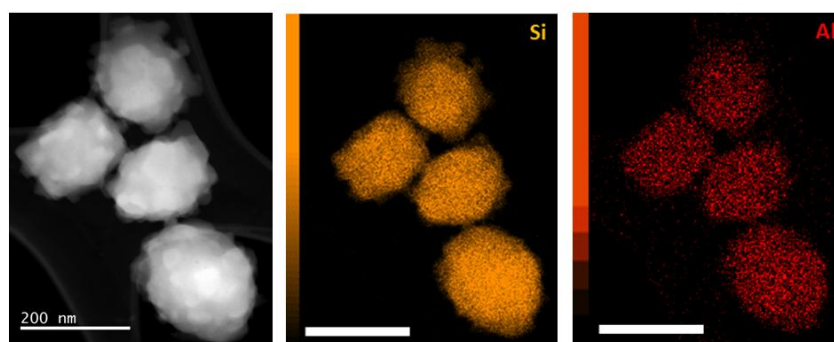


Figure S3. STEM-EDS elemental maps of pristine ZSM-5 sample: from left to right are Si and Al. All scale bars are 200 nm.

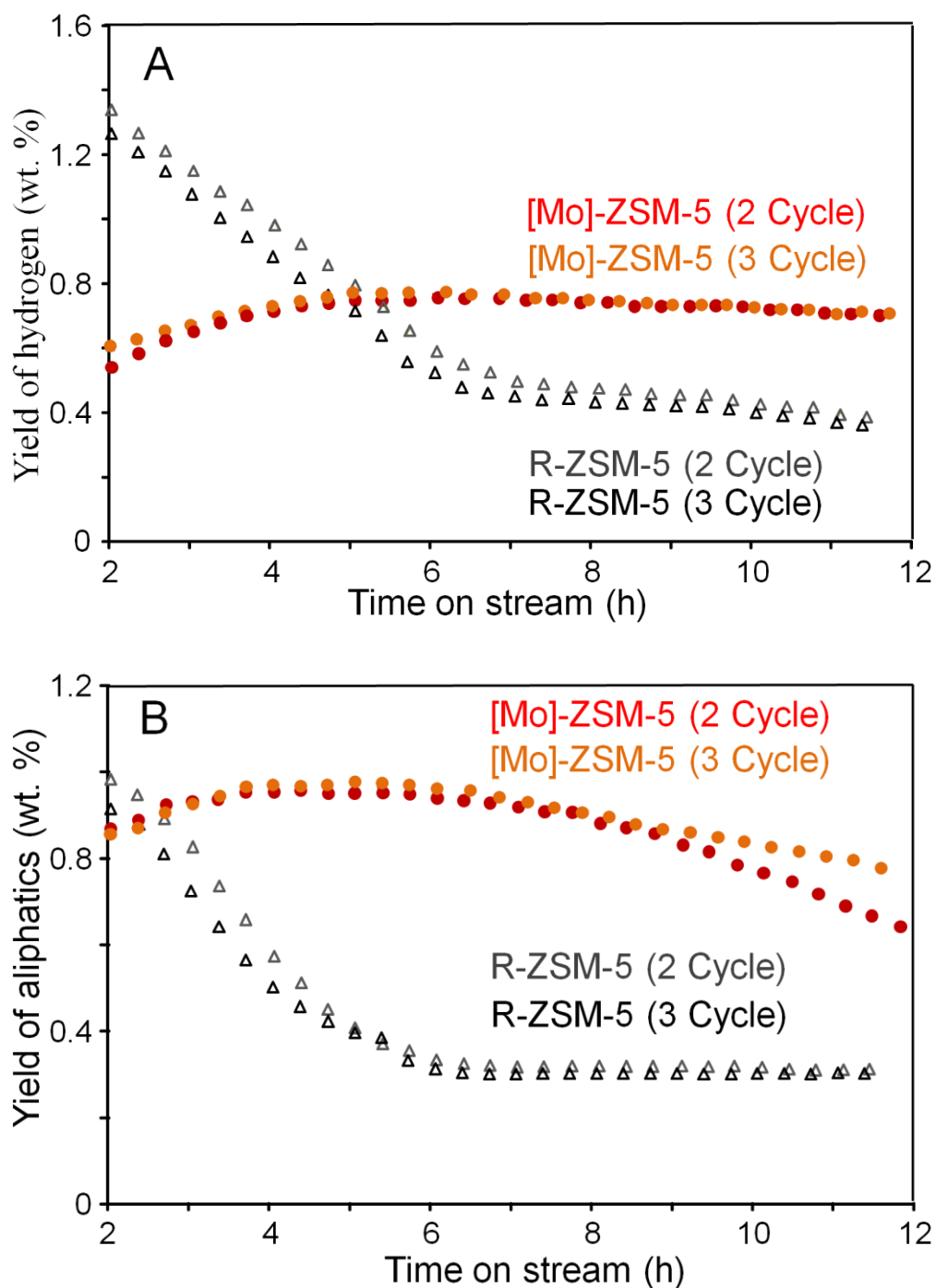


Figure S4. (A) H₂ yield, and (B) aliphatics yield after the second and third consecutive cycles of reaction-regeneration as a function of time on stream for the [Mo]-ZSM-5 and reference R-ZSM-5 zeolite samples. Reaction conditions: 850 °C, atmospheric pressure, 0.3 g of catalyst, WHSV 1.2 h⁻¹.

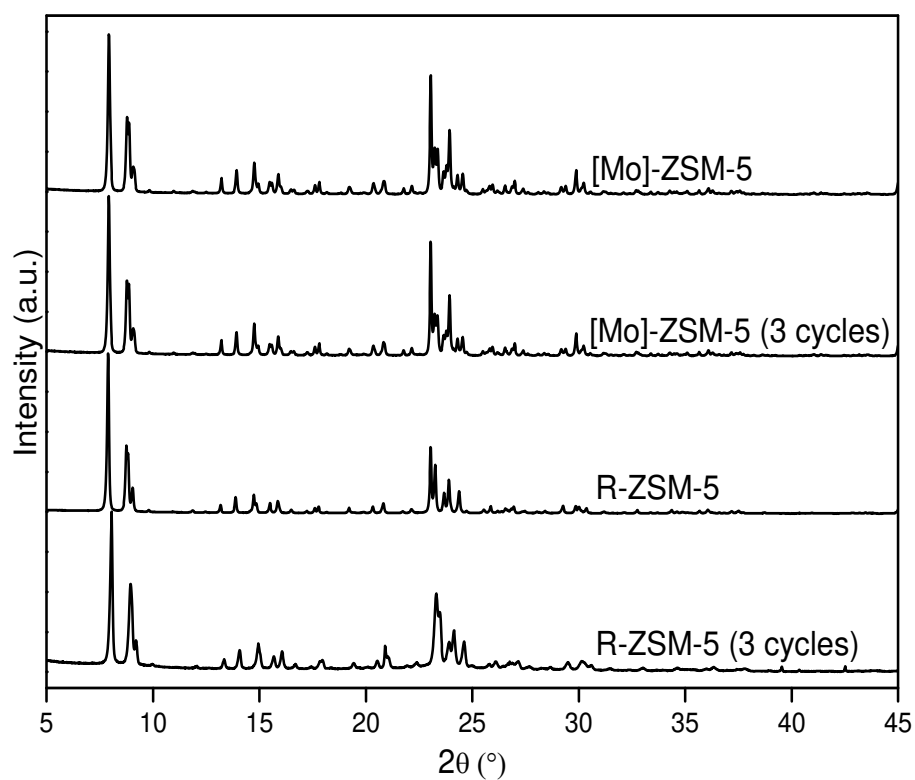


Figure S5. XRD patterns of as-synthesized [Mo]-ZSM-5, used [Mo]-ZSM-5 (3 cycles), as-synthesized R-ZSM-5, and used R-ZSM-5 (3 cycles).

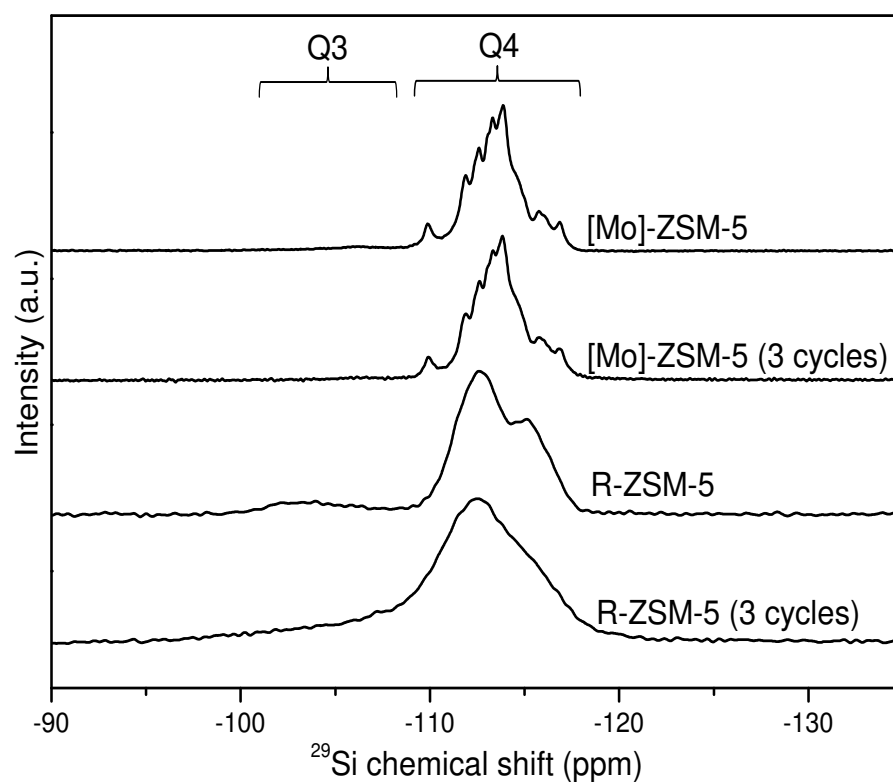


Figure S6. ^{29}Si MAS NMR spectra of as-synthesized [Mo]-ZSM-5, used [Mo]-ZSM-5 (3 cycles), as-synthesized R-ZSM-5, and used R-ZSM-5 (3 cycles) zeolite samples.

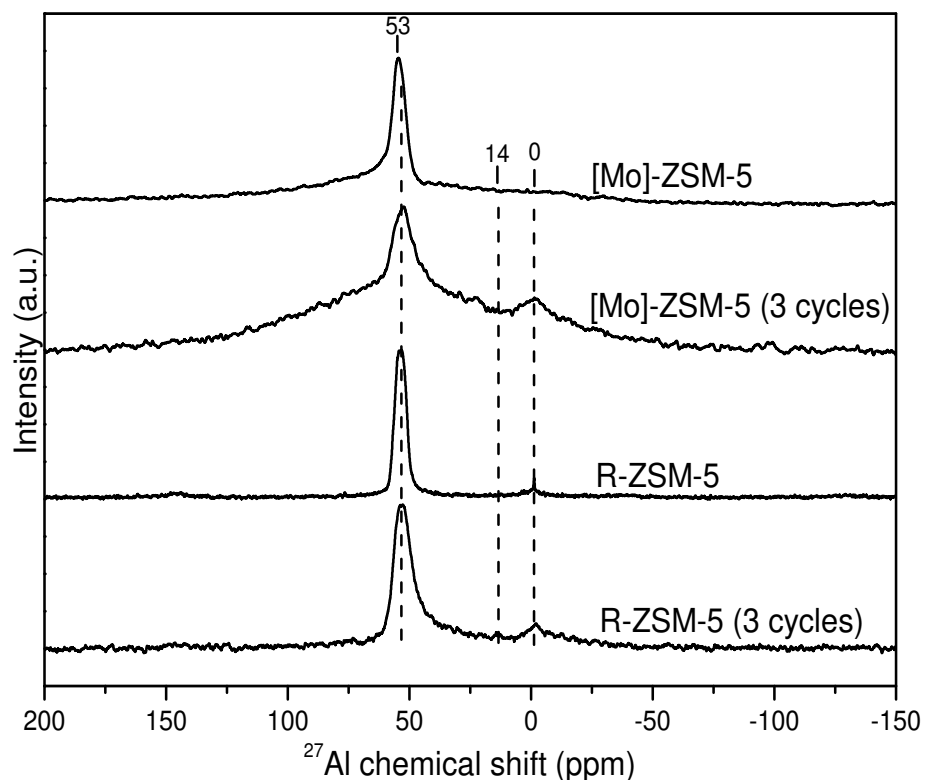


Figure S7. ^{27}Al MAS NMR spectra of as-synthesized [Mo]-ZSM-5, used [Mo]-ZSM-5 (3 cycles), as-synthesized R-ZSM-5, and used R-ZSM-5 (3 cycles) zeolite samples.

Table S1. Le Bail profile refinement of XRD patterns of fresh and used catalysts [Mo]-ZSM-5, [Mo]-ZSM-5 (3 cycles), R-ZSM-5, and R-ZSM-5 (3 cycles).

Sample	Symmetry	<i>a</i> (Å)	<i>b</i> (Å)	<i>c</i> (Å)	β (°)	Volume (Å ³)	GOF	R _p	wR _p
[Mo]-ZSM-5	<i>P2₁/n</i>	19.910	20.139	13.392	90.609	5369.266	1.5	2.89	3.97
[Mo]-ZSM-5 (3 cycles)	<i>P2₁/n</i>	19.908	20.136	13.391	90.583	5367.941	1.6	3.05	4.26
R-ZSM-5	<i>Pnma</i>	19.862	20.097	13.397	90.000	5359.283	2.58	3.99	5.87
R-ZSM-5 (3 cycles)	<i>Pnma</i>	19.862	20.188	13.330	90.000	5344.653	3.37	5.48	8.48

Conclusions and perspectives

The development of catalysts that can operate under harsh catalytic conditions such as high temperature is of critical importance for the development of industrial process able to convert natural gas into valuable chemicals. From that point of view, metal containing zeolite-based catalysts are shown as promising candidates, but their stability under harsh conditions remains an open question. However, high hopes are dedicated to the introduction of metals as framework species in zeolite framework, through a process called isomorphous substitution, because of the properties it brings to the resulting materials. Among these properties, atomic metal dispersion, low metal loading, high interaction with the zeolite support, or hydrophobicity are properties that are limiting or preventing sintering, metal leaching, metal fouling, zeolite amorphization for instance, and thus, stabilize the catalysts against irreversible deactivation in harsh catalytic conditions. The introduction of metal in zeolite framework can be performed in two main synthetic way: (i) direct synthesis, and (ii) post synthesis. However, both methods have drawbacks, and neither are ideal. Indeed, the influence of metal ions on crystallization is of a big concern as far as direct synthesis is concerned, while selectivity and silanol content are of concern for post synthesis treatments.

During this PhD thesis, the synthesis of molybdenum containing MFI zeolite was investigated and optimized. Several attempts were made so as to perform isomorphous substitution of Mo, and among them, the first main synthesis method used was a state of the art direct synthesis approach in which Mo source and the required alkali metal source were combined and introduced together in the precursor gel suspension of the corresponding MFI structure. After observation that Mo species were not reacting at early stage of the crystallization process, a new alternative synthetic method was developed: the staged synthesis. The idea behind this new synthetic process was to introduce a delay for the metal (Mo and alkali) addition to the precursor gel suspension, after a pre-crystallization step was conducted under hydrothermal conditions. The introduction of this delay allowed a drastic particle size reduction, and with a slightly higher local homogeneity based on ^{29}Si MAS NMR. This resulted from the fact that by adding a delay before the metal addition, the metal was no longer able to influence the nucleation process, as well as the initial crystallization of the MFI structure. After further observation of the staged synthesis process, it occurred that the delay could be higher than the crystallization time, leading to the conclusion that Mo was not meant to be present alongside other reactants during the crystallization process itself, so as to be embedded in the zeolite framework. The post hydrothermal synthesis was consequently developed as a second novel synthetic alternative allowing to perform isomorphous substitution. In post hydrothermal synthesis treatment, a parent zeolite was first prepared from a precursor gel suspension, crystallized under hydrothermal conditions, purified, and calcined. Then only, the Mo and alkali metal sources are introduced in the form of an aqueous metallic solution in which the zeolite is added. The suspension is then

hydrothermally treated, resulting in the incorporation of Mo in the parent zeolite framework. Both novel methods and especially the post hydrothermal synthesis are improvements to the state-of-the-art direct synthesis approach. Indeed, these treatments are much more versatile and adaptable, interactions with the initial crystallization are fully removed, and the quality of the samples is not degraded, but improved by doing so. The post hydrothermal synthesis treatment was for instance the milestone allowing to prepare highly homogeneous silanol defect free and Mo containing ZSM-5 nanocrystals.

Then, the complete characterization of a Mo containing silicalite-1 sample (Mo-MFI) as prepared by state-of-the-art direct synthesis approach was described and compared to a reference silicalite-1 sample in which Mo was impregnated as non framework species. Mo-MFI displays high local homogeneity of the atomically dispersed Mo atoms, low silanol content, and high hydrophobicity. The insertion of Mo in the MFI structure induces a space group symmetry transition and increases the unit cell volume of the MFI crystals. The uniform nature of Mo species incorporated in the MFI framework was demonstrated by IR spectroscopy (using deuterated acetonitrile probe molecule), ^{31}P MAS NMR (using trimethylphosphine oxide probe molecule), and the homogeneous metal distribution proved based on STEM-HAADF coupled with EDS analysis. The materials open many opportunities of catalyst and adsorbents design for applications in both mature and emerging fields.

The influence of silanol on the parent zeolite prior Mo addition was highlighted as being of prime importance for the actual occurrence of isomorphous substitution. Indeed, Mo addition is always taking place with silanol defect healing, because Mo is reacting with these species during isomorphous substitution. It is therefore of prime importance to be able to correctly assess the nature and amount of silanol species in zeolite, for subsequent optimization of the Mo-MFI synthesis procedure. Therefore, hydroxyl groups in three nanosized MFI type zeolites (Si-MFI, Al-MFI, and Mo-MFI) with identical particle size have been characterized in depth using IR, Raman, and NMR spectroscopies. The nature and amount of the various silanols were determined unambiguously by cross-checking the results from the different techniques used. The complete removal of silanol nests upon Mo isomorphous substitution was demonstrated, while only a fraction of the isolated silanol species (around 50%) were healed. Based on the corresponding study, guidelines for the characterization of hydroxyls species in zeolites are provided, and ^1H MAS NMR was highlighted as the most efficient way to simultaneously identify and quantify silanol species, with the help of IR for unambiguous attribution.

The stability and activity of [Mo]-ZSM-5 zeolite prepared by post hydrothermal synthesis treatment was evaluated for methane dehydroaromatization (MDA) reaction. The single-site [Mo]-ZSM-5 contains highly disperse Mo (0.5 wt. %) according to EDS-TEM and ICP analysis, and unaltered Brønsted acid sites; the [Mo]-ZSM-5 catalyst was compared with state of the art ZSM-5 impregnated with 1 wt. % Mo, as non framework species. The introduction of Mo in the ZSM-5 zeolite

framework healed silanol nests defects, resulting in a stable material, resistant to severe structural degradation. The novel [Mo]-ZSM-5 material exhibits superior performances for methane conversion into hydrogen and higher hydrocarbons, and remarkable stability over successive reaction-regeneration cycles (3.9 vs 3.0 % conversion after 3 catalytic cycles), once compared to the state-of-the-art catalyst. The stability of the Mo framework sites from [Mo]-ZSM-5 catalyst was further evaluated up to 1000 °C, and under steaming conditions at 550 °C. Still, based on detailed characterization of the sample, the Mo sites remained perfectly unaltered, even though some dealumination did occur, but without generation of any silanol species, the material remaining silanol defect-free. This material is therefore a strong example of a zeolite material that is able to operate in a stable manner under harsh conditions (high temperature under reductive and oxidative atmosphere, and under hydrothermal conditions).

Following this work, there is still room for the optimization of isomorphous substitution procedure using the novel hydrothermal post synthesis approach. Such optimization would start with the enhancement of the silanol species in the parent zeolite (to be treated). Questions such as “What kind of silanol species are healed by metal addition?” are for instance fundamental questions that need to be addressed by studying in depth the ^1H MAS NMR spectra of silicalite-1 samples having different silanol content, prior Mo isomorphous substitution. The synthesis process could also be generalized to other metals (such as Cu, W, Sn) introduction in other zeolite structures (such as MWW or BEA). This would in turn allow the preparation of other resilient catalysts with new catalytic properties that might be of interest for other catalytic processes. However, the development of our understanding of the nature and amount of the silanol species as well as the relation between these parameters and the initial zeolite synthesis process is central and will probably represent the next milestone for the design of metal containing zeolite frameworks. Optimization for scale-up is also foreseen, with optimization of treatments times, concentrations, recycling of metal containing solutions, removal of useless calcination steps, use of steaming pre-treatment or not, etc. Based on the first optimisation steps that were performed during the PhD and for the post hydrothermal synthesis approach, the recycling of the metallic solution can be performed without any drawback, the treatment time can be reduced, the concentrations can be changed freely in a wide range, and the calcination treatment performed after Mo introduction (and before ion exchange with NH_4Cl) is not absolutely necessary. Also, the optimization of the metal containing catalyst for the MDA catalytic reaction is still an open question. The framework Mo atoms are catalyzing the formation of C2 products, and acid sites are promoting the C2 polymerization into aromatics. Questions such as “do we need both functionalities on the same catalyst?” or “what amount of acid sites is needed?” or also “what are the optimum temperature and contact time?” are still subject of discussion and needs to be addressed.

The new catalysts prepared according to the methodologies presented in this PhD thesis work are very promising from an industrial point of view due to their properties and possible applications. The advances made on the synthesis of framework metal containing zeolites and their applications as stable catalysts for new industrial processes are now attracting many interests. Due to the high concurrence in this field, this PhD thesis work was followed by the deposition of three patents protecting the synthesis processes (staged synthesis and novel post synthesis approach), and the catalytic applications of the corresponding materials, with the following application numbers: 19315123.0-1105; 19315122.2-1105; 19315132.1-1109. In addition, this work was the object of three publications: one communication in the Journal of American Chemical Society (chapter 2: “*Direct evidence for single molybdenum atoms incorporated in the framework of MFI zeolite nanocrystals*”, J. Am. Chem. Soc. 2019, 141, 22, 8689), and one full article as well as one review paper in Angewandte Chemie (chapter 5: DOI:10.1002/anie.202006524, “*Novel strategy for the synthesis of ultra-stable single-site Mo-ZSM-5 zeolite nanocrystals*”; and a part of chapter 1: DOI:10.1002/anie.202005498, “*Emphasis on the properties of metal-containing zeolites operating outside the comfort zone of current heterogeneous catalytic reactions*”). The present research was also the subject of several oral and poster presentations in international conferences. Moreover, chapter 4 of the present PhD thesis will soon be submitted as well for publication.

French conclusions and perspectives

Le développement de catalyseurs capables d'opérer sous des conditions de catalyse difficiles tels que les hautes températures, est d'une importance critique pour le développement de procédés industriels permettant la conversion du gaz naturel en composés chimiques à haute valeur ajoutée. De ce point de vue, les zéolithes comportant des métaux sont montrées comme étant des candidats prometteurs, mais leur stabilité en condition catalytiques difficiles demeure une question ouverte. Cependant, de grands espoirs sont dévoués à l'introduction de métaux dans la structure cristalline des supports zéolithiques via un processus appelé substitution isomorphe, du fait des propriétés apportées au matériau résultant. Parmi ces propriétés, la dispersion atomique des métaux, la faible teneur en métaux, et la forte interaction avec le support zéolithe, ou encore le caractère hydrophobe des matériaux générés sont autant de points qui permettent de limiter ou prévenir le frittage des métaux, leur démétallation, la dégradation des sites métalliques, ou l'amorphisation du support zéolithique par exemple. Par conséquent, la substitution isomorphe de métaux stabilise les catalyseurs contre les phénomènes de désactivation irréversible rencontrés lors de l'usage en catalyse sous conditions difficiles. L'introduction de métaux dans les réseaux zéolithiques peut être conduite de deux façons : (i) la synthèse directe, ou (ii) la post synthèse. Cependant, les deux méthodes possèdent leurs désavantages, et aucune n'est idéale. En effet, l'influence des ions métalliques sur le phénomène de cristallisation des zéolithes est une grande limitation liée à l'usage de la synthèse directe, alors que la sélectivité et la quantité d'espèce silanols posent également problèmes pour la post synthèse.

Au cours de cette thèse de doctorat, la synthèse de zéolithes MFI contenant du Mo introduit dans la structure cristalline a été étudiée et optimisée. Plusieurs essais ont été réalisés afin de réaliser la substitution isomorphe de Mo dans la structure MFI ; parmi ces derniers, la synthèse directe conventionnelle a été la première méthode principalement utilisée, dans laquelle les sources de Mo et de l'alcalin requis étaient combinées et introduites ensemble dans la suspension initiale permettant la cristallisation de la structure MFI. Après observation que les espèces Mo ne réagissaient pas avec les cristaux de MFI en formation lors des étapes initiales de synthèse, une nouvelle alternative de synthèse a été développée : la synthèse par étape. L'idée derrière cette nouvelle synthèse était d'introduire un délai avant l'ajout des sources de Mo et d'alcalin dans le gel de synthèse, après qu'un premier prétraitement hydrothermal soit conduit en l'absence de celles-ci. L'ajout de ce délai a permis de fortement réduire la taille des cristaux formés, et l'obtention d'échantillons ayant une homogénéité locale légèrement améliorée, basée sur une étude par ^{29}Si MAS NMR. Cela résulte du fait que l'addition retardée de Mo a permis de supprimer l'influence des ions Mo en solution, sur le processus de nucléation et de cristallisation des zéolithes MFI. Après observation détaillée du procédé de synthèse par étape, il a été montré que le délai avant l'addition du Mo et des ions alcalins pouvait être augmenté au-delà du temps de traitement hydrothermal

nécessaire pour la cristallisation complète de la structure MFI, menant à la conclusion que la présence de Mo n'était pas nécessaire aux côtés des autres espèces chimiques permettant la synthèse des cristaux de zéolithe MFI, lors de la synthèse de Mo-MFI. Par conséquent, la post synthèse hydrothermal a été développée comme une seconde alternative permettant la substitution isomorphe des zéolithes. Dans le cadre de cette seconde nouvelle approche, une zéolithe « parente » est préparée depuis une suspension initiale qui est cristallisée, lavée, et calcinée. Alors seulement, le Mo et la source de métal alcalin sont ajoutés sous la forme d'une solution aqueuse, dans laquelle les cristaux de zéolithes sont placés en suspension. La suspension ainsi préparée est traitée en conditions hydrothermales, ce qui résulte dans l'incorporation du Mo dans les cristaux de la zéolithe parente. Ces deux nouvelles méthodes de préparation permettant la substitution isomorphe, et plus spécialement la post synthèse hydrothermale, sont des améliorations de la synthèse directe classique décrite dans la littérature. De fait, ces traitements sont bien plus versatiles et adaptables, les interactions avec le processus de cristallisation sont totalement supprimées, et la qualité des échantillons ainsi formés n'est pas dégradée, mais améliorée. La post synthèse hydrothermale a été par exemple le jalon permettant la co-introduction de Mo et d'Al dans la structure MFI, formant une nanozéolithe Mo-ZSM-5 hautement homogène et hydrophobe.

Ensuite, la caractérisation complète d'une zéolithe MFI comportant du Mo en position intra-réseau de sa structure (Mo-MFI), préparée via une procédure classique de synthèse directe, a été décrite et comparée à une zéolithe MFI de référence dans laquelle du Mo a été introduit en position extra-réseau par imprégnation. Mo-MFI montre une haute homogénéité de sa structure au niveau local des atomes de Mo, une faible teneur en silanols, et une forte hydrophobicité. L'insertion de Mo dans la structure MFI induit une transition de symétrie, et accroît le volume de maille cristalline des cristaux de MFI. La nature uniforme des sites Mo incorporés dans le réseau MFI a été démontrée par IR (avec l'usage d'acétonitrile deutéré comme molécule sonde) et par ^{31}P MAS NMR (avec l'usage d'oxyde de triméthylphosphine comme molécule sonde), et la distribution homogène des métaux a été prouvée par STEM-HAADS combinée à une analyse EDS. Ce matériau ouvre de nouvelles opportunités pour le design de catalyseurs ou d'absorbants, pour des applications dans des domaines de l'industrie matures et émergents.

L'influence des silanols sur la zéolithe « parente » avant l'addition de Mo dans sa structure a permis de mettre en lumière l'importance centrale de ces espèces silanols sur le processus de substitution isomorphe. En effet, l'addition de Mo est toujours accompagnée d'une réduction de la quantité de silanols, car les Mo réagissent avec ces espèces lors de leur substitution isomorphe dans la structure zéolithique. Il est par conséquent important d'être en mesure d'évaluer la nature et la quantité des espèces silanols dans les zéolithes, afin d'ensuite optimiser la procédure de synthèse des matériaux Mo-MFI. En conséquence, les groupements hydroxyls, les silanols en particuliers, ont été caractérisés en profondeur dans trois

nanocristaux de MFI différents ayant la même taille de particules (Si-MFI, Al-MFI, and Mo-MFI), par IR, Raman et RMN. La nature et la quantité des sites silanols a été déterminée sans ambiguïté par vérification avec l'ensemble des techniques de caractérisation impliquées. La disparition totale des nids de silanols lors de la substitution isomorphe de Mo dans la structure MFI a été démontrée, alors que seulement une fraction des silanols externes isolés (environ 50 %) l'ont été. Basé sur cette étude, des directives pour la caractérisation des espèces hydroxyles dans les zéolithes sont émises, et la ^1H MAS NMR est montrée comme la méthode la plus efficace pour l'identification et la quantification simultanée des espèces silanols, avec l'aide de l'IR pour attribuer les signaux sans ambiguïté.

La stabilité et l'activité des zéolithes [Mo]-ZSM-5 préparés par post synthèse hydrothermale a été évaluée pour l'aromatisation du méthane (MDA). Les sites singuliers [Mo]-ZSM-5 contiennent du Mo hautement dispersé (0.5 wt. %) selon les analyses EDS-TEM et ICP, et des sites de Brønsted préservés. Le [Mo]-ZSM-5 a été comparé avec un catalyseur standard composé d'une zéolite ZSM-5 imprégnée avec 1 wt. % de Mo, extra-réseau. L'introduction de Mo dans la structure ZSM-5 ([Mo]-ZSM-5) a permis de supprimer les nids de silanols du matériau, résultant en un matériau stable, hydrophobe, et résistant contre les dégradations structurales sévères. Le nouveau matériau [Mo]-ZSM-5 montre des performances supérieures pour la conversion du méthane en hydrogène et en composés carbonés dits « supérieurs », et une stabilité remarquable sur les cycles de réaction-régénération successifs appliquées, une fois comparé au catalyseur de référence. La stabilité des Mo intra-réseau a été évaluée jusque 1000 °C, et sous conditions hydrothermales à 550 °C. A partir de caractérisations détaillées du catalyseur, les sites Mo restent parfaitement inchangés, même après qu'une partie de l'aluminium soit sortie du réseau MFI, et sans génération d'espèces silanols, le matériau demeurant hydrophobe. Ce matériau est par conséquent un exemple fort d'un matériau zéolithique capable d'opérer une catalyse stable à haute température, sous des conditions difficiles (haute température en présence d'une atmosphère oxydante, réductrice, ou hydrothermale).

A la suite de cette thèse de doctorat, il reste du travail à accomplir pour l'optimisation de la procédure de substitution isomorphe utilisant la nouvelle approche de post synthèse hydrothermale. Cette optimisation débiterait avec l'optimisation des propriétés et de la nature et quantité des silanols présents dans le matériau zéolithique initiale avant traitement au molybdène. Des questions comme « Quels types de silanols précisément réagissent avec le molybdène » sont par exemple des questions fondamentales qui doivent être adressées. La synthèse peut également être généralisée à d'autres métaux introduits dans d'autres structures zéolithiques que la MFI. Cependant, le développement de notre compréhension de la nature et quantification des espèces silanols, et la relation entre celles-ci et l'introduction de métaux par substitution isomorphe est centrale, et représente probablement le prochain jalon permettant un meilleur design de zéolithes contenant

des espèces métalliques intra-réseau. L'optimisation pour le scale-up représente également une nouvelle étape à franchir, avec l'optimisation des temps de traitements, les concentrations utilisées, le recyclage des solutions métalliques utilisées dans le post traitement, la suppression de certaines étapes de calcinations inutiles, ou encore l'addition d'un pré-traitement hydrothermale à haute température (steaming), ... Enfin, l'optimisation du catalyseur pour l'aromatization du méthane est encore une question ouverte. Les espèces molybdène intra-réseau catalysent la formation des C2, et les sites acides permettent la polymérisation des C2 ainsi formés en aromatiques. Des questions comme « A-t-on besoin des deux fonctionnalités acides et métalliques sur le même catalyseur ? » ou « quelle quantité de sites acides sont nécessaires ? » ou encore « quels sont les temps de résidences optimums, et les températures optimales ? » sont encore sujet à discussion, et doivent recevoir des réponses claires et précises.

Les nouveaux catalyseurs développés au cours de cette thèse de doctorat sont très prometteurs d'un point de vue industriel, du fait de leurs propriétés et de leurs applications potentielles. Les progrès réalisés sur la synthèse par substitution isomorphe de zéolithes contenant des métaux, et leurs applications comme catalyseurs exceptionnellement stables pour de nouveaux procédés industriels attirent en conséquence l'attention dans la communauté scientifique. Du fait de la haute concurrence dans ce domaine précis, cette thèse a été l'objet du dépôt de trois brevets protégeant les nouveaux procédés de synthèse, et les applications catalytiques des matériaux ainsi formés, avec les numéros d'application suivants : 19315123.0-1105; 19315122.2-1105 ; 19315132.1-1109. De plus, ce travail a fait l'objet de trois publications : une communication dans le Journal of American Chemical Society (chapitre 3 : J. Am. Chem. Soc. 2019, 141, 22, 8689), ainsi qu'un article et une revue de littérature dans Angewandte Chemie International Edition (Chapitre 5 : DOI :10.1002/anie.202006524, et première partie du chapitre 1 : DOI :10.1002/anie.202005498). La recherche ici présentée a également fait l'objet de plusieurs présentations orales et par poster lors de conférences internationales. De plus, le chapitre 4 de la présente thèse devrait être bientôt soumis pour publication également.

Incorporation of metals in zeolite frameworks for catalytic applications

Incorporation de métaux dans des zéolithes, pour des applications en catalyse

Short Abstract: The development of resilient metal containing zeolite based catalysts able to withstand harsh catalytic conditions is a milestone required for the industrialization of many catalytic processes involved in the energy transition. Among them, methane aromatization (MDA) stands as a promising alternative for the valorization of methane resources into value-added hydrogen and heavier hydrocarbons. The metal stability in a zeolite against irreversible deactivation processes such as metal leaching or metal sintering is mainly ruled by the way the metal is introduced in the zeolite support. Therefore, the introduction of molybdenum (Mo) in MFI zeolite frameworks by isomorphous substitution was studied in depth. Two novel synthesis processes were designed for the synthesis of highly hydrophobic Mo-containing MFI zeolite nanocrystals. The catalytic performances and stability of the as-prepared Mo-ZSM-5 material were then evaluated for methane dehydroaromatization (MDA) catalytic reaction over 3 successive reaction-regeneration cycles. The novel Mo-ZSM-5 catalyst showed superior conversion and selectivities compared to state-of-the-art MDA catalyst. In addition, the remarkable stability of the catalytic performances and of the catalyst itself was demonstrated over several reaction-regeneration cycles, and against thermal (up to 1000 °C) and hydrothermal (steaming, 550 °C) treatments. Some dealumination occurred, but no silanol species were generated, and the Mo atoms remained perfectly unaltered in the MFI zeolite structure.

Keywords: Zeolite, molybdenum, isomorphous substitution, MFI, ZSM-5, methane dehydroaromatization, MDA

Résumé: Le développement de catalyseurs zéolithiques contenant des métaux capables de résister à des conditions de travail difficiles représente un jalon requis pour l'industrialisation de nombreux procédés catalytiques impliqués dans la transition énergétique. Parmi ces réactions, l'aromatization du méthane est une alternative prometteuse pour la valorisation du méthane en hydrogène et en hydrocarbures à haute valeur ajoutée. La stabilité d'un métal dans une zéolithe contre les procédés de désactivation irréversibles comme la démetalation ou le frittage dépend principalement de la façon avec laquelle le métal est introduit dans le support zéolithique. Par conséquent, l'introduction de molybdène (Mo) dans les réseaux MFI par substitution isomorphe a été étudiée en profondeur. Deux nouveaux processus de synthèse ont été conçus pour la synthèse de nanocristaux de zéolithe Mo-MFI hautement hydrophobes. Les performances catalytiques et la stabilité du catalyseur Mo-ZSM-5 ainsi préparé ont été évaluées pour la réaction d'aromatization du méthane, sur 3 cycles de réaction-régénération successifs. Le nouveau catalyseur Mo-ZSM-5 montre une conversion et une sélectivité supérieure comparé à un catalyseur correspondant à l'état de l'art. De plus, la remarquable stabilité des performances catalytiques ainsi que du catalyseur lui-même a été démontrée sur plusieurs cycles de réaction-régénération, contre les traitements thermiques (jusqu'à 1000 °C) et contre les traitements hydrothermaux (550 °C). Le catalyseur subit une déalumination partielle, mais aucun silanol n'est généré, et les atomes de Mo demeurent parfaitement inchangés dans la structure zéolithique MFI.

Mots clés: Zéolithes, molybdène, substitution isomorphe, MFI, ZSM-5, aromatization du méthane, MDA